FLUID ALTERATION AND MAGNETITE-APATITE MINERALIZATION OF THE LYON MOUNTAIN GRANITE: ADIRONDACK MOUNTAINS, NEW YORK STATE

PETER M. VALLEY

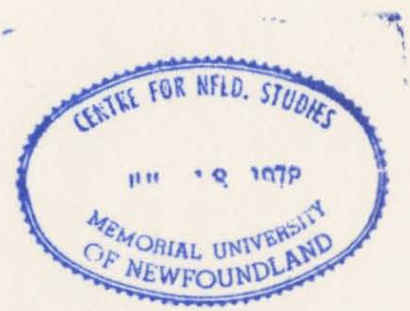
CENTRE FOR NFLD. STUDIES
MEMORIAL UNIVERSITY
OF NEWFOUNDLAND

FLUID ALTERATION AND MAGNETITE-APATITE MINERALIZATION OF THE LYON MOUNTAIN GRANITE: ADIRONDACK MOUNTAINS, NEW YORK STATE

by

Peter M. Valley

A thesis submitted to the School of Graduate Studies in partial fulfillment of the requirements for the degree of Doctor of Philosophy

Department of Earth Sciences/Faculty of Science

Memorial University of Newfoundland

October, 2010

St. John's

Newfoundland

ABSTRACT

The Lyon Mountain granite (LMG) is exposed in the Adirondack Mountains of northern New York State and is the host to numerous magnetite-apatite (Kiruna type) deposits. The results in this study suggest that the LMG was emplaced in the middle to late Ottawan orogeny between 1065 and 1045 Ma, along extensional shear zones during the onset of orogenic collapse. The original protolith, perthitic granite, has been extensively altered by subsequent Na- and K-rich fluids. Early-formed, zircon-poor clinopyroxene-magnetite-apatite deposits related to granite emplacement were remobilized and chemically modified by Na- and F-bearing fluids to form new deposits that crystallized hydrothermal zircon. Age determinations using U-Th-Pb geochronology of these hydrothermal zircon indicate that Na alteration and second generation mineralization occurred between 1040 Ma and 1000 Ma, 20 to 60 million years after crystallization of the host granite. Hafnium isotopes in zircon suggest that Lu-rich apatite and clinopyroxene associated with early-formed ore deposits broke down during Na and F alteration releasing radiogenic Hf from apatite and Zr from clinopyroxene. Granitic dikes and pegmatites which crosscut the fabric of the LMG, are dated between 1040 Ma and 1015 Ma and are contemporaneous with zircon growth in the iron ore deposits. This implies that Na alteration and Fe-mineralization were the result of externally derived fluids that penetrated the Lyon Mountain granite along extensional shear zones during orogenic collapse or by fluids related to granitic dike and pegmatite emplacement.

The presence of U-Th-Pb zircon ages that are 20 to 60 m.y. younger than the host granites of the magnetite ores, and the highly variable mineralogy of the ore deposits,

suggests that multiple fluid and mineralization processes were responsible for ore formation and periodic modification of preexisting ores. However, the presence of magnetite-apatite ore deposits almost exclusively within the LMG implies a "fertility" requirement of the host granite and hence that mineralization was in part related to magmatism.

ACKNOWLEDGEMENTS

I would like to thank my supervisor John Hanchar for his funding and support throughout the duration of this thesis. This research was supported by an NSERC Discovery Grant and startup funds to JMH provided by Memorial University of Newfoundland. Additional thanks goes to my thesis committee, Mark Wilson, Greg Dunning, Toby Rivers and Graham Layne who made themselves available when I needed them and Martin Whitehouse at NORDSIMS, for the use of the ion probe at the Swedish Museum of Natural History.

To my Adirondack mentors and now colleagues Marian Lupulescu, Phil Whitney, Jeff Chianrenzelli, and Jim McLelland, thanks for your helpful discussions and debates and for the good times in the ADK.

To Helen Mango, Ed Hasenohr and especially Tim Grover, thank you for giving me my start, believing in me, and being there when things got/get rough. To Chris Kopf and Marybeth Johnson, thanks for making me laugh and feeding me on holidays at the compound and keeping my head above water when the ship went down.

I would like to thank my mother and father for all your love and support over the years. It took a long time to get here, far longer than I ever imagined, but I finally did it. Even though my father could not be here to see me complete my thesis I think he would be proud.

To dance beneath the diamond sky with one hand waving free.....

(Bob Dylan)

One of my wishes is that those dark trees,

So old and firm they scarcely show the breeze,

Were not, as 'twere, the merest mask of gloom,

But stretched away unto the edge of doom.

I should not be withheld but that some day

Into their vastness I should steal away,

Fearless of ever finding open land,

Or highway where the slow wheel pours the sand.

I do not see why I should e'er turn back,

Or those should not set forth upon my track

To overtake me, who should miss me here

And long to know if still I held them dear.

They would not find me changed from him they knew—

Only more sure of all I thought was true.

(Robert Frost, Into My Own)

TABLE OF CONTENTS

LIST OF TABLES

LIST OF FIGURES

LIST OF ABBREVIATIONS AND SYMBOLS

AB	albite
ADK	Adirondack
ALT	alteration
AMCG	anorthosite-mangerite-charnockite-granite
AN	anorthite
APT	apatite
BSE	back scattered electron
CCSZ	Carthage-Colton shear zone
CHUR	chondritic uniform reservoir
CL	cathodoluminescence
CPX	clinopyroxene
εHf (t)	epsilon hafnium at time (t)
EPMA	electron probe microanalyzer
FG	fayalite granite
FIA	fluid inclusion assemblage
FLD	feldspar
FT	fluorite
HFSE	high field strength element(s)
HG	Hawkeye granite
HM	hematite
HREE	heavy rare earth element(s)

IL	ilmenite
IOCG	Iron oxide, copper, gold
KSP	K-feldspar
LA-ICPMS	laser ablation inductively-coupled plasma, mass spectrometry
LMG	Lyon Mountain granite
LILE	large ion lithophile element(s)
LREE	light rare earth element(s)
MC-ICPMS	multi-collector inductively-coupled mass spectrometry
MREE	middle rare earth element(s)
MSWD	mean square of weighted deviates
MT	magnetite
MUN	Memorial University
NIST	National Institute of Standards
OR	orthoclase
PG	perthite granite
QTZ	quartz
REE	rare earth element(s)
SEM	scanning electron microscope
SIMS	secondary ion mass spectrometer
TTN	titanite
ZR	zircon

LIST OF APPENDICES

CO-AUTHORSHIP STATEMENT

The manuscript presented as Chapter 2 has been published in "Geology" 2009, volume 37, pages 223-226 entitled "Direct dating of Fe-oxide (-Cu-Au) mineralization by U/Pb zircon geochronology ". The paper is co-authored by Dr. John Hanchar (Memorial University) and Dr. Martin Whitehouse (Swedish Museum of Natural History). As the first author, I was responsible for all aspects of the project including formulating specific research questions and conclusions, literature review, data collection, and analysis. Coauthors gave guidance for data collection, reduction and interpretation and corrected the written manuscript before submission. The manuscript was written and submitted to Geology by me.

The manuscript presented as Chapter 3 is entitled "Hafnium isotopes in zircon: A tracer of fluid-rock interaction during magnetite-apatite ("Kiruna-type") mineralization" and has been published in "Chemical Geology" volume 275 (3-4), pages 208-220. The manuscript is currently "in press". The paper is co-authored with Christopher Fisher (Memorial University), Dr. John Hanchar (Memorial University) dr. Rebecca Lam (Memorial University) and Michael Tubrett (Memorial University). I was responsible for all aspects of the project including formulating specific research questions and conclusions, literature review, data collection, and analysis. Chris Fisher assisted with data collection and interpretation. Rebecca Lam and Mike Tubrett assisted with the operation of the MC-ICPMS. Coauthors gave guidance and suggestions in writing of the

manuscript and corrected the original manuscript before submission. The manuscript was written and submitted to Chemical Geology by me.

The manuscript presented as Chapter 4 entitled "New insights on the evolution of the Lyon Mountain granite and associated magnetite-apatite ("Kiruna type") deposits, Adirondack Mountains, New York State" is in press with the journal Geosphere. The manuscript is co-authored by Dr. John Hanchar (Memorial University) and Dr. Martin Whitehouse (Swedish Museum of Natural History). As the first author, I was responsible for all aspects of the project including formulating specific research questions and conclusions, literature review, data collection, and analysis. Co-authors gave guidance for data collection, reduction and interpretation and have assisted in the correction of the written manuscript. The manuscript was written by me.

CHAPTER 1

INTRODUCTION AND OVERVIEW

Magnetite-apatite (Kiruna-type) deposits have often been placed in the all-encompassing group of iron oxide copper-gold (IOCG) deposits (e.g., Hitzman et al. 1992; Barton and Johnson, 1996). Iron oxide copper-gold deposits are highly variable in regards to their mineral content and the inferred fluid chemistry associated with mineralization, the timing of fluid alteration, geologic setting and host rock affinity. Some deposits contain significant amounts of Cu, Au and U such as those at Olympic Dam, Australia, whereas others like those in the Norrbotten region of Sweden (e.g., Kirunavaara, Malmberget) comprise mainly magnetite and apatite (e.g. Reynolds, 2000; Harlov et al., 2002). Most deposits contain significant quantities of rare earth elements (REE). Because of these variations, several different models for the origin of IOCG deposits and associated fluids have been proposed which can be included in two main groups: those that are directly related to magmatism and those related to coeval or older brines (Barton and Johnson, 2004). Magmatic IOCG deposits are characterized by a direct relation to a particular intrusion and typically occur in an arc setting. Mineralization is associated with widespread K-alteration and the deposits are enriched in Au and Cu with moderate amounts of magnetite and few rare earth elements (REE) (Barton and Johnson, 2004). Brine-related IOCG deposits are characterized by Na, K or acid alteration, abundant magnetite and apatite, high concentrations of REE, and are correlated with the presence of evaporites. Many deposits contain evidence for multiple generations of Fe mineralization and the remobilization of early-formed ores. In addition

to the magmatic and brine models, certain deposits have been proposed to be the result of Fe-rich magmas (like those at El Laco in Chili) (Naslund et al., 2002) and fluids related to metamorphic dehydration (Hagner and Collins, 1967). The unifying characteristics of all these deposits, regardless of the preferred model, are low-Ti Fe-oxides (magnetite, hematite), extensive hydrothermal Na and K metasomatic alteration, and typically form in an extensional tectonic setting (Hitzman et al., 1992). Fundamental questions, however, still exist about the relationship of magmatic activity, mineralization, fluid alteration and fluid sources, and the relative timing of these processes.

The Lyon Mountain granite crops out extensively in the northeastern Adirondack Mountains and is the host to numerous magnetite-apatite deposits. These deposits are variable in their constituent minerals, but nearly all contain low-Ti magnetite as the main Fe-bearing phase. Most include anomalous abundances of rare earth element (REE)-rich apatite (Roeder et al., 1987), quartz, variable amounts of clinopyroxene and trace abundances of zircon. Multiple generations of Fe mineralization and alkali fluid alteration are common even within a single deposit, but the majority of magnetite deposits are associated with Na alteration and pyroxene-bearing rocks.

1-1 HISTORY AND PREVIOUS WORK

The discovery of so-called "iron sands" at Fort St. Frederick, Crown Point, New York is mentioned in the writings of Swedish naturalist Peter Kalm in 1749 (Farrel, 1996). The first ironworks, utilizing the locally obtained ores were established at Skenesborough (now Whitehall, New York) around 1761. Magnetite ore deposits hosted

by the Lyon Mountain granite were mined extensively starting in the second half of the 19th century, and the last mine was closed by the Republic Steel Corporation at Mineville, NY in 1972.

Serious scientific inquiry into the origins of the LMG ores began in the first half of the 20th century. Kemp (1908) described in detail the mineralogy and structure of the orebodies and associated rocks in the Mineville area and the association of orebodies with pyroxene-bearing "syenite gneiss" host rock. The ores are described by Kemp (1908) as layers which trend NE-SW, conformable to the "banding or foliation" of the enclosing rock and may pinch and swell in a "pod-like or lenticular form". Gallagher (1937) described in detail the magnetite ores at Lyon Mountain. Gallagher concluded that the mineralization process was the result of late-stage iron-bearing fluids that were differentiated from granitic magma. A comprehensive study by Postel (1952) reported on the geology of the Clinton County magnetite district in the northeastern Adirondack Mountains. Postel's study included 1:62,500 scale bedrock mapping, structural analysis and petrology of the rocks in this area and an examination of all the mines and prospects in Clinton County. Postel identified the different lithologies within the LMG using names that are still in use today, including perthite granite, microcline granite and plagioclase granite. Postel concluded that the ore deposits and associated alteration were the result of Fe-bearing magmatic fluids and gasses. Hagner and Collins (1967) recognized that the LMG becomes depleted in disseminated magnetite (and any Fe-bearing minerals) as the ore zone is approached. They proposed that magnetite in the granite was removed by pervasive hydrothermal fluids and the Fe carried to areas of

lower pressure and subsequently redeposited. The source of the hydrothermal fluids was thought by those authors to be hornblende and biotite that broke down during regional metamorphism. Whitney and Olmsted (1988) theorized that the high Na- and K-bearing rocks of the LMG were the result of diagenetic alteration of felsic volcanic ash that was deposited in an evaporitic environment that were subsequently metamorphosed by the Ottawan orogeny.

The extensive body of work produced by James McLelland and colleagues in the past 25 years has led to a better understanding of the regional tectonics of the Adirondack Mountains, as well as the age of the LMG and processes associated with fluid alteration and Fe mineralization within the LMG. The LMG was proposed to be emplaced between 1060 and 1045 Ma (McLelland et al., 2001) based on U-Pb dating of zircon grains. This is substantially younger than either the Hawkeye granite (~1100 Ma) or rocks of the AMCG suite (~ 1150 Ma). It had been postulated previously by both Buddington (1948) and by Postel (1952) that the LMG was younger than other Grenvillian Adirondack rocks. Based on the deformational character of the LMG and the presence of magnetite-bearing granitic dikes crosscutting the Hawkeye granite that texturally and mineralogically resemble the LMG. McLelland et al. (2001) cited the lack of a penetrative fabric in the LMG to indicate that it had not experienced the granulite-facies metamorphism associated with the Ottawan orogeny. Furthermore, it was concluded that intrusion of the LMG marked the onset of extension and orogenic collapse following the Ottawan orogeny (McLelland et al., 2001; Selleck et al., 2005). McLelland (2002) and Selleck (2004) proposed that the extensive Fe mineralization was the result of magmatic-

hydrothermal processes during the last stages of pluton emplacement and that emplacement of the LMG drove fluid circulation during orogenic unroofing of the Adirondack Highlands.

1-2 THESIS OBJECTIVES

The main objectives of this thesis are:

1. *To establish whether there is a link between magnetite-apatite ores and the granites that host these deposits.*

The Lyon Mountain granite is the host to numerous magnetite-apatite deposits in the Adirondack Highlands. This suggests that there is a genetic link between this intrusive phase and the ore bodies. Understanding this link may have important implications for developing a model for the origin of magnetite-apatite deposits;

2. *To determine the absolute timing of magnetite-apatite mineralization relative to hydrothermal alteration and magmatism.*

Knowledge of the timing of mineralization and fluid alteration history is essential to understand the origins of magnetite-apatite deposits. Direct dating of such deposits establishes the link, or lack thereof, between granitic magmatism, hydrothermal alteration, and ore mineralization. Direct dating also links mineralization to tectonics and provides information on the type(s) of tectonic environments in which magnetite-apatite deposits may form;

3. *To determine fluid sources and fluid processes responsible for magnetite-apatite mineralization.*

Identification of the source and composition of the fluids responsible for mineralization and the processes driving fluid flow, fluid transport of metals and areas of mineralization is important for understanding how magnetite-apatite deposits form and whether mineralization is related to a particular magma type or certain tectonic environments or conditions

4. *To determine the extent, sequence and style of alteration associated with mineralization.*

The extent and type(s) of fluid alteration associated with mineralization are important for factors controlling how magnetite-apatite deposits form and evolve, and for identification of possible new deposits. Is mineralization associated with one type of alteration or all types? Are different types of alteration separated in time and space? What is the link between fluid alteration, mineralization and magmatism?

1-3 METHODS

The complex relationships among igneous and metamorphic processes, magnetite-apatite mineralization and fluid alteration requires a multidisciplinary approach to resolve the questions proposed in this thesis. Specifically, field work was conducted in order to better to understand the regional extent of LMG magmatism and the local extent and distribution of fluid alteration and mineralization within the LMG. Detailed

petrography (including color cathodoluminescence) was essential for understanding the origins of the LMG, its metamorphic history (if any) and the characterization and evolution of fluid alteration and Fe mineralization. Various types of geochemical analyses were used to characterize the chemistry of the ores, the host rocks, and the fluids related to alteration and mineralization and the elemental effects of the fluids on the original chemistry of the LMG. These techniques include whole rock major and trace element geochemistry, electron probe microanalysis (EPMA) of minerals, U-Th-Pb geochronology and trace element and Hf isotopic compositions of zircon and apatite.

1-4 CHAPTER OVERVIEWS

Chapter 1 Direct dating of Fe-oxide (-Cu-Au) mineralization by U/Pb zircon geochronology.

Zircon crystals were identified in samples collected from various magnetite-apatite ore bodies and dated by U-Th-Pb zircon geochronology along with zircon from the granite host in contact with the immediate ore body. Zircon grains were dated in situ using the secondary ion mass spectrometer (SIMS). These data provide an absolute age on at least one phase of Fe mineralization and provide information on the relationship, or lack there of, between granite magmatism and Fe mineralization as well as fluid processes.

Zircon grains from the studied magnetite-apatite ore deposits reveal that Fe mineralization associated with the growth of zircon is 20 to 60 m.y. younger than the crystallization of the granite host. Samples from the Palmer Hill ore yielded an age of

1038.9 ± 4.4 Ma (2σ) whereas zircon from the host granite less than a meter above the contact with the ore body yielded a concordant age of 1062.6 ± 5.5 Ma (2σ). The age of zircon crystals from the Arnold Hill ore is 1014.0 ± 7.4 Ma (2σ) and the granite host at Arnold Hill is 1060.7 ± 4.5 Ma (2σ). The Skiff Mountain ore is dated at 1000.9 ± 9.2 Ma (2σ). The Old Bed ore body contains zircon crystals that are very large (e.g., up to 10mm). Because of the extreme metamictization of these zircon grains, variable degrees of Pb loss have affected this sample. A statistically valid age was calculated using a weighted mean average and produced an average $^{207}Pb/^{206}Pb$ age of 1000.7 ± 4.2 Ma (2σ) for the Old Bed ore. However, this is a weighted average of samples that have undergone significant Pb loss. If we assume the oldest ages represent the least amount of Pb loss, then the oldest analyses should be a better representation of the true age or at least a minimum age. A weighted average of the four oldest samples produces a $^{207}Pb/^{206}Pb$ age of 1020.0 ± 11 Ma (2σ).

Zirconium is generally thought to be an immobile element during rock alteration. However, in the presence of F and alkaline fluids, Zr may become available, and mobile, from the breakdown of aegerine and arfedsonite in the host rocks (Rubin et al., 1993). The presence of altered aegerine, fluorite, fluoroapatite, NaCl-rich fluid inclusions and extensive albitization in the LMG is consistent with the conditions necessary for the supply and transport of Zr during at least one stage of Fe mineralization.

Previous age determinations of these deposits were constrained by the age of the host granitoids and the assumption that Fe mineralization was directly related to pluton emplacement. Zircon crystals extracted from the ore yield ages that show ore

mineralization was episodic and significantly younger than pluton emplacement. Host granites that intruded at ~1060 Ma cannot be the source of heat or fluids required for this period of Fe mineralization. Zircon ages in the ore bodies are similar in age to dikes which crosscut the regional fabric of the Adirondack Highlands (McLelland et al., 2001; Selleck et al., 2005). This suggests that the fluids responsible for this stage of Fe mineralization and hydrothermal zircon growth may be the result of fluid penetration along extensional structures related to orogenic collapse or that fluids were related to the emplacement of late dikes and pegmatite bodies that have a similar age relationship to the zircon ages in the ore.

Chapter 2 Hafnium isotopes in zircon: A tracer of fluid-rock interaction during magnetite-apatite ("Kiruna-type") mineralization.

The measurement of Hf isotopes in zircon provides a "snapshot" of the fluid or magma from which the zircon crystallized. Additionally, Lu/Hf offers a proxy for the ratio of heavy rare earth element (HREE) to high field strength element (HFSE) concentration in source materials, which vary significantly between minerals and rock types. The Hf isotopic composition of zircon from magnetite-apatite ore bodies, when combined with U-Pb zircon ages and trace element data can provide important information on the mineralizing fluids and evolution of these deposits. Hafnium isotopes were measured *in situ* by laser ablation inductively coupled plasma mass spectrometry (LA-ICP-MS) from the same zircon grains that were dated by SIMS. Hafnium isotopic compositions of zircon from the magnetite-apatite ore bodies and the host granite (as well

as the nearby Hawkeye granite and Tahawas ilmenite ore) were compared in order to characterize the fluids responsible for Fe mineralization.

The results of this study show that the Hf isotopic compositions of zircon from the LMG, Hawkeye granite, Tahawas ilmenite mine as well as the Palmer Hill ore body all have εHf (t) values similar to those predicted for juvenile Proterozoic crust (~εHf (t) less than +7 at 1060 Ma). However, Hf isotopic compositions from the magnetite-apatite ores at Skiff Mountain, Arnold Hill, and Old bed, all contain zircon with extremely radiogenic Hf (as high as εHf (t) +40) . These high values can only be explained by the breakdown of a Lu-rich mineral in the absence of a Hf-rich mineral (which would lower the radiogenic signature). Two plausible explanations exist for the highly radiogenic Hf isotopic compositions in these ores: 1) first-generation orebodies containing magnetite, clinopyroxene, and Lu-rich apatite were subsequently reworked 20 to 60 m.y. later during secondary fluid alteration and ore remobilization. This process released highly radiogenic Hf from the apatite, less radiogenic Hf and Zr from clinopyroxene, and mobilized Fe. Zircon then crystallized during the formation of these second-generation orebodies; alternatively 2) fluids responsible for zircon-bearing ores may have interacted with garnet-rich crust during rapid decompression and retrograde metamorphism of the Adirondack Highlands and radiogenic Hf was released from garnet and, as above, Zr and less radiogenic Hf from clinopyroxene. Model 1 is supported by (i) the high Lu/Hf ratios in apatite, (ii) zircon with the highest εHf (t) values correspond to deposits which contain the most REE-rich apatite, (iii) the observed alteration in thin section of apatite and clinopyroxene, and (iv) the overprinting nature of Na-rich fluids observed in the field and

in thin sections. Model 2, is supported by the close proximity of garnet-bearing rocks with the LMG and some of the ore deposits. In both models the association of fluorite and fluorine-bearing minerals and NaCl-rich fluid inclusions with Na alteration and Fe mineralization suggests that F- and Cl-bearing fluid may have been responsible for the breakdown of early formed apatite and clinopyroxene or garnet and clinopyroxene and for transportation of the REE.

Chapter 3 New insights on the evolution of the Lyon Mountain granite and associated magnetite-apatite ("Kiruna type") deposits, Adirondack Mountains, New York State

The combination of field observations, cathodoluminescence (CL) and traditional transmitted and reflected light petrography, whole rock and mineral chemistry and *in situ* U-Th-Pb zircon geochronology can be used for recognizing the type, sequence, and timing of fluid alteration and Fe mineralization associated with magnetite-apatite deposits. Representative samples of the different LMG rock types, orebodies, amphibolite layers from within the LMG, crosscutting granitic dikes, Hawkeye granite and AMCG suite charnockite were systematically collected and analyzed.

The LMG consists of 3 main rock types: perthite granite, microcline granite and albite granite and a fourth minor rock type fayalite granite. Both the microcline granite and the albite granite are probably the result of hydrothermal alteration. The perthite granite, containing the mineral assemblage perthitic feldspar, quartz, magnetite, and minor clinopyroxene, biotite, amphibole, titanite, apatite, zircon, and hematite-ilmenite intergrowths, has been overprinted by potassic alteration (microcline, quartz, magnetite

and minor titanite), which in turn has been overprinted by extensive Na alteration (albite, quartz, magnetite, apatite ± clinopyroxene, amphibole, biotite, titanite, garnet, and fluorite). The fayalite granite (perthitic feldspar, quartz, clinopyroxene, fayalite and zircon) has also been overprinted by Na-rich fluids. During Na alteration, preexisting ore bodies consisting of magnetite, clinopyroxene, and apatite, were overprinted and remobilized to form new deposits that comprise magnetite, apatite, quartz, albite, and zircon.

Whole rock geochemistry shows that the LMG may contain up to 10 weight percent K or Na in the most extremely altered samples and that Na altered samples have the highest and most variable concentration of REE. Potassic alteration had little effect on the trace element budget of the LMG except for an increase in large ion lithophile elements. Electron microprobe analyses reveal that the feldspar grains analyzed are close to end-member albite or orthoclase regardless of whether the feldspars are primary perthitic feldspar or produced as a product of K and Na fluid alteration. Clinopyroxene is typically aegerine-augite except in the fayalite granite where clinopyroxene is hedenbergite with exsolution of Fe-rich orthopyroxene.

The LMG contains ubiquitous 1060-1050 Ma zircon with minor ~1150 Ma cores regardless of the rock type they were collected from. However, zircon from the albite granite yielded a subset of ages (~1030 Ma) which is coincident with zircon ages from some of the ore bodies. Zircon from the LMG have small (<5 μm) rims that were observed in BSE images but could not be dated. The LMG contains amphibolite layers of uncertain origin, one of which was dated as coeval with the last stage of probable LMG

emplacement at 1046 ± 11 Ma (Skiff Mountain) and an amphibolite layer in Ausable Forks yielded zircon at 1019 ± 8 Ma. Zircon from granitic dikes and pegmatites which crosscut the fabric of the LMG are dated at 1041 ± 7 Ma at Lyon Mountain, 1030 ± 11 Ma at Skiff Mountain and 1017 ± 7 Ma at Dannemora.

The most likely model suggested by the data presented here is that the LMG is a syn- to late-tectonic granite as proposed by McLelland et al. (2001). Intrusion of the LMG began during the Ottawan Orogeny around 1060 Ma and lasted at least until 1047 Ma. The formation of early clinopyroxene-magnetite-apatite ore bodies occurred during the latest stages of pluton emplacement as the result of Fe-rich immiscible liquids or incorporation of Fe-rich wall-rock into the Lyon Mountain magmas. By ~1047 Ma the orogen had cooled sufficiently for the preservation of feldspars and clinopyroxene more typical of intrusive felsic igneous rocks that have not experienced long periods at elevated temperatures as evidenced by the mineralogy of the fayalite granite. We suggest that the LMG intruded along extensional shear zones that developed at the onset of orogenic collapse. Initial ore deposits (or Fe-rich immiscible liquids) formed as a result of LMG magmatism. From 1040 Ma to 1000 Ma a period of widespread extension is evidenced by the emplacement of dikes and pegmatites which crosscut the regional fabric of the LMG, which was accompanied by massive remobilization and modification of preexisting ore bodies by K-, Na-, Cl and F-rich fluids.

1-5 SUMMARY

The data presented in this thesis suggest that the LMG intruded the northeastern Adirondack Highlands between 1060 and 1050 Ma. First generation ore deposits consisting of clinopyroxene, magnetite and apatite formed as a result of granite crystallization. The granite and these early deposits were altered and remobilized 20 to 60 million years later by K- and Na-rich fluids that penetrated the LMG following the Ottawan Orogeny. These second-generation deposits comprise magnetite, apatite, quartz, albite, and minor zircon. Fluid alteration and Fe mineralization associated with the development of magnetite-apatite (Kiruna-type) deposits occurred episodically, long after crystallization or formation of the ore host rock.

REFERENCES

Barton, M.D., and Johnson, D.A., 1996, Evaporitic-source model for igneous-related Fe oxide- (REE-Cu-Au-U) mineralization: Geology, v. 24, p. 259-262.

Barton, M.D., and Johnson, D.A., 2004, Footprints of Fe-oxide (-Cu-Au) systems: SEG 2004 Predictive Mineral Discovery Under Cover - Extended Abstracts, Centre for Global Metallogeny, The University of Western Australia, v. 33, p. 112-116.

Bouvier A., Vervoort J.D., and Patchett P.J., 2007, The Lu-Hf CHUR value: Geochimica et Cosmochimica Acta Supplement, Vol. 71, Goldschmidt Conference Abstracts 2007, A116.

Buddington, A.F., 1948, Origin of granitic rocks of the northwest Adirondacks [New York]: Memoir - Geological Society of America, p. 21-43.

Farrel, P., 1996, Through the Light Hole: North Country Books, Utica New York, p. 1-291

Gallagher, D., 1937, Origin of the magnetite deposits at Lyon Mountain, N. Y: New York State Museum Bulletin, p. 85.

Hagner, A.F., and Collins, L.G., 1967, Magnetite ore formed during regional metamorphism, Ausable magnetite district, New York: Economic Geology, v. 62, p. 1034-1071.

Harlov, D.E., Andersson, U.B., Foerster, H.-J., Nyström, J.O., Dulski, P., and Broman, C., 2002, Apatite-monazite relations in the Kiirunavaara magnetite-apatite ore, northern Sweden: Chemical Geology, v. 191, p. 47-72.

Hitzman, M.W., Oreskes, N., and Einaudi, M.T., 1992, Geological characteristics and tectonic setting of proterozoic iron oxide (Cu-U-Au-REE) deposits: Precambrian Research, v. 58, p. 241-287.

Hitzman, M. W., 2000, Iron Oxide-Cu-Au Deposits: What, Where, When, and Why: In, Porter T.M. (eds.), Hydrothermal Iron Oxide Copper-Gold & Related Deposits: A Global Perspective. Volume 1, PGC Publishing, Adelaide, p. 9-25.

Kemp, J. F., 1908, The Mineville-Port Henry mine group: Bulletin N.Y. State. Museum, v. 119, p. 57-88.

McLelland, J., Hamilton, M., Selleck, B., McLelland, J., Walker, D., and Orrell, S., 2001, Zircon U-Pb geochronology of the Ottawan Orogeny, Adirondack Highlands, New York; regional and tectonic implications: Precambrian Research, v. 109, p. 39-72.

McLelland, J., Morrison, J., Selleck, B., Cunningham, B., Olson, C., and Schmidt, K., 2002, Hydrothermal alteration of late- to post-tectonic Lyon Mountain granitic gneiss, Adirondack Mountains, New York; origin of quartz-sillimanite segregations, quartz-albite lithologies, and associated Kiruna-type low-Ti Fe-oxide deposits: Journal of Metamorphic Geology, v. 20, p. 175-190.

McLelland, J.M., Bickford, M.E., Hill, B.M., Clechenko, C.C., Valley, J.W., and Hamilton, M.A., 2004, Direct dating of Adirondack massif anorthosite by U-Pb SHRIMP analysis of igneous zircon: Implications for AMCG complexes: Geological Society of America Bulletin, v. 116, p. 1299-1317.

Naslund, H.R., Henríquez, F., Nyström, J.O., Vivallo, W., & Dobbs, F.M., 2002, Magmatic iron ores and associated mineralization: Examples from the Chilean High Andes and Coastal Cordillera: in Porter, T.M., ed., Hydrothermal iron oxide copper-gold & related deposits: A global perspective, v. 2, PGC Publishing, Adelaide, p. 207-226.

Postel, A.W., 1952, Geology of the Clinton County magnetite district: United States Geological Survey Professional Paper, v. 237, p. 88.

Reynolds L.J., 2000, Geology of the Olympic Dam Cu-U-Au-Ag-REE Deposit, In Porter T.M. (Ed.) Hydrothermal Iron Oxide Copper-Gold & Related Deposits: A Global Perspective. Volume 1. PGC Publishing, Adelaide,

pp.93-104.

Roeder, P.L., MacArthur, D., Ma, X.-P., Palmer, G.R., and Mariano, A.N., 1987, Cathodoluminescence and microprobe study of rare-earth elements in apatite: American Mineralogist, v. 72, p. 801-811.

Rubin, J.N., Henry, C.D., and Price, J.G., 1993, The mobility of zirconium and other "immobile" elements during hydrothermal alteration: Chemical Geology, v. 110, p. 29-47.

Selleck, B., McLelland, J., and Hamilton, M.A., 2004, Magmatic-hydrothermal leaching and origin of late to post-tectonic quartz-rich rocks, Adirondack Highlands, New York: Geological Society of America Memoirs, v. 197, p. 379-390.

Selleck, B.W., McLelland, J.M., and Bickford, M.E., 2005, Granite emplacement during tectonic exhumation: The Adirondack example: Geology, v. 33, p. 781-784.

Whitney, P.R., and Olmsted, J.F., 1988, Geochemistry and origin of albite gneisses, northeastern Adirondack Mountains, New York: Contributions to Mineralogy and Petrology, v. 99, p. 476–484, doi: 10.1007/BF00371938.

CHAPTER 2

In:

Valley, P.M., Hanchar, J.M. and Whitehouse, M.J. (2009) Direct dating of Fe-oxide (-Cu-Au) mineralization by U/Pb zircon geochronology. Geology, 37: 223-226, doi: 10.1130/G25439A.1

DIRECT DATING OF FE-OXIDE (-CU-AU) MINERALIZATION BY U/PB ZIRCON GEOCHRONOLOGY

Peter M. Valley[1], John M. Hanchar[1], and Martin J. Whitehouse[2]

[1]*Department of Earth Sciences, Memorial University of Newfoundland, St. John's, NL A1B 3X5 Canada*

[2]*Laboratory for Isotope Geology, Swedish Museum of Natural History S-104 05 Stockholm, Sweden*

E-mail: pvalley@mun.ca

ABSTRACT

We present results for direct dating of Fe-oxide (-Cu-Au) (IOCG) mineralization by U/Pb zircon geochronology. Constraining the timing of mineralization has important geodynamic implications for the processes involved in the genesis of these types of deposits and the tectonic evolution of rocks associated with these deposits. Hydrothermal zircon crystals were separated from four IOCG-type ore deposits associated with the Lyon Mountain Granite (LMG) in the Adirondack Mountains. Zircon grains from these low-Ti magnetite deposits reveal at least two periods of mineralization: one episode at ~1039 Ma and a second between ~1015 and 1000 Ma. Previous age determinations of these deposits were constrained by the age of the altered host granitoids, and the assumption that Fe mineralization was directly related to pluton emplacement. Zircon

crystals extracted from the ore yield ages that show ore mineralization was episodic and younger than pluton emplacement.

2-1 INTRODUCTION

Iron oxide (-Cu-Au) (so called IOCG) deposits are a class of ore deposits whose defining characteristics vary significantly (e.g., Hitzman 1992). Some deposits contain significant amounts of Cu, Au, and U, such as those at Olympic Dam, Australia (e.g., Reynolds, 2000), whereas the dominant ore at Kiruna, Sweden, is magnetite and apatite (Harlov et al., 2002). The unifying characteristics of all these deposits are high concentrations of low-Ti Fe-oxide minerals (magnetite and hematite), pervasive hydrothermal alteration (Na, K, Si, seritization), and an extensional tectonic setting (Hitzman et al., 1992).

Several studies have attempted to constrain the timing of IOCG-type mineralization by dating zircon in the altered host rocks associated with these deposits (e.g., Mortimer et al., 1988). Other studies have dated minerals in the ore such as apatite and titanite (e.g., Romer et al., 1994; Gelcich et al., 2005), or monazite (e.g., Grainger et al., 2008), or Re-Os dating of molybdenite (e.g., Mathur et al., 2002). Dating the host rock, however, assumes that the growth of zircon is coeval with Fe mineralization. Accessory minerals that are directly linked with ore mineralization provide a less ambiguous means of dating IOCG mineralization. Iron oxide mineralization is often accompanied by the growth of apatite and titanite (Hitzman et al., 1992); however, those minerals may incorporate common Pb (i.e., ^{204}Pb) in their structure, and if their $^{238}U/^{204}Pb$ ratios are low this will preclude obtaining precise ages. In this study, we have

directly dated Fe mineralization by identifying hydrothermal zircon from four IOCG-type ore deposits in the Lyon Mountain Granite (LMG) from the Adirondack Highlands in New York State. Zircon is a more robust geochronometer and as such should provide more reliable age constraints on the timing of mineralization.

2-2 GEOLOGICAL SETTING

The Adirondack Highlands (Fig. 2-1) are dominated by a ca. 1150 anorthosite-mangerite-charnockite-granite (AMCG) suite that was metamorphosed during the Ottawan orogeny between 1090 and 1040 Ma and is intruded by syn- to late-tectonic granites (McLelland et al., 2001). The LMG crops out extensively in the northeastern Adirondack Highlands and is the host to numerous low-titanium magnetite IOCG-type deposits (e.g., Whitney and Olmsted, 1988). The LMG has experienced extreme metasomatism by potassic- and sodic-rich fluids, accompanied by enrichment in F and P, and mobilization of high field strength elements (HFSE) including Zr, Y, U, and light and middle rare earth elements (LREEs, and MREEs, respectively) during Fe mineralization (Foose and McLelland, 1995; Whitney et al., 1993; McLelland et al., 2002). The LMG consists of mesoperthite granite and where altered microcline granite and/or albitic granite. All lithologies contain disseminated magnetite as the predominant mafic mineral. A gneissic fabric may be present but varies from pronounced to non-existent.

2-3 LOW TITANIUM MAGNETITE DEPOSITS

The ores are comprised of magnetite, and/or hematite, and typically include apatite, quartz, feldspar, clinopyroxene, and minor zircon. Fluid temperatures of 565-675°C were estimated from quartz-magnetite $\delta^{18}O$ fractionation (McLelland et al., 2002).

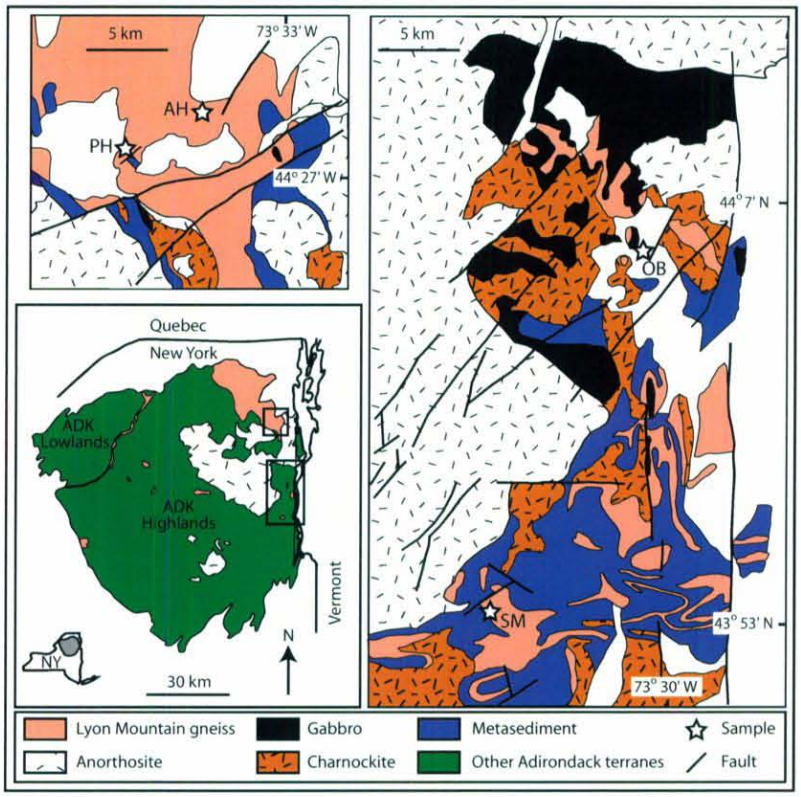

Figure 2-1. Simplified geologic map of the northeastern Adirondack Mountains with sample locations for this study marked on detailed maps: PH = Palmer Hill; AH = Arnold Hill; OB = Old Bed; SM = Skiff Mountain (modified from Isachsen and Fisher, 1970 and Whitney et al., 1993)

The LMG orebodies are associated with shear zones, fold hinges, and at the contact of the LMG with other units (Postel, 1952; Whitney et al., 1993). The orebodies are generally conformable with the gneissic fabric, but locally crosscut the fabric at a high angle. Barren zones nearly devoid of magnetite up to 150 m wide occur in the granite immediately adjacent to the ore bodies (Hagner and Collins, 1967). Locations of samples used in this study are shown in Figure 2-1. Detailed descriptions of the individual ore deposits in this study are given in section 2-7, data repository 1.

Numerous workers have discussed the origin of low-Ti magnetite ores in the LMG and include: 1) immiscible magmatic Fe-rich fluids (e.g., Postel, 1952); 2) the breakdown of preexisting mafic silicates (Hagner and Collins, 1967); 3) eruption of Fe-oxide magmas (Whitney et al., 1993); and 4) surface derived saline fluids that have interacted with the latest stages of pluton emplacement (McLelland et al., 2002). Previously, the timing of Fe mineralization in the LMG was constrained through inference by its close association with the LMG host rocks (Foose and McLelland, 1995; Selleck et al., 2004).

2-4 U-Pb SIMS GEOCHRONOLOGY

Uranium-Th-Pb zircon analyses for the four ore and two granite host samples were done using the Cameca IMS 1270 ion-microprobe at the Swedish Museum of Natural History following the methods described by Whitehouse et al. (1999) and later modified in Whitehouse and Kamber (2004). Concordia ages for samples that yield overlapping concordant points were calculated using Isoplot (Ludwig, 2003). The mean square of weighted deviates (MSWD) indicates whether uncertainties in the Concordia

age can be explained entirely by assigned analytical error on individual data points (MSWD ~1 or lower). Details of the analytical techniques are given in section 2-8 data repository 2. All age uncertainties in the paper and associated figures are 2σ. Errors in Table 2-1 are 1σ.

Magmatic zircon crystals from the host granite typically are brown to pink, elongate, well faceted, and highly fractured (Fig. 2-2A) and may contain inclusions of apatite or quartz. These grains are often zoned with respect to U and Hf and some contain older inherited cores (Fig. 2-2). Zircon is typically found as inclusions in quartz or feldspar or at grain boundaries.

Hydrothermal zircon grains from the magnetite ore are typically blocky, clear and featureless in back-scattered electron (BSE) images (Figs. 2-2B and 2-3). Some contain irregular, patchy, zoning in BSE or cathodoluminescence (CL) imaging. Some of the ore zircon crystals analyzed contain interior regions with different U and Hf contents that produce variations in the BSE signal and appear to be "cores" (Fig. 2-3); however, these inner zones yield ages within error of the outer regions in the crystals. Zircon grains are generally free of melt or fluid inclusions, but may contain small apatite, Fe-oxide, or quartz inclusions. Zircon crystals occur in association with magnetite, apatite, fluorite, calcite, quartz, and chlorite.

Zircon grains from the granite less than a meter above the contact with the ore body at Palmer Hill yield a concordant age of 1062.6 ± 5.5 Ma (2σ) (Fig. 2-4A). Samples from the ore yield an age of 1038.9 ± 4.4 Ma (2σ) (Fig. 2-4B). Zircon from the granite adjacent to the ore body at Arnold Hill yield an age of 1060.7 ± 4.5 Ma (2σ) (Fig. 2-4C).

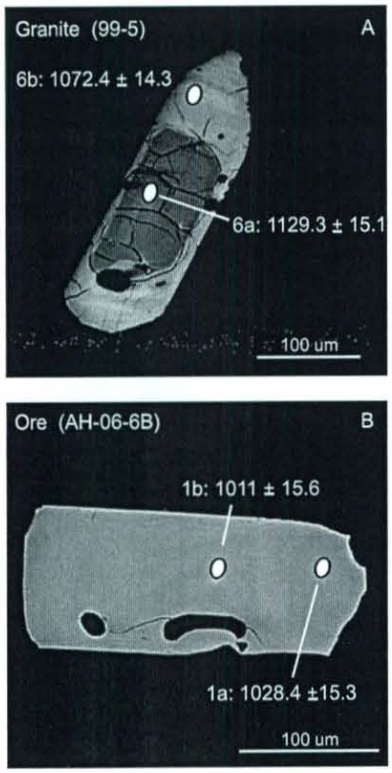

Figure 2-2. Representative BSE images of zircon grains from (A) typical host granite zircon from Arnold Hill and (B) ore zircon . Single spot ages are given as $^{207}Pb/^{206}Pb$ ages corrected for common Pb. Sample names correspond to Table 2-1.

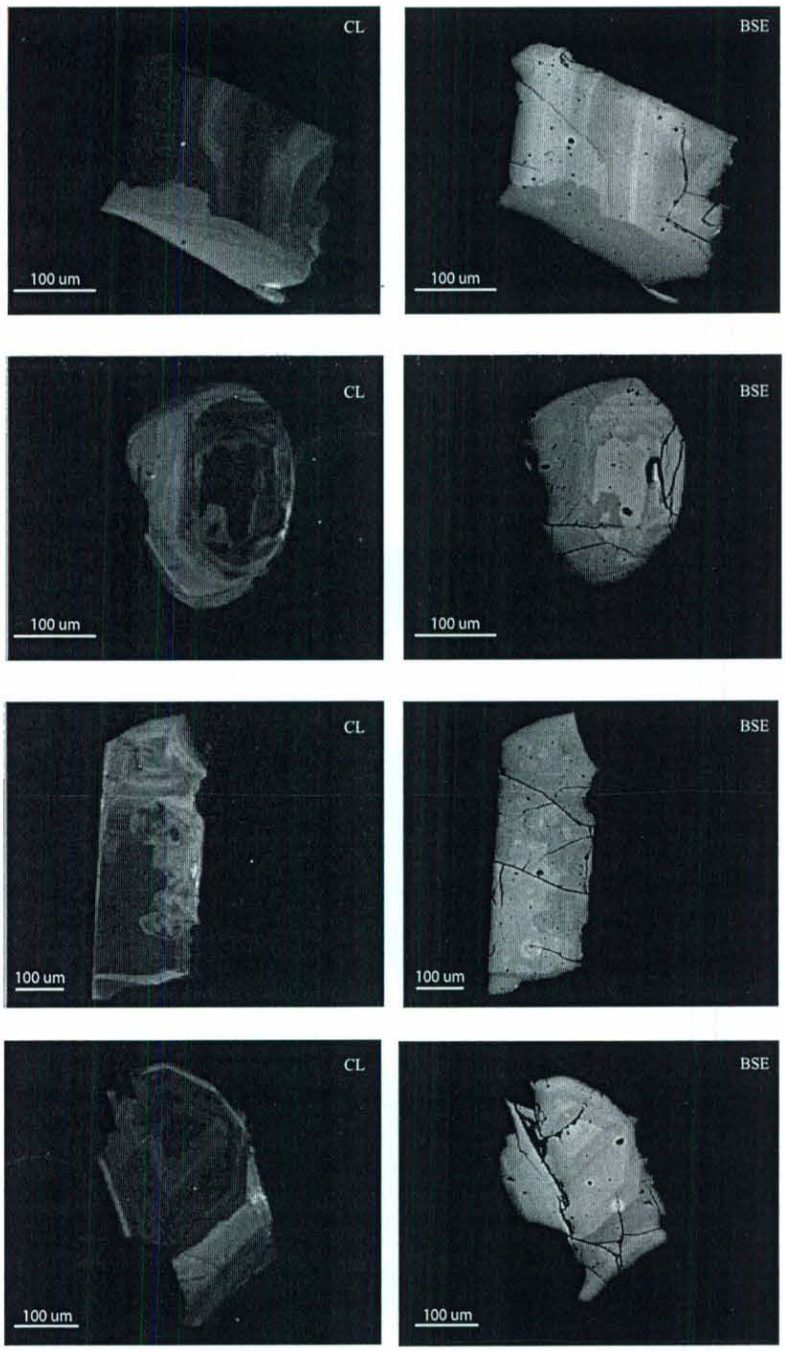

Figure 2-3. Additional CL and BSE images of representative zircon samples from the Palmer Hill ore (99-4a).

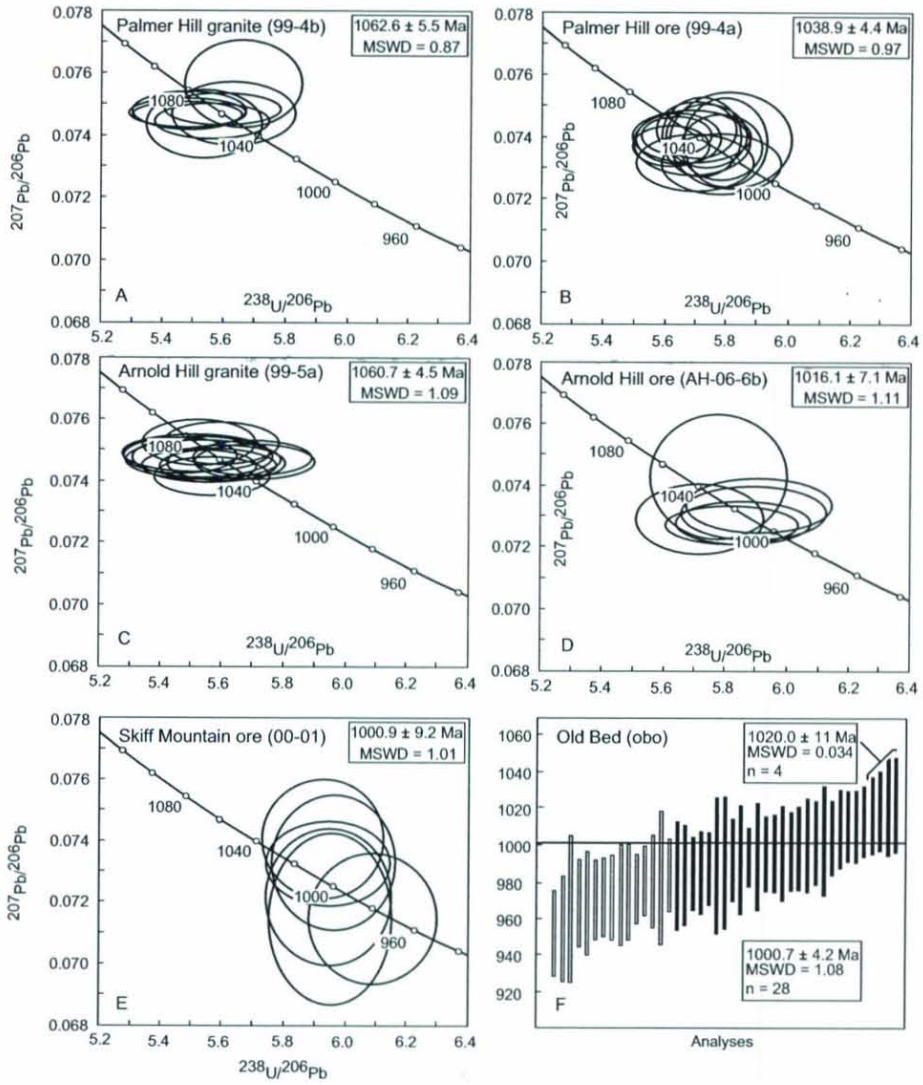

Figure 2-4. Tera-Wasserburg Concordia diagrams ($^{207}Pb/^{206}Pb$ versus $^{238}U/^{206}Pb$) zircon ages for Palmer Hill granite (A), Palmer Hill ore (B), Arnold Hill granite (C), Arnold Hill ore (D), and Skiff Mountain ore (E). Uncertainties on quoted concordia ages (a-e) are 2σ. Weighted mean averages of common Pb corrected $^{207}Pb/^{206}Pb$ age for Old Bed Ore (n = 28, filled black errors bars on plot). Bracketed error bars are $^{207Pb}/^{206}Pb$ age of samples assumed to be least a ffected by Pb loss (n=4) and used to calculate separate weighted average age for the Old Bed Ore,(F). Open error bars in (F) are not used in age calculation. Error ellipses and error bars are in all samples.

Table 2-1 Ion microprobe U-Th-Pb results for the Lyon Mountain Granite and associated iron ores.

Sample	U(ppm)	Th (ppm)	Pb (ppm)	Th/U	f206 *	238U/206Pb	sigma%	207Pb/206Pb	sigma%	207Pb/206Pb	Ma error	206Pb/238U	Ma error
Palmer Hill granite (99-4b)													
1B	1166	159	234	0.138	{0.01}	5.558	1.38	0.07442	0.32	1052.8	6.4	1066.5	13.6
2A	2165	201	436	0.089	0.02	5.472	1.38	0.07468	0.25	1059.9	5.0	1082.0	13.8
~~2B**~~	~~69~~	~~28~~	~~16~~	~~0.419~~	~~{0.21}~~	~~5.297~~	1.38	~~0.07868~~	~~1.41~~	~~1164.0~~	~~27.8~~	~~1114.9~~	~~14.1~~
~~3B~~	~~125~~	~~62~~	~~30~~	~~0.427~~	~~{0.03}~~	~~5.086~~	1.39	~~0.07728~~	~~0.89~~	~~1128.4~~	~~17.7~~	~~1157.1~~	~~14.7~~
3C	380	110	80	0.318	{0.04}	5.535	1.40	0.07434	0.60	1050.6	12.1	1070.6	13.8
4B	1063	104	214	0.104	{0.01}	5.482	1.38	0.07477	0.32	1062.3	6.4	1080.2	13.8
5A	201	108	44	0.552	{0.03}	5.660	1.38	0.07561	0.75	1084.8	15.1	1048.9	13.3
~~5B~~	~~157~~	~~87~~	~~37~~	~~0.583~~	~~{0.08}~~	~~5.241~~	1.38	~~0.07659~~	~~0.81~~	~~1110.4~~	~~16.2~~	~~1125.7~~	~~14.3~~
5C	1955	307	401	0.164	0.01	5.481	1.38	0.07461	0.24	1058.1	4.8	1080.4	13.7
6B	418	182	84	0.172	0.15	5.626	1.46	0.07468	0.55	1060.0	11.0	1054.6	14.3
6D	1628	338	327	0.164	0.06	5.592	1.39	0.07480	0.27	1063.1	5.4	1060.6	13.6
Arnold Hill granite (99-5a)													
1A	1544	333	310	0.221	{0.01}	5.697	1.38	0.07466	0.32	1059.3	6.4	1042.5	13.2
1B	2145	413	435	0.205	0.01	5.606	1.38	0.07457	0.28	1057.1	5.7	1058.1	13.4
2A	1469	358	301	0.250	{0.00}	5.617	1.38	0.07448	0.30	1054.4	6.0	1056.2	13.5
3A	2116	503	445	0.253	{0.00}	5.464	1.38	0.07479	0.26	1062.8	5.2	1083.4	13.7
3B	1242	354	257	0.282	0.01	5.614	1.38	0.07448	0.33	1054.6	6.6	1056.8	13.4
~~4A~~	~~154~~	~~72~~	~~37~~	~~0.481~~	~~{0.07}~~	~~5.101~~	1.38	~~0.07895~~	~~0.86~~	~~1170.9~~	~~17.0~~	~~1154.1~~	~~14.6~~
4B	1637	346	337	0.218	0.02	5.526	1.39	0.07440	0.29	1052.4	5.8	1072.2	13.7
~~4C2~~	~~138~~	~~64~~	~~33~~	~~0.450~~	~~{0.09}~~	~~5.091~~	1.29	~~0.07871~~	~~1.14~~	~~1164.9~~	~~22.5~~	~~1156.1~~	~~13.7~~
5A	1335	294	273	0.225	{0.00}	5.598	1.38	0.07516	0.37	1072.7	7.4	1059.6	13.5
5B	2059	380	419	0.190	{0.01}	5.570	1.38	0.07484	0.30	1064.3	5.9	1064.4	13.5
~~6A~~	~~115~~	~~67~~	~~27~~	~~0.454~~	~~0.20~~	~~5.217~~	1.38	~~0.07808~~	~~1.19~~	~~1148.8~~	~~23.5~~	~~1130.4~~	~~14.3~~
6B	1100	175	224	0.166	0.03	5.526	1.38	0.07520	0.39	1073.7	7.9	1072.3	13.6
7A	1403	265	284	0.187	{0.01}	5.587	1.38	0.07445	0.33	1053.7	6.6	1061.5	13.5
7B	1378	185	268	0.116	0.03	5.706	1.39	0.07456	0.31	1056.5	6.2	1041.0	13.4
8B	1991	443	415	0.234	0.02	5.494	1.38	0.07480	0.34	1063.0	6.8	1078.1	13.7
9A	1225	217	248	0.186	{0.01}	5.568	1.39	0.07409	0.34	1044.0	6.8	1064.7	13.6
~~9C~~	~~1901~~	~~826~~	~~465~~	~~0.469~~	~~0.01~~	~~4.958~~	1.39	~~0.07797~~	~~0.24~~	~~1146.2~~	~~4.7~~	~~1184.3~~	~~15.1~~
10A	1178	256	246	0.228	0.01	5.478	1.42	0.07461	0.32	1058.1	6.5	1080.9	14.2
Palmer Hill magnetite ore (99-4a)													
1A	432	180	90	0.438	0.04	5.782	1.38	0.07311	0.54	1016.9	10.8	1028.3	13.1
2B	408	405	99	1.035	0.05	5.684	1.38	0.07381	0.58	1036.2	11.7	1044.7	13.3
3A	502	380	115	0.778	0.05	5.698	1.38	0.07317	0.51	1018.6	10.4	1042.4	13.3
4A	611	656	151	1.107	0.03	5.689	1.38	0.07402	0.47	1042.1	9.4	1043.8	13.3
4B	188	78	39	0.413	0.12	5.812	1.39	0.07389	0.87	1038.5	17.4	1023.4	13.2
1a	184	131	41	0.698	0.10	5.720	0.94	0.07399	0.71	1041.2	14.3	1038.7	9.1
1b	716	670	171	0.898	0.03	5.622	0.94	0.07404	0.36	1042.5	7.2	1055.4	9.2
1c	177	89	37	0.457	0.15	5.795	0.94	0.07383	0.78	1036.7	15.8	1026.2	9.0
3a	401	474	99	1.102	0.11	5.702	0.95	0.07422	0.50	1047.5	10.0	1041.7	9.1
4a	308	151	65	0.480	0.12	5.784	0.94	0.07366	0.58	1032.1	11.7	1027.9	9.0
4b	299	210	67	0.669	0.06	5.736	0.94	0.07402	0.56	1042.1	11.2	1035.9	9.0
5a	716	151	144	0.195	0.04	5.619	0.94	0.07371	0.36	1033.5	7.2	1055.8	9.2
6a	533	424	123	0.772	0.04	5.652	0.94	0.07393	0.45	1039.5	9.0	1050.2	9.1

Table 2-1 continued

Sample	U(ppm)	Th (ppm)	Pb (ppm)	Th/U	f206 *	238U/206Pb	sigma%	207Pb/206Pb	sigma%	207Pb/206Pb	Ma error	206Pb/238U	Ma error
Arnold Hill magnetite ore (ah-6b)													
1a	1363	302	268	0.207	0.02	5.777	1.53	0.07415	0.76	1045.5	15.2	1029.2	14.6
1b	1660	269	316	0.152	0.02	5.888	1.59	0.07305	0.46	1015.4	9.2	1011.2	14.9
3a	1617	336	310	0.195	0.01	5.905	1.63	0.07331	0.48	1022.6	9.7	1008.5	15.3
~~10a~~	~~131~~	~~65~~	~~30~~	~~0.487~~	~~0.05~~	~~5.311~~	1.55	~~0.07725~~	~~0.48~~	~~1127.6~~	~~30.6~~	~~1112.1~~	~~15.9~~
~~10b~~	~~102~~	~~38~~	~~23~~	~~0.359~~	~~0.12~~	~~5.174~~	1.50	~~0.07738~~	~~1.55~~	~~1130.9~~	~~37.4~~	~~1139.0~~	~~15.7~~
11b	1742	319	343	0.180	0.03	5.714	1.49	0.07287	0.63	1010.2	12.6	1039.7	14.3
11c	1810	377	344	0.133	0.04	5.853	1.50	0.07277	0.37	1007.5	7.6	1016.7	14.2
15b	2307	358	443	0.151	0.02	5.815	1.51	0.07268	0.34	1005.0	6.9	1022.9	14.3
Skiff Mountain magnetite ore (00-01)													
2A	327	158	67	0.449	0.08	5.948	1.38	0.07324	0.76	1020.7	15.2	1007.7	10.1
2B	144	34	27	0.216	{0.04}	5.949	1.41	0.07216	1.27	990.3	25.5	998.1	12.1
3A	166	54	33	0.279	{0.07}	5.927	1.39	0.07403	1.08	1042.2	21.7	1016.8	11.4
4B	150	40	29	0.224	{0.17}	5.964	1.38	0.07327	1.24	1021.5	25.0	1006.3	11.9
4C	209	42	39	0.176	{0.06}	6.091	1.41	0.07144	1.22	970.2	24.7	977.0	11.8
5A	158	44	30	0.243	0.15	5.954	1.38	0.07143	1.59	969.9	32.2	991.2	13.4
Old Bed Ore (obo)													
n2273_Pb_7@10				0.26	0.02			0.0733	1.27	1022.7	12.7		
n2270_Pb_7@16				0.16	0.14			0.0722	1.41	1021.7	13.4		
n2273_Pb_7@6				0.18	0.02			0.0732	1.07	1019.4	10.7		
n2273_Pb_7@15				0.17	0.01			0.0731	0.99	1018.1	10.0		
n2273_Pb_7@8				0.22	0.03			0.0730	0.96	1013.6	9.6		
n2273_Pb_7@14				0.19	0.01			0.0728	0.98	1011.1	9.9		
n2270_Pb_7@36				0.15	0.09			0.0722	0.99	1011.0	9.5		
n2270_Pb_7@19				0.17	0.13			0.0719	1.19	1009.6	10.4		
n2270_Pb_7@2				0.15	0.06			0.0722	1.09	1004.5	10.0		
n2270_Pb_7@21				0.12	0.07			0.0721	1.52	1003.0	14.9		
n2270_Pb_7@25				0.17	0.06			0.0726	1.19	1002.3	11.4		
n2273_Pb_7@13				0.12	0.03			0.0725	1.25	1000.5	12.5		
n2273_Pb_7@3				0.12	0.04			0.0725	1.14	998.7	11.3		
n2273_Pb_7@12				0.12	0.04			0.0724	1.06	996.8	10.5		
n2273_Pb_7@17				0.12	0.03			0.0724	1.28	996.0	12.8		
n2270_Pb_7@1				0.15	0.04			0.0720	1.04	995.9	10.4		
n2273_Pb_7@11				0.14	0.02			0.0723	0.98	995.3	9.9		
n2270_Pb_7@18				0.11	0.11			0.0714	1.53	994.3	14.6		
n2273_Pb_7@2				0.14	0.02			0.0723	0.78	994.1	7.8		
n2270_Pb_7@29				0.10	0.20			0.0707	1.75	992.5	14.8		
n2270_Pb_7@5				0.13	0.04			0.0722	1.13	992.4	11.1		
n2270_Pb_7@31				0.11	0.18			0.0708	2.11	991.1	18.2		
n2270_Pb_7@28				0.13	0.13			0.0711	1.89	989.0	18.5		
n2270_Pb_7@27				0.16	0.08			0.0721	1.04	987.4	9.7		
n2273_Pb_7@16				0.11	0.04			0.0720	1.10	985.1	11.0		
n2270_Pb_7@26				0.15	0.11			0.0720	1.08	984.8	9.8		
n2270_Pb_7@22				0.12	0.07			0.0714	1.38	984.3	13.5		
n2270_Pb_7@34				0.13	0.12			0.0719	1.53	983.7	14.7		
n2270_Pb_7@4				0.16	0.05			0.0719	1.00	983.6	9.8		
n2270_Pb_7@12				0.10	0.15			0.0719	1.91	983.0	18.3		
n2270_Pb_7@20				0.16	0.21			0.0718	1.37	980.9	12.7		
n2273_Pb_7@9				0.07	0.02			0.0718	0.91	980.8	9.2		
n2270_Pb_7@24				0.18	0.12			0.0707	0.97	976.2	9.2		
n2270_Pb_7@3				0.12	0.03			0.0716	1.28	974.5	12.9		
n2270_Pb_7@8				0.12	0.09			0.0715	1.42	972.9	13.5		
n2270_Pb_7@15				0.16	0.05			0.0715	1.14	971.6	11.3		
n2270_Pb_7@23				0.15	0.06			0.0715	1.05	971.4	10.3		
n2273_Pb_7@4				0.13	0.04			0.0714	1.04	969.9	10.4		
n2270_Pb_7@7				0.11	0.09			0.0714	1.44	968.5	13.9		

Table 2-1 continued

Sample	U(ppm)	Th (ppm)	Pb (ppm)	Th/U	f206 *	238U/206Pb	sigma%	207Pb/206Pb	sigma%	207Pb/206Pb	Ma error	206Pb/238U	Ma error
n2270_Pb_7@9				0.13	0.10			0.0714	1.20	967.8	11.3		
n2270_Pb_7@13				0.10	0.13			0.0713	2.10	965.4	19.9		
n2270_Pb_7@33				0.12	0.21			0.0709	1.73	954.3	14.2		
n2270_Pb_7@17				0.17	0.12			0.0708	1.22	951.6	11.4		
n2270_Pb_7@11				0.10	0.16			0.0707	1.56	949.4	14.1		
n2270_Pb_7@10				0.11	0.19			0.0705	2.45	942.8	23.4		
n2270_Pb_7@30				0.10	0.24			0.0704	1.75	941.1	15.7		
~~n2270_Pb_7@6~~				~~0.14~~	~~0.24~~			~~0.0699~~	1.49	~~925.9~~	~~11.6~~		
~~n2270_Pb_7@14~~				~~0.10~~	~~0.34~~			~~0.0698~~	1.44	~~921.8~~	~~11.8~~		
~~n2270_Pb_7@32~~				~~0.10~~	~~0.21~~			~~0.0697~~	1.76	~~919.4~~	~~15.9~~		
~~n2273_Pb_7@21~~				~~0.11~~	~~0.49~~			~~0.0696~~	3.93	~~915.9~~	~~32.9~~		
~~n2273_Pb_7@1~~				~~0.09~~	~~0.08~~			~~0.0687~~	0.75	~~889.4~~	~~7.2~~		
~~n2270_Pb_7@35~~				~~0.14~~	~~0.08~~			~~0.0639~~	22.49	~~738.4~~	~~218.7~~		
~~n2273_Pb_7@20~~				~~0.04~~	~~2.11~~			~~0.0565~~	32.05	~~473.3~~	~~175.0~~		

Notes:

All errors are 1 sigma

*Percent of Pb206 that is common Pb, brackets indicate 204 was too small to measure

**Analyses with crossed out data are inherited zircon cores or points that have experienced excessive Pb loss and have been eliminated from concordia plots for clarity

The age for zircon crystals from the Arnold Hill ore is 1016.1 ± 7.1 Ma (2σ) (Fig. 2-4D). The Skiff Mountain ore is dated at 1000.9 ± 9.2 Ma (2σ) (Fig. 2-4E). The Old Bed ore body contains zircon crystals that are very large (up to 10mm). They are typically dark brown and highly metamict. Because of the extreme metamictization, variable degrees of Pb loss have affected this sample. Two approaches were therefore used to calculate a minimum $^{207}Pb/^{206}Pb$ age. A statistically valid age was calculated using a weighted mean average. Analyses were added (n = 28) until the MSWD exceeded one. This approach produced an average $^{207}Pb/^{206}Pb$ age of 1000.7 ± 4.2 Ma (2σ) for the Old Bed ore (Fig. 2-4F). However, this is a weighted average of samples that have undergone significant Pb loss. Analytical error alone cannot explain the difference between the oldest measured ages and the age calculated by this weighted average. If we assume the oldest ages represent the least amount of Pb loss, then the oldest analyses are a minimum age. A weighted average of the four oldest samples (n = 4) yields a $^{207}Pb/^{206}Pb$ age of 1020.0 ± 11 Ma (2σ) (Fig. 2-4f).

2-5 DISCUSSION

Uranium-Pb zircon ages calculated from low-Ti magnetite deposits in the LMG are 20–60 million years younger than their host granites. These age data are supported by the earlier work of McLelland and co-workers who dated the LMG with the sensitive high-resolution ion microprobe (SHRIMP) from several nearby localities between 1059 and 1047 Ma (McLelland et al., 2001). It seems unlikely, therefore, that the iron mineralization is directly related to emplacement of the granites that host the ore deposits. Three possibilities for the formation of zircon in these iron oxide deposits are: 1) post-

emplacement metamorphic fluids; 2) Fe-oxide rich magmas intruding as dikes and sills; and 3) the zircon in the ores are hydrothermal in origin with mineralizing fluids coming from deep circulating meteoric waters and /or brines or younger, and as yet, unidentified magmatism.

Metamorphic fluids seem the least likely hypothesis. Small leucogranite bodies that were emplaced during regional extension and numerous dikes that crosscut the gneissic fabric of the LMG have been dated between 1045 Ma and 1030 Ma in the Adirondacks (McLelland et al., 2001; Selleck et al., 2005). Because U/Pb ages from the ore deposits have contemporaneous or younger ages than these dikes, the ore bodies could not have been significantly metamorphosed or deformed.

Some evidence exists that these deposits could be Fe-rich magmas (e.g., nelsonites) intruding the LMG as dikes and sills. The contacts of some deposits are very sharp with the surrounding granite or ores may be pegmatitic in nature. Iron oxide magmas have been proposed sources for other IOCG deposits (e.g., Naslund et al., 2002). The similarity of magnetite, apatite, and quartz ores with nelsonite magmas is compelling; however, nelsonite magmas are enriched in Ti (as well as Fe and P) and all of these ore bodies contain low-Ti oxides. Also, nelsonite magmas are typically associated with anorthosite-gabbro intrusions. Though very large anorthosite bodies are common in the Adirondack highlands, these intrusions are ~100 to 150 million years too old to be responsible for ore formation in the LMG (McLelland et al., 2001).

Several papers have been written on the hydrothermal origin of IOCG deposits (e.g., Hitzman et al., 1992; Barton and Johnson, 1996, and references therein). The

presence of vein fluorite and fluorite intergrown with magnetite and apatite at the Palmer Hill mine suggests that the ore is hydrothermal. At the Arnold Hill mine the presence of calcite, microcrystalline quartz, and chlorite in brecciated zones associated with Fe mineralization also suggests a hydrothermal origin. Extensive Na and K alteration of perthitic feldspar in the host granites requires a hydrothermal fluid or late magmatic/hydrothermal fluid. The scavenging of disseminated magnetite from the host rock and production of magnetite from the breakdown of clinopyroxene is also consistent with an ore that is hydrothermal in nature and may be the source of Fe for the ore body (Hagner and Collins, 1967).

The presence of hydrothermal zircon in an ore requires that Zr was highly mobile during mineralization. Zirconium is generally thought to be an immobile element during rock alteration; however, in the presence of F and alkaline fluids, Zr may become available, and mobile, from the breakdown of aegerine and arfedsonite in the host rocks (Rubin et al., 1993). The presence of F-bearing minerals indicates F was present during mineralization. Other possible reservoirs of Zr include ilmenite, titanite, rutile, and garnet (Bea et al., 2006). It may, in some cases, be possible to use Th/U ratios to distinguish hydrothermal from magmatic zircon grains. However, some hydrothermal zircon show depletion in Th (Rubin et al., 1993), while others may show an increase in Th (Hoskin, 2005). Thorium/uranium ratios in the Arnold Hill ore zircon are virtually indistinguishable from those of the host granite, whereas at Palmer Hill there is a distinct difference in Th/U ratios of the ore and granite zircon (Table 2-1). These differences alone do not preclude that ore-related zircon at Palmer Hill or Arnold Hill is

hydrothermal in origin. Zircon grains in the ore could not have been inherited from the host LMG, however, because of the discrepancy in ages between the host rocks and the ore and the textural association of ore zircon to possible hydrothermal minerals such as apatite, fluorite and altered feldspars.

The most plausible explanation for the origin of the Fe mineralization is penetration of hydrothermal fluids along faults related to extension and orogenic collapse. These fluids were presumably rich in alkalis, F, P, Fe, REEs, Y, U, and Zr. Initial Fe mineralization at ~1039 Ma at the Palmer Hill mine is coeval with syn-extensional leucogranite bodies and dikes. Fluids and heat required for the formation of the oldest ore deposits may be supplied by these intrusions. However, the older granites that host the ore deposits are too old to supply the heat and fluids needed for mineralization. It is not clear if subsequent Fe mineralization at ~1020 Ma and ~1000 Ma is the result of as yet undiscovered plutonism and/or episodic extension and secondary fluid penetration. If these younger ages were the result of Pb-loss we would expect to see a continuum of ages with each sample.

2-6 CONCLUSIONS

The first direct dating of low-Ti magnetite ores by U/Pb zircon geochronology indicates that Fe mineralization was protracted and episodic and not related to emplacement of the host granites. These data are consistent with Fe mineralization being the result of hydrothermal fluid alteration during a period of extensional tectonics. Direct U/Pb dating of zircon crystals from the ore provides a more robust method for dating IOCG deposits than other minerals which may be susceptible to the effects of common

Pb or that provide only indirect dates from the host rocks. Understanding the timing of Fe mineralization and hydrothermal alteration provides important information for ore petrogenesis, crustal fluids, and the tectonic evolution of the regions that host these deposits.

ACKNOWLEDGEMENTS

This research was supported by an NSERC Discovery Grant and startup funds provided by Memorial University of Newfoundland to JMH. The NordSIM ion microprobe facility is financed and operated under an agreement between the research councils of Denmark, Norway, Sweden, and the Geological Survey of Finland and the Swedish Museum of Natural History; this is NordSIM publication number 219. We wish to thank Greg Dunning, Mark Wilson, Toby Rivers, Marian Lupulescu, Phil Whitney, and James McLelland for their helpful discussions, and Don Davis, Richard Tosdal, David John, and an anonymous reviewer, for their insightful reviews.

REFERENCES CITED

Bea, F., Montero, P., and Ortega, M., 2006, A LA-ICP-MS evaluation of Zr reservoirs in common crustal rocks: Implications for Zr and Hf geochemistry, and zircon-forming processes: Canadian Mineralogist, v. 44, p. 693-714.

Barton, M.D., and Johnson, D.A., 1996, Evaporitic-source model for igneous-related Fe oxide- (REE-Cu-Au-U) mineralization: Geology, v. 24, p. 259–262, doi: 10.1130/0091-7613(1996)024<0259:ESMFIR>2.3.CO;2.

Foose, M.P., and McLelland, J.M., 1995, Proterozoic low-Ti iron-oxide deposits in New York and New Jersey; relation to Fe-oxide (Cu-U-Au-rare earth element) deposits

and tectonic implications: Geology (Boulder), v. 23, p. 665–668, doi: 10.1130/0091-7613(1995)023<0665:PLTIOD>2.3.CO;2.

Gelcich, S., Davis, D.W., and Spooner, E.T.C., 2005, Testing the apatite-magnetite geochronometer; U/Pb and $^{40}Ar/^{39}Ar$ geochronology of plutonic rocks, massive magnetite-apatite tabular bodies, and IOCG mineralization in northern Chile: Geochimica et Cosmochimica Acta, v. 69, p. 3367–3384, doi: 10.1016/j.gca.2004.12.020.

Grainger, C.J., Groves, D.I., Tallarico, F.H.B., and Fletcher, I.R., 2008, Metallogenesis of the Carajás Mineral Province, Southern Amazon Craton, Brazil: Varying styles of Archean through Paleoproterozoic to Neoproterozoic base- and precious-metal mineralisation: Ore Geology Reviews, v. 33, p. 451, doi: 10.1016/j.oregeorev.2006.10.010.

Hagner, A.F., and Collins, L.G., 1967, Magnetite ore formed during regional metamorphism, Ausable magnetite district, New York: Economic Geology and the Bulletin of the Society of Economic Geologists, v. 62, p. 1034–1071.

Harlov, D.E., Andersson, U.B., Foerster, H.-J., Nyström, J.O., Dulski, P., and Broman, C., 2002, Apatite-monazite relations in the Kiirunavaara magnetite-apatite ore, northern Sweden: Chemical Geology, v. 191, p. 47–72, doi: 10.1016/S0009-2541(02)00148-1.

Hitzman, M.W., Oreskes, N., and Einaudi, M.T., 1992, Geological characteristics and tectonic setting of proterozoic iron oxide (Cu—U—Au—REE) deposits: Precambrian Research, v. 58, p. 241–287, doi: 10.1016/0301-9268(92)90121-4.

Hoskin, P.W.O., 2005, Trace element composition of hydrothermal zircon and the alteration of Hadean zircon from the Jack Hills, Australia: Geochimica et Cosmochimica Acta, v. 69, p. 637–648, doi: 10.1016/j.gca.2004.07.006.

Isachsen, Y. W., and Fisher, D. W. (1970) Geologic map of New York State Adirondack Sheet. New York State Museum Science Service Map Chart Series 16.

Ludwig, K.R., 2003, User's Manual for Isoplot 3.00, A geochronological toolkit for Microsoft Excel: Berkley Geochronology Center Special Publication No. 4.

Mathur, R., Marschik, R., Ruiz, J., Munizaga, F., Leveille, R.A., and Martin, W., 2002, Age of mineralization of the Candelaria Fe oxide Cu-Au deposit and the origin of the Chilean iron belt, based on Re-Os isotopes: Economic Geology and the Bulletin of the Society of Economic Geologists, v. 97, p. 59–71.

McLelland, J., Hamilton, M., Selleck, B., McLelland, J., Walker, D., and Orrell, S., 2001, Zircon U-Pb geochronology of the Ottawan Orogeny, Adirondack Highlands, New York; regional and tectonic implications: Precambrian Research, v. 109, p. 39–72, doi: 10.1016/S0301-9268(01)00141-3.

McLelland, J., Morrison, J., Selleck, B., Cunningham, B., Olson, C., and Schmidt, K., 2002, Hydrothermal alteration of late- to post-tectonic Lyon Mountain granitic gneiss, Adirondack Mountains, New York; origin of quartz-sillimanite segregations, quartz-albite lithologies, and associated Kiruna-type low-Ti Fe-oxide deposits: Journal of Metamorphic Geology, v. 20, p. 175–190, doi: 10.1046/j.0263-4929.2001.00345.x.

Mortimer, G.E., Cooper, J.A., Paterson, H.L., Cross, K., Hudson, G.R.T., and Uppill, R.K., 1988, Zircon U-Pb dating in the vicinity of the Olympic Dam Cu-U-Au deposit, Roxby Downs, South Australia: Economic Geology and the Bulletin of the Society of Economic Geologists, v. 83, p. 694–709.

Naslund, H.R., Henriquez, F., Nystrom, J.O., Vivallo, W., and Dobbs, F.M., 2002, Magmatic iron ores and associated mineralisation; examples from the Chilean High Andes and Coastal Cordillera, Australian Mineral Foundation, Glenside, South Aust., Australia (AUS). v. 2, p.207–226.

Postel, A.W., 1952, Geology of the Clinton County magnetite district: United States Geological Survey Professional Paper, v. 237, p. 88.

Reynolds, L.J., 2000, Geology of the Olympic Dam Cu-U-Au-Ag-REE deposit, Australian Mineral Foundation, Glenside, South Aust., Australia (AUS).

Romer, R.L., Martinsson, O., and Perdahl, J.A., 1994, Geochronology of the Kiruna iron ores and hydrothermal alterations: Economic Geology and the Bulletin of the Society of Economic Geologists, v. 89, p. 1249–1261.

Rubin, J.N., Henry, C.D., and Price, J.G., 1993, The mobility of zirconium and other "immobile" elements during hydrothermal alteration: Chemical Geology, v. 110, p. 29–47, doi: 10.1016/0009-2541(93)90246-F.

Selleck, B.W., McLelland, J.M., and Hamilton, M.A., 2004, Magmatic-hydrothermal leaching and origin of late- to post-tectonic quartz-rich rocks, Adirondack Highlands, New York; in Tollo, R.P., Corriveau, L., McLelland, J., and Bartholomew, M. J.,

eds., Proterozoic Tectonic Evolution of the Grenville Orogen in North America: Geological Society of America Memoir no. 197, p. 379–390.

Selleck, B.W., McLelland, J.M., and Bickford, M.E., 2005, Granite emplacement during tectonic exhumation: The Adirondack example: Geology, v. 33, p. 781–784, doi: 10.1130/G21631.1.

Whitehouse, M.J., Kamber, B.S., and Moorbath, S., 1999, Age significance of U-Th-Pb zircon data from early Archaean rocks of west Greenland–a reassessment based on combined ion-microprobe and imaging studies: Chemical Geology, v. 160, p. 201, doi: 10.1016/S0009-2541(99)00066-2.

Whitehouse, M.J., and Kamber, B.S., 2004, Assigning dates to thin gneissic veins in high-grade metamorphic terranes: A cautionary tale from Akilia, southwest Greenland: Journal of Petrology, v. 46, p. 291–318, doi: 10.1093/petrology/egh075.

Whitney, P.R., and Olmsted, J.F., 1988, Geochemistry and origin of albite gneisses, northeastern Adirondack Mountains, New York: Contributions to Mineralogy and Petrology, v. 99, p. 476–484, doi: 10.1007/BF00371938.

Whitney, P.R., Olmsted, J.F., and New York State Geological, Survey., 1993, Bedrock geology of the Au Sable Forks quadrangle, northeastern Adirondack Mountains, New York: New York State Museum Map and Chart Series 43, 48 pp and map.

2-7 DATA REPOSITORY 1

ORE DEPOSIT DESCRIPTIONS
Palmer Hill

The Palmer Hill ore body consists of massive magnetite, with quartz, apatite, microcline, albite, fluorite, and zircon. Disseminated magnetite is common throughout the host granites in the Palmer Hill mine area, but is generally lacking in depleted zones up to 100 meters wide adjacent to the ore body (Hagner and Collins, 1967). The ore was approximately 3 meters thick at Palmer Hill over a distance of ~600m narrows to 1 meter (Postel, 1952). The orebody lies in the axis of a northeast plunging syncline with brecciated and mylonitized zones in the hanging wall and footwall. The ore body and fold are bounded on the southeast by a northeast trending fault. The host rock in the vicinity of the ore is dominated by microcline granite gneiss. Microcline is partially corroded or crosscut by albite and hematite partially replaces magnetite in the host granite.

Arnold Hill

The orebodies at Arnold Hill are a mixture of magnetite, hematite, martite (pseudomorphic hematite after magnetite) and minor apatite and zircon. Calcite, jasper, and amphibole/chlorite breccia are common at the margins of the ore adjacent to the host rock. Three main ore bodies were mined here two of which were magnetite and one martite. The thickness of all 3 ore bodies ranges from 1 to 7 meters. The ore bodies plunge to the northeast and may occupy the east limb of a syncline (Postel, 1952). The host rock at Arnold Hill is dominated by albitic gneiss. Albite has replaced the perthitic feldspar granite.

Skiff Mountain

The ore consists of two main bodies approximately 40 meters apart and is concordant with the gneissic foliation. The lower ore has been mined out and is inaccessible. The upper ore consists of a half-meter thick body of massive magnetite, apatite, and quartz. The host rock immediately above and below the ore consists of quartz-albite gneiss and is depleted in disseminated magnetite for 0.5 meters above the ore. Thirty to 40 meters above the orebody, the host rock returns to perthitic granite (McLelland et al., 2002).

Old Bed

Ore samples from the Old Bed mine consist of magnetite, apatite, clinopyroxene, and quartz. Early workers described the Old Bed ore as part of a larger ore body that "pinches and swells" and is thickest in the hinge of an overturned antiform that is dissected by faulting (Kemp, 1908; Gallagher, 1937). The ore is up to 15m thick. This series of orebodies is greater than 800 meters long and in some regions of the fold hinge is 60 meters thick. Perthitic granite is common in the hanging wall of the Old Bed ore.

2-8 DATA REPOSITORY 2

ANALYTICAL TECHNIQUES

Zircon separation was done using standard crushing, heavy liquids, and magnetic methods, following removal of magnetite using a hand magnet on the crushed ore. Zircon crystals were hand picked from the non-magnetic fraction (the remaining magnetite, hematite, and martite, were removed during this stage) and mounted in epoxy resin and polished to reveal the crystal interiors. The mounts were gold coated and imaged with a Hitachi S-4300 scanning electron microscope (SEM) using cathodoluminescence (CL) to identify internal structures and zoning. Back-scattered electron (BSE) imaging was used to identify fractures and inclusions within the grains and to identify analytical spot locations precisely after the analyses were done.

Uranium-Th-Pb and Pb-Pb zircon analyses for the 4 samples in this study were done using the Cameca IMS 1270 ion-microprobe at the Swedish Museum of Natural History following the methods first described by Whitehouse et al. (1999) and later modified in Whitehouse and Kamber (2005). The calibration of U/Pb ratios is based on the 1065 Ma zircon standard 91500 with U and Pb concentrations of 80 and 15 ppm, respectively (Weiedenbeck et al., 1995). For our sample in which high U concentrations precluded accurate U/Pb calculations only $^{207}Pb/^{206}Pb$ ages were calculated. Data reduction is done using Excel macros developed at the Swedish Museum of Natural History in Stockholm. Applicable to all material, age determinations and errors were calculated using Isoplot version 3.34 (Ludwig, 2003). U-Pb data are plotted as 2σ error ellipses. All age errors quoted in the text are 2σ unless specifically stated otherwise.

Common Pb corrections were applied to all ion probe data. An average composition for modern day terrestrial common Pb is assumed (Stacey and Kramers, 1975).

REFERENCES CITED

Gallagher, D., 1937, Origin of the magnetite deposits at Lyon Mountain, N. Y: New York State Museum Bulletin, p. 85.

Hagner, A.F., and Collins, L.G., 1967, Magnetite ore formed during regional metamorphism, Ausable magnetite district, New York: Economic Geology, v. 62, p. 1034-1071.

Kemp, J. F., 1908 - The Mineville-Port Henry mine group: in Newland, David H., Geology of the Adirondack magnetite iron ores, New York State Museum Bulletin 119, p. 57-123.

Ludwig, K.R., 2003, User's Manual for Isoplot 3.00, A geochronological toolkit for Microsoft Excel: Berkley Geochronology Center Special Publication No. 4

Stacey, J.S., and Kramers, J.D., 1975, Approximation of terrestrial lead isotope evolution by a two-stage model: Earth and Planetary Science Letters, v. 26, p. 207.

McLelland, J., Morrison, J., Selleck, B., Cunningham, B., Olson, C., and Schmidt, K., 2002, Hydrothermal alteration of late- to post-tectonic Lyon Mountain granitic gneiss, Adirondack Mountains, New York; origin of quartz-sillimanite segregations, quartz-albite lithologies, and associated Kiruna-type low-Ti Fe-oxide deposits: Journal of Metamorphic Geology, v. 20, p. 175-190.

Postel, A.W., 1952, Geology of the Clinton County magnetite district: United States Geological Survey Professional Paper, v. 237, p. 88.

Stacey, J.S., and Kramers, J.D., 1975, Approximation of terrestrial lead isotope evolution by a two-stage model: Earth and Planetary Science Letters, v. 26, p. 207.

Whitehouse, M.J., Kamber, B.S., and Moorbath, S., 1999, Age significance of U-Th-Pb zircon data from early Archaean rocks of west Greenland--a reassessment based on combined ion-microprobe and imaging studies: Chemical Geology, v. 160, p. 201.

Whitehouse, M.J., and Kamber, B.S., 2005, Assigning Dates to Thin Gneissic Veins in High-Grade Metamorphic Terranes: A Cautionary Tale from Akilia, Southwest Greenland: J. Petrology, v. 46, p. 291-318.

Wiedenbeck, M., Alle, P., Corfu, F., Griffin, W.L., Meier, M., Oberli, F., Quadt, A.V., Roddick, J.C., and Spiegel, W., 1995, Three natural zircon standards for U-Th-Pb, Lu-Hf, trace element and REE analyses: Geostandards and Geoanalytical Research, v. 19, p. 1-23.

CHAPTER 3

In:

Valley, P.M., Fisher, C.M., Hanchar, J.M., Lam, R. and Tubrett, M. (2010) Hafnium isotopes in zircon: A tracer of crust-fluid interactions during iron oxide-apatite (IOA) mineralization. Chemical Geology. doi: 10.1016/j.chemgeo.2010.05.011.

HAFNIUM ISOTOPES IN ZIRCON: A TRACER OF FLUID-ROCK INTERACTION DURING MAGNETITE-APATITE ("KIRUNA-TYPE") MINERALIZATION

Peter M. Valley[a]*, Christopher M. Fisher[a], John M. Hanchar[a],

Rebecca Lam[b], Michael Tubrett[b]

[a]*Department of Earth Sciences, Memorial University of Newfoundland, St. John's, NL A1B 3X5 Canada*

[b]*INCO Innovation Centre, MicroAnalysis Facility, Memorial University of Newfoundland, St. John's, NL A1C 5S7 Canada*

ABSTRACT

In situ analyses of hafnium isotopes in zircon combined with existing U-Pb zircon ages and trace element data provide new information on the characterization and evolution of magnetite-apatite ("Kiruna-type") deposits and the tectonic environments in which they occur. The Lyon Mountain granite in the Adirondack Mountains of New York, USA, is the host to numerous zircon-bearing magnetite-apatite deposits. Hafnium isotopic compositions and rare earth element contents in individual zircon crystals were measured in situ in both the host granites and the ore bodies by laser ablation inductively coupled plasma-mass spectrometry. Hafnium isotopic compositions in the ore zircon can

be divided into two groups: those that have initial εHf (t) values that are indistinguishable from those of the host granites (e.g., εHf (t) less than +7) and are typical of relatively juvenile Proterozoic crust, and those that have extremely radiogenic εHf (t) values (as high + 40). Two models are proposed to explain the observed εHf (t) values in the zircon crystals: 1) early-formed ore bodies containing magnetite, apatite, and clinopyroxene were remobilized by secondary fluid alteration, releasing Zr and Hf for the crystallization of new zircon; or alternatively, 2) fluids responsible for ore formation have interacted with garnet-bearing rocks during retrograde metamorphism, scavenging rare earth elements and radiogenic Hf.

Previous work done to determine the U-Pb ages from the same zircon crystals, which were analyzed for the Hf isotopic composition in this study, revealed that ore bodies record a mineralizing event that is 20 to 60 m.y. younger than the age of granite emplacement (Valley et al., 2009). This age discrepancy, plus the highly radiogenic εHf (t) values in the ore zircon crystals, suggests that the fluids responsible for this younger event could not have been derived from the granite hosts. These data argue that magnetite-apatite deposits in the LMG have multiple mineralizing events superimposed upon one another and that early-formed deposits may be reworked, modified and redeposited by fluids subsequent to magma crystallization

Keywords: magnetite-apatite ("Kiruna-type") deposits, IOCG deposits, Kiruna, Hf isotopes, zircon, REE, trace elements, garnet, fluid alteration, fluorine, Adirondack

Mountains, Lyon Mountain granite, accessory minerals, LA-MC-ICPMS, LA-ICPMS, apatite, magnetite.

*Corresponding author: pvalley@mun.ca

3-1 INTRODUCTION

The Hf isotopic composition of zircon combined with U-Pb age data and trace element data from the same region in the crystal provides an unparalleled way to infer the Hf isotopic composition of the fluid or melt from which the zircon crystallized, in a temporal context (Kemp et al., 2005; Hawkesworth and Kemp, 2006). The ability of zircon to record the Hf isotopic composition of the fluid or melt in which it crystallized is due to the refractory nature of zircon, as well as low Lu/Hf (e.g., Lu is a trace element whereas Hf is a minor element and $^{176}Lu/^{177}Hf$ are typically less than 0.002; Kinny and Maas, 2003) intrinsic to zircon, resulting in minimal growth of ^{176}Hf (from the decay of ^{176}Lu) through time.

Additionally, the Lu/Hf offers a proxy for the heavy rare earth element (HREE) to high field strength element (HFSE) ratio in source materials, which varies significantly between minerals and rock types. This means that Lu-Hf isotopic systematics in zircon can potentially be a more sensitive indicator of the source region of melts and fluids than isotopic systems such as Sm/Nd that not only combine two geochemically similar elements (Patchett et al., 1981) but also occur in much lower abundances than Lu or Hf. Typical crustal rocks have $^{176}Lu/^{177}Hf$ of ~0.01 (granite) to ~0.03 (basalt); however, these

averages represent a composite Lu/Hf of their constituent minerals, many of which strongly fractionate Lu from Hf. For example, garnet has high Lu/Hf (0.1 to 8.0, e.g. Scherer et al., 1997, Duchéne et al.; 1997) resulting in very radiogenic $^{176}Hf/^{177}Hf$ over geologically short periods of time, but relatively low total Hf concentration (< 0.01 wt%, e.g., Hickmott et al., 1987; Sisson and Bacon, 1992). Conversely, zircon has extremely low Lu/Hf with high Hf contents (typically between 1-4 wt. % HfO_2; e.g., Hoskin and Schaltegger, 2003). This range of Lu/Hf offers the possibility of extreme Hf isotopic composition (relative to the chrondritic uniform reservoir [CHUR]) to develop in some minerals and rock types. Such Hf isotopic compositions are also transferred to the new materials derived from these protoliths, providing a powerful tool to identify the composition of the fluid or melt and important mineral reactions occurring in the source region.

We have applied this method for the first time to zircon associated with the development of magnetite-apatite ("Kiruna-type") deposits. We have determined in situ the trace element and Hf isotopic composition of previously dated hydrothermal and igneous zircon grains associated with magnetite-apatite deposits and their respective host granites in the Adirondack Highlands to better characterize the processes and origins of these ore deposits and their associated fluids (Valley et al., 2009).

Low-Ti magnetite-apatite ("Kiruna-type") deposits are considered an end-member of the Fe-oxide-Cu-Au (IOCG) group of deposits, whose characteristics are widely variable (e.g., Hitzman et al., 1992; Barton and Johnson, 1996). Some IOCG deposits contain economic abundances of Cu, Au, and U such as those at Olympic Dam,

Australia, whereas the deposits in the Norrbotten region of northern Sweden (e.g., Kiruna), contain primarily iron oxide and apatite (e.g., Reynolds, 2000; Harlov et al., 2002). Additionally, many of these IOCG deposits concentrate rare earth elements (REE) in minerals such as apatite (Hitzman et al., 2000). Genetic models for the origin of IOCG deposits include two main groups: those that are directly related to magmatism and those related to coeval or older brines (Barton and Johnson, 2004). The deposits that are clearly magmatic are characterized by a direct relation to a particular intrusion (intermediate to felsic calc-alkaline or alkaline), occur in an arc setting (extensional or compressional), have widespread K-alteration, and are enriched in Au and Cu with moderate amounts of magnetite and minor REE. Brine-related deposits are characterized by Na, K or acid alteration, abundant magnetite, REE and apatite, and are correlated with the presence of evaporites. Additionally, brine-related deposits lack a direct connection to any particular intrusive event but are commonly associated with an extensional tectonic setting (Barton and Johnson, 2004). The unifying characteristics of all these deposits are low-Ti Fe-oxides (magnetite and hematite), extensive replacement by Na-, K-, Ca-, Si-, or Al-bearing fluids, and their association with an extensional tectonic setting (Hitzman et al., 1992). Deposits within the Lyon Mountain Granite (LMG) in the Adirondack Highlands of New York belong to the magnetite-apatite (Kiruna-type") group of deposits and lack Cu and Au in economic concentrations.

3.2 GEOLOGICAL SETTING

The Adirondack Mountains are a 27,000 km^2 area of exposed Proterozoic rocks in northern New York State, USA and represents the southern extension of the Grenville Province of Ontario and Quebec. The region is divided into the Adirondack Lowlands in the northwest and the Adirondack Highlands to the east and south (Fig. 3-1). The Adirondack Lowlands comprise amphibolite grade metasedimentary or metavolcanic rocks and granitoid intrusive bodies that range in age from ~1300-1150 Ma (Wasteneys et al., 1999; Rivers, 1997). A large suite of anorthosite-mangerite-charnockite-granite (AMCG) rocks dominate the Adirondack Highlands with minor metasedimentary rocks separating the various domical intrusive bodies. Rocks in the Adirondack Highlands contain mineral assemblages that are the result of granulite-facies metamorphism. The Adirondack Highlands are separated from the Adirondack Lowlands by the Carthage-Colton shear zone (CCSZ), which is defined by highly ductile fabrics and small granitic intrusions which yield U-Pb zircon ages between 1045 and 1037 Ma (Selleck et al., 2005). Tonalite and granodiorite magmas were emplaced into the southern and eastern Adirondacks in the interval between 1350 to 1250 Ma (McLelland and Chiarenzelli, 1988). These rocks are interpreted to be juvenile, arc-related magmas emplaced along an Andean-style margin prior to the onset of the Shawinigan orogeny (McLelland and Chiarenzelli, 1990, Rivers, 1997). Widespread metamorphism and deformation affected the whole of the Adirondacks during the 1210 and 1170 Ma Shawinigan orogeny. Immediately following cessation of the Shawinigan orogeny extensive AMCG suite magmas were emplaced into the Adirondack Highlands from 1170 to 1120 Ma

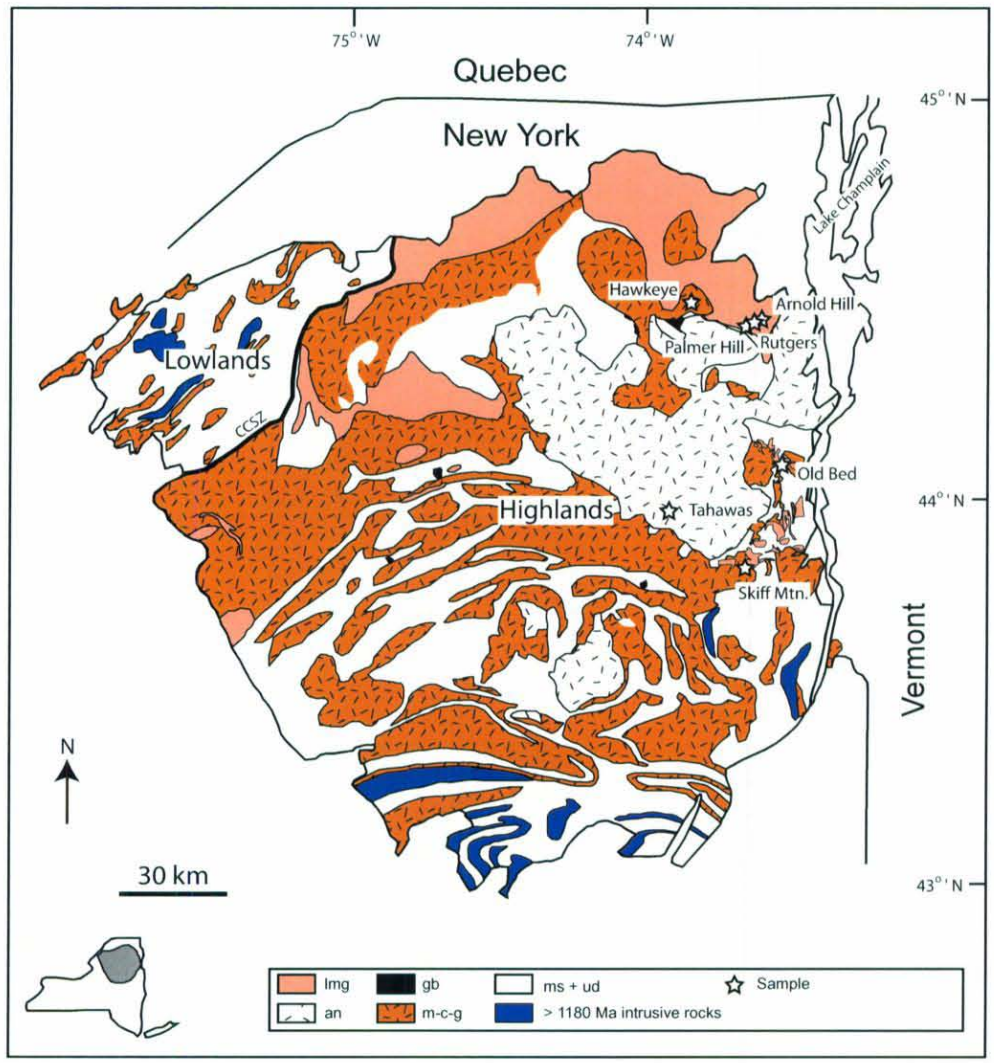

Figure 3-1. Simplified geology of the Adirondack Mountains with sample locations for this study. The Adirondack Highlands are dominated by the ~1150-1120 Ma, anorthosite-mangerite-charnockite granite suite. The Adirondack Lowlands comprise ~1300-1150 Ma metasedimentary and metaigneous rocks separated from the Adirondack Highlands by the Carthage-Colton shear zone (CCSZ). Abbreviations: lmg = Lyon Mountain granite; an = anorthosite; gb = gabbro; m-c-g = mangerite-charnockite-granite; ms + ud = metasediments and undivided, (modified after Isachsen and Fisher, 1970; McLelland and Isachsen, 1985; and Davidson, 1998).

(McLelland et al., 2001; Hamilton et al., 2004; McLelland et al. 2004) and are coincident with amphibolite grade metamorphism in the Adirondack Lowlands. The main period of deformation and metamorphism in the Adirondack Highlands was during the Ottawan phase of the Grenville Orogeny. The Ottawan metamorphism is thought to occur between 1100 and 1040 Ma based on the ages of the penetratively deformed Hawkeye granite (1100 Ma) and emplacement of the less deformed LMG (1060-1040 Ma) (McLelland et al. 2001, Selleck et al., 2005).

The LMG crops out extensively in the northeastern Adirondack Highlands (Fig.3-1) and is the host to numerous economic grade magnetite-apatite ("Kiruna-type") deposits (e.g., Whitney and Olmsted, 1988). The LMG experienced multiple periods of alteration by potassium- and sodium-rich fluids which are superimposed on one another. One or more of these fluid events are accompanied by Fe mineralization or reworking of older ore deposits and the addition of F, Cl and P, and mobilization of HFSE including Zr Y, U, and REE (Lindberg and Ingram, 1964; Roeder et al., 1987; Foose and McLelland, 1995).

3-3 MAGNETITE-APATITE DEPOSITS

The locations of the samples investigated in this study are shown in Figure 3-1. The ores comprise magnetite, or rarely martite (hematite replacing preexisting magnetite), and typically include one or more of the following: apatite, quartz, alkali feldspar, clinopyroxene or amphibole, and minor zircon. The earliest Fe mineralization is associated with "skarn-like", clinopyroxene-magnetite ± apatite deposits. Clinopyroxene

crystals contain small inclusions of magnetite and are commonly altered to amphibole and coarse magnetite. Clinopyroxene-magnetite mineralization may be associated with migmatization and mylonitization and occasionally potassic alteration. A second period of Fe mineralization is associated with Na alteration (specifically albitization) (e.g., Postel, 1952; McLelland et al., 2002). These secondary ore deposits were formed in part from the dissolution and re-precipitation of magnetite from the "skarn-like" deposits and leaching of disseminated magnetite from the granite immediately adjacent to the ores (Hagner and Collins, 1967). Magnetite-apatite deposits associated with Na alteration commonly occur without the obvious presence of the "skarn-like" deposits but, most "skarn-like" deposits contain evidence of replacement and reworking by sodic fluids.

Fluid temperatures between 675 and 565 °C were estimated from quartz-magnetite $\delta^{18}O$ fractionation in LMG ore bodies (McLelland et al., 2002). The location of mineralization and alteration is associated with shear zones, the hinge regions of folds, and near the contact of the LMG with other units (Postel 1952; Whitney and Olmsted, 1993). The ore deposits often occur as "tubes" or "cigar -shaped" bodies that plunge to the NE in the direction of the main regional lineation (Postel, 1952). Ore bodies are generally parallel to the foliation in the host granite, but locally crosscut the fabric at a high angle.

The primary Fe mineralization ("skarn-like" deposits) appears to be related to emplacement of the LMG at the onset of regional extension. Secondary Fe mineralization, associated with zircon growth, may be the result of continued and

prolonged fluid penetration along extensional shear zones during orogenic collapse. (Valley et al., 2009).

3-4 ANALYTICAL TECHNIQUES

3-4-1 TRACE ELEMENTS

Zircon crystals were separated from the ore and host rock using conventional heavy liquids, magnetic, and hand-picking techniques. The crystals were then mounted in epoxy and polished to reveal the crystal centers and then characterized using back-scattered electron (BSE) and cathodoluminescence (CL) imaging. Selected zircon crystals were analyzed using an electron probe microanalyzer (EPMA) to determine their Zr, Si, and Hf compositions for normalization of laser ablation-inductively coupled plasma mass spectrometry (LA-ICPMS) trace element results. The EPMA analyses were done using a JEOL 8900 at the University of Maryland. Operating conditions used were an accelerating voltage of 15 kV and a beam current of 100 nA with 30 second count times on peak and each background using a focused beam. Synthetic zircon (for Zr and Si) and synthetic hafnon (for Hf) were used as standards. The data were reduced using standard ZAF procedures in the JEOL software. The zircon grains were then analyzed for their trace element compositions using a Finnigan ELEMENT XR double focusing magnetic sector field LA-ICPMS coupled to a Geolas 193 nm ArF excimer laser at the Inco Innovation Centre, Memorial University of Newfoundland (MUN), Canada. The LA-ICPMS analysis locations were placed as close as possible to the EPMA analysis spots. The crystals were ablated using a 40 μm laser beam with a laser energy of 3 J/cm^2,

and a repetition rate of 10 Hz. Helium was used as a carrier gas to transport the ablated material from the laser-ablation cell to the LA-ICPMS torch.

Concentrations were calibrated using NIST 612 glass. Hf was used as an internal standard (obtained from the EPMA analyses) to correct for differences in ablation yields and matrix effects between the zircon and the calibration material (NIST glass). Approximately 30 seconds of gas background data were collected prior to each 60-second ablation of both standards and unknowns.

The data acquisition methodology used an analytical sequence of two analyses of the NIST 612 standard, one analysis of zircon 91500 (Wiedenbeck et al., 2004), followed by analyses of 14 unknowns, closing the sequence with a repetition of the same standards in reverse order. The zircon 91500 was treated as an unknown and data were acquired to monitor the accuracy and precision of the dataset. The uncertainty for this method when measuring homogeneous materials is estimated to be between 4 to 7 % relative error based on the reproducibility of results for various reference materials measured from day to day over several years of analyses in the MUN LA-ICPMS laboratory. Elements showing high relative standard deviation (RSD) values can be directly attributed to heterogeneities in 91500 for particular elements, especially at low concentrations, and for elements prone to being affected by elemental fractionation.

Data were reduced using MUN's in-house CONVERT and LAMTRACE spreadsheet programs, which use procedures described in Longerich et al. (1996). LAMTRACE allows for the selection of representative signal intervals, background subtraction and internal standard correction for ablation yield differences, instrument

sensitivity drift during the analytical session, and perform calculations converting count rates into concentrations by reference to the standards.

3-4-2 Lu-Hf:

The Lu-Hf isotopic analyses of the zircon crystals used in this study were done on the same grains used in the U/Pb and trace element studies, either directly on top of, or as close as possible to the SIMS U/Pb and LA-ICPMS trace element analysis pits. Lu-Hf analyses consume the greatest amount of zircon material during an analysis, and as such, those data were acquired as the last step of this three-step process. The Lu-Hf analyses were acquired using a Finnigan NEPTUNE double focusing, high-resolution multi-collector inductively coupled mass spectrometer (MC-ICPMS) operated in static mode at Memorial University of Newfoundland.

Due to the relatively high concentration of Yb found in typical natural zircon crystals (up to a few hundred ppm) (Hoskin & Schaltegger, 2003), the interference correction of ^{176}Yb on ^{176}Hf must be able to accommodate a wide range of Yb/Hf ratios. The accuracy of this correction is monitored by repeated (e.g., every 4-6 analyses) measurements of reference zircons (Fig. 3-2a). Reference zircons 91500 (^{176}Yb/^{177}Hf = 0.005 to 0.012), Plešovice (^{176}Yb/^{177}Hf = 0.003 to 0.008), and FC-1 (^{176}Yb/^{177}Hf = 0.02 to 0.07), were ablated under identical analytical conditions as the unknowns. The average value of ^{176}Hf/^{177}Hf obtained for the 91500 zircon during the time frame of this study using the MUN Neptune LA-MC-ICPMS facility was 0.282302 ± 52 2 SD (n=229) compared to a literature value of (0.282308 ± 6, 2SD, Blichert-Toft, 2008) . Analysis of Plešovice zircon yielded 0.282482 ± 34, 2SD, (n=114), compared with a literature value

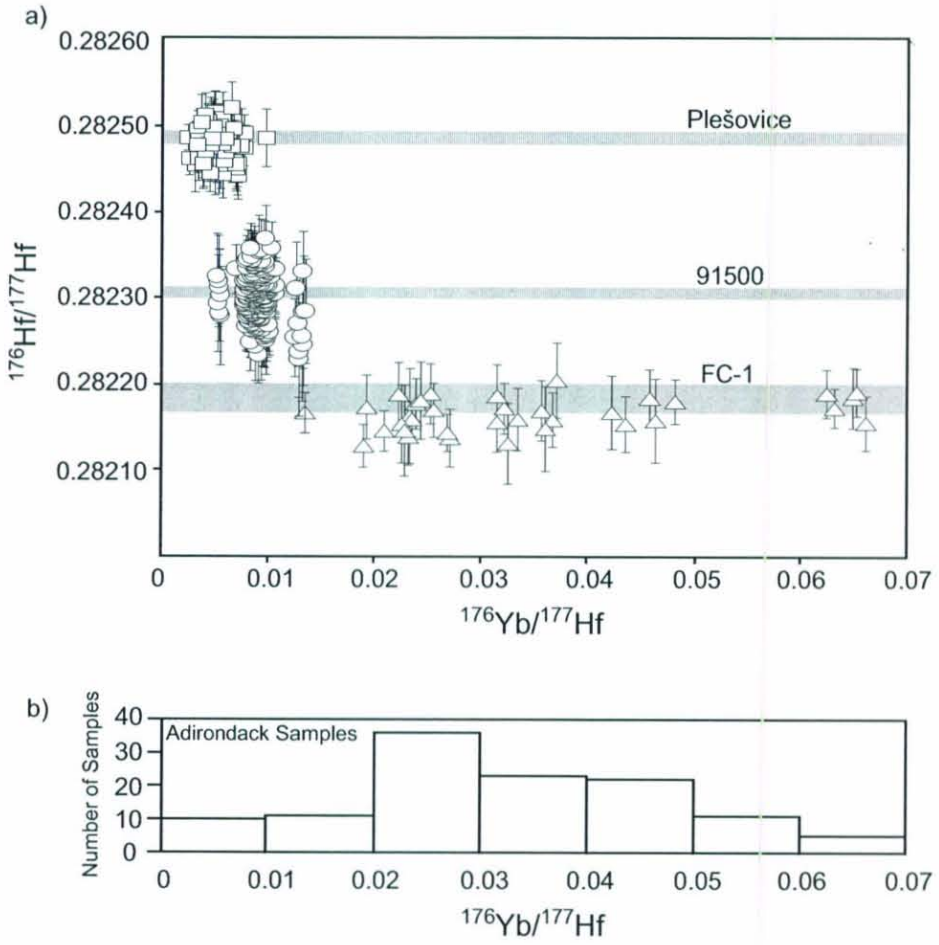

Figure 3-2. (a) Laser ablation Hf and Yb isotope data from three zircon standards with different Yb/Hf ratios as measured at Memorial University over a one-year period. Error bars are shown at 2σ standard error. Accepted values are shown as gray bars representing the mean ± 2σ standard deviation from Blichert-Toft, 2008 (91500), Sláma et al., 2008 (Plešovice) and Woodhead and Hergt, 2005 (FC-1). (b) Histogram of $^{176}Yb/^{177}Hf$ of unknowns analyzed in this study. 118 out 122 (97%) of the analyses are represented at this $^{176}Yb/^{177}Hf$ scale.

of (0.282482 ± 13, Sláma et al., 2008). Analysis of zircon FC-1 gave a value of 0.282168 ± 37 (2SD; n=35) compared to (0.282184 ± 16, Woodhead and Hergt, 2005). Ninety-seven percent of the zircon analyzed in this study have $^{176}Yb/^{177}Hf$ less than our standards, confirming the accuracy our interference correction on these samples (Fig. 3-2b). A detailed method and data reduction description, as well as further verification of our Yb interference correction is given in 3-8 Data Repository 1. Validity of the mass bias correction can be assessed by comparison of the calculated invariant $^{178}Hf/^{177}Hf$ to accepted values (1.46734 ± 17; Thirlwall and Anczkiewicz, 2004). The results of these measurements are given in Table 3-1.

Epsilon Hf (t) values were calculated using the present day CHUR $^{176}Hf/^{177}Hf$ value of 0.282802 and $^{176}Lu/^{177}Hf$ 0.0337 (Bouvier et al., 2007). The ^{176}Lu decay constant of 1.93×10^{-11} yr^{-1} was used in the data calculations (Blichert-Toft and Albarede, 1997). The linear depleted mantle model of Nowell et al. (1998) is used as reference in Figure 3-4 and 3-6.

3-5 RESULTS

Lutetium-Hf isotopic and trace element analyses were done on granite host and hydrothermal ore zircon (Fig. 3-3) and are presented in Figure 3-4 and 3-5. Individual Lu-Hf analyses are presented in Table 3-1. Uranium-Th-Pb age data for these LMG zircon samples were previously reported in Valley et al.; (2009) and are presented again for reference in Figures 3-4 and 3-6. Non-LMG Hf zircon data from the Hawkeye granite and Tahawas magnetite-ilmenite mine are presented for comparison (Figs. 3-4 and 3-6b).

The U-Pb age data from McLelland et al., (2001) were used for plotting the Hawkeye and Tahawas samples in Figures 3-4 and 3-6.

3-5-1 ZIRCON MORPHOLOGY

Magmatic zircon crystals from the LMG typically are brown to pink, elongate, well faceted, and highly fractured and may contain inclusions of apatite or quartz and commonly contain inherited cores (Fig. 3-3a). Inherited cores are typically lower in U and Hf concentration than primary rims and single age zircon grains. The zircon grains occur along grain boundaries or as inclusions in feldspar and quartz.

Ore samples collected for zircon separation are hosted by rocks that have experienced extensive sodium alteration or sodium alteration overprinting potassium alteration in the case of Palmer Hill. The Skiff Mountain ore sample comprises quartz-magnetite-apatite and minor zircon and biotite whereas the Arnold Hill ore contains martite as the main oxide mineral, apatite, quartz, chlorite, calcite and minor clinopyroxene, amphibole and zircon. The Palmer Hill ore consists of remnant microcline replaced by albite, magnetite, apatite, quartz, fluorite and minor zircon and biotite. The Old Bed ore is a quartz-magnetite pegmatite with apatite and zircon grains up to 2cm in length and minor clinopyroxene.

Hydrothermal zircon grains from the magnetite ore are commonly clear and featureless in transmitted light and frequently are larger than the granite host zircon crystals. Irregular, patchy, zoning in BSE or CL imaging is common (Figs. 3-3b and 3-3c). Some of the ore zircon crystals that were analyzed contain interior regions with different U and Hf contents that produce variations in the BSE signal and appear to be

"cores" (Figs. 3-3b and 3c); however, as reported in Valley et al. (2009) the majority of those ages are within error of the "rim" ages. Rare inherited, AMCG age zircon cores do occur in Arnold Hill ore zircon grains. The hydrothermal zircon grains are generally free of melt or fluid inclusions, but may contain small apatite, Fe-oxide, or quartz inclusions. Zircon grains from the ore are rarely observed in thin sections, but when identified, occur as inclusions in magnetite, along grain boundaries, or in the case of the Old Bed ore as large, mm-scale crystals surrounded by coarse grains of magnetite. There is no clear association between zircon growth and any one particular mineral in the ore bodies

Zircon crystals from the nearby 1100 Ma Hawkeye granite (Fig. 3-1) which has not undergone magnetite-apatite mineralization or K and Na metasomatic alteration have been used as a comparison to zircon crystals in the LMG (McLelland, 2001). These zircon grains are dark brown, fractured, and may contain inclusions of apatite and quartz and in some samples have older inherited cores (Fig. 3-3d). Zircon from the Tahawas magnetite-ilmenite mine (Fig. 3-1) has also been used as an additional comparison to those of the LMG and associated magnetite-apatite ores. The Tahawas mine samples are thought to be contemporaneous with emplacement of the AMCG-related Marcy anorthosite at 1165 Ma (McLelland et al., 1988; McLelland et al., 2004) but unrelated to the metasomatic alteration and magnetite-apatite mineralization discussed in this study. Numerous sensitive, high-resolution ion microprobe (SHRIMP) data points from McLelland et al. (2004) show that there is a significant population of younger ages in zircon from Tahawas between 1060 and 1000 Ma. Zircon crystals from Tahawas are

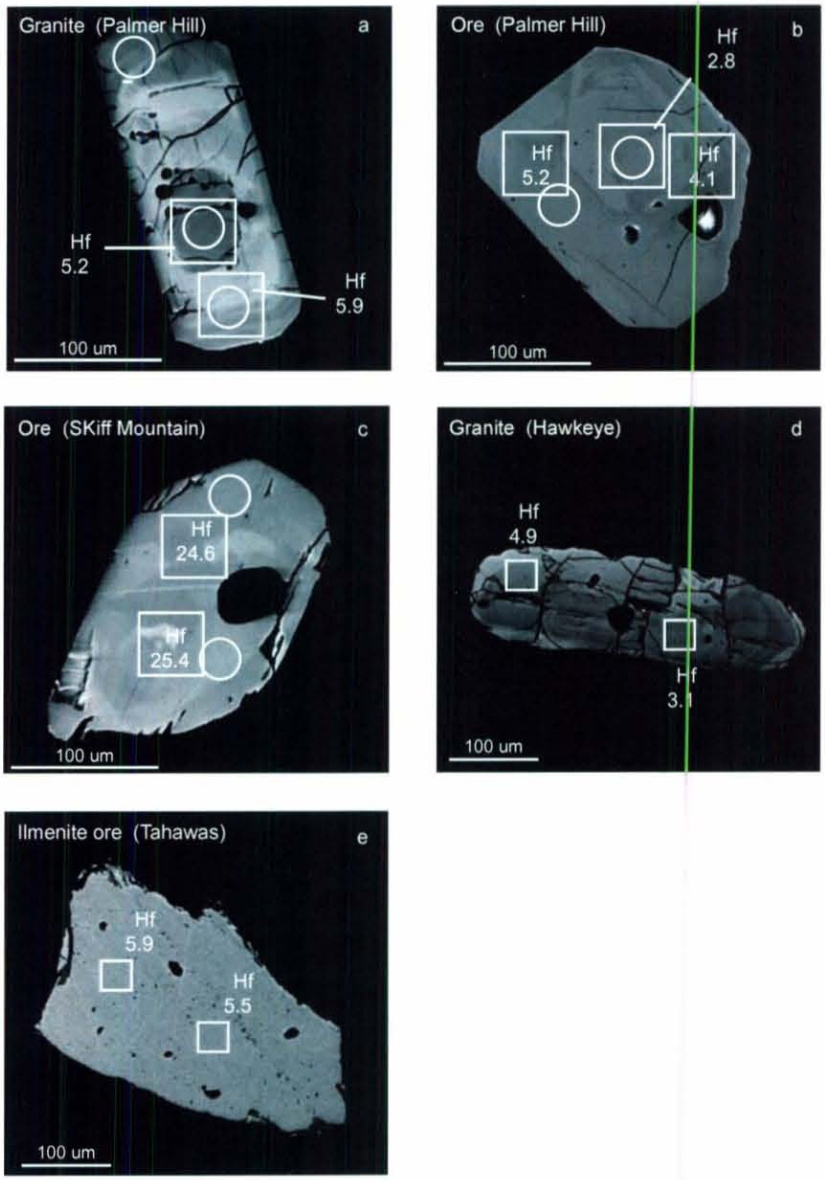

Figure 3-3. Representative BSE images of zircon grains from (a) host granite zircon grain from Palmer Hill, (b) low εHf (t) zircon grain from the Palmer Hill ore body, (c) high εHf zircon grain from the Skiff Mountain ore body, (d) Hawkeye granite zircon grain and (e) zircon grain from the Tahawas ilmenite ore. Circles indicate trace element analyzes and squares indicate Hf isotope analyzes.

typically pink, clear, fragments of broken larger grains with patchy irregular zoning in CL or BSE (see McLelland et al., 2004; Fig. 3-3f)

3-5-2 HAFNIUM ISOTOPES

Hafnium data are presented in Table 3-1 and Figure 3-4. Zircon grains from the Palmer Hill granite have εHf (t) values ranging from +4.3 to +7.1 and a U-Pb age of ~1062 Ma (Valley et al., 2009). Samples from the Palmer Hill ore have εHf (t) values that are indistinguishable from the granite host, but its U-Pb age is ~20 m.y. younger (~1039 Ma). At Arnold Hill, zircon from the granite host have εHf(t) values that range from +4.5 to +7.6, whereas zircon grains from the ore have highly radiogenic εHf(t) values ranging from +13.6 to +40.1. The age of the Arnold Hill granite is ~1061 Ma, whereas the ore is ~1016 Ma (Valley et al., 2009). Epsilon Hf (t) values in the Skiff Mountain ore zircon range from +19.8 to +34, this sample has been dated at ~1001 (Valley et al., 2009). The Old Bed ore sample contains zircon crystals that are very large (up to 2cm). These zircon grains are dark brown to opaque and highly metamict. The εHf (t) values are consistent, (+19.2 to +20.3) and are dated between 1030 and 1000 Ma (Valley et al., 2009).

Zircon from the Hawkeye granite have εHf (t) values ranging from + 3.7 to +6.1 similar to zircon from all of the LMG. The Hawkeye granite is dated at 1103 ± 15 Ma (McLelland et al., 2001). At Tahawas, the zircon crystals separated from the magnetite-ilmenite ore have εHf (t) values that vary little from +5.1 to +7.6.

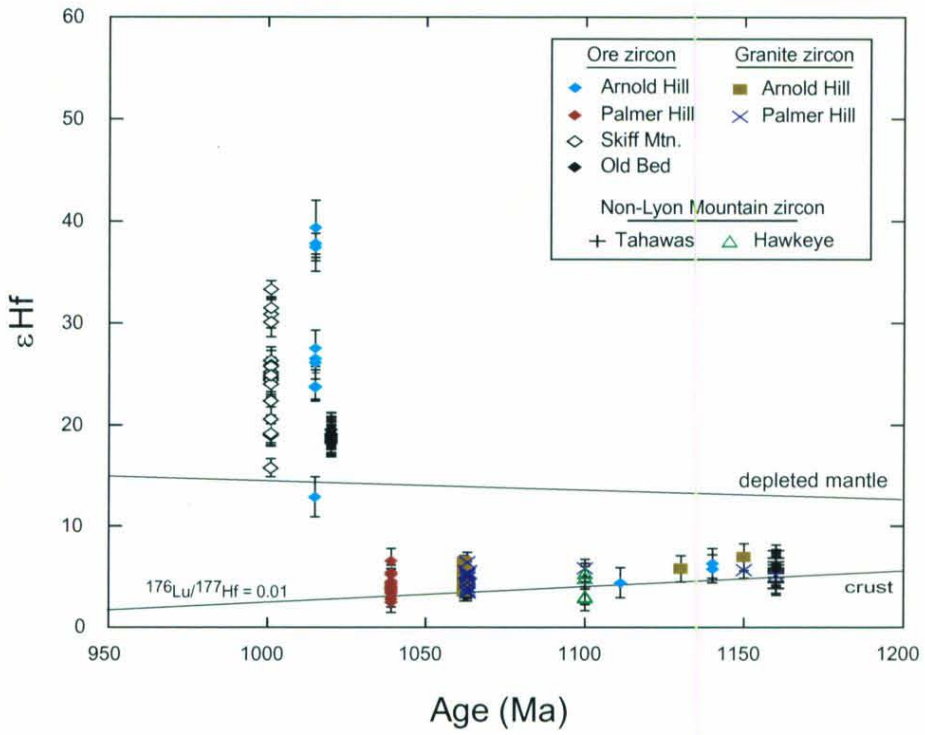

Figure 3-4. Hafnium isotope composition of zircon verses crystallization age from the Lyon Mountain granite (LMG), associated ore, Hawkeye granite, and anorthosite related Tahawas ilmenite ore compared with their crystallization age. Linear depleted mantle model from Nowell et al. (1998). Present day $^{176}Hf/^{177}Hf$ and $^{176}Lu/^{177}Hf$ of CHUR from Bouvier et al., (2007). The ^{176}Lu decay constant is from Blichert-Toft and Albarede (1997).

Table 3-1 Hafnium isotopic analyses of magnetite-apatite ore and host rock zircon*

Sample	Analysis	176Hf/177Hf**	2SE	176Lu/177Hf	2SE	176Yb/177Hf	2SE	corr 178Hf/177Hf	2SE	ε Hf (t)***	2SE
OBO grn 1	no13a4	0.282695	0.000054	0.001417	0.000002	0.046246	0.000264	1.467212	0.000052	18.95	1.91
OBO grn 1	no13a5	0.282676	0.000033	0.001447	0.000005	0.047724	0.000304	1.467225	0.000048	18.26	1.17
OBO grn 1	no13a6	0.282681	0.000061	0.000511	0.000015	0.016565	0.000624	1.467231	0.000046	19.10	2.17
OBO grn 1	no13a7	0.282682	0.000060	0.000530	0.000014	0.017405	0.000594	1.467206	0.000056	19.11	2.11
OBO grn 1	no13a8	0.282696	0.000048	0.001348	0.000006	0.043931	0.000227	1.467210	0.000043	19.03	1.69
OBO grn 1	no13a9	0.282679	0.000041	0.000438	0.000002	0.013925	0.000073	1.467211	0.000034	19.07	1.44
OBO grn 1	no13a10	0.282687	0.000042	0.001661	0.000005	0.053814	0.000296	1.467188	0.000046	18.48	1.48
OBO grn 1	no13a12	0.282686	0.000040	0.001407	0.000158	0.044397	0.004910	1.467205	0.000039	18.64	1.41
OBO grn 1	no13a13	0.282691	0.000031	0.001530	0.000122	0.048309	0.003784	1.467226	0.000042	18.72	1.09
OBO grn 1	no13a14	0.282714	0.000037	0.001553	0.000127	0.049275	0.003942	1.467217	0.000044	19.55	1.30
OBO grn 1	no13a15	0.282705	0.000033	0.001618	0.000108	0.051356	0.003336	1.467231	0.000044	19.16	1.18
OBO grn 1	no13a16	0.282701	0.000038	0.001501	0.000179	0.047243	0.005514	1.467241	0.000041	19.11	1.33
OBO grn 1	no13a17	0.282678	0.000044	0.001270	0.000198	0.039618	0.006164	1.467218	0.000043	18.47	1.55
OBO grn 1	no13a18	0.282695	0.000031	0.001372	0.000168	0.042671	0.005207	1.467201	0.000035	18.97	1.11
AHG grn 1	no13a38	0.282256	0.000019	0.001243	0.000075	0.035256	0.002271	1.467209	0.000041	4.47	0.67
AHG grn 1	no13a39	0.282269	0.000023	0.001483	0.000081	0.039034	0.002061	1.467222	0.000033	4.77	0.81
AHG grn 2	no13a40	0.282253	0.000019	0.001361	0.000006	0.035803	0.000311	1.467195	0.000034	4.29	0.67
AHG grn 2	no13a41	0.282261	0.000021	0.001305	0.000042	0.037556	0.001796	1.467201	0.000040	4.61	0.73
AHG grn 5 core	no13a42	0.282234	0.000033	0.001122	0.000059	0.038277	0.002216	1.467190	0.000040	3.78	1.15
AHG grn 5 inner rim	no13a43	0.282261	0.000021	0.001244	0.000016	0.032189	0.000409	1.467195	0.000040	4.64	0.73
AHG grn 5 outer rim	no13a44	0.282245	0.000020	0.001200	0.000014	0.033744	0.000428	1.467221	0.000034	4.12	0.69
AHG grn 9 rim	no13a45	0.282259	0.000025	0.001498	0.000052	0.043960	0.001812	1.467191	0.000034	4.40	0.90
AHG grn 9 core	no13a46	0.282280	0.000024	0.001413	0.000068	0.040612	0.002522	1.467200	0.000033	5.18	0.86
AHG grn 10 core	no13a48	0.282304	0.000023	0.001356	0.000012	0.037139	0.000550	1.467159	0.000041	6.09	0.80
AHG grn 10 rim	no13a49	0.282301	0.000025	0.001041	0.000009	0.027617	0.000236	1.467260	0.000039	6.23	0.88
AHG grn 12 core	no13a50	0.282277	0.000037	0.001597	0.000065	0.050647	0.002611	1.467186	0.000044	6.94	1.32
AHG grn 12 rim	no13a51	0.282249	0.000029	0.000994	0.000069	0.028204	0.002510	1.467162	0.000048	4.39	1.04
AHG grn 13 center	no13a52	0.282304	0.000028	0.001413	0.000062	0.040921	0.002131	1.467159	0.000033	6.06	1.00
AHG grn 13 rim	no13a53	0.282253	0.000016	0.000876	0.000012	0.023973	0.000507	1.467238	0.000031	4.05	0.56
AHG grn 14 core	no13a54	0.282249	0.000037	0.001233	0.000060	0.040178	0.002199	1.467175	0.000043	5.77	1.30
AHG grn 14 rim	no13a55	0.282246	0.000027	0.000913	0.000010	0.024209	0.000476	1.467221	0.000042	4.37	0.97
PHG grn5 rim	jl10a93	0.282304	0.000028	0.000976	0.000064	0.023532	0.001211	1.467258	0.000044	6.40	0.98
PHG grn 5 core	jl10a94	0.282238	0.000029	0.000964	0.000028	0.027645	0.000420	1.467219	0.000038	4.07	1.01
PHG grn 2	jl10a95	0.282277	0.000023	0.001114	0.000016	0.025189	0.000413	1.467224	0.000038	5.32	0.82
PHG grn 2	jl10a96	0.282224	0.000028	0.000863	0.000025	0.023366	0.000377	1.467224	0.000037	3.62	0.99
PHG grn 3 (dark)	no13a58	0.282262	0.000018	0.000688	0.000005	0.016825	0.000157	1.467221	0.000041	5.10	0.64
PHG grn 3 (bright)	no13a59	0.282259	0.000021	0.000943	0.000033	0.024428	0.001101	1.467171	0.000037	4.82	0.73

Table 3-1 continued

Sample	Analysis	176Hf/177Hf**	2SE	176Lu/177Hf	2SE	176Yb/177Hf	2SE	corr 178Hf/177Hf	2SE	ε Hf (t)***	2SE
PHG grn 7 core	no13a60	0.282215	0.000031	0.001310	0.000138	0.046654	0.005414	1.467190	0.000043	5.17	1.11
PHG grn 7 rim	no13a61	0.282265	0.000024	0.000974	0.000023	0.028409	0.000589	1.467201	0.000041	5.86	0.85
PHG grn 10 core	no13a62	0.282267	0.000025	0.001334	0.000049	0.042477	0.001562	1.467197	0.000041	4.82	0.87
PHG grn 10 rim	no13a63	0.282231	0.000026	0.001006	0.000025	0.032509	0.000581	1.467210	0.000036	3.78	0.91
PHG grn 12 core	no13a65	0.282224	0.000023	0.000819	0.000014	0.024475	0.000780	1.467136	0.000036	5.68	0.81
PHG grn 12 rim	no13a66	0.282246	0.000020	0.000823	0.000016	0.021964	0.000429	1.467205	0.000039	4.45	0.70
PHG grn 14 rim	no13a67	0.282258	0.000022	0.000914	0.000037	0.024154	0.001133	1.467206	0.000037	4.82	0.77
PHG grn 17 rim	no13a68	0.282326	0.000039	0.003782	0.000068	0.140655	0.002719	1.467193	0.000048	5.11	1.37
PHG grn 17 rim	no13a69	0.282254	0.000027	0.001845	0.000013	0.068476	0.000490	1.467197	0.000045	3.99	0.97
PHO grn3 rim	jl10a75	0.282251	0.000017	0.000953	0.000055	0.024188	0.001412	1.467194	0.000033	3.99	0.60
PHO grn3 core	jl10a76	0.282263	0.000024	0.002400	0.000084	0.063432	0.002068	1.467167	0.000037	3.37	0.84
PHO grn4 rim	jl10a77	0.282284	0.000017	0.000898	0.000004	0.022269	0.000173	1.467227	0.000034	5.19	0.62
PHO grn4 core	jl10a78	0.282255	0.000018	0.001143	0.000071	0.029517	0.001835	1.467199	0.000035	3.99	0.65
PHO grn4 core	jl10a79	0.282258	0.000023	0.002933	0.000009	0.078944	0.000520	1.467221	0.000033	2.81	0.81
PHO grn2 rim	jl10a81	0.282248	0.000023	0.000939	0.000033	0.023451	0.000835	1.467195	0.000029	3.89	0.81
PHO grn2 core	jl10a82	0.282248	0.000027	0.001308	0.000066	0.033247	0.001664	1.467201	0.000036	3.63	0.94
PHO grn2 core	jl10a83	0.282270	0.000016	0.001946	0.000022	0.050359	0.000506	1.467212	0.000031	3.95	0.56
PHO grn 1	no13a71	0.282285	0.000031	0.001884	0.000029	0.053982	0.000598	1.467171	0.000032	4.52	1.11
PHO grn 1	no13a72	0.282287	0.000041	0.000963	0.000013	0.030535	0.000591	1.467211	0.000056	5.24	1.44
PHO grn 3	no13a73	0.282309	0.000044	0.000720	0.000005	0.021244	0.000202	1.467199	0.000047	6.22	1.54
PHO grn 3	no13a74	0.282253	0.000051	0.000633	0.000018	0.020184	0.000545	1.467181	0.000047	4.30	1.81
PHO grn 3	no13a75	0.282225	0.000029	0.001725	0.000102	0.050620	0.002711	1.467191	0.000043	2.51	1.04
SMO grn4	jl10a84	0.283105	0.000023	0.001042	0.000049	0.029658	0.001300	1.467207	0.000040	33.32	0.83
SMO grn4	jl10a85	0.282905	0.000038	0.000869	0.000015	0.024670	0.000403	1.467235	0.000042	26.34	1.33
SMO grn5 rim	jl10a87	0.283061	0.000040	0.002231	0.000290	0.093125	0.013192	1.467230	0.000038	30.93	1.41
SMO grn5 core	jl10a88	0.282702	0.000027	0.000752	0.000025	0.021067	0.000601	1.467192	0.000042	19.23	0.96
SMO grn5 rim	jl10a89	0.282885	0.000038	0.000362	0.000008	0.010344	0.000260	1.467239	0.000062	25.98	1.35
SMO grn1	jl10a90	0.282850	0.000018	0.000532	0.000006	0.014204	0.000215	1.467213	0.000030	24.62	0.64
SMO grn1	jl10a91	0.282889	0.000026	0.001496	0.000062	0.041386	0.001783	1.467175	0.000042	25.36	0.92
SMO grn 3 rim	no13b5	0.283002	0.000040	0.000403	0.000008	0.012697	0.000197	1.467193	0.000041	30.11	1.43
SMO grn 3 core	no13b6	0.282857	0.000035	0.001818	0.000033	0.062906	0.001270	1.467207	0.000035	24.01	1.25
SMO grn 3 rim	no13b7	0.282846	0.000031	0.000664	0.000014	0.022518	0.000531	1.467213	0.000036	24.40	1.11
SMO grn 6	no13b8	0.283041	0.000031	0.000397	0.000003	0.013218	0.000193	1.467175	0.000041	31.49	1.10
SMO grn 6	no13b9	0.282697	0.000032	0.000783	0.000017	0.026587	0.000480	1.467205	0.000032	19.04	1.12

Table 3-1 continued

Sample	Analysis	176Hf/177Hf**	2SE	176Lu/177Hf	2SE	176Yb/177Hf	2SE	corr 178Hf/177Hf	2SE	ε Hf (t)***	2SE
SMO grn 15	no13b10	0.282738	0.000033	0.000583	0.000066	0.020060	0.002426	1.467152	0.000050	20.62	1.18
SMO grn 15	no13b11	0.282882	0.000022	0.000394	0.000010	0.013328	0.000448	1.467209	0.000034	25.86	0.79
SMO grn 15	ja16a35	0.282609	0.000025	0.000955	0.000039	0.038157	0.001378	1.467336	0.000039	15.80	0.90
SMO grn 14	ja16a36	0.282801	0.000039	0.001312	0.000081	0.053179	0.002884	1.467345	0.000039	22.37	1.38
SMO grn 13	ja16a37	0.282707	0.000033	0.001065	0.000055	0.042411	0.002271	1.467331	0.000048	19.19	1.16
SMO grn 11	ja16a38	0.282836	0.000028	0.000660	0.000050	0.027733	0.001998	1.467324	0.000045	24.05	1.00
SMO grn 11	ja16a39	0.282857	0.000026	0.000517	0.000008	0.020930	0.000191	1.467332	0.000041	24.89	0.93
AHO grn 1	no13b13	0.283210	0.000064	0.001045	0.000026	0.029957	0.000644	1.467214	0.000047	37.35	2.26
AHO grn 1	no13b14	0.282893	0.000046	0.000963	0.000032	0.026510	0.001102	1.467210	0.000049	26.16	1.63
AHO grn 3	no13b15	0.282527	0.000055	0.001358	0.000057	0.046139	0.002439	1.467177	0.000065	12.92	1.96
AHO grn 6	no13b16	0.283272	0.000074	0.001266	0.000030	0.038225	0.000461	1.467223	0.000083	39.38	2.63
AHO grn 10	no13b17	0.282248	0.000041	0.000788	0.000024	0.026807	0.000794	1.467181	0.000046	6.31	1.44
AHO grn 10	no13b18	0.282239	0.000039	0.001032	0.000011	0.039505	0.000520	1.467204	0.000059	5.79	1.38
AHO grn 11	no13b19	0.282840	0.000039	0.001810	0.000111	0.056230	0.005130	1.467175	0.000045	23.71	1.37
AHO grn 11	no13b20	0.282915	0.000031	0.001581	0.000091	0.039479	0.001694	1.467181	0.000057	26.54	1.11
AHO grn 15	no13b22	0.283227	0.000039	0.001221	0.000101	0.032976	0.001945	1.467221	0.000051	37.83	1.38
AHO grn 15	no13b23	0.283214	0.000038	0.001125	0.000021	0.030188	0.000581	1.467155	0.000044	37.45	1.34
AHO grn 1 rim	ja16a12	0.282834	0.000037	0.001306	0.000030	0.045651	0.000758	1.467296	0.000056	23.84	1.29
AHO grn 18 core	ja16a22	0.282218	0.000042	0.001018	0.000043	0.043316	0.001610	1.467338	0.000050	4.41	1.50
AHO grn 1 core	ja16a32	0.282932	0.000050	0.000992	0.000009	0.034072	0.000525	1.467431	0.000066	27.53	1.77
TW grn 3	no12c04	0.282205	0.000040	0.000013	0.000000	0.000463	0.000020	1.467237	0.000047	5.86	1.43
TW grn 3	no12c05	0.282196	0.000039	0.000010	0.000000	0.000385	0.000015	1.467175	0.000056	5.54	1.39
TW grn 4	no12c06	0.282164	0.000035	0.000004	0.000000	0.000144	0.000016	1.467249	0.000043	4.44	1.24
TW grn 4	no12c07	0.282179	0.000030	0.000004	0.000000	0.000161	0.000028	1.467176	0.000042	4.96	1.05
TW grn 4a	no12c08	0.282174	0.000034	0.000265	0.000009	0.008626	0.000263	1.467237	0.000048	4.57	1.20
TW grn 4a	no12c09	0.282222	0.000035	0.000023	0.000001	0.000744	0.000041	1.467209	0.000054	6.46	1.22
TW grn 6	no12c10	0.282235	0.000034	0.000005	0.000001	0.000221	0.000029	1.467219	0.000052	6.94	1.21
TW grn 6	no12c11	0.282213	0.000036	0.000014	0.000002	0.000632	0.000070	1.467219	0.000051	6.16	1.26
TW grn 5	no12c13	0.282201	0.000038	0.000020	0.000002	0.000610	0.000052	1.467217	0.000054	5.73	1.34
TW grn 5	no12c14	0.282224	0.000030	0.000028	0.000004	0.000831	0.000114	1.467257	0.000040	6.54	1.07
HWKY grn 17	no12c27	0.282183	0.000025	0.000770	0.000123	0.027503	0.004914	1.467227	0.000051	3.11	0.87
HWKY grn 17	no12c28	0.282229	0.000032	0.000535	0.000044	0.017242	0.001222	1.467226	0.000059	4.90	1.12
HWKY grn 10	no12c29	0.282244	0.000026	0.000613	0.000031	0.019959	0.000562	1.467212	0.000041	5.40	0.92
HWKY grn 10	no12c30	0.282176	0.000037	0.000601	0.000010	0.020773	0.000468	1.467251	0.000051	2.99	1.32

* Notes: Abbreviations: OBO = Old Bed ore, AHG = Arnold Hill granite, PHG = Palmer Hill granite, PHO = Palmer Hill ore, SMO = Skiff Mountain ore, AHO = Arnold Hill ore, TW = Tahawas ilmenite ore, HWKY = Hawkeye granite, SE = standard error

Errors are absolute

** 176Hf/177Hf (measured)

*** ε Hf (t) calculated using SIMS U-Pb age of Valley et al., 2009

3-5-3 TRACE ELEMENTS

Representative zircon trace element data are presented in Table 3-2 and Figure 3-5a. Rare earth element data show that ore zircon grains have a narrower range of compositions and higher ratios of HREE to middle rare earth elements (MREE) when compared with their granite counterparts. The Yb/Sm for the LMG vary between ~50 and 100. The Yb/Sm for ore zircon range from ~250 to 450 regardless of whether the zircon contains a high amount of radiogenic Hf. Additionally, the ore zircon crystals have smaller negative Eu anomalies compared to LMG zircon samples. Whole rock REE data demonstrate that the ores that contain the most radiogenic Hf compositions are enriched in all REE relative to the granite (Fig. 3-5b and Table 3-3). In contrast, Palmer Hill ore, which contains the lowest εHf (t) values of the ore zircons have whole rock compositions identical in slope and total REE to their respective host granite.

Apatite REE data from LMG ore samples are presented in Figure 3-5c and Table 3-4. Ores with the highest εHf (t) values contain the most REE-enriched apatite. The chondrite normalized REE patterns are broadly similar between apatite and whole rock suggesting apatite controls the REE budget of the rock. The Skiff Mountain apatite, however, exhibit a negative light rare earth element (LREE) slope, whereas whole rock REE pattern is positive. This implies that a second REE-bearing mineral such as monazite is present at Skiff Mountain that is not present in the other ores.

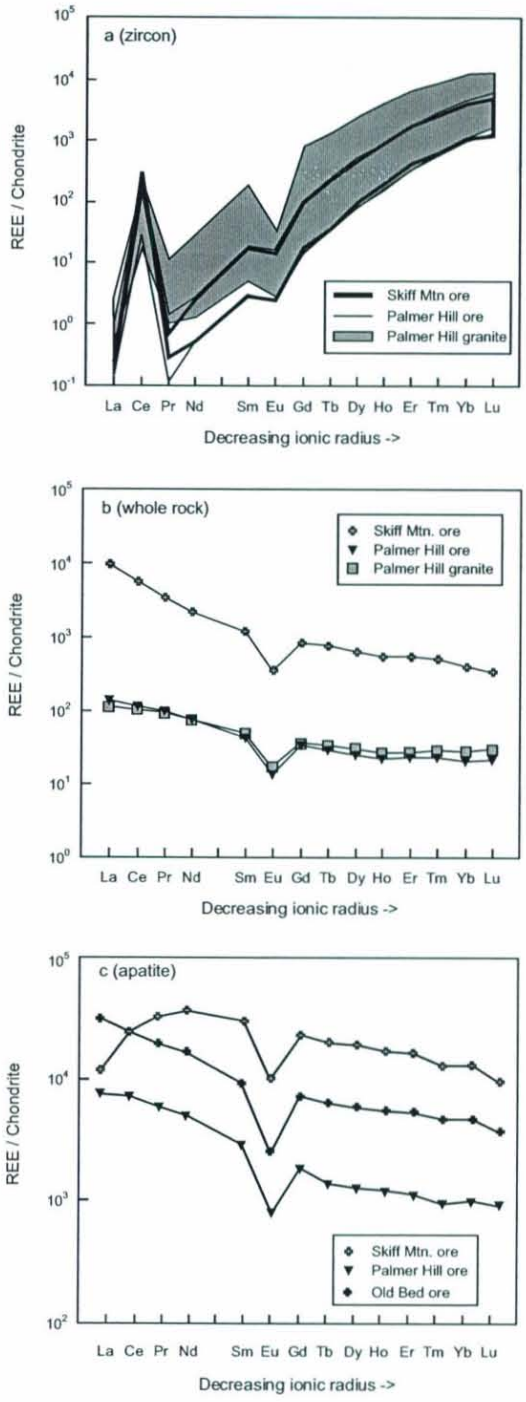

Figure 3-5. (a) Range of chondrite-normalized REE patterns for representative zircon from the Lyon Mountain granite (Palmer Hill), low εHf(t) ore (Palmer Hill) and high εHf(t) ore (Skiff Mountain) and (b) chondrite normalized whole rock REE patterns and (c) chondrite-normalized apatite REE patterns.

Table 3-2 Representative zircon trace element data (ppm)

Sample	Palmer Hill granite	Palmer Hill granite	Palmer Hill ore	Palmer Hill ore	Skiff Mtn. ore	Skiff Mtn. ore
Element						
Y	169.3	4512	402.2	1618	391.7	1832
Nb	33.27	48.73	16.16	9.54	12.75	26.69
Ta	8.47	15.42	5.10	3.80	6.82	7.74
Pb	100.7	204.0	8.51	34.33	2.18	10.91
Th	869.4	1498	84.38	308.4	21.52	109.9
U	1763	1438	210.8	344.2	119.0	273.4
Nb/Ta	3.93	3.16	3.17	2.51	1.87	3.45
Th/U	0.49	1.04	0.40	0.90	0.18	0.40
La	0.12	0.19	n.d.	n.d.	0.06	n.d.
Ce	40.10	96.56	71.51	122.0	57.24	175.3
Pr	0.72	0.68	0.02	0.07	0.03	0.07
Nd	9.98	9.30	0.25	1.25	0.30	1.24
Sm	18.60	21.12	0.54	3.38	0.55	2.80
Eu	0.58	1.39	0.19	0.99	0.15	0.85
Gd	113.4	123.5	4.29	22.90	3.91	21.61
Tb	41.34	38.41	1.84	9.05	1.72	8.94
Dy	560.8	456.4	30.67	135.6	27.66	135.1
Ho	214.0	155.6	13.65	56.25	12.23	56.62
Er	1001	644.8	78.06	305.4	68.74	306.4
Tm	210.2	124.0	21.08	77.77	17.99	71.97
Yb	1852	992.3	236.3	829.1	187.1	707.8
Lu	320.9	170.6	48.12	165.4	33.59	132.0
Yb/Sm	99.58	46.98	437.5	245.3	340.2	252.8

Table 3-3 Representative rare earth element data of whole rock samples (ppm)

Sample Element	Palmer Hill granite	Palmer Hill ore	Skiff Mtn. ore
La	26.71	32.21	2300
Ce	60.77	69.35	3390
Pr	8.47	8.81	311.40
Nd	34.39	33.65	993.36
Sm	7.26	6.32	175.67
Eu	0.94	0.77	19.49
Gd	7.23	6.70	168.23
Tb	1.25	1.06	28.28
Dy	7.27	6.05	153.30
Ho	1.48	1.25	30.67
Er	4.34	3.66	86.26
Tm	0.71	0.56	12.52
Yb	4.47	3.34	66.22
Lu	0.73	0.51	8.13
Yb/Sm	0.56	0.47	0.34

Table 3-4 Representative trace element data of apatite

Sample Element	Palmer Hill ore	Old bed ore	Skiff Mtn ore
F	3.94	3.61	3.55
Cl	0.08	0.07	0.10
Sc	0.35	0.16	0.57
V	0.88	1.38	0.30
Co	-	0.54	0.17
Cu	0.28	-	1.35
Zn	0.27	0.28	0.68
As	911	2690	1170
Sr	173	283	202
Y	2320	11800	34400
Zr	0.29	6.82	4.83
Nb	0.49	0.09	2.55
Sn	1.07	0.70	1.37
Ba	0.24	0.56	1.26
La	2550	10300	4060
Ce	6300	21100	22100
Pr	744	2410	4300
Nd	3090	10200	23900
Sm	538	1960	6380
Eu	57.70	189	724
Gd	503	1960	6480
Tb	73.00	311	1040
Dy	417	1930	6250
Ho	90.10	425	1310
Er	245	1200	3470
Tm	32.10	162	455
Yb	212	1020	2740
Lu	30.60	125	323
Hf	0.04	0.17	0.38
Th	229	1540	961
U	17.40	236	302
Lu/Hf	765	735	850

Data are in ppm except Cl and F which are reported as weight percent

3-6 DISCUSSION

The extremely radiogenic εHf (t) (up to + 40) found in the hydrothermal zircon grains from the Arnold Hill, Skiff Mountain, and Old Bed ores provide unique information regarding the formation of these zircon crystals as well as magnetite-apatite ("Kiruna-type") deposits in general. The εHf (t) values in zircon for the LMG hosts (Palmer Hill granite and Arnold Hill granite), Palmer Hill ore, Hawkeye granite, and the anorthosite-related Tahawas magnetite-ilmenite ore, all plot along a curve defined by a $^{176}Lu/^{177}Hf$ of 0.01 (average continental crust) from an initial $\varepsilon Hf_{1150\ Ma} = +5$ at 1150 Ma ($^{176}Hf/^{177}Hf$ ~0.282200) (Fig 3-4). The suites of zircon in the younger ores in the LMG (Arnold Hill, Old Bed, and Skiff Mountain) are up to 30 εHf units higher than those of the host granites and the Palmer Hill ore body. Models for the Hf isotopic evolution of the LMG ores and associated rocks are presented in Figure 3-6.

Two plausible possibilities exist to explain the highly radiogenic Hf isotopic compositions in the younger ores: 1) first generation "skarn-like" ore bodies contained magnetite, clinopyroxene, and Lu-rich apatite, which were subsequently dissolved during secondary fluid alteration and ore remobilization. This process released highly radiogenic Hf from the apatite, less radiogenic Hf and Zr from clinopyroxene and mobilized magnetite. Zircon then crystallized during the formation of these second-generation ore bodies. Alternatively: 2) fluids responsible for zircon-bearing ores interacted with garnet-rich crust during rapid decompression of the Adirondack Highlands and radiogenic Hf was released from garnet and as above Zr and less radiogenic Hf from clinopyroxene.

3-6-1 MODEL 1: REMOBILIZATION OF LU-RICH APATITE

In this model, early-formed, "skarn-like", ore bodies, related to crystallization of the LMG, contain clinopyroxene and magnetite ± apatite (Fig. 3-7a and 7b) and no zircon. Field relations and thin section petrography clearly show Na-alteration overprinting the earlier "skarn-like" mineralization (Postel, 1952; McLelland, 2002; Valley et al., chapter 4). Additionally, no zircon grains were identified during the mineral separation process (i.e., in the > 3.3 g/cm^3 fraction) or in the thin section from the "skarn-like" sample shown in Figure 3-7a and 7b. The breakdown of early-formed apatite and clinopyroxene during secondary fluid alteration in the LMG resolves the conflict of zircon ages in the Lyon Mountain ore deposits being 20 to 60 m.y. younger than the host granite, as well as supplying a source of radiogenic Hf and Zr for zircon (Valley et al., 2009).

Apatite from the same samples that contain high εHf (t) zircon (Skiff Mountain, Arnold Hill and Old Bed) is enriched in most REE and HFSE (including Lu and Hf) relative to the samples that contain low εHf (t) zircon (Palmer Hill) (Fig. 3-5c). Lu/Hf are, however, similar for all apatite. The presence of REE-rich apatite may be the result of elemental partitioning during late stage granite crystallization, or alternatively the development of F and Cl-rich, orthomagmatic fluids that fractionated or scavenged REE and HFSE from granites that had already crystallized (Salvi and William-Jones, 1996; Schmidt et al., 2007).

A model for the release and mobilization of radiogenic Hf from apatite is presented in Figure 3-6a. The apatite grains studied can be divided into high Lu (~320

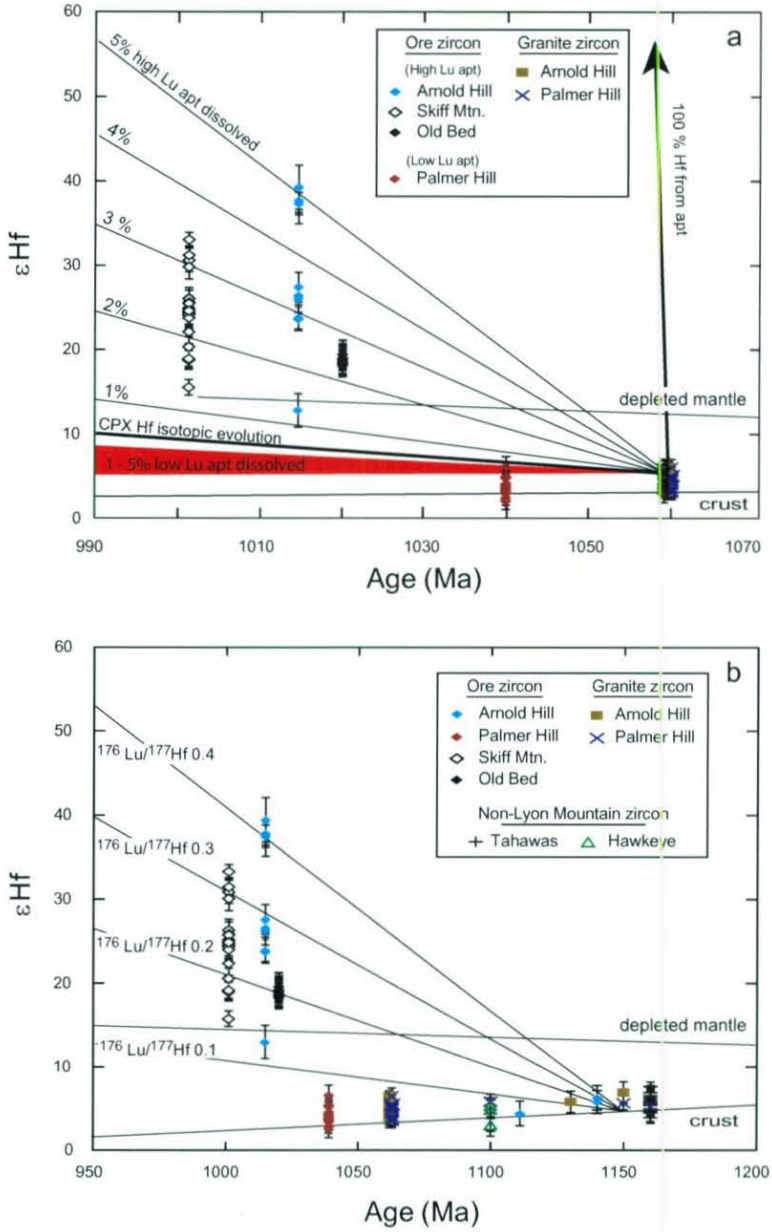

Figure 3-6. (a) Model 1 showing the production of observed Hf isotopic compositions in zircon as a result of variable apatite dissolution (1-5%) and variable Hf incorporation into zircon (0.2-1%) (see text for details). In this model the amount of Hf provided by; clinopyroxene = 2 ppm, high Lu apatite = 0.4 ppm, and low Lu apatite = 0.04 ppm (b) Model 2 showing the production of observed Hf isotopic compositions in zircon as a result of fluid interaction with garnet-rich (high Lu/Hf) crust during retrograde metamorphism (see text for details). The starting 176Lu/177Hf in garnet is varied from 0.1 to 0.4 to produce the given Hf isopleths. Abbreviations as in Figures 3-1 and 3-3.

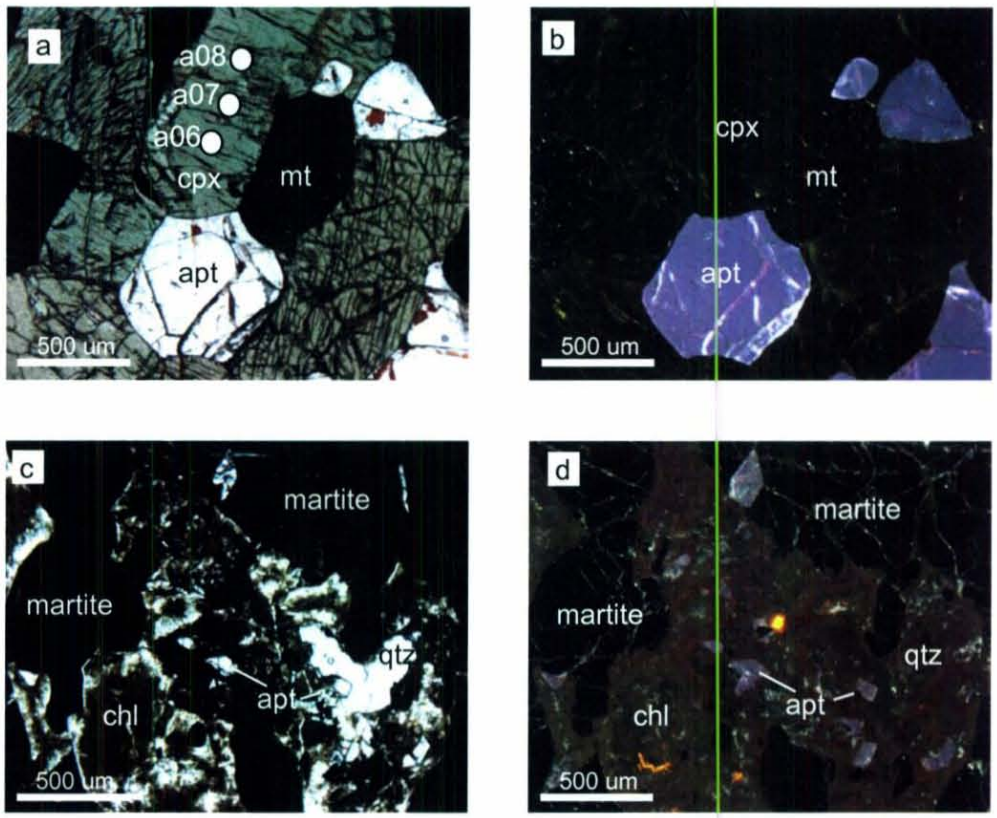

Figure 3-7. Photomicrographs in cross-polarized light (a and c) and color cathodoluminescence (b and d) of early-formed and secondary ore bodies. Photomicrographs a and b show primary apatite, clinopyroxene, and magnetite from the Rutgers mine. White circles indicate locations of trace element analyses and labels correspond to data in Table 3-5. Photomicrographs c and d show remnant apatite, hematite after magnetite (martite) and alteration of probable clinopyroxene to chlorite from the Arnold Hill ore (highly radiogenic Hf).

ppm) and low Lu (~30 ppm) groups (Table 3-4; Fig 3-6a). The Hf concentrations of these apatite display a similar relationship; high Lu apatite contain ~0.4 ppm Hf and low Lu apatite ~0.04 ppm Hf. Thus, both the higher and lower Lu apatite have similar, and extremely high, calculated $^{176}Lu/^{177}Hf$ of ~105, which were determined from the measured ^{175}Lu and ^{178}Hf concentrations (as measured by single collector LA-ICPMS, see methods section 4.2 above and Appendix 1). Thus, the measured Hf concentrations do not reflect in-growth of ^{176}Hf but are an estimate of the initial Hf concentrations at the time of ore formation.

Assuming breakdown of apatite was the only source of Hf for zircon, then εHf (t) values measured in zircon could be as high as +5000, depending on the time of apatite dissolution (Fig 3-6a). The highest εHf (t) value measured in zircon in this study was +40. This requires that measured Hf isotopic compositions were lowered, or diluted, by the introduction of high concentrations non-radiogenic Hf from a different source. The breakdown of pyroxene and the accompanying release of non-radiogenic Hf (as well as a source of zirconium for the crystallization of zircon) are consistent with the observed Hf isotopic compositions in zircon. Concentrations of Hf in clinopyroxene from an unaltered ore sample at the Rutgers mine are ~2 ppm and have a $^{176}Lu/^{177}Hf$ of 0.07 (Table 3-5, Fig. 3-7).

Epsilon Hf(t) data for Palmer Hill, Arnold Hill, Skiff Mountain, and Old Bed zircon are plotted in Figure 3-6a along with time-integrated mixing lines of constant proportions of apatite dissolution for ore samples containing both high and low Lu apatite with attendant Hf concentrations. A concentration of 2 ppm Hf (with an initial $\varepsilon Hf_{1060\ Ma}$

Table 3-5 Representative trace element data (ppm) of clinopyroxene

Sample Element	Rutgers (a06)	Rutgers (a07)	Rutgers (a08)
Sr	15.67	17.04	17.38
Y	34.59	27.77	21.87
Zr	77.70	73.22	68.58
Nb	0.44	0.43	1.66
Ba	86.84	95.91	100.83
La	5.17	5.83	5.84
Ce	17.26	16.16	15.36
Pr	2.86	2.53	2.25
Nd	14.22	12.60	10.52
Sm	4.36	3.47	2.75
Eu	0.66	0.60	0.48
Gd	4.30	3.61	2.95
Tb	0.82	0.68	0.50
Dy	5.61	4.58	3.56
Ho	1.26	1.02	0.76
Er	3.88	3.05	2.44
Tm	0.65	0.54	0.42
Yb	5.96	4.81	3.70
Lu	1.24	0.98	0.72
Hf	2.08	1.92	1.67
Ta	0.03	0.02	0.02
Pb	3.06	5.77	9.23
Th	0.65	1.97	8.84
U	0.16	0.31	0.91

~6 $^{176}Hf/^{177}Hf$ of 0.282270 and $^{176}Lu/^{177}Hf = 0.07$ at 1060 Ma) from pyroxene is used in all mixing calculations. The model assumes all ore deposits (and associated minerals) initially formed at 1060 Ma prior to subsequent alteration and secondary mineralization. This model can be used effectively to explain observed εHf (t) values of the ore zircon crystals. For example, Arnold Hill contains apatite with high concentrations of Lu (Hf ~0.4 ppm) with zircon crystals that display a wide range of εHf (t) values up to +40. The most radiogenic Hf isotopic compositions observed at Arnold Hill can be accounted for by 45 m.y. of ^{176}Hf in-growth in apatite at which time some or part of the apatite is dissolved and 1% of the released Hf is incorporated into zircon. The remaining Hf in zircon could have been supplied from clinopyroxene.

In comparison, zircon crystals in the Palmer Hill ore, which also contains apatite but with low concentrations of Lu (and 0.04 ppm Hf), display relatively un-radiogenic εHf(t) values. These values can be achieved by similar mixing contributions for Arnold Hill ore, but will not produce radiogenic Hf compositions owing to the very low Lu concentrations in these apatite. Alternatively, the relatively low εHf (t) observed in the Palmer Hill zircon can also be achieved with a larger contribution of Hf from un-radiogenic sources like pyroxene or the surrounding country rock. Projected apatite εHf (t) values for low Lu apatite are still substantial (~ +1450 epsilon units) by the 1040 Ma crystallization age of the Palmer Hill ore deposit when only apatite is allowed to contribute its Hf. Furthermore, the εHf (t) observed at Palmer Hill could be accounted for solely by the breakdown of clinopyroxene or surrounding country rock (see cpx evolution curve Fig. 3-6a). An important outcome of this model is that the observed εHf

(t) in high Lu ores cannot be accounted for solely by breakdown of pyroxene or country rock and requires a source with much higher $^{176}Lu/^{177}Hf$.

The observed range of εHf (t) in the Arnold Hill and Skiff Mountain ore zircon may be the result of incomplete mixing of Hf from different sources within individual samples, an increase in the breakdown of cpx over time (or exhaustion or lack of apatite input), or the influence of inherited low εHf (t) zircon which are present in the Arnold Hill ore (Valley et al., 2009). Additionally, these ore zircon grains exhibit patchy zoning in BSE images (which may indicate chemical as well as structural variations in the crystal) and may suggest that the zircon is zoned with respect to Hf as well.

For this model to be effective, three requirements need to be met: the breakdown of clinopyroxene and apatite; the mobilization of typically immobile elements like Hf and Zr; and time for radiogenic Hf to accumulate. The breakdown of REE- and HFSE-bearing minerals and the redistribution of HFSE and REE by halogen-bearing fluids (especially F and Cl) is well documented (e.g., Rubin et al. 1993; Bau and Dulski, 1995; Schmidt et al., 2007). The presence of halogen-bearing fluids in model 1 is a means to selectively breakdown apatite and clinopyroxene and redistribute their constituent REE and HFSE. The presence of fluorite in the alteration halo and within the ore itself (e.g., Hagner and Collins, 1967) implies that F activity was high during at least one stage of alteration and Fe mineralization. Apatite in these ore deposits have high F/Cl (Table 4), which is typical in many felsic rocks (Piccoli and Candela, 2002). The presence of fluoroapatite does not confirm that the fluids from which apatite crystallized were overly enriched in F, but the occurrence of fluoroapatite that is extremely enriched in REE, does

imply that REE and F must have coexisted in the same fluid. This association of F and REE has been recognized in many REE deposits (e.g., Salvi and Williams-Jones, 1996; Halden and Fryer, 1999; Smith and Wu, 2000).

Alternatively, or additionally, Cl may play a significant role in model 1. High concentrations of LREE and MREE in apatite can be the result of Cl-rich fluids (Schmidt et al., 2007). Evidence of NaCl bearing fluids in the LMG comes from NaCl-rich fluid inclusions (12-21 % NaCl), quartz-albite veins, and extensive albitization of the granite and in the alteration zones around the ore (McLelland et al., 2002). The role of halogens may seem obvious for HFSE and REE mobility, but other less readily identifiable fluid processes should be considered including the role of OH, changing fO_2, the low activity of S, and pH of the hydrothermal fluid (Barton et al., 1991; Barton and Johnson, 1996). The role of acidic fluids in the LMG is suggested by presence of sillimanite nodules which formed by the leaching of alkali cations from feldspar leaving behind quartz-sillimanite segregations (McLelland et al. 2002).

Zircon from the ore bodies are 20 to 60 m.y. younger than the granites immediately adjacent to the ore (Valley et al., 2009). It is unlikely that these ages could be the result Pb loss from a circa 1060 Ma zircons, given the precision of the data points for the U-Th-Pb concordia ages and the lack of obvious zircon crystal damage (Valley et al., 2009). Whether the ore zircon ages represent primary mineralization or secondary remobilization, the fluids responsible for zircon growth cannot be derived from the granite bodies that are in contact with the ore. This requires that the source of the fluid is external. Possibilities include: as yet undated magmatism, deep circulating brines related

to extension, or that the magnetite-apatite deposits are not hydrothermal at all, but Fe-rich melts of uncertain origin. Whatever the ultimate source of the fluid, the presence of so much radiogenic Hf requires a two-stage process whereby a Lu-rich source has enough time for radiogenic Hf to accumulate and that subsequent breakdown did not involve Hf-bearing minerals.

3-6-2 MODEL 2: RETROGRADE METAMORPHISM INVOLVING GARNET

An alternative hypothesis for the source of radiogenic Hf is that pervasive fluid interactions with garnet-rich material have produced the observed εHf (t) values and high REE concentrations. Garnet incorporates Lu over Hf due to strong partitioning of HREE (e.g., Irving and Frey, 1978). Typical initial $^{176}Lu/^{177}$ Hf values in garnet are variable from 0.03 to 8.0 (e.g., Scherer et al., 1997; Duchéne et al., 1997; Blichert-Toft and Frei, 2001), and as a result, highly radiogenic Hf compositions may evolve over time. Figure 6b shows $^{176}Lu/^{177}Hf$ evolution curves emanating from the starting composition at 1150 Ma using $^{176}Lu/^{177}Hf$ (in garnet) = 0.1, 0.2, 0.3 and 0.4. An 1150 Ma age is used as the probable age of garnet-bearing crust in this region given the prevalence of 1150 Ma AMCG rocks in the Adirondack Highlands (e.g. Daly and McLelland, 1991; McLelland et al., 2001). Given an initial $\varepsilon Hf_{1150\ Ma}$ = +5 at 1150 Ma ($^{176}Hf/^{177}Hf$ ~0.282200), the most radiogenic Hf compositions for the Old Bed ore zircon crystals can be accounted for by a garnet source with a $^{176}Lu/^{177}Hf$ = 0.2, the radiogenic Hf composition of the Arnold Hill ore zircon requires a $^{176}Lu/^{177}Hf$ = 0.4 in the garnet source, and those of Skiff Mountain ore zircon requires $^{176}Lu/^{177}Hf$ = 0.3. The $^{176}Lu/^{177}$ Hf evolution curves using

values of 0.1 to 0.4 in Figure 3-6b are well within the accepted values for garnet. For this radiogenic Hf signature to be passed on to zircon elsewhere, minerals containing non-radiogenic Hf (e.g., zircon, rutile) in the garnet-bearing source, must not be involved in the process, or be present in very low modal abundance. Thus, if zircon breakdown accompanies garnet breakdown, radiogenic Hf ratios produced by garnet will be "diluted" by non-radiogenic Hf contained in zircon.

Emplacement of the LMG is syn- to post-tectonic and related to regional extension (McLelland et al., 2001; Selleck, 2005; Valley et al., 2009). If extension and uplift of rocks containing garnet are rapid, garnet may react to form plagioclase. This solid-state reaction without melting would release REE and HFSE from garnet, while preexisting zircon should remain unchanged. Garnet grains with coronas of plagioclase are a common feature throughout the Adirondack Highlands

The selective breakdown of garnet in model 2 is achieved through retrograde metamorphic reactions without the need for fluids. However, transport of REE and HFSE from the garnet-bearing source rock to the LMG does require fluid circulation. Without the interaction of halogen-rich fluids, REE typically are redistributed only locally during metamorphism (e.g., Grauch, 1989; Seifert, 1989). Field relations show the LMG is currently in contact with garnet-bearing calc-silicate marble and gabbro. Fluid conduits between the garnet-bearing rocks and the LMG have not commonly recognized, but in many localities, ore deposits occur only 10s of meters away from the contacts of the two rock types.

3-6-3 IMPLICATIONS FOR ORE FORMATION

The data presented here have important implications for fluid-rock interactions and the processes associated with the formation of magnetite-apatite ("Kiruna-type") deposits. Chondrite-normalized zircon REE patterns for all the ore bodies are nearly identical in slope and total REE regardless or whether the ore contains low Lu apatite or high Lu apatite (Fig. 3-5a). This suggests that despite differences in age and REE content, all hydrothermal zircon formed as a result of similar processes. Both U-Pb age data and Hf isotopes suggest that secondary ore formation or modification post-dates LMG magmatic activity by 20 to 60 m.y. Additionally, the modification of preexisting ores suggests that once a fluid pathway has been created, fluid will continue to follow the same route. The existence of ore deposits only in the LMG (with rare exceptions) indicates that there is a direct relationship between original granite and these deposits. In addition to the skarn-like deposits, disseminated magnetite that is pervasive throughout the LMG has apparently been stripped from the granite directly adjacent to the ore body and concentrated in the ore (Hagner and Collins, 1967).

Much evidence exists to suggest that the magnetite-apatite ("Kiruna-type") deposits in the LMG were emplaced during regional extension following the Ottawan orogeny (e.g., Selleck et al., 2005; Valley et al., 2009). The ore bodies are either coeval or younger in age than the emplacement of dikes and small magmatic bodies that crosscut the main tectonic fabric in the Adirondack Highlands. The alignment of the ore bodies with the NE plunging regional lineation is coincident with a lineation that developed during extension along the Tawachiche shear zone in the Maurice region of Quebec along

strike with outcrops of the LMG (Corrigan and Nadeau, 1997). Extension in the Maurice region was active from 1090 to 1040 Ma and is contemporaneous with emplacement of younger granitoids, similar to the tectonic associations in the LMG. If granite emplacement was related to orogenic extension then certainly the ore deposits associated with these granites must be directly or indirectly related to extension as well. The deposits in the LMG contain many of the characteristics of brine-related deposits which typically occur in extensional tectonic settings (Barton and Johnson, 2004).

The source of fluids and the driving mechanism for fluid circulation in extensional settings is debated, but the association of a variety of ore deposits (including magnetite-apatite deposits) with extensional tectonics is well documented in the literature (e.g., Cathles,1981; Hitzman, 2000; Staude et al., 2009). In the Adirondack Highlands fluid circulation could have been driven by rapid uplift of the hot interior of the orogen during regional extension or magmatic underplating of a thinning crust. The ubiquity of the aforementioned, dikes and leucogranite bodies from this time period requires high heat flow throughout the region (Selleck et al., 2004; Selleck et al., 2005). Given the wide-spread occurrence of dry granulite facies rocks in Adirondack Highlands, fluids probably were externally derived. Halogen-bearing fluids or brines could have used these extensional shear zones and interacted with early-formed "skarn-like" ore deposits related to granite emplacement (model 1) or garnet-bearing calc-silicate marble and meta-gabbro that are pervasive throughout the Adirondack Highlands during retrograde metamorphism (model 2).

3-7 CONCLUSIONS

Hafnium isotopes combined with trace element data for zircon and apatite may be used to characterize fluids and fluid processes responsible for hydrothermal alteration and magnetite-apatite mineralization. Extremely radiogenic Hf values in zircon from some of the ore bodies indicate that the fluids responsible for Fe mineralization or remobilization may have: 1) interacted with preexisting Lu-rich apatite and clinopyroxene from early formed ore bodies related to granite emplacement; or 2) that fluids interacted and scavenged HFSE and REE from preexisting garnet bearing rocks most likely during garnet breakdown. Zircon and whole rock REE patterns are similar between ore deposits and independent of Hf isotopic compositions. This suggests that similar fluids and processes were responsible for their formation regardless of their original Lu content. The presence of radiogenic Hf in hydrothermal zircon and U-Pb ages 20 to 60 m.y. younger than the host granites of the ores, suggests that multiple processes are responsible for ore formation and periodic modification of preexisting ores.

ACKNOWLEDGEMENTS

This research was supported by an NSERC Discovery Grant and startup funds to JMH provided by Memorial University of Newfoundland. We wish to thank Marian Lupulescu, Phil Whitney, and James McLelland for their helpful discussions. Phil Piccoli, John Fournelle and Matt McInnis are also thanked for their contributions.

REFERENCES

Barton, M. D., Ilchik, R. P., and Marikos, M. A., 1991, Metasomatism: in Kerrick, D. M., Contact Metamorphism, Reviews in Mineralogy 26, p. 321-350.

Barton, M.D., and Johnson, D.A., 1996, Evaporitic-source model for igneous-related Fe oxide- (REE-Cu-Au-U) mineralization: Geology, v. 24, p. 259-262.

Barton, M.D., and Johnson, D.A., 2004, Footprints of Fe-oxide (-Cu-Au) systems. SEG 2004 Predictive Mineral Discovery Under Cover - Extended Abstracts, Centre for Global Metallogeny, The University of Western Australia, v. 33, p. 112-116.

Bau, M., and Dulski, P., 1995, Comparative study of yttrium and rare-earth element behaviors in fluorine-rich hydrothermal fluids. Contributions to Mineralogy and Petrology, v. 119, p. 213.

Blichert-Toft, J., and Frei, R., 2001, Complex Sm-Nd and Lu-Hf isotope systematics in metamorphic garnets from the Isua supracrustal belt, West Greenland: Geochimica et Cosmochimica Acta, v. 65, p. 3177-3189.

Blichert-Toft, J., and Albarede F., 1997, The Lu-Hf isotope geochemistry of chondrites and the evolution of the mantle-crust system. Earth Planet. Sci. Lett. v. 148, 243–258.

Blichert-Toft, J., 2008, The Hf isotopic composition of zircon reference material 91500. Chemical Geology, v. 253, no. 3-4, p. 252-257.

Bouvier A., Vervoort J.D., and Patchett P.J., 2007, The Lu-Hf CHUR value. Geochimica et Cosmochimica Acta Supplement, Vol. 71, Goldschmidt Conference Abstracts 2007, A116.

Cathles, L. M., 1981, Fluid flow and genesis of hydrothermal ore deposits. Economic Geology Seventy-Fifth Anniversary Volume. B. J. Skinner, Society of Economic Geologists: p. 1905-1980.

Corrigan, D., and Nadeau, L., 1997, U-Pb age constraints for the lithotectonic evolution of the Grenville Province along the Mauricie transect, Quebec. Canadian Journal of Earth Sciences, vol. 34, no. 3, p. 299-316.

Daly, J.S., and McLelland, J.M., 1991, Juvenile middle Proterozoic crust in the Adirondack highlands, Grenville province, northeastern North America. Geology, v. 19, p. 119-122

Davidson, A., 1998, Geological map of the Grenville Province, Canada and adjacent parts of the United States of America. Geol. Surv. Can., Map 1947A (scale 1:2,000,000).

Duchéne, S., Blichert-Toft, J., Luais, B., Telouk, P., Lardeaux, J.M., and Albarede, F., 1997, The Lu-Hf dating of garnets and the ages of the Alpine high-pressure metamorphism: Nature, v. 387, p. 586-589.

Foose, M.P., and McLelland, J.M., 1995, Proterozoic low-Ti iron-oxide deposits in New York and New Jersey; relation to Fe-oxide (Cu-U-Au-rare earth element) deposits and tectonic implications. Geology, v. 23, p. 665-668.

Grauch, R.I., 1989, Rare earth elements in metamorphic rocks. Reviews in Mineralogy and Geochemistry, v. 21, p. 147-167.

Hagner, A.F., and Collins, L.G., 1967, Magnetite ore formed during regional metamorphism, Ausable magnetite district, New York. Economic Geology, v. 62, p. 1034-1071.

Halden, N.M., and Fryer, B.J., 1999, Geochemical characteristics of the Eden Lake Complex: evidence for anorogenic magmatism in the Trans-Hudson orogen: Canadian Journal of Earth Sciences, v. 36, p. 91-103.

Hamilton, M.A., McLelland, J., and Selleck, B., 2004, SHRIMP U-Pb zircon geochronology of the anorthosite-mangerite-charnockite-granite (AMCG) suite, Adirondack Mountains, New York: Ages of emplacement and metamorphism, In Tollo, R.P., Corriveau, L., McLelland, J., and Bartholomew, M.J., eds., Proterozoic tectonic evolution of the Grenville orogen in North America. Geological Society of America Memoir 197, p. 337–355.

Harlov, D.E., Andersson, U.B., Foerster, H.-J., Nystrom, J.O., Dulski, P., and Broman, C., 2002, Apatite-monazite relations in the Kiirunavaara magnetite-apatite ore, northern Sweden. Chemical Geology, v. 191, p. 47-72.

Hawkesworth, C.J., and Kemp, A.I.S., 2006, Using hafnium and oxygen isotopes in zircons to unravel the record of crustal evolution. Chemical Geology, v. 226, p. 144.

Hickmott, D.D., Shimizu, N., Spear, F.S., and Selverstone, J., 1987, Trace-element zoning in a metamorphic garnet. Geology, v. 15, p. 573-576.

Hitzman, M.W., Oreskes, N., and Einaudi, M.T., 1992, Geological characteristics and tectonic setting of Proterozoic iron oxide (Cu-U-Au-REE) deposits. Precambrian Research, v. 58, p. 241-287.

Hitzman, M.C., 2000, Iron oxide-Cu-Au deposits: What, where, when, and why?, in Porter, T.M., ed., Hydrothermal iron oxide copper-gold and related deposits: A global perspective: PGC Publishing, Adelaide, v. 1, p. 9-25.

Hoskin, P.W.O., and Schaltegger, U., 2003, The Composition of Zircon and Igneous and Metamorphic Petrogenesis: Reviews in Mineralogy and Geochemistry, v. 53, p. 27-62.

Isachsen, Y. W., and Fisher, D. W., 1970, Geologic map of New York State Adirondack Sheet. New York State Museum Science Service Map Chart Series 16.

Irving, A.J., and Frey, F.A., 1978, Distribution of trace elements between garnet megacrysts and host volcanic liquids of kimberlitic to rhyolitic composition: Geochimica et Cosmochimica Acta, v. 42, p. 771-787.

Kemp, A.I.S., Wormald, R.J., Whitehouse, M.J., and Price, R.C., 2005, Hf isotopes in zircon reveal contrasting sources and crystallization histories for alkaline to peralkaline granites of Temora, southeastern Australia. Geology, v. 33, p. 797-800.

Kinny, P.D., and Maas, R., 2003, Lu-Hf and Sm-Nd isotope systems in zircon. Reviews in Mineralogy and Geochemistry v. 53, p. 327-341.

Lindberg, M L., and Ingram, B., 1964, Rare-earth silicatian apatite from the Adirondack Mountains, New York. U.S. Geological Survey Professional Paper 501-B, 864-865.

Longerich, H. P., S. E. Jackson, and D. Gunther., 1996, Laser ablation ICP-MS spectrometric transient signal data acquisition and analyte concentration calculation. Journal of Analytical Atomic Spectrometry, v 11, 899-904.

McLelland, J., and Isachsen, Y. W., 1985, Geologic evolution of the Adirondack Mountains: a review, *in* Tobi, A., and Touret, J., eds., The deep Proterozoic crust in the North Atlantic provinces: NATO Advanced Study Institute Series C, v. 158, 175-215.

McLelland, J. and Chiarenzelli, J., 1988, Geochronology and geochemistry of 1.3 Ga tonalitic gneisses of the Adirondack Highlands and their implications for the tectonic evolution of the Grenville Province: *In* Middle Proterozoic Crustal evolution of the North American and Baltic Shields, Geological Association of Canada Special paper 38, p. 175-196.

McLelland, J., Chianrenzelli, J., Whitney, P., and Isachsen, Y., 1988, U-Pb zircon geochronolgy of the Adirondack Mountains and implications for their geologic evolution. Geology, v. 16, p. 920-924.

McLelland, J.M., and Chiarenzelli, J. 1990, Isotopic constraints on emplacement age of anorthositic rocks of the Marcy Massif, Adirondack Mts., New York: Journal of Geology, v. 98, p. 19–41.

McLelland, J., Hamilton, M., Selleck, B., McLelland, J., Walker, D., and Orrell, S., 2001, Zircon U-Pb geochronology of the Ottawan Orogeny, Adirondack Highlands, New York; regional and tectonic implications. Precambrian Research, v. 109, p. 39-72.

McLelland, J., Morrison, J., Selleck, B., Cunningham, B., Olson, C., and Schmidt, K., 2002, Hydrothermal alteration of late- to post-tectonic Lyon Mountain granitic gneiss, Adirondack Mountains, New York; origin of quartz-sillimanite segregations, quartz-albite lithologies, and associated Kiruna-type low-Ti Fe-oxide deposits. Journal of Metamorphic Geology, v. 20, p. 175-190.

McLelland, J.M., Bickford, M.E., Hill, B.M., Clechenko, C.C., Valley, J.W., and Hamilton, M.A., 2004, Direct dating of Adirondack massif anorthosite by U-Pb SHRIMP analysis of igneous zircon: Implications for AMCG complexes. Geological Society of America Bulletin, v. 116, p. 1299-1317.

Nowell, G.M., Kempton, P.D., Noble, S.R., Fitton, J.G., Saunders, A.D., Mahoney, J.J., and Taylor, R.N., 1998, High precision Hf isotope measurements of MORB and OIB by thermal ionization mass spectrometry: insights into the depleted mantle. Chemical Geology, v. 149, p. 211.

Patchett, P.J., Kouvo O., Hedge C.E., Tatsumoto M., 1981, Evolution of continental crust and mantle heterogeneity: evidence from Hf isotopes. Contributions to Mineralogy and Petrology, v. 78, p. 279–297.

Postel, A.W., 1952, Geology of the Clinton County magnetite district. United States Geological Survey Professional Paper, v. 237, p. 88.

Reynolds, L.J., 2000, Geology of the Olympic Dam Cu-U-Au-Ag-REE deposit, Australian Mineral Foundation, Glenside, South Aust., Australia (AUS).

Rivers, T., 1997, Lithotectonic elements of the Grenville Province: review and tectonic implications: Precambrian Research, v. 86, p. 117-154.

Roeder, P.L., MacArthur, D., Ma, X.-P., Palmer, G.R., and Mariano, A.N., 1987, Cathodoluminescence and microprobe study of rare-earth elements in apatite. American Mineralogist, v. 72, p. 801-811.

Salvi, S., and Williams-Jones, A.E., 1996, The role of hydrothermal processes in concentrating high-field strength elements in the Strange Lake peralkaline complex, northeastern Canada. Geochimica et Cosmochimica Acta, v. 60, p. 1917.

Scherer, E.E., Cameron, K.L., Johnson, C.M., Beard, B.L., Barovich, K.M., and Collerson, K.D., 1997, Lu-Hf geochronology applied to dating Cenozoic events affecting lower crustal xenoliths from Kilbourne Hole, New Mexico: Chemical Geology, v. 142, p. 63-78.

Schmidt, C., Rickers, K., Bilderback, C.H., and Huang, R., 2007, In situ synchrotron-radiation XRF study of REE phosphate dissolution in aqueous fluids to 800° C. Lithos, v. 95, p. 87-102

Seifert, K.E., and Chadima, S.A., 1989, Depletion of heavy rare-earth elements in metamorphic minerals from Adirondack anorthosites. Geology, v. 17, p. 1004-1006.

Selleck, B.W., McLelland, J.M., and Hamilton, M. A., 2004, Magmatic-hydrothermal leaching and origin of late- to post-tectonic quartz-rich rocks, Adirondack Highlands, New York. In Tollo, R.P., Corriveau, L., McLelland, J., and Bartholomew, M. J., eds., Proterozoic Tectonic Evolution of the Grenville Orogen in North America: Geological Society of America Memoir no. 197, p. 379-390.

Selleck, B.W., McLelland, J.M., and Bickford, M.E., 2005, Granite emplacement during tectonic exhumation: The Adirondack example. Geology, v. 33, p. 781-784.

Sisson, T. W., and Bacon, C. R., 1992, Garnet—high-silica rhyolite trace element partition coefficients measured by ion microprobe: Geochimica et Cosmochimica Acta, v. 56, p. 2133-2136

Sláma, J., Kosler, J., Condon, D.J., Crowely, J.L., Gerdes, A., Hanchar, J.M., Horstwood, M.S.A, Morris, G.A., Nasdala, L., Norberg, N., Schaltegger, U., Schoene, B., Tubrett, M.N., and Whitehouse, M.J., 2008, Plesovice zircon- a new natural reference material for U-Pb and Hf isotopic microanalysis. Chemical Geology, v. 249, n. 1-2, p. 1-35.

Smith, M. Wu, C., 2000, The Geology and genesis of the Bayan Obo Fe-REE-Nb deposit: A review. In Porter, T. M. (ed.) Hydrothermal iron oxide copper-gold and related deposits: A global perspective. AMF, Adelaide, 1, 271–281.

Staude, S., Bons, P.D., and Markl, G., 2009, hydrothermal vein formation by extension-driven dewatering of the middle crust: An example from SW Germany: Earth and Planetary Science Letters, v. 286, p. 387-395.

Thirlwall, M.F., and Anczkiewicz, R., 2004, Multidynamic isotope ratio analysis using MC-ICP-MS and the causes of secular drift in Hf, Nd, and Pb isotope ratios. International Journal of Mass Spectrometry, v. 235, p. 59.

Valley, P. M., Hanchar, J. M., and Whitehouse, M.J., 2009, Direct dating of Fe-oxide (-Cu-Au) mineralization by U-Pb zircon geochronology. Geology v. 37, p. 223-226.

Wasteneys, H., McLelland, J., and Lumbers, S., 1999, Precise zircon geochronology in the Adirondack Lowlands and implications for revising plate-tectonic models of the Central Metasedimentary Belt and Adirondack Mountains, Grenville Province, Ontario and New York: Canadian Journal of Earth Sciences, v. 36, p. 967-984.

Whitney, P.R., and Olmsted, J.F., 1988, Geochemistry and origin of albite gneisses, northeastern Adirondack Mountains, New York: Contributions to Mineralogy and Petrology, v. 99, p. 476–484, doi: 10.1007/BF00371938.

Whitney, P.R., Olmsted, J.F., and New York State Geological, S., 1993, Bedrock geology of the Au Sable Forks quadrangle, northeastern Adirondack Mountains, New York: Albany, N.Y., University of the State of New York, State Education Dept., New York State Museum/Geological Survey.

Wiedenbeck, M., Hanchar, J.M., Peck, W.H., Sylvester, P., Valley, J., Whitehouse, M., Kronz, A., Morishita, Y., Nasdala, L. and 21 others, 2004, Further Characterization of the 91500 zircon crystal. Geostandards and Geoanalysis, 28, 9-39.

Woodhead, J.D., and Hergt, J.M., 2005, A preliminary appraisal of seven natural zircon reference materials for in situ Hf isotopic determination. Geostandards and Geoanalytical Research, v. 29, n. 2, p.183-195.

3-8 DATA REPOSITORY 1

LU-HF ISOTOPIC ANALYSIS OF ZIRCON BY LA-MC-ICPMS: DATA COLLECTION AND REDUCTION

Laser ablation- multicollector- inductively coupled plasma mass spectrometry (LA-MC-ICPMS) Lu-Hf isotopic analyses of zircon were conducted using a high-resolution Finnigan NEPTUNE double focusing MC-ICPMS at Memorial University of Newfoundland. The Neptune was operated in static mode at low mass resolution, and coupled to a GeoLas 193 nm ArF excimer laser. The eight Faraday cup configuration allows for the simultaneous collection of a number of Lu, Yb, and Hf masses as follows: ^{171}Yb (low 4); ^{173}Yb (low 3); ^{174}(Hf+Yb) (low 2); ^{175}Lu (low 1); ^{176}(Hf+Yb+Lu) (axial); ^{177}Hf (high 1); ^{178}Hf (high 2); and ^{179}Hf (high 3).

Each LA-MC-ICPMS analysis consists of 30 seconds of gas background data followed by 60 seconds of ablation, typically using a 50 um laser beam diameter (depending on grain being analyzed and its zonation, a larger or smaller beam diameter may be used), a laser fluence of 5 J/cm^2 and repetition rate of 10 Hz. On-peak integration time is 1 second, thus each analysis typically produces 50-60 isotopic ratios. This results in a precision for the measured ^{176}Hf/^{177}Hf of +/- 1 to 2 ε_{Hf} units. Data were processed off-line using an in-house Excel spreadsheet program, which allows the data to be visually assessed using plots of time *vs.* intensity and time *vs.* isotope ratio. This approach allows detection of changes in ^{176}Hf/^{177}Hf as a function of laser sampling depth within the zircon crystal, and provides the user the ability to selectively integrate different portions of the laser ablation signal.

Accurate $^{176}Hf/^{177}Hf$ ratio determination requires proper handling of the instrument mass bias as well as the ^{176}Lu and ^{176}Yb isobaric interferences on ^{176}Hf (Hawkesworth and Kemp, 2006). Mass bias effects on Hf and Yb were corrected using the exponential law. The mass bias for Hf, β(Hf), was determined using a recommended $^{179}Hf/^{177}Hf$ value of 0.7325 (e.g., Patchett et al., 1981); β(Yb) was determined using $^{173}Yb/^{171}Yb$ and a recommended value of 1.13014 (Segal et al., 2003).

Data were reduced in the following order, based upon user-selected background and sample integration intervals. First, the mean signal intensity of the 30 second gas background was subtracted from the gross signal intensity measured for the same isotope when the laser was firing. These background-corrected signal intensities were then used throughout the following calculations. The signal measured for mass 176 is combination of ^{176}Hf, ^{176}Yb, and ^{176}Lu. In order to determine the ^{176}Hf, the interference for ^{176}Yb and ^{176}Lu must be removed. The ^{176}Yb isobaric interference on ^{176}Hf was determined using the measured, interference-free ^{173}Yb mass, itself corrected for mass bias effects using β(Yb), and the accepted $^{176}Yb/^{173}Yb$ of 0.79383 (Segal et al., 2003), as follows;

$$^{176}Yb_{meas} = {}^{173}Yb_{meas} * \left(\frac{^{176}Yb}{^{173}Yb}\right)_{true} * \left(\frac{M_{173Yb}}{M_{176Yb}}\right)^{\beta(Yb)}$$

where *meas* denotes the measured (background-corrected) signal intensity of the isotope of interest, *true* denotes the recommended isotopic composition, and M_{173X} is the mass of the isotope. The ^{176}Lu isobaric interference on ^{176}Hf was determined using the measured, interference-free ^{175}Lu mass, itself corrected for mass bias effects using β(Yb), and the accepted $^{176}Lu/^{175}Lu$ of 0.2656 (Chu et al., 2002);

$$^{176}Lu_{meas} = {}^{175}Lu_{meas} * \left(\frac{^{176}Lu}{^{175}Lu}\right)_{true} * \left(\frac{M_{175Lu}}{M_{176Lu}}\right)^{\beta(Yb)}$$

Following determination of the ^{176}Lu and ^{176}Yb on the total 176 signal intensity, the mass bias and interference corrected ^{176}Hf/^{177}Hf is calculated as follows;

$$\frac{^{176}Hf}{^{177}Hf}_{corrected} = \left(\frac{^{176}(Hf+Yb+Lu)_{meas} - {}^{176}Yb_{meas} - {}^{176}Lu_{meas}}{^{177}Hf_{meas}}\right) * \left(\frac{M_{176Hf}}{M_{177Hf}}\right)^{\beta(Hf)}$$

^{176}Lu/^{176}Hf and ^{176}Yb/^{176}Hf were calculated using β(Hf), as follows;

$$\frac{^{176}Lu}{^{177}Hf}_{corrected} = \left(\frac{^{176}Lu_{meas}}{^{177}Hf_{meas}}\right) * \left(\frac{M_{176Hf}}{M_{177Hf}}\right)^{\beta(Hf)}$$

$$\frac{^{176}Yb}{^{177}Hf}_{corrected} = \left(\frac{^{176}Yb_{meas}}{^{177}Hf_{meas}}\right) * \left(\frac{M_{176Yb}}{M_{177Hf}}\right)^{\beta(Hf)}$$

Both the mass bias and interference corrections were calculated for each individual replicate measurement to account for both time-dependent mass bias changes as well as natural zonation of Yb/Hf within the sample (Sylvester and Lam, 2007). Outlier rejection of the Hf isotopic ratio for each analysis is done using a 2 standard deviation (2SD)

criterion, while no outlier rejections were performed for $^{176}Lu/^{177}Hf$ and $^{176}Yb/^{177}Hf$ as these ratios often vary within natural zircons. The reported uncertainty is calculated based on the interference and mass bias corrected ratios and is expressed as the 2σ standard error of the mean (2 SE).

Verification of the Yb interference correction:

Due to the relatively high concentration of Yb found in typical natural zircon crystals (up to a few hundred ppm) (Hoskin and Schaltegger, 2003), the interference correction of ^{176}Yb on ^{176}Hf must be able to accommodate a wide range of Yb/Hf ratios. The magnitude of this correction can be as high as 30-40% in some zircon crystals, but more commonly is 20% (Yb/Hf ~0.1) or less. In comparison, the ^{176}Lu correction is typically 0.1% or less. The magnitude of these corrections, expressed as percent of the total 176 signal, for different $^{176}Yb/^{177}Hf$ values is shown in Figure 3-8, using data from 373 zircon samples (measured in house as part of this study and other studies) from low Yb/Hf anorthositic rocks to high Yb/Hf felsic granites and volcanics. There is strong correlation between Yb and Lu contents, and thus interference corrections, in zircon such that large corrections for ^{176}Yb also require large corrections for ^{176}Lu, albeit insignificant relative to the ^{176}Yb correction.

Due to the importance of this correction, the proper Yb isotopic compositions to be used for the interference correction must be determined. The isotopic composition of Yb has been determined using both TIMS (McCulloch et al., 1977; IUPAC, De Bierve and Taylor, 1997; Vervoort et al., 2004; Amelin and Davis, 2005) and MC-ICPMS (Chu

et al., 2002; Segal et al., 2003), and these studies report a range of compositions. The reason for this is unknown, but may reflect using different normalizing ratios or may be a more instrument-specific phenomenon (Kemp et al., 2009). The effects of using different Yb isotopic compositions on the $^{176}Hf/^{177}Hf$ was first evaluated by spiking a pure Hf solution (JMC-14374) with variable amounts of Yb, and using Yb isotopic compositions reported in the literature to perform both the Yb mass bias and ^{176}Yb interference correction. The results of this experiment are shown in Figure 3-9. Recently published Yb isotopic compositions determined by both TIMS and MC-ICPMS produce similar corrected $^{176}Hf/^{177}Hf$ for Yb/Hf ratios typical of zircon (within 1 ε_{Hf} unit of Yb-free analyses), whereas the Yb isotopic compositions of IUPAC and McCulloch et al., 1977 produce under-corrected $^{176}Hf/^{177}Hf$. These results are in agreement with those of Hawkesworth and Kemp (2006) and Kemp et al., 2009, who performed a similar study using Yb spiked JMC-475. An additional test to examine the effects of using different Yb isotopic compositions on the $^{176}Hf/^{177}Hf$ determined using laser ablation was preformed using the reference zircon FC-1, which displays a wide range of Yb/Hf (Fig. 3-10) (Woodhead and Hergt, 2005). Similar to the results of our Yb spiked solution experiment, both the TIMS and MC-ICPMS Yb composition yield similar corrected $^{176}Hf/^{177}Hf$ values with a 1.5 ε_{Hf} unit difference between the values of Chu et al., (2003) and Vervoort et al., 2004 at $^{176}Yb/^{177}Hf$ of ~0.07. Moreover, all studies shown here are in close agreement with the Yb-free analyses of FC-1 obtained by Woodhead and Hergt (2005), within ~1 ε_{Hf} unit at $^{176}Yb/^{177}Hf$ of ~0.07.

In order to evaluate and the accuracy of our LA-MC-ICPMS Hf isotopic analyses on a daily basis, analyses of multiple reference zircons were interspersed with unknowns and ablated under identical conditions. Analyses of reference zircons 91500, FC-1, and Plesovice (collected during the course of this study) are shown in Figure 3-2 of the text and discussed in section 3-4-2. A final check on accuracy is provided by the invariant $^{178}Hf/^{177}Hf$ which acts as an internal monitor of the Hf mass bias correction. The $^{178}Hf/^{177}Hf$ for reference zircons analyzed during the course of this study are given in Table 3-6. These values fall in range of those (1.46734 ± 17) reported by Thirlwall and Anczkiewicz (2004).

REFERENCES

Amelin, Y., and Davis, W.J., 2004, Geochemical test for branching decay of 176Lu: Geochim. Cosmochim. Acta, v. 69, p. 465-473.

Chu, N., Taylor, R.N., Chavagnac, V., Nesbitt, R.W., Boella, R.M., Milton, J.A., German, C.R., Bayon, G., and Burton, K., 2002, Hf isotope ratio analysis using multi-collector inductively coupled plasma mass spectrometry: an evaluation of isobaric interference corrections: Journal of Analytical Atomic Spectrometry, v. 17, p. 1567-1574.

De Bievre, P., and Taylor, P.D.P., 1993, Table of the isotopic composition of the elements: Int. J. Mass Spectrom. Ion Process. , v.123, p. 149.

Hawkesworth, C.J., and Kemp, A.I.S., 2006, Using hafnium and oxygen isotopes in zircons to unravel the record of crustal evolution. Chemical Geology, v. 226, p. 144.

Hoskin, P.W.O., and Schaltegger, U., 2003, The Composition of Zircon and Igneous and Metamorphic Petrogenesis: Reviews in Mineralogy and Geochemistry, v. 53, p. 27-62.

Kemp, A.I.S., Foster, G.L., Schersten, A., Whitehouse, M.J., Darling, J., C. Storey, 2009, Concurrent Pb-Hf isotope analysis of zircon by laser ablation multi-collector ICP-MS, with implication for the crustal evolution of Greenland and the Himalayas: Chemical Geology, v. 261, p. 244-260.

McCulloch, M.T., Rosman, K.J.R., and De Laeter, J.R., 1977, The isotopic and elemental abundance of ytterbium in meteorites and terrestrial samples: Geochimica. Cosmochimica et Acta, v. 41, p. 1703-1707.

Patchett, P.J., Kuovo, O., Hedge, C.E., Tatsumoto, M.,, 1981, Evolution of the continental crust and mantle heterogeneity: evidence from Hf isotoptes: Contributions to Mineralogy and Petrology, v. 78, p. 279-297..

Segal, I., Halicz, L., and Platzner, I.T., 2003, Accurate isotope ratio measurements of ytterbium by multiple collection inductively coupled plasma mass spectrometry applying erbium and hafnium in an improved double external normalization procedure: Journal of Analytical Atomic Spectrometry, v. 18, p. 1217-1223.

Thirlwall, M.F., and Anczkiewicz, R., 2004, Multidynamic isotope ratio analysis using MC-ICP-MS and the causes of secular drift in Hf, Nd, and Pb isotope ratios. International Journal of Mass Spectrometry, v. 235, p. 59.

Vervoort, J.D., Patchett, P.J., Soderlund, U., and Baker, M., 2004, Isotopic composition of Yb and the determination of Lu concentrations and Lu/Hf by isotope dilution using MC-ICPMS: Geochemistry, Geophysics, Geosystems, v. 5, p. 1-15.

Woodhead, J.D., and Hergt, J.M., 2005, A preliminary appraisal of seven natural zircon reference materials for in situ Hf isotope determination: Geostandards and Geoanalytical Research, v. 29, p. 183-195.

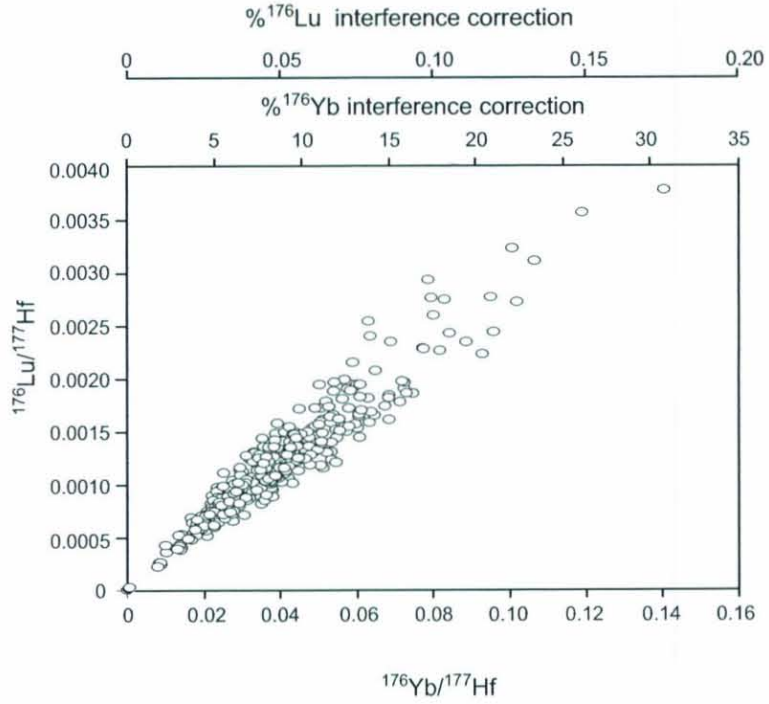

Figure 3-8. $^{176}Yb/177Hf$ vs. $^{176}Lu/177Hf$ for 373 zircon analyses from a wide range of rock types illustrating the magnitude of the ^{176}Yb and ^{176}Lu interference corrections and the correlation of Yb and Lu contents within zircon.

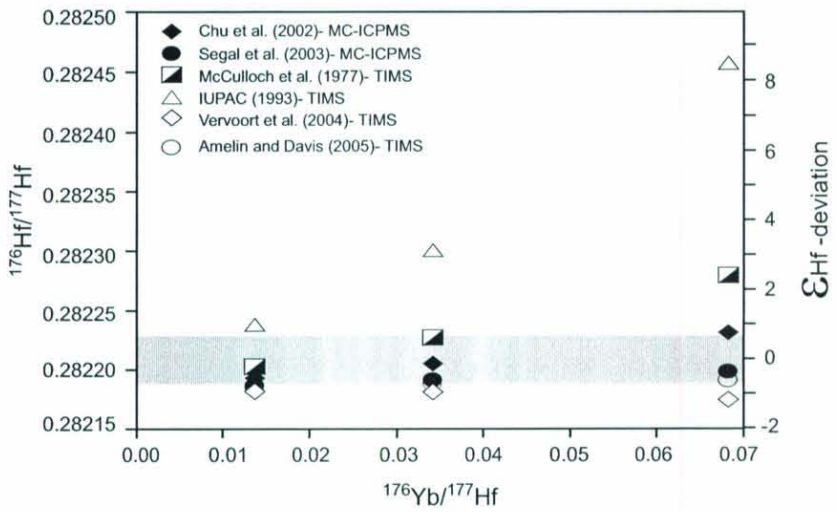

Figure 3-9. Solution MC-ICPMS analyses of JMC-14374 spiked with variable amounts of Yb cover the Yb/Hf range found in typical zircons. Data was reduced using 173Yb/171Yb and 176Yb/171Yb determined from both MC-ICPMS (Chu et al., 2002; Segal et al., 2003) and TIMS studies TIMS (McCulloch et al., 1977; IUPAC, De Bierve and Taylor, 1997; Vervoort et al., 2004; Amelin and Davis, 2005). 176Hf/177Hf was mass bias corrected using the exponential law and 179Hf/177Hf =0.7325. Error bars are omitted for clarity; typical 176Hf/177Hf 2SE for analyses is ± .000008 (~0.3 εHf units). Grey area represents the mean ± 2 standard deviations of unspiked analyses of JMC-14374. Shown on the right-hand y-axis are the results expressed in εHf relative to the unspiked analyses of JMC-14374.

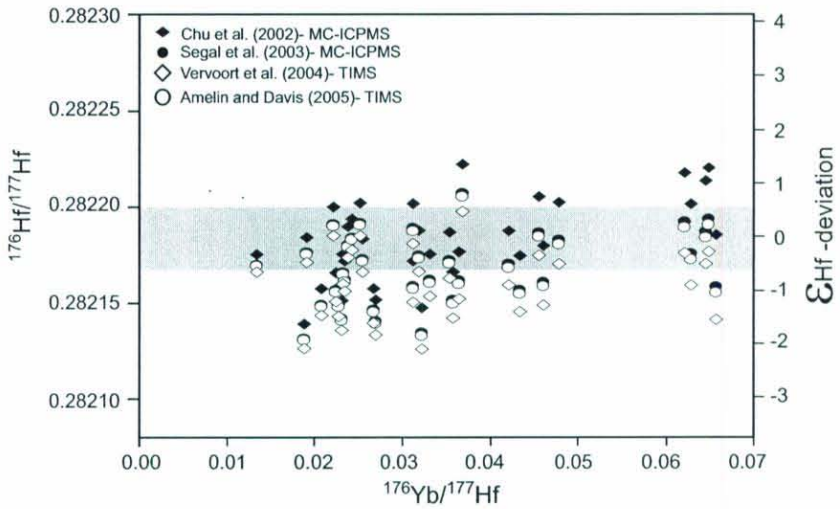

Figure 3-10. LA-MC-ICPMS analyses of FC-1 conducted during the course of this study. Data were reduced using $^{173}Yb/^{171}Yb$ and $^{176}Yb/^{171}Yb$ determined from both MC-ICPMS (Chu et al., 2002; Segal et al., 2003) and TIMS studies (Vervoort et al., 2004; Amelin and Davis, 2005). 176Hf/177Hf was mass bias corrected using the exponential law and 179Hf/177Hf =0.7325. Error bars are omitted f or clarity, typical 176Hf/177Hf 2SE for analyses is ± .000030 (~1 εHf unit). Grey area represents the mean ± 2 standard deviations of Yb free solution analyses of FC-1 from Woodhead and Hergt, 2005. Shown on the right-hand y-axis are the results expressed in εHf relative to the Yb free solution analyses of Woodhead and Hergt, 2005.

Table 3-6 Analytical Standards

File name Plesovice	max 178Hf signal (V)	176Hf/177Hf	2SE	176Lu/177Hf	2SE	176Yb/177Hf	2SE	178Hf/177Hf	2SE
PL.1	3.7	0.282484	0.000026	0.000089	0.000001	0.004444	0.000030	1.467441	0.000049
PL.2	3.7	0.282496	0.000032	0.000086	0.000002	0.004291	0.000068	1.467466	0.000046
PL.3	3.6	0.282509	0.000024	0.000096	0.000001	0.004836	0.000090	1.467448	0.000038
PL.4	3.6	0.282510	0.000032	0.000100	0.000001	0.004912	0.000079	1.467478	0.000044
PL.5	4.6	0.282461	0.000022	0.000076	0.000002	0.004286	0.000159	1.467485	0.000036
PL.6	5.2	0.282476	0.000024	0.000066	0.000000	0.003712	0.000019	1.467461	0.000033
PL.7	3.6	0.282459	0.000032	0.000057	0.000001	0.003107	0.000023	1.467460	0.000041
PL.8	3.5	0.282451	0.000028	0.000091	0.000001	0.005005	0.000094	1.467436	0.000056
PL.9	3.3	0.282482	0.000032	0.000093	0.000001	0.004641	0.000072	1.467312	0.000050
PL.10	3.1	0.282457	0.000034	0.000146	0.000001	0.007145	0.000075	1.467354	0.000046
PL.11	3.2	0.282472	0.000027	0.000143	0.000004	0.006967	0.000221	1.467329	0.000047
PL.12	4.4	0.282454	0.000022	0.000144	0.000001	0.007168	0.000056	1.467359	0.000038
PL.13	4.3	0.282496	0.000026	0.000151	0.000001	0.007487	0.000060	1.467352	0.000036
PL.14	4.3	0.282480	0.000028	0.000143	0.000001	0.007104	0.000058	1.467373	0.000040
PL.15	4.5	0.282446	0.000028	0.000143	0.000001	0.007200	0.000063	1.467337	0.000046
PL.16	4.4	0.282454	0.000026	0.000141	0.000001	0.007070	0.000050	1.467345	0.000039
PL.17	4.3	0.282470	0.000026	0.000110	0.000001	0.005527	0.000102	1.467342	0.000031
PL.18	5.8	0.282482	0.000018	0.000121	0.000000	0.005293	0.000029	1.467204	0.000035
PL.19	4.7	0.282474	0.000017	0.000095	0.000000	0.004339	0.000057	1.467251	0.000038
PL.20	4.8	0.282496	0.000017	0.000106	0.000000	0.004708	0.000036	1.467257	0.000036
PL.21	4.7	0.282470	0.000028	0.000082	0.000001	0.003738	0.000068	1.467252	0.000040
PL.22	4.3	0.282476	0.000027	0.000104	0.000001	0.004800	0.000020	1.467249	0.000043
PL.23	4.1	0.282505	0.000031	0.000098	0.000000	0.004589	0.000041	1.467266	0.000050
PL.24	3.9	0.282504	0.000027	0.000102	0.000001	0.004712	0.000028	1.467238	0.000033
PL.25	4.1	0.282487	0.000023	0.000086	0.000000	0.003832	0.000020	1.467249	0.000036
PL.26	4.2	0.282479	0.000019	0.000077	0.000000	0.003363	0.000038	1.467244	0.000035
PL.27	3.9	0.282504	0.000027	0.000102	0.000001	0.004712	0.000028	1.467238	0.000033
PL.28	4.1	0.282487	0.000023	0.000086	0.000000	0.003832	0.000020	1.467249	0.000036
PL.29	4.2	0.282479	0.000019	0.000077	0.000000	0.003363	0.000038	1.467244	0.000035
PL.31	4.5	0.282501	0.000022	0.000142	0.000001	0.006027	0.000024	1.467176	0.000038
PL.32	4.5	0.282506	0.000022	0.000125	0.000001	0.005209	0.000025	1.467249	0.000043
PL.33	4.7	0.282487	0.000017	0.000103	0.000000	0.004225	0.000017	1.467213	0.000036
PL.34	3.8	0.282474	0.000020	0.000107	0.000001	0.004446	0.000047	1.467189	0.000033
PL.35	6.3	0.282497	0.000015	0.000109	0.000001	0.004400	0.000018	1.467203	0.000034
PL.36	5.6	0.282478	0.000017	0.000099	0.000000	0.004058	0.000029	1.467191	0.000030
PL.37	5.3	0.282490	0.000015	0.000060	0.000000	0.002454	0.000029	1.467207	0.000035
PL.38	5.3	0.282466	0.000020	0.000063	0.000000	0.002585	0.000011	1.467228	0.000033
PL.39	5.2	0.282499	0.000020	0.000109	0.000000	0.004535	0.000016	1.467195	0.000036
PL.40	6.1	0.282482	0.000019	0.000151	0.000001	0.006027	0.000018	1.467218	0.000036
PL.41	5.7	0.282492	0.000015	0.000134	0.000000	0.005392	0.000013	1.467209	0.000032
PL.42	6.2	0.282470	0.000017	0.000111	0.000001	0.004445	0.000015	1.467226	0.000036
PL.43	4.8	0.282474	0.000015	0.000176	0.000001	0.006979	0.000017	1.467213	0.000040
PL.44	4.8	0.282478	0.000021	0.000198	0.000001	0.007763	0.000021	1.467222	0.000029
PL.45	8.2	0.282486	0.000019	0.000180	0.000000	0.007182	0.000021	1.467257	0.000028
PL.46	7.4	0.282473	0.000019	0.000154	0.000002	0.006141	0.000048	1.467223	0.000027
PL.47	6.5	0.282487	0.000023	0.000172	0.000000	0.006885	0.000016	1.467221	0.000031
PL.48	5.9	0.282491	0.000021	0.000137	0.000000	0.005424	0.000036	1.467193	0.000033
PL.49	5.4	0.282463	0.000025	0.000169	0.000001	0.006621	0.000025	1.467207	0.000033
PL.50	5.1	0.282458	0.000020	0.000131	0.000000	0.005150	0.000030	1.467196	0.000036

Table 3-6 continued

File name Plesovice	max 178Hf signal (V)	176Hf/177Hf	2SE	176Lu/177Hf	2SE	176Yb/177Hf	2SE	178Hf/177Hf	2SE
PL.51	5.4	0.282518	0.000024	0.000128	0.000001	0.004994	0.000020	1.467228	0.000043
PL.52	4.6	0.282473	0.000027	0.000157	0.000001	0.006135	0.000067	1.467202	0.000037
PL.53	4.6	0.282512	0.000030	0.000148	0.000001	0.005685	0.000047	1.467180	0.000043
PL.54	4.8	0.282524	0.000029	0.000169	0.000000	0.006576	0.000045	1.467213	0.000042
PL.55	5.4	0.282475	0.000029	0.000103	0.000001	0.004202	0.000018	1.467230	0.000036
PL.56	5.2	0.282501	0.000022	0.000087	0.000001	0.003559	0.000056	1.467215	0.000033
PL.57	5.2	0.282496	0.000027	0.000119	0.000000	0.004958	0.000032	1.467252	0.000036
PL.58	5.6	0.282482	0.000022	0.000127	0.000001	0.005102	0.000026	1.467211	0.000038
PL.59	4.8	0.282501	0.000027	0.000149	0.000000	0.006145	0.000023	1.467197	0.000040
PL.60	4.7	0.282482	0.000023	0.000119	0.000000	0.004744	0.000014	1.467205	0.000041
PL.61	4.8	0.282478	0.000022	0.000114	0.000000	0.005732	0.000048	1.467297	0.000042
PL.62	4.7	0.282462	0.000030	0.000077	0.000001	0.003936	0.000084	1.467276	0.000038
PL.63	4.5	0.282481	0.000026	0.000117	0.000001	0.005898	0.000036	1.467271	0.000038
PL.64	4.0	0.282489	0.000033	0.000188	0.000001	0.009869	0.000109	1.467290	0.000044
PL.65	4.1	0.282447	0.000028	0.000118	0.000000	0.005747	0.000062	1.467360	0.000046
PL.66	4.0	0.282470	0.000027	0.000096	0.000000	0.004676	0.000047	1.467383	0.000037
PL.67	4.0	0.282463	0.000023	0.000118	0.000001	0.005706	0.000034	1.467352	0.000038
PL.68	3.8	0.282462	0.000037	0.000108	0.000002	0.005356	0.000143	1.467385	0.000036
PL.69	3.9	0.282467	0.000025	0.000113	0.000000	0.005567	0.000041	1.467407	0.000036
PL.70	4.0	0.282461	0.000019	0.000103	0.000000	0.005093	0.000028	1.467345	0.000036
PL.71	3.8	0.282460	0.000023	0.000155	0.000001	0.007216	0.000087	1.467364	0.000053
PL.72	3.9	0.282463	0.000026	0.000148	0.000001	0.006833	0.000073	1.467354	0.000038
PL.73	3.6	0.282464	0.000025	0.000096	0.000001	0.004682	0.000024	1.467394	0.000044
PL.74	3.6	0.282458	0.000028	0.000115	0.000001	0.005550	0.000071	1.467423	0.000038
PL.75	3.4	0.282487	0.000031	0.000113	0.000002	0.005296	0.000110	1.467392	0.000038
PL.76	3.5	0.282478	0.000025	0.000100	0.000001	0.004795	0.000063	1.467441	0.000047
PL.78	5.0	0.282484	0.000020	0.000172	0.000001	0.006760	0.000031	1.467234	0.000032
PL.79	5.2	0.282462	0.000018	0.000172	0.000000	0.006864	0.000035	1.467203	0.000030
PL.80	5.2	0.282493	0.000016	0.000167	0.000001	0.006659	0.000023	1.467222	0.000029
PL.81	4.8	0.282495	0.000021	0.000198	0.000000	0.007800	0.000040	1.467208	0.000034
PL.82	5.0	0.282484	0.000020	0.000162	0.000000	0.006420	0.000024	1.467209	0.000037
PL.83	3.5	0.282497	0.000026	0.000167	0.000001	0.006574	0.000053	1.467183	0.000035
PL.85	4.7	0.282485	0.000022	0.000138	0.000001	0.005086	0.000028	1.467231	0.000040
PL.86	4.8	0.282499	0.000021	0.000140	0.000001	0.005183	0.000029	1.467206	0.000034
PL.87	4.8	0.282492	0.000024	0.000169	0.000000	0.006406	0.000029	1.467261	0.000037
PL.88	4.7	0.282449	0.000022	0.000116	0.000001	0.004534	0.000033	1.467183	0.000038
PL.89	5.5	0.282499	0.000024	0.000096	0.000001	0.003799	0.000048	1.467222	0.000036
PL.90	6.5	0.282466	0.000026	0.000086	0.000000	0.003405	0.000031	1.467235	0.000040
PL.91	6.5	0.282459	0.000029	0.000097	0.000000	0.003819	0.000030	1.467243	0.000038
PL.92	5.7	0.282503	0.000025	0.000103	0.000001	0.005472	0.000058	1.467255	0.000038
PL.93	5.7	0.282487	0.000028	0.000119	0.000001	0.006258	0.000085	1.467253	0.000034
PL.94	5.8	0.282493	0.000021	0.000112	0.000001	0.005841	0.000030	1.467209	0.000033
PL.95	5.2	0.282480	0.000023	0.000147	0.000000	0.007472	0.000076	1.467205	0.000036
PL.96	4.9	0.282459	0.000029	0.000138	0.000000	0.006938	0.000061	1.467192	0.000032
PL.97	5.8	0.282463	0.000017	0.000130	0.000001	0.005876	0.000079	1.467218	0.000034
PL.98	5.2	0.282473	0.000019	0.000132	0.000001	0.005992	0.000036	1.467184	0.000038
PL.99	5.1	0.282481	0.000018	0.000148	0.000000	0.006559	0.000042	1.467164	0.000035
PL.100	4.9	0.282489	0.000021	0.000124	0.000000	0.005655	0.000049	1.467167	0.000036
PL.102	4.7	0.282494	0.000021	0.000121	0.000001	0.005634	0.000037	1.467210	0.000039

Table 3-6 continued

File name Plesovice	max 178Hf signal (V)	176Hf/177Hf	2SE	176Lu/177Hf	2SE	176Yb/177Hf	2SE	178Hf/177Hf	2SE
PL.103	5.1	0.282500	0.000018	0.000152	0.000000	0.006779	0.000038	1.467234	0.000042
PL.104	4.4	0.282489	0.000028	0.000101	0.000001	0.004752	0.000039	1.467197	0.000039
PL.105	5.1	0.282509	0.000018	0.000093	0.000001	0.004328	0.000014	1.467218	0.000037
PL.106	4.8	0.282474	0.000020	0.000088	0.000000	0.004112	0.000028	1.467214	0.000039
PL.107	4.9	0.282499	0.000022	0.000070	0.000000	0.003311	0.000032	1.467208	0.000035
PL.108	4.2	0.282486	0.000033	0.000111	0.000001	0.005467	0.000029	1.467194	0.000042
PL.109	4.4	0.282515	0.000025	0.000088	0.000000	0.004042	0.000066	1.467218	0.000040
PL.110	4.3	0.282480	0.000024	0.000148	0.000000	0.006633	0.000061	1.467199	0.000041
PL.111	5.1	0.282482	0.000020	0.000123	0.000001	0.005724	0.000088	1.467203	0.000031
PL.112	5.0	0.282502	0.000016	0.000103	0.000001	0.004886	0.000032	1.467174	0.000034
PL.114	4.0	0.282488	0.000026	0.000105	0.000001	0.006008	0.000049	1.467295	0.000044
PL.115	3.7	0.282487	0.000028	0.000059	0.000000	0.003408	0.000039	1.467269	0.000036
PL.116	3.9	0.282482	0.000029	0.000078	0.000001	0.004588	0.000054	1.467279	0.000040
PL.117	3.8	0.282488	0.000028	0.000081	0.000001	0.004705	0.000068	1.467302	0.000047
PL.118	3.7	0.282481	0.000033	0.000057	0.000000	0.003291	0.000018	1.467309	0.000046
PL.119	3.4	0.282507	0.000031	0.000064	0.000001	0.003696	0.000042	1.467358	0.000045
91500									
H91500.1	1.5	0.282230	0.000066	0.000335	0.000001	0.012917	0.000182	1.467357	0.000081
H91500.2	2.5	0.282235	0.000033	0.000308	0.000001	0.009090	0.000049	1.467239	0.000040
H91500.3	1.9	0.282239	0.000053	0.000335	0.000000	0.012914	0.000128	1.467364	0.000056
H91500.4	2.3	0.282245	0.000039	0.000303	0.000001	0.008800	0.000029	1.467217	0.000042
H91500.5	1.9	0.282247	0.000048	0.000351	0.000001	0.013309	0.000074	1.467416	0.000059
H91500.6	2.6	0.282250	0.000033	0.000292	0.000001	0.008328	0.000055	1.467238	0.000052
H91500.7	2.2	0.282252	0.000040	0.000309	0.000001	0.009844	0.000052	1.467252	0.000042
H91500.8	2.0	0.282255	0.000045	0.000331	0.000001	0.012504	0.000121	1.467365	0.000066
H91500.9	2.7	0.282255	0.000035	0.000349	0.000001	0.009652	0.000067	1.467174	0.000053
H91500.10	3.2	0.282256	0.000024	0.000347	0.000000	0.009947	0.000071	1.467234	0.000039
H91500.11	1.5	0.282257	0.000075	0.000353	0.000001	0.013180	0.000129	1.467335	0.000086
H91500.12	2.8	0.282259	0.000031	0.000345	0.000000	0.009895	0.000069	1.467193	0.000040
H91500.13	2.0	0.282261	0.000055	0.000271	0.000003	0.009330	0.000046	1.467254	0.000051
H91500.14	2.3	0.282262	0.000033	0.000297	0.000001	0.009235	0.000048	1.467217	0.000057
H91500.15	2.1	0.282262	0.000041	0.000307	0.000001	0.009551	0.000048	1.467247	0.000056
H91500.16	2.8	0.282262	0.000027	0.000346	0.000000	0.010100	0.000061	1.467241	0.000048
H91500.17	2.6	0.282262	0.000031	0.000316	0.000001	0.008685	0.000043	1.467251	0.000044
H91500.18	2.4	0.282264	0.000035	0.000302	0.000001	0.008904	0.000065	1.467218	0.000041
H91500.19	2.3	0.282265	0.000037	0.000302	0.000001	0.009539	0.000062	1.467199	0.000054
H91500.20	2.7	0.282265	0.000033	0.000297	0.000001	0.008373	0.000054	1.467216	0.000040
H91500.21	2.5	0.282266	0.000032	0.000303	0.000000	0.008987	0.000045	1.467238	0.000052
H91500.22	2.7	0.282267	0.000030	0.000292	0.000000	0.008625	0.000045	1.467174	0.000048
H91500.23	2.7	0.282267	0.000034	0.000301	0.000000	0.008673	0.000026	1.467240	0.000050
H91500.24	2.7	0.282268	0.000035	0.000293	0.000001	0.008314	0.000051	1.467168	0.000053
H91500.25	2.9	0.282269	0.000030	0.000277	0.000000	0.007922	0.000067	1.467243	0.000050
H91500.26	2.5	0.282269	0.000032	0.000287	0.000001	0.008486	0.000057	1.467157	0.000043
H91500.27	1.7	0.282270	0.000047	0.000277	0.000001	0.009460	0.000058	1.467215	0.000054
H91500.28	2.5	0.282270	0.000031	0.000346	0.000001	0.010026	0.000026	1.467233	0.000049
H91500.29	2.6	0.282271	0.000039	0.000295	0.000000	0.008584	0.000043	1.467238	0.000053
H91500.30	1.9	0.282271	0.000037	0.000251	0.000006	0.008585	0.000120	1.467218	0.000060
H91500.31	2.2	0.282272	0.000050	0.000333	0.000000	0.012778	0.000110	1.467311	0.000068

Table 3-6 continued

File name 91500	max 178Hf signal (V)	176Hf/177Hf	2SE	176Lu/177Hf	2SE	176Yb/177Hf	2SE	178Hf/177Hf	2SE
H91500.32	2.8	0.282274	0.000032	0.000288	0.000000	0.008166	0.000042	1.467226	0.000049
H91500.33	2.9	0.282274	0.000032	0.000287	0.000000	0.008210	0.000106	1.467244	0.000041
H91500.34	2.4	0.282275	0.000031	0.000321	0.000001	0.008777	0.000025	1.467238	0.000054
H91500.35	2.3	0.282275	0.000036	0.000293	0.000000	0.009206	0.000048	1.467221	0.000038
H91500.36	2.3	0.282276	0.000035	0.000300	0.000001	0.009339	0.000035	1.467201	0.000053
H91500.37	2.3	0.282277	0.000038	0.000299	0.000000	0.009326	0.000042	1.467245	0.000050
H91500.38	2.2	0.282278	0.000044	0.000295	0.000000	0.009047	0.000044	1.467243	0.000052
H91500.39	2.9	0.282278	0.000040	0.000296	0.000000	0.008154	0.000055	1.467277	0.000052
H91500.40	2.7	0.282279	0.000031	0.000294	0.000000	0.008340	0.000038	1.467245	0.000061
H91500.41	2.2	0.282279	0.000030	0.000294	0.000000	0.009032	0.000047	1.467242	0.000053
H91500.42	2.9	0.282280	0.000039	0.000280	0.000002	0.007965	0.000069	1.467230	0.000050
H91500.43	1.7	0.282280	0.000057	0.000132	0.000002	0.005453	0.000117	1.467302	0.000073
H91500.44	2.7	0.282281	0.000036	0.000295	0.000002	0.008627	0.000048	1.467206	0.000045
H91500.45	2.6	0.282281	0.000039	0.000294	0.000000	0.008391	0.000038	1.467220	0.000048
H91500.46	2.7	0.282282	0.000030	0.000285	0.000000	0.008199	0.000050	1.467236	0.000049
H91500.47	3.1	0.282282	0.000029	0.000309	0.000001	0.008498	0.000029	1.467238	0.000045
H91500.48	3.3	0.282283	0.000031	0.000322	0.000001	0.008865	0.000045	1.467228	0.000040
H91500.49	2.4	0.282284	0.000033	0.000155	0.000001	0.005356	0.000127	1.467294	0.000049
H91500.50	2.6	0.282284	0.000032	0.000295	0.000000	0.008312	0.000042	1.467249	0.000046
H91500.51	2.7	0.282284	0.000030	0.000344	0.000000	0.009687	0.000052	1.467265	0.000058
H91500.52	2.7	0.282284	0.000032	0.000343	0.000000	0.009825	0.000079	1.467195	0.000056
H91500.53	1.3	0.282285	0.000065	0.000354	0.000001	0.013303	0.000140	1.467379	0.000084
H91500.54	2.3	0.282285	0.000033	0.000300	0.000001	0.008677	0.000033	1.467244	0.000057
H91500.55	2.6	0.282285	0.000038	0.000347	0.000001	0.009940	0.000038	1.467218	0.000048
H91500.56	2.4	0.282286	0.000033	0.000307	0.000001	0.009055	0.000046	1.467214	0.000051
H91500.57	2.8	0.282286	0.000030	0.000285	0.000000	0.008209	0.000056	1.467248	0.000054
H91500.58	2.5	0.282286	0.000030	0.000296	0.000000	0.008619	0.000032	1.467227	0.000057
H91500.59	2.7	0.282286	0.000030	0.000349	0.000001	0.009648	0.000049	1.467259	0.000050
H91500.60	2.8	0.282286	0.000028	0.000291	0.000001	0.008242	0.000055	1.467208	0.000048
H91500.61	2.9	0.282286	0.000035	0.000284	0.000000	0.008161	0.000066	1.467220	0.000046
H91500.62	1.5	0.282286	0.000061	0.000352	0.000001	0.013497	0.000187	1.467309	0.000065
H91500.63	2.7	0.282288	0.000031	0.000321	0.000000	0.008714	0.000044	1.467239	0.000057
H91500.64	2.7	0.282288	0.000028	0.000289	0.000001	0.008502	0.000043	1.467259	0.000045
H91500.65	2.8	0.282288	0.000035	0.000280	0.000002	0.007949	0.000036	1.467234	0.000055
H91500.66	2.6	0.282289	0.000035	0.000290	0.000000	0.008518	0.000073	1.467239	0.000045
H91500.67	2.8	0.282289	0.000031	0.000291	0.000000	0.008481	0.000050	1.467228	0.000048
H91500.68	2.7	0.282289	0.000027	0.000346	0.000000	0.009867	0.000046	1.467184	0.000052
H91500.69	2.8	0.282289	0.000041	0.000285	0.000000	0.008044	0.000051	1.467224	0.000047
H91500.70	2.6	0.282290	0.000032	0.000341	0.000000	0.009818	0.000057	1.467174	0.000057
H91500.71	2.3	0.282290	0.000028	0.000291	0.000000	0.009040	0.000059	1.467264	0.000052
H91500.72	2.7	0.282290	0.000033	0.000344	0.000001	0.010004	0.000060	1.467226	0.000038
H91500.73	2.3	0.282290	0.000026	0.000296	0.000000	0.009209	0.000051	1.467312	0.000052
H91500.74	2.6	0.282292	0.000031	0.000344	0.000001	0.009977	0.000052	1.467219	0.000049
H91500.75	2.2	0.282292	0.000034	0.000291	0.000001	0.009071	0.000050	1.467223	0.000050
H91500.76	2.6	0.282293	0.000030	0.000342	0.000000	0.009722	0.000085	1.467223	0.000044
H91500.77	2.8	0.282293	0.000034	0.000291	0.000001	0.008143	0.000057	1.467200	0.000045
H91500.78	3.0	0.282293	0.000026	0.000279	0.000000	0.007716	0.000070	1.467184	0.000057
H91500.79	2.7	0.282293	0.000037	0.000292	0.000000	0.008222	0.000057	1.467269	0.000042
H91500.80	2.6	0.282294	0.000035	0.000299	0.000000	0.008524	0.000047	1.467254	0.000047

Table 3-6 continued

File name 91500	max 178Hf signal (V)	176Hf/177Hf	2SE	176Lu/177Hf	2SE	176Yb/177Hf	2SE	178Hf/177Hf	2SE
H91500.81	2.8	0.282294	0.000031	0.000317	0.000000	0.008670	0.000025	1.467259	0.000052
H91500.82	2.8	0.282294	0.000024	0.000304	0.000001	0.008599	0.000027	1.467222	0.000053
H91500.83	2.7	0.282294	0.000034	0.000344	0.000000	0.009893	0.000065	1.467243	0.000052
H91500.84	2.7	0.282294	0.000028	0.000342	0.000000	0.009734	0.000046	1.467202	0.000052
H91500.85	2.7	0.282294	0.000032	0.000277	0.000001	0.007818	0.000049	1.467246	0.000046
H91500.86	1.5	0.282295	0.000056	0.000125	0.000001	0.005232	0.000082	1.467318	0.000062
H91500.87	3.0	0.282296	0.000029	0.000304	0.000000	0.008700	0.000029	1.467242	0.000052
H91500.88	2.6	0.282296	0.000026	0.000296	0.000000	0.008656	0.000038	1.467243	0.000050
H91500.89	2.8	0.282296	0.000032	0.000280	0.000001	0.008136	0.000072	1.467262	0.000043
H91500.90	2.8	0.282296	0.000036	0.000294	0.000000	0.008738	0.000048	1.467228	0.000047
H91500.91	2.5	0.282296	0.000044	0.000340	0.000000	0.009704	0.000054	1.467208	0.000048
H91500.92	2.7	0.282297	0.000035	0.000343	0.000000	0.009790	0.000072	1.467255	0.000060
H91500.93	2.4	0.282297	0.000036	0.000280	0.000000	0.008589	0.000043	1.467289	0.000050
H91500.94	2.6	0.282297	0.000035	0.000348	0.000001	0.009989	0.000060	1.467229	0.000056
H91500.95	2.7	0.282297	0.000032	0.000347	0.000001	0.009812	0.000043	1.467257	0.000038
H91500.96	2.8	0.282298	0.000031	0.000278	0.000000	0.008064	0.000047	1.467243	0.000050
H91500.97	2.8	0.282298	0.000029	0.000276	0.000001	0.007805	0.000091	1.467229	0.000046
H91500.98	2.5	0.282299	0.000035	0.000307	0.000001	0.008944	0.000054	1.467249	0.000053
H91500.99	3.0	0.282299	0.000038	0.000310	0.000002	0.008585	0.000027	1.467203	0.000053
H91500.100	3.1	0.282300	0.000028	0.000329	0.000002	0.009095	0.000043	1.467272	0.000055
H91500.101	2.6	0.282300	0.000028	0.000283	0.000000	0.008190	0.000048	1.467255	0.000052
H91500.102	2.6	0.282300	0.000035	0.000276	0.000001	0.008041	0.000031	1.467238	0.000056
H91500.103	2.2	0.282300	0.000040	0.000305	0.000001	0.009537	0.000062	1.467211	0.000057
H91500.104	2.7	0.282301	0.000033	0.000340	0.000000	0.009618	0.000056	1.467211	0.000052
H91500.105	2.6	0.282302	0.000032	0.000343	0.000000	0.009710	0.000049	1.467235	0.000047
H91500.106	2.5	0.282302	0.000030	0.000326	0.000000	0.008765	0.000034	1.467206	0.000052
H91500.107	2.6	0.282302	0.000035	0.000289	0.000000	0.008193	0.000043	1.467237	0.000044
H91500.108	2.6	0.282302	0.000035	0.000344	0.000001	0.009748	0.000056	1.467246	0.000050
H91500.109	2.7	0.282303	0.000037	0.000292	0.000000	0.008396	0.000052	1.467129	0.000042
H91500.110	2.7	0.282303	0.000032	0.000283	0.000001	0.008042	0.000051	1.467227	0.000043
H91500.111	2.5	0.282303	0.000043	0.000306	0.000001	0.008840	0.000030	1.467179	0.000042
H91500.112	2.8	0.282304	0.000033	0.000296	0.000000	0.008382	0.000042	1.467193	0.000050
H91500.113	2.7	0.282304	0.000032	0.000290	0.000000	0.008477	0.000045	1.467238	0.000049
H91500.114	2.4	0.282305	0.000030	0.000167	0.000001	0.005431	0.000059	1.467280	0.000045
H91500.115	2.3	0.282305	0.000033	0.000297	0.000001	0.009194	0.000071	1.467249	0.000053
H91500.116	2.6	0.282305	0.000026	0.000346	0.000001	0.010615	0.000106	1.467194	0.000053
H91500.117	2.7	0.282305	0.000034	0.000294	0.000001	0.008648	0.000041	1.467199	0.000047
H91500.118	2.6	0.282306	0.000033	0.000293	0.000001	0.008610	0.000028	1.467215	0.000048
H91500.119	2.9	0.282307	0.000029	0.000346	0.000001	0.010628	0.000088	1.467208	0.000041
H91500.120	2.0	0.282307	0.000051	0.000276	0.000001	0.008570	0.000070	1.467205	0.000064
H91500.121	2.8	0.282307	0.000027	0.000283	0.000000	0.007794	0.000046	1.467243	0.000047
H91500.122	2.3	0.282307	0.000042	0.000305	0.000001	0.009538	0.000053	1.467187	0.000049
H91500.123	2.8	0.282308	0.000032	0.000348	0.000001	0.010084	0.000037	1.467296	0.000059
H91500.124	2.8	0.282308	0.000032	0.000297	0.000001	0.008498	0.000070	1.467267	0.000043
H91500.125	2.6	0.282309	0.000033	0.000292	0.000001	0.008290	0.000078	1.467236	0.000053
H91500.126	2.7	0.282309	0.000031	0.000345	0.000001	0.009900	0.000052	1.467245	0.000049
H91500.127	2.4	0.282309	0.000029	0.000303	0.000001	0.009612	0.000042	1.467250	0.000048
H91500.128	2.3	0.282309	0.000026	0.000305	0.000001	0.009631	0.000083	1.467263	0.000055

Table 3-6 continued

File name 91500	max 178Hf signal (V)	176Hf/177Hf	2SE	176Lu/177Hf	2SE	176Yb/177Hf	2SE	178Hf/177Hf	2SE
H91500.130	2.5	0.282310	0.000025	0.000289	0.000000	0.008478	0.000068	1.467208	0.000047
H91500.131	2.9	0.282310	0.000041	0.000307	0.000001	0.008349	0.000029	1.467191	0.000057
H91500.132	2.3	0.282311	0.000037	0.000300	0.000000	0.008937	0.000058	1.467251	0.000060
H91500.133	2.5	0.282311	0.000031	0.000279	0.000000	0.007764	0.000028	1.467265	0.000050
H91500.134	3.0	0.282311	0.000023	0.000345	0.000000	0.010067	0.000120	1.467209	0.000037
H91500.135	2.8	0.282311	0.000034	0.000298	0.000001	0.008547	0.000032	1.467238	0.000046
H91500.136	2.5	0.282311	0.000030	0.000299	0.000000	0.008742	0.000035	1.467205	0.000045
H91500.137	2.2	0.282312	0.000027	0.000310	0.000001	0.009766	0.000048	1.467189	0.000052
H91500.138	2.5	0.282312	0.000031	0.000293	0.000000	0.008460	0.000036	1.467228	0.000050
H91500.139	2.7	0.282312	0.000031	0.000350	0.000001	0.010048	0.000045	1.467172	0.000050
H91500.140	2.0	0.282312	0.000054	0.000338	0.000001	0.012605	0.000070	1.467408	0.000065
H91500.141	3.1	0.282313	0.000028	0.000354	0.000000	0.010320	0.000033	1.467277	0.000046
H91500.142	2.8	0.282313	0.000033	0.000282	0.000001	0.008234	0.000031	1.467178	0.000039
H91500.143	3.0	0.282313	0.000033	0.000320	0.000002	0.008800	0.000031	1.467232	0.000049
H91500.144	2.8	0.282313	0.000033	0.000286	0.000000	0.008188	0.000048	1.467227	0.000053
H91500.145	2.7	0.282313	0.000029	0.000347	0.000001	0.009769	0.000054	1.467242	0.000055
H91500.146	2.8	0.282314	0.000032	0.000297	0.000000	0.008764	0.000036	1.467239	0.000037
H91500.147	1.6	0.282314	0.000043	0.000130	0.000001	0.005316	0.000060	1.467519	0.000062
H91500.148	2.4	0.282314	0.000033	0.000299	0.000001	0.008880	0.000090	1.467209	0.000057
H91500.149	2.6	0.282314	0.000034	0.000339	0.000000	0.009892	0.000052	1.467232	0.000051
H91500.150	2.8	0.282315	0.000029	0.000361	0.000001	0.010605	0.000061	1.467215	0.000045
H91500.151	2.9	0.282316	0.000033	0.000351	0.000001	0.009759	0.000030	1.467226	0.000046
H91500.152	2.2	0.282316	0.000037	0.000317	0.000001	0.009945	0.000037	1.467192	0.000061
H91500.153	3.0	0.282316	0.000028	0.000332	0.000002	0.009268	0.000048	1.467264	0.000050
H91500.154	2.6	0.282316	0.000032	0.000347	0.000001	0.010696	0.000082	1.467227	0.000052
H91500.155	3.2	0.282316	0.000025	0.000303	0.000001	0.008227	0.000029	1.467246	0.000054
H91500.156	2.6	0.282316	0.000036	0.000293	0.000000	0.008459	0.000034	1.467258	0.000049
H91500.157	2.7	0.282316	0.000027	0.000296	0.000000	0.008177	0.000036	1.467231	0.000038
H91500.158	2.7	0.282317	0.000022	0.000296	0.000000	0.008183	0.000052	1.467225	0.000048
H91500.159	2.4	0.282317	0.000036	0.000346	0.000001	0.009969	0.000051	1.467202	0.000057
H91500.160	2.9	0.282317	0.000033	0.000309	0.000000	0.008434	0.000035	1.467217	0.000043
H91500.161	2.9	0.282317	0.000030	0.000344	0.000000	0.009540	0.000057	1.467198	0.000049
H91500.162	2.7	0.282317	0.000029	0.000341	0.000001	0.009410	0.000055	1.467238	0.000055
H91500.163	2.7	0.282317	0.000033	0.000344	0.000000	0.009759	0.000056	1.467240	0.000053
H91500.164	2.4	0.282317	0.000028	0.000299	0.000001	0.009336	0.000056	1.467224	0.000053
H91500.165	2.9	0.282318	0.000028	0.000288	0.000001	0.007999	0.000071	1.467259	0.000046
H91500.166	2.8	0.282318	0.000035	0.000279	0.000000	0.007863	0.000028	1.467219	0.000047
H91500.167	2.3	0.282318	0.000029	0.000299	0.000000	0.009161	0.000063	1.467251	0.000051
H91500.168	2.6	0.282318	0.000029	0.000283	0.000000	0.008003	0.000041	1.467269	0.000046
H91500.169	2.5	0.282319	0.000033	0.000297	0.000001	0.008712	0.000045	1.467199	0.000044
H91500.170	2.8	0.282319	0.000035	0.000294	0.000000	0.008322	0.000031	1.467244	0.000053
H91500.171	2.7	0.282320	0.000032	0.000302	0.000000	0.008949	0.000044	1.467256	0.000045
H91500.172	1.8	0.282321	0.000037	0.000158	0.000006	0.005304	0.000186	1.467263	0.000067
H91500.173	1.5	0.282321	0.000053	0.000127	0.000001	0.005257	0.000071	1.467324	0.000057
H91500.174	2.9	0.282321	0.000026	0.000276	0.000000	0.007747	0.000043	1.467271	0.000051
H91500.175	2.8	0.282322	0.000034	0.000290	0.000001	0.008404	0.000043	1.467245	0.000047
H91500.176	2.7	0.282322	0.000031	0.000289	0.000000	0.008196	0.000042	1.467174	0.000054
H91500.177	2.4	0.282323	0.000043	0.000302	0.000001	0.009484	0.000071	1.467195	0.000059

Table 3-6 Analytical Standards

File name 91500	max 178Hf signal (V)	176Hf/177Hf	2SE	176Lu/177Hf	2SE	176Yb/177Hf	2SE	178Hf/177Hf	2SE
H91500.179	2.3	0.282323	0.000025	0.000308	0.000001	0.009805	0.000050	1.467251	0.000055
H91500.180	2.4	0.282323	0.000037	0.000292	0.000000	0.008761	0.000042	1.467247	0.000040
H91500.181	2.8	0.282323	0.000021	0.000346	0.000000	0.009732	0.000047	1.467255	0.000044
H91500.182	2.7	0.282324	0.000034	0.000291	0.000000	0.008455	0.000037	1.467249	0.000053
H91500.183	2.6	0.282325	0.000031	0.000291	0.000001	0.008350	0.000042	1.467243	0.000044
H91500.184	2.6	0.282325	0.000025	0.000295	0.000000	0.008703	0.000063	1.467275	0.000058
H91500.185	2.8	0.282325	0.000032	0.000293	0.000000	0.008296	0.000031	1.467221	0.000048
H91500.186	3.0	0.282325	0.000029	0.000314	0.000000	0.008590	0.000043	1.467231	0.000047
H91500.187	2.8	0.282326	0.000027	0.000340	0.000000	0.009688	0.000062	1.467252	0.000040
H91500.188	2.8	0.282326	0.000025	0.000290	0.000000	0.008536	0.000042	1.467195	0.000048
H91500.189	3.0	0.282326	0.000024	0.000356	0.000001	0.010250	0.000032	1.467254	0.000052
H91500.190	1.5	0.282327	0.000050	0.000123	0.000002	0.005115	0.000128	1.467326	0.000068
H91500.191	2.7	0.282327	0.000035	0.000348	0.000001	0.009588	0.000069	1.467226	0.000056
H91500.192	2.7	0.282327	0.000030	0.000286	0.000000	0.008051	0.000045	1.467255	0.000042
H91500.193	2.5	0.282327	0.000025	0.000289	0.000001	0.008506	0.000031	1.467236	0.000042
H91500.194	2.5	0.282328	0.000027	0.000288	0.000000	0.008429	0.000068	1.467171	0.000042
H91500.195	2.7	0.282328	0.000031	0.000344	0.000001	0.009758	0.000040	1.467207	0.000045
H91500.196	2.7	0.282329	0.000028	0.000302	0.000000	0.008632	0.000057	1.467202	0.000046
H91500.197	2.9	0.282331	0.000031	0.000349	0.000000	0.009974	0.000048	1.467269	0.000044
H91500.198	2.7	0.282332	0.000036	0.000344	0.000000	0.009721	0.000065	1.467227	0.000048
H91500.199	1.9	0.282332	0.000046	0.000348	0.000000	0.013238	0.000122	1.467324	0.000054
H91500.200	2.7	0.282333	0.000029	0.000344	0.000000	0.009356	0.000065	1.467242	0.000049
H91500.201	2.5	0.282333	0.000038	0.000293	0.000000	0.008437	0.000047	1.467210	0.000050
H91500.202	2.6	0.282333	0.000023	0.000341	0.000000	0.010565	0.000097	1.467223	0.000051
H91500.203	2.7	0.282334	0.000033	0.000353	0.000001	0.010707	0.000049	1.467206	0.000044
H91500.204	2.4	0.282335	0.000028	0.000208	0.000002	0.006899	0.000048	1.467251	0.000048
H91500.205	3.2	0.282335	0.000035	0.000325	0.000001	0.009209	0.000025	1.467250	0.000034
H91500.206	2.7	0.282336	0.000032	0.000282	0.000000	0.007973	0.000056	1.467245	0.000054
H91500.207	3.0	0.282337	0.000030	0.000294	0.000001	0.008727	0.000032	1.467199	0.000043
H91500.208	1.6	0.282338	0.000047	0.000306	0.000001	0.008675	0.000052	1.467257	0.000059
H91500.209	2.6	0.282339	0.000028	0.000348	0.000001	0.009765	0.000051	1.467256	0.000057
H91500.210	2.2	0.282340	0.000036	0.000298	0.000001	0.009266	0.000071	1.467254	0.000053
H91500.211	2.3	0.282341	0.000033	0.000294	0.000000	0.009093	0.000068	1.467219	0.000050
H91500.212	2.9	0.282341	0.000039	0.000293	0.000000	0.008454	0.000034	1.467197	0.000047
H91500.213	3.1	0.282341	0.000034	0.000313	0.000000	0.008500	0.000028	1.467189	0.000044
H91500.214	2.7	0.282343	0.000036	0.000342	0.000000	0.009734	0.000072	1.467186	0.000048
H91500.215	2.6	0.282344	0.000029	0.000301	0.000000	0.008618	0.000037	1.467260	0.000041
H91500.216	2.7	0.282344	0.000034	0.000343	0.000001	0.009418	0.000048	1.467246	0.000047
H91500.217	3.1	0.282344	0.000030	0.000282	0.000001	0.007899	0.000047	1.467268	0.000051
H91500.218	3.0	0.282344	0.000026	0.000310	0.000001	0.008521	0.000032	1.467262	0.000044
H91500.219	2.7	0.282345	0.000034	0.000285	0.000000	0.008320	0.000046	1.467243	0.000055
H91500.220	2.8	0.282345	0.000025	0.000291	0.000000	0.008506	0.000042	1.467250	0.000047
H91500.221	2.7	0.282345	0.000033	0.000293	0.000001	0.008528	0.000038	1.467259	0.000047
H91500.222	2.8	0.282346	0.000034	0.000283	0.000000	0.008019	0.000063	1.467211	0.000051
H91500.223	2.6	0.282349	0.000028	0.000290	0.000000	0.008398	0.000045	1.467235	0.000046
H91500.224	2.3	0.282354	0.000037	0.000306	0.000001	0.009596	0.000063	1.467199	0.000058
H91500.225	2.2	0.282355	0.000043	0.000291	0.000001	0.009072	0.000058	1.467230	0.000052
H91500.226	2.2	0.282357	0.000036	0.000300	0.000000	0.009265	0.000040	1.467315	0.000057

Table 3-6 continued

File name 91500	max 178Hf signal (V)	176Hf/177Hf	2SE	176Lu/177Hf	2SE	176Yb/177Hf	2SE	178Hf/177Hf	2SE
H91500.228	2.3	0.282359	0.000031	0.000337	0.000001	0.010318	0.000050	1.467241	0.000059
H91500.229	2.2	0.282370	0.000039	0.000310	0.000001	0.009728	0.000067	1.467211	0.000047
FC1									
FC1.1	5.6	0.282170	0.000023	0.000535	0.000018	0.013502	0.000458	1.467262	0.000040
FC1.2	4.7	0.282187	0.000035	0.002299	0.000142	0.064732	0.004046	1.467235	0.000035
FC1.3	5.0	0.282183	0.000026	0.001715	0.000013	0.047975	0.000400	1.467245	0.000040
FC1.4	4.6	0.282187	0.000033	0.001636	0.000016	0.045665	0.000521	1.467247	0.000036
FC1.5	4.4	0.282176	0.000023	0.002390	0.000036	0.062986	0.000870	1.467264	0.000036
FC1.6	4.5	0.282192	0.000028	0.002307	0.000002	0.062288	0.000074	1.467249	0.000048
FC1.7	4.7	0.282159	0.000031	0.002408	0.000002	0.065939	0.000104	1.467253	0.000037
FC1.8	5.4	0.282192	0.000035	0.000925	0.000078	0.025211	0.002164	1.467294	0.000047
FC1.9	6.9	0.282162	0.000036	0.001188	0.000077	0.033315	0.002316	1.467293	0.000050
FC1.10	3.9	0.282173	0.000031	0.000962	0.000004	0.025515	0.000144	1.467275	0.000044
FC1.11	4.0	0.282141	0.000034	0.000998	0.000012	0.027047	0.000344	1.467268	0.000045
FC1.12	4.1	0.282172	0.000035	0.001315	0.000007	0.035535	0.000209	1.467248	0.000047
FC1.13	4.2	0.282175	0.000029	0.001171	0.000015	0.032029	0.000452	1.467239	0.000052
FC1.14	3.5	0.282166	0.000055	0.000876	0.000010	0.023302	0.000309	1.467310	0.000061
FC1.15	3.4	0.282180	0.000029	0.000889	0.000002	0.023876	0.000040	1.467241	0.000052
FC1.16	3.9	0.282149	0.000023	0.000789	0.000009	0.020867	0.000259	1.467274	0.000047
FC1.17	3.5	0.282142	0.000032	0.000850	0.000011	0.023164	0.000346	1.467275	0.000048
FC1.19	4.5	0.282147	0.000021	0.000986	0.000015	0.026793	0.000422	1.467304	0.000040
FC1.20	3.8	0.282194	0.000027	0.002404	0.000009	0.065060	0.000139	1.467302	0.000055
FC1.21	4.4	0.282162	0.000020	0.000846	0.000006	0.023472	0.000148	1.467242	0.000040
FC1.22	3.8	0.282131	0.000025	0.000689	0.000014	0.018948	0.000345	1.467262	0.000045
FC1.23	3.5	0.282157	0.000032	0.001600	0.000103	0.043479	0.002750	1.467270	0.000052
FC1.24	3.5	0.282159	0.000034	0.001136	0.000101	0.031385	0.002829	1.467227	0.000043
FC1.25	3.6	0.282191	0.000037	0.000813	0.000010	0.022219	0.000274	1.467246	0.000054
FC1.26	4.2	0.282157	0.000045	0.000817	0.000001	0.022521	0.000099	1.467223	0.000050
FC1.27	3.5	0.282189	0.000036	0.001120	0.000004	0.031389	0.000156	1.467257	0.000044
FC1.28	3.6	0.282162	0.000032	0.001289	0.000001	0.036642	0.000122	1.467257	0.000038
FC1.29	3.6	0.282149	0.000053	0.000843	0.000002	0.022803	0.000048	1.467214	0.000059
FC1.30	3.6	0.282170	0.000042	0.001501	0.000017	0.042228	0.000588	1.467257	0.000055
FC1.31	3.7	0.282176	0.000037	0.000728	0.000001	0.019215	0.000034	1.467249	0.000041
FC1.32	4.2	0.282134	0.000047	0.001145	0.000001	0.032391	0.000083	1.467234	0.000055
FC1.33	3.3	0.282184	0.000045	0.000907	0.000002	0.024302	0.000039	1.467234	0.000059
FC1.34	3.3	0.282161	0.000049	0.001658	0.000003	0.046179	0.000071	1.467276	0.000054
FC1.35	3.5	0.282207	0.000044	0.001288	0.000001	0.037031	0.000148	1.467259	0.000055

CHAPTER 4

In:

Valley, P.M., Hanchar, J.M. and Whitehouse, M.J. New insights on the evolution of the Lyon Mountain granite and associated magnetite-apatite "Kiruna-type" deposits, Adirondack Mountains, New York State (in press, Geosphere).

NEW INSIGHTS ON THE EVOLUTION OF THE LYON MOUNTAIN GRANITE AND ASSOCIATED "KIRUNA-TYPE" MAGNETITE-APATITE DEPOSITS, ADIRONDACK MOUNTAINS, NEW YORK STATE

Peter M. Valley[1], John M. Hanchar[1], Martin J. Whitehouse[2]

[1]Department of Earth Sciences, Memorial University of Newfoundland

St. John's, NL A1B 3X5

Canada

[2]Laboratory for Isotope Geology, Swedish Museum of Natural History, S-104 05

Stockholm, Sweden

ABSTRACT

The integrated approach of field work, microscopy, whole rock and mineral-scale geochemistry, and in situ U-Th-Pb zircon geochronology have proven to be useful tools for recognizing the type, timing, and sequence, of complex Na and K fluid alteration related to the development of "Kiruna-type" magnetite-apatite deposits and the tectonic evolution of the granites that host these deposits. The Lyon Mountain granite in the northeastern Adirondack Mountains of New York State has experienced multiple episodes of hydrothermal fluid alteration and Fe-mineralization. Perthite granite containing ubiquitous 1060-1050 Ma zircon grains has been overprinted by potassic-

alteration, which in turn has been overprinted by pervasive Na-alteration. During the Na-alteration, preexisting ore bodies consisting of magnetite, clinopyroxene, and apatite, were overprinted and remobilized to form new deposits that contain magnetite, apatite, quartz, and zircon.

Uranium-Th-Pb zircon geochronology data suggests the Lyon Mountain granite intruded the Adirondack Highlands during the Ottawan orogeny between ca. 1060 and 1050 Ma. However, subsequent alteration has obscured much of the pre-history of the LMG. Amphibolite layers within the Lyon Mountain granite and granitic dikes and pegmatites that crosscut the foliation in the Lyon Mountain granite have been dated between 1045 and 1016 Ma. These ages coincide with previous published zircon age data from second-generation ore bodies associated with Na-alteration.

Keywords: magnetite-apatite Kiruna-type deposits, IOA deposits, IOCG deposits, perthite, zircon, U-Pb, geochronology, SIMS, fluid alteration, albitization, Adirondack Mountains, Lyon Mountain Granite, trace elements, accessory minerals

Corresponding author: pvalley@mun.ca

4-1 INTRODUCTION

Low-Ti "Kiruna-type" magnetite-apatite, economic-grade mineral deposits are often included with the class of deposits commonly referred to as Fe-oxide [-Cu-Au] (IOCG) deposits whose characteristics are variable (e.g., Hitzman et al., 1992; Barton and

Johnson, 1996; Corriveau et al., 2007). Some of these deposits contain significant amounts of Cu, Au and U such as those at Olympic Dam, Australia, where the IOCG name is appropriately used (e.g., Reynolds, 2000), whereas in the Norrbotten region of northern Sweden (e.g., Kiirunavaara, Luossavaara, Svappavaara, Malmberget) the ores are comprised mainly of magnetite and apatite (e.g., Hitzman et al., 1992; Harlov et al., 2002) and lack economic concentrations of Cu or Au. Genetic models for the origin of IOCG deposits include two main types; those that are directly related to magmatism, and those related to brines and evaporites (Barton and Johnson, 2004). The deposits that are clearly magmatic are characterized by a direct relation to a particular intrusion (e.g., intermediate to felsic calc-alkaline or alkaline), typically occur in an arc setting, have widespread K-alteration, and are enriched in Au and Cu with moderate amounts of magnetite and few rare earth elements (REE) (e.g., Olympic Dam). Brine-related deposits are characterized by Na, K or acid alteration (sericite and chlorite production), abundant magnetite and apatite, enrichment in REE, and are correlated with the presence of evaporites (e.g., Kiruna). Additionally, brine-related deposits lack a direct connection to any particular intrusive event; however, they still require magmatism to drive hydrothermal fluid circulation in an extensional tectonic setting (Barton and Johnson, 2004). Specifically, the Kiruna-type ores have been debated as being volcanic-sedimentary in origin (Parák, 1975) or magmatic (Frietsch, 1978). In general, many deposits contain evidence for multiple generations of fluid alteration including Na, K, Ca and Si; Fe-mineralization; and trace element enrichment (REE and high field strength

elements [HFSE]) and the remobilization of early-formed ores (e.g., Hitzman et al., 1992).

The magnetite-apatite deposits that occur within the Lyon Mountain Granite (LMG) in the northeastern Adirondack Highlands of New York, USA are similar to the deposits in northern Sweden and lack Cu and Au in economic concentrations, but have high concentrations of REE in some apatite associated with mineralization (Lindberg and Ingram, 1964; Roeder et al., 1987; Valley et al., 2010). Extensive outcrops and relatively easy access make the LMG and its associated ore deposits an ideal natural laboratory for studying the relationships and hydrothermal alteration of the host rocks and the magnetite-apatite Kiruna-type mineralization. Understanding the timing and geochemical evolution of the hydrothermal alteration and related Fe-mineralization, as well as the origin and geologic history of the LMG has important implications for the origins of magnetite-apatite deposits globally, the conditions through which they form, and for further exploration in other locations.

4-1-1 GEOLOGICAL SETTING

The Adirondack Mountains are a 27,000 km^2 area of exposed Proterozoic, Grenville Province rocks in northern New York State. The region is divided into the Adirondack Lowlands in the northwest and the Adirondack Highlands to the east and south (Fig. 4-1). The Adirondack Highlands are separated from the Adirondack Lowlands by the Carthage-Colton shear zone (CCSZ), which is marked by highly ductile fabrics and small granitic intrusions. Tonalite- and granodiorite-composition magmas were emplaced into the southern and eastern Adirondacks in the interval between 1350 to

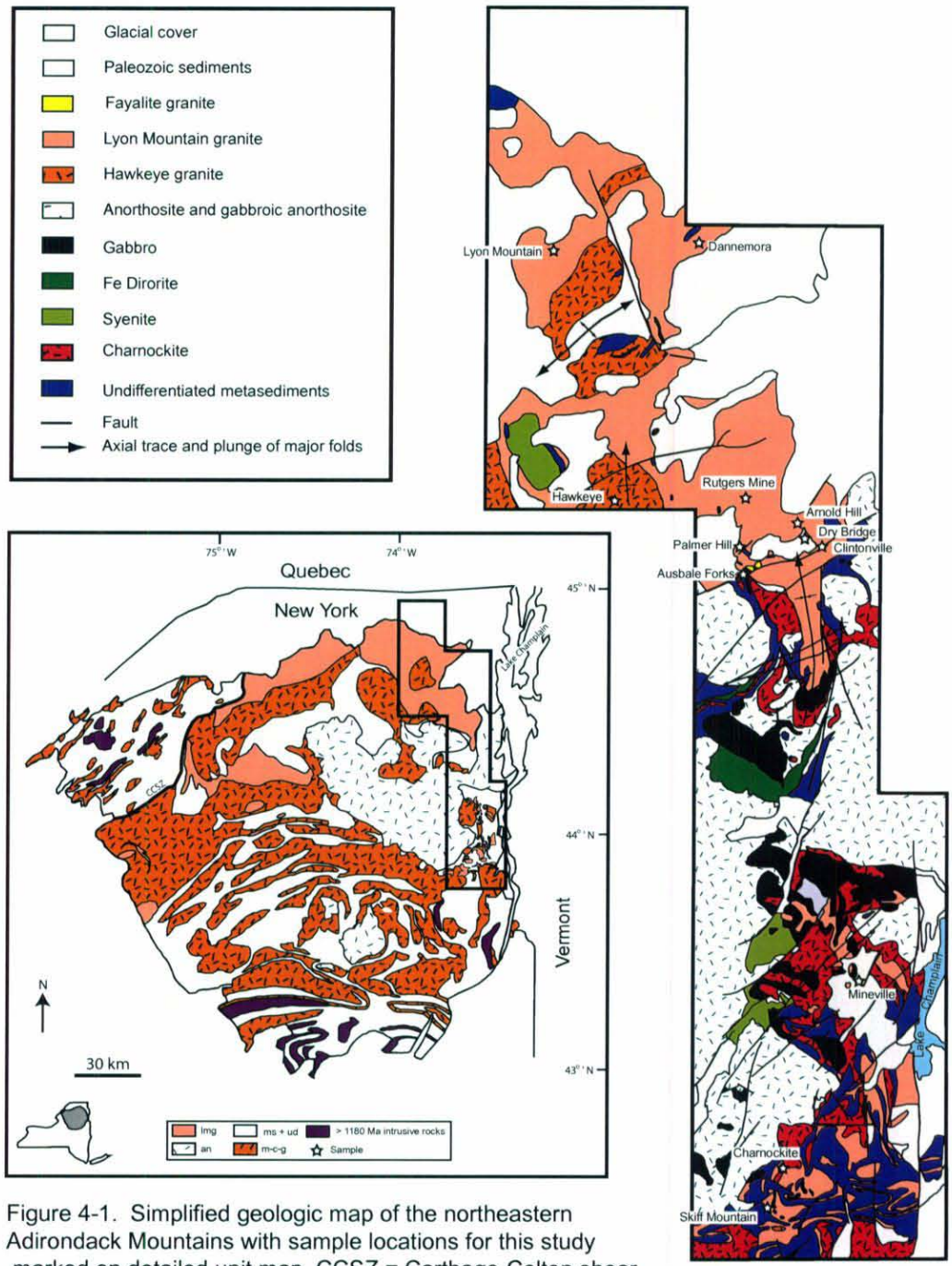

Figure 4-1. Simplified geologic map of the northeastern Adirondack Mountains with sample locations for this study marked on detailed unit map. CCSZ = Carthage-Colton shear zone (modified after Postel, 1952; Isachsen and Fisher, 1970; McLelland and Isachsen, 1985; Whitney and Olmsted, 1993; and Davidson, 1998).

1250 Ma (McLelland and Chiarenzelli, 1988). These rocks are interpreted to be juvenile, arc related, magmas emplaced along an Andean style active margin prior to the onset of the Shawinigan orogeny (e.g., 1210 to 1170 Ma) (McLelland and Chiarenzelli, 1990, Rivers, 1997). Widespread metamorphism and deformation affected the whole of the Adirondacks during the Shawinigan orogeny as a result of the Adirondack-Green Mountain block colliding with the southeast margin of Laurentia (Wasteneys et al., 1999). Immediately following cessation of the contractional phase of the Shawinigan orogeny, extensive anorthosite, mangerite, charnockite and granitic (AMCG) magmas were emplaced into the Adirondack Highlands between 1170 to 1120 Ma (e.g., McLelland et al., 2004; Hamilton et al., 2004). This time period is coincident with amphibolite grade metamorphism in the Adirondack Lowlands. A subsequent period of deformation and metamorphism in the Adirondack Highlands was during the Ottawan phase of the Grenville Orogeny. The timing of Ottawan metamorphism and deformation in the Highlands has been determined to be between 1100 and 1040 Ma based on U-Pb zircon dating of deformed and undeformed intrusions (McLelland et al., 2001). The penetratively deformed Hawkeye granite, dated at 1100 Ma was used as an upper age limit for Ottawan deformation whereas emplacement of the LMG during extension along the CCSZ and elsewhere has been proposed to mark the end of the Ottawan orogeny (Mezger,1990; McLelland et al., 2001; Selleck et al., 2005).

The LMG crops out extensively in the northeastern Adirondack Highlands (Fig.4-1) and is the host to numerous Kiruna-type magnetite-apatite deposits (e.g., Whitney and Olmsted, 1988; McLelland et al., 2002). The LMG experienced widespread K and Na

fluid alteration, accompanied by the addition of F, Cl and P, and mobilization of high field strength elements (HFSE) including Zr, Y, U, and REE during at least one stage of Fe-mineralization (Lindberg and Ingram, 1964; Roeder et al., 1987; Foose and McLelland, 1995). Sample localities for this project include Lyon Mountain, Dannemora, Hawkeye, Ausable Forks (fayalite granite), Palmer Hill, Arnold Hill, Clintonville, Dry Bridge, Rutgers, Mineville, and Skiff Mountain. Some these localities were previously reported in McLelland et al. (2001) (Dannemora, fayalite granite, and Dry Bridge) and McLelland et al. (2002) (Lyon Mountain, Dannemora, and Skiff Mountain). Outcrops of mineralogically similar, and possibly LMG-related, rocks occur throughout the western Adirondack Highlands some of which contain magnetite ore deposits (e.g., Star Lake). These deposits, however, remain to be explored in detail and their similarities (or lack there of) to the ore deposits studied here is unclear. Quartz-sillimanite vein emplacement as a result of fluid alteration is present in some outcrops of the LMG in the western Adirondacks but is rare in the northeastern Adirondacks (Selleck et al., 2004)

4-2 ANALYTICAL METHODS

4-2-1 FIELD WORK

Sampling of the LMG host rock and ores, and other nearby units, was undertaken to quantify the extent of fluid alteration within the LMG and throughout the northeastern Adirondack Highlands. Detailed sampling and mapping was done in and around (i.e., from the host rock to the ore) a number of ore bodies in the LMG to characterize fluid

alteration and Fe-mineralization associated with a given deposit. Similarly, sampling and mapping across contacts between the LMG and neighboring units was undertaken to better understand the origins of the LMG.

4-2-2 CATHODOLUMINESCENCE IMAGING

Cathodoluminescence microscopy was done with a PATCO ELM-3 Cathodoluminoscope at Memorial University. Operating conditions were 12 kV and 0.7mA, a vacuum of 50–70 mTorr, and an unfocused beam. Images were acquired using a KAPPA DX-30C Peltier cooled charge-coupled device (CCD) camera and KAPPA Image software. All CL images were acquired using consistent red-green-blue (RGB) settings so that CL colors could be directly compared between samples.

4-2-3 WHOLE ROCK GEOCHEMISTRY

Whole rock powders were prepared by using a tile saw to remove weathered material, a "chipmunk" jaw crusher (to produce "pea" sized material), a disk mill (set to produce material with a grain size between 500 and 63 micrometers) and an alumina ceramic shatter box to produce pulverized powders in house and subsequently analyzed for major and trace elements by Activation Laboratories Ltd. (Ancaster, Ontario, Canada) for the Actlabs "WRA +trace 4Lithoresearch" analysis package. Reference materials AGV-1 and BCR-1 were also analyzed as unknowns and are included in Table 4-1 (Govindaraju, 1994).

4-2-4 ELECTRON PROBE MICROANALYSIS

Electron microprobe analyses were done using a Cameca SX-51 electron probe microanalyzer (EPMA) with Probe for Windows software at the University of Wisconsin-Madison. Feldspars were analyzed for Si, Al, Fe, Ca, Na, K, and Ba. The operating conditions were an accelerating voltage of 15 kV, a Faraday cup current of 10 nA and a defocused beam of 10 μm. Clinopyroxene and olivine were analyzed for Si, Ti, Al, Fe, Mn, Mg, Ca, Na, K, and Cr, and magnetite was analyzed for Si, Ti, Al, Fe, Mg, Mn, Ca, Cr, V and Zn. The operating conditions for both minerals were an accelerating voltage of 15 kV, a Faraday cup current of 20 nA and a focused beam. Twenty second count-times on peak and background were used for all the elements that were measured. Natural mineral standards were used and the matrix correction algorithm of Armstrong/Love Scott phi-rho-z (Armstrong, 1988) was used for all analyzes.

4-2-5 ZIRCON PROCESSING AND IMAGING

Zircon separation was done using standard crushing (to produce material with a grain size between 500 and 63 micrometers), heavy liquids (bromoform and methylene iodide), and magnetic methods (i.e., Frantz isodynamic magnetic separator). Zircon crystals were hand picked from the non-magnetic fraction and mounted in epoxy resin and polished to reveal the crystal centers. The epoxy mounts were gold coated and imaged with a Hitachi S-4300 scanning electron microscope (SEM) using cathodoluminescence (CL) to identify internal structures and zoning prior to ion probe microanalysis. Back-scattered electron (BSE) imaging was also used to identify fractures

and inclusions within the grains and to identify analytical spot locations precisely after the SIMS analyses were done at Memorial University of Newfoundland using a FEI Quanta 400 environmental SEM. A 20 kV accelerating voltage and 50 nA current were used for BSE imaging.

4-2-6 SECONDARY ION MASS SPECTROMETRY

Uranium-Th-Pb and Pb-Pb zircon data were acquired to determine the ages of the samples in this study using the Cameca IMS 1270 ion microprobe at the Swedish Museum of Natural History (Nordsim) following the methods first described by Whitehouse et al. (1999) and later modified in Whitehouse and Kamber (2005). The calibration of U/Pb is based on the 1065 Ma zircon standard 91500 with U and Pb concentrations of 80 and 15 ppm, respectively (Wiedenbeck et al., 1995). Initial data reductions were done using Excel macros developed at the Swedish Museum of Natural History. Age determinations and errors were calculated using Isoplot version 3.34 (Ludwig, 2003). U-Pb data are plotted as 2σ error ellipses. All age errors quoted in the text are 2σ unless specifically stated otherwise. Common Pb corrections were applied to all ion probe data; an average composition for modern day terrestrial common Pb is assumed (Stacey and Kramers, 1975).

4-3 RESULTS

4-3-1 FIELD RELATIONS, STRUCTURE, AND DEFORMATION OF THE LMG

Several authors have discussed the extent of deformation within the LMG, and the name of the Lyon Mountain suite of rocks has varied between Lyon Mountain granite

(e.g., McLelland et al., 2001a; Selleck et al., 2005), Lyon Mountain granite gneiss (e.g., Postel, 1952) and Lyon Mountain gneiss (e.g., Whitney and Olmsted, 1993). We have adopted the term Lyon Mountain granite as the unit is not always a gneiss but it is always a granite and most igneous rock types in the Adirondack Highlands retain their igneous name regardless of their deformational or metamorphic history (e.g., Marcy anorthosite, Hawkeye granite).

Contacts between the LMG and other lithologies in the Adirondack Highlands are typically poorly exposed and the nature of these contacts (tectonic vs. intrusive) is not obvious. However, dikes of probable LMG intrude the ~1100 Ma Hawkeye granite near the town of Hawkeye, New York, and a gabbronorite body (~1150 Ma AMCG suite) on the south side of Skiff Mountain. In the northern part of the study area, the LMG overlies domes or core complexes of Hawkeye granite and anorthosite (Fig. 4-1). Much of the Fe-mineralization in the northern area occurs just above the contact with one these domes of Hawkeye granite. The dominant mineral lineation and trend of the ore bodies in the LMG plunges to the north-northeast parallel to the axis of this regional folding (Postel, 1952). In the cores of some of the synforms (e.g., Dannemora) an assemblage of highly deformed and migmatized metasedimentary rocks are present above the LMG. In the central part of the study area, the LMG has been folded into a north plunging, upright syncline between domes of anorthosite (Whitney and Olmsted, 1993) (Fig. 4-1). Mineralization in the central area is associated with faults or the hinge regions of folds (Postel, 1952). In the southern part of the study area, the LMG is typically in contact with calc-silicate marbles, other metasedimentary rocks, and gabbros (Isachsen and

Fisher, 1970) (Fig. 4-1). Iron-mineralization in the southeastern LMG frequently occurs near these contacts (e.g., Skiff Mountain, Mineville). Late northeast trending faults of uncertain age crosscut all lithologies in the southern and central study area (Isachsen and Fisher, 1970).

There is little evidence of widespread penetrative deformation in the LMG but localized deformation is present in the form of stretched or sheared clinopyroxene layers (Fig. 4-2a), and quartz veins (Fig. 4-2b). These layers and veins are typically ambiguous as to the direction of shearing, showing only stretching without rotation. Migmatization and mylonitization were observed in and around the zone of mineralization of some ore bodies (e.g., Lyon Mountain) (Figs. 4-2c and 4-2d). At these localities, melting has taken place *in situ*, as revealed by mafic selvages around the leucosome.

4-3-2 ROCK DESCRIPTIONS AND PETROGRAPHY

Detailed rock and petrographic descriptions of all the LMG rock types and associated rocks for this study are presented at the end of this chapter. A brief summary is presented here.

Lyon Mountain granite

The LMG consists of three primary end-member rock types based on the dominant feldspar present: perthite granite; microcline granite; and albite granite. The microcline granite and the albite granite are most likely the result of fluid alteration and do not constitute true magmatic compositions. Mineral assemblages related to Na alteration clearly overprint the perthite and microcline granite. The paragenetic sequence for the LMG and subsequent alteration events is presented in Figure 4-3a.

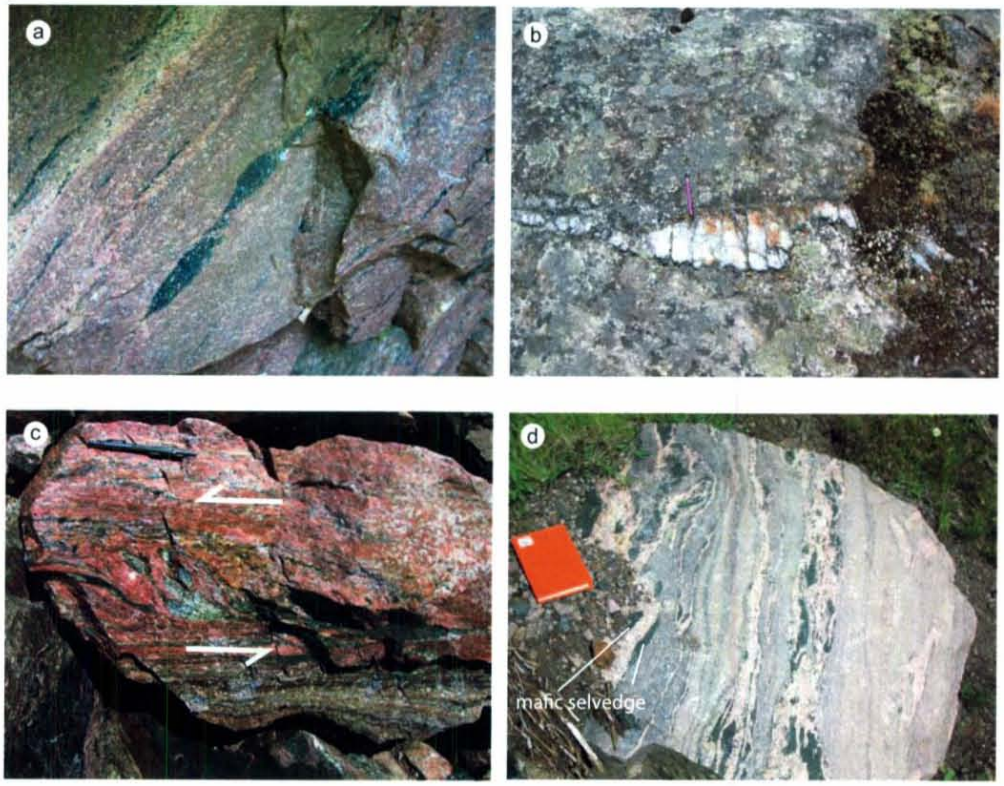

Figure 4-2. Deformation and partial melting in the Lyon Mountain granite. a) Stretched clinopyroxene layer at Lyon Mountain. b) Stretched quartz vein at Skiff Mountain. c) Mylonite sample from the immediate footwall of the Chateaugay mine in Lyon Mountain. Mylonite mineral assemblage is dominated by "crushed" albite and minor remnant perthite grains. d) Migmatization around the ore zone at Lyon Mountain. Leucosomes typically are bordered by mafic selvages of clinopyroxene and amphibole.

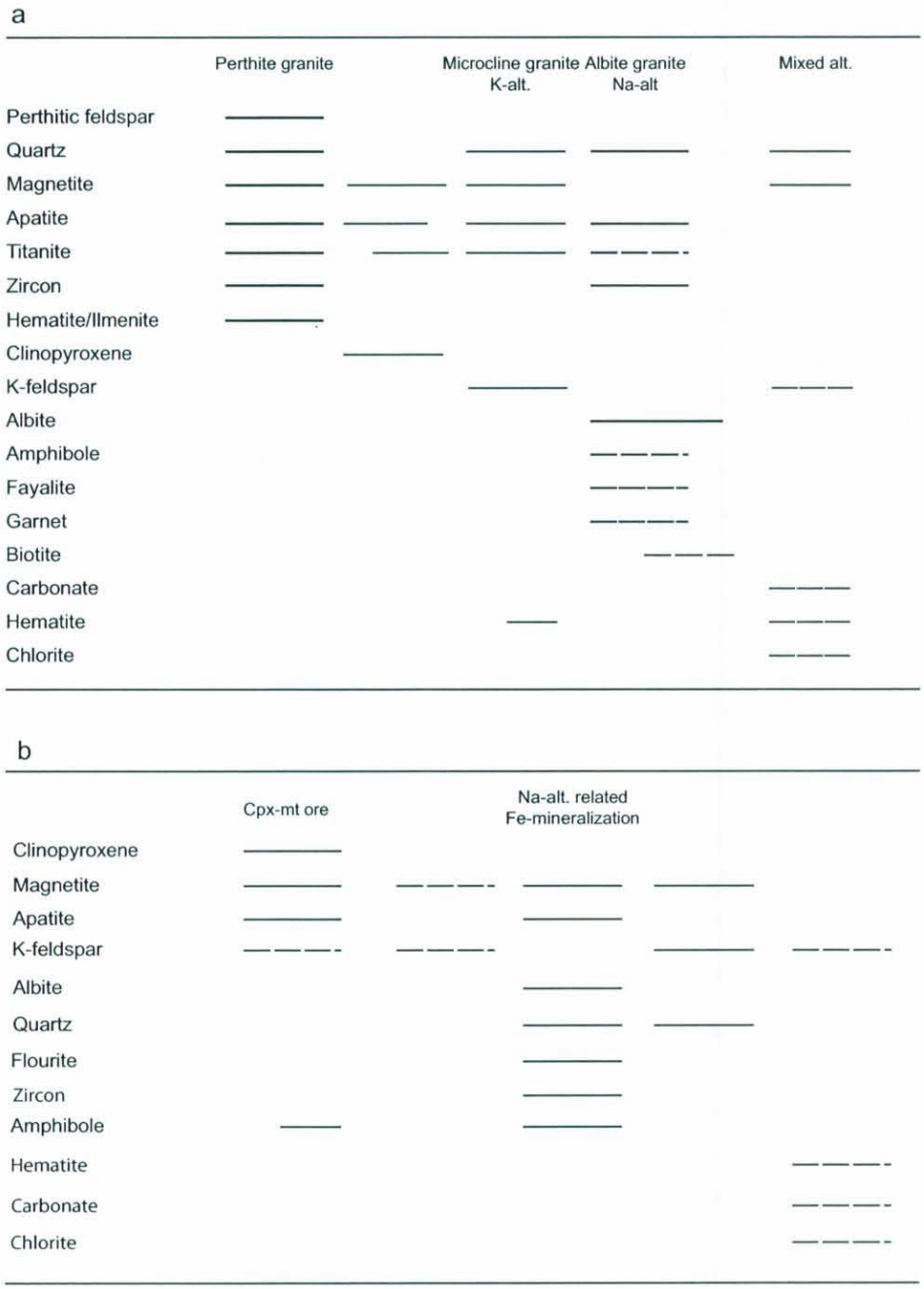

FIGURE 4-3. a) Paragenetic sequence for the Lyon Mountain granite and subsequent fluid alteration. Solid lines indicate widespread mineral growth; dashed lines indicate minor mineral formation or alteration event. b) Paragenetic sequence for Fe mineralization and associated alteration within the Lyon Mountain granite. Solid lines indicate widespread mineral growth; dashed lines indicate minor mineral formation or mineralizing event.

The perthite granite (e.g., Clintonville, sample 99-1a; Rutgers Mine, sample 06-4d; Lyon Mountain, sample LM-06-2a) is the dominant rock type of the LMG suite of rocks. The perthite granite is considered unaltered, or the least altered, due to its occurrence away from ore bodies and hydrothermal alteration zones. Its general resemblance to perthitic granites from other igneous and metamorphic terranes in the Adirondacks and elsewhere, and the coherent or semi-coherent nature and regular distribution of lamellae throughout the feldspar grains suggests that it is a primary igneous or metaigneous rock type (e.g., Parsons et al., 2005).

The primary mineral assemblage in the perthite granite is perthitic feldspar, quartz, euhedral magnetite, and minor zircon, hematite-ilmenite intergrowths, titanite and apatite. Perthite grains exhibit coarse, anastomosing albite lamellae hosted by microcline (Fig 4-4a, b). Many samples of the perthite granite contain secondary clinopyroxene and coarse masses of magnetite. Additionally, the unit commonly contains minerals related to subsequent Na- and K-rich fluid alteration especially albite replacement of perthite grains. In CL, microcline regions in perthite grains luminesce blue (typical of microcline; e.g., Finch and Klein, 1999) and albite lamellae are brownish-gray-green to red. Red CL in feldspars is attributed to the presence of Fe^{3+} or trivalent REE (e.g., Sm, or Eu) (Finch and Klein, 1999).

The microcline granite is the simplest mineralogically and typically more homogeneous than either the perthite or albite granite. Foliations in the microcline granite are much less distinct and difficult to observe than in the perthite granite owing to the lack of mafic and planar minerals or subsequent K alteration and recrystallization.

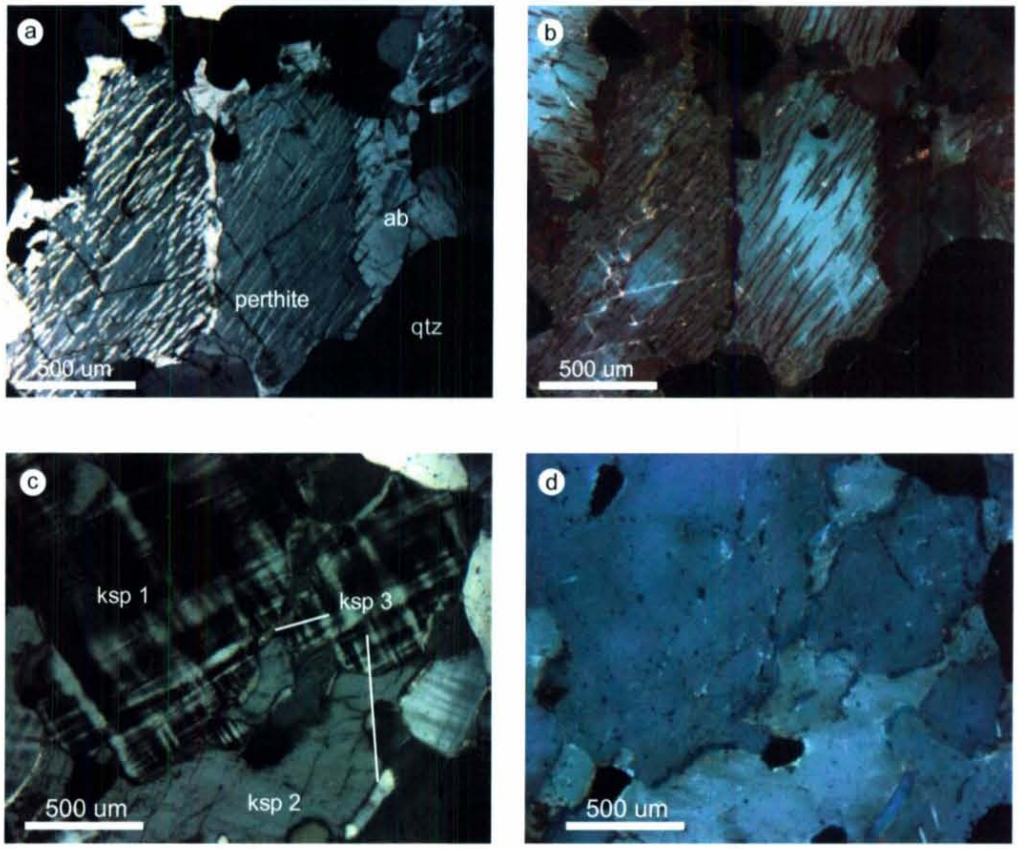

Figure 4-4. Photomicrographs of the Lyon Mountain granite. a) Cross-polarized light image and b) color CL image of perthite grains with minor Na-alteration in the form of albite rims and veins. Note albite lamellae protruding into alteration related albite and red luminescence associated with alteration related albite. c) Cross-polarized light image and d) color C L image of the microcline granite. Note multiple generations of K-feldspar in CL image.

The mineral assemblage consists predominately of microcline, quartz, magnetite or hematite, and minor titanite, apatite, and zircon. The microcline granite is "pristine" in some localities (e.g., Dannemora, sample 99-6c) or overprinted by minerals related to Na-rich fluid alteration (e.g., Palmer Hill, sample 99-4b). Additionally, CL imaging shows multiple generations of K-feldspar growth (Figs. 4-4 c and d).

The albite granite, like its potassium counterpart the microcline granite, is probably the product of pervasive Na-rich fluid alteration and overprints both the perthite granite and the microcline granite. Earlier rock types are completely converted to albite granite (e.g., albitized) with only small remnants of the preexisting lithology remaining or veins and patches of albite are present where replacement is incomplete (Figs.4- 5). The albite granite is little deformed except in localized shear zones where the unit has a moderate foliation. The mineral assemblage of the albite granite is highly variable consisting of granoblastic albite, quartz, zircon, apatite, magnetite ± clinopyroxene ± amphibole ± titanite ± garnet ± fluorite. The albite granite in some localities (e.g., Arnold Hill, sample AH-06-1a) has been overprinted by a second phase of K alteration as well as by Ca, or Si-rich fluids in the form of untwinned K-feldspar, calcite, and jasper.

In addition to the three main rock types in the LMG, there is small body of hydrothermally altered fayalite granite (Ausable Forks, sample 99-3a) that crops out in the town of Ausable Forks and probably represents a later intrusion or reduced magma of the LMG series (Fig. 4-1) (Postel, 1952; Whitney and Olmsted, 1993). The primary mineral assemblage consists of perthitic feldspar, quartz, clinopyroxene, minor zircon, and fayalite. It is not clear if the fayalite is primary or the result of hydrothermal

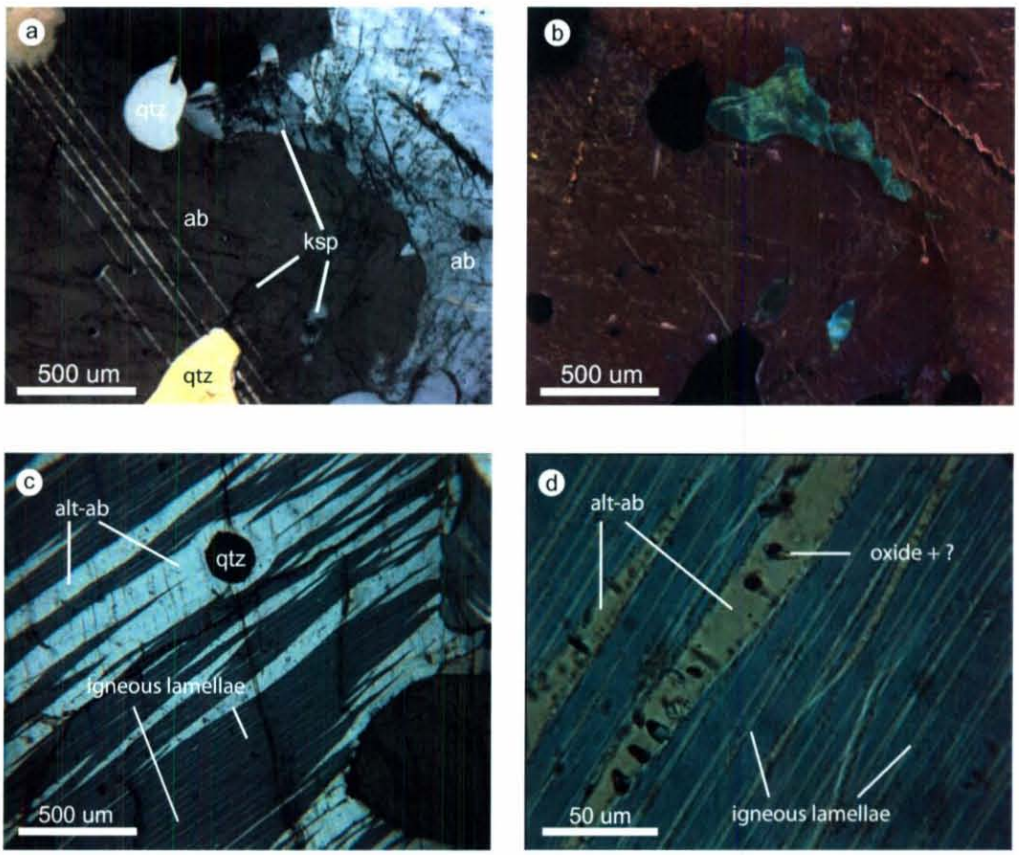

Figure 4-5. Photomicrographs of the Lyon Mountain granite. a) Cross-polarized light image and b) color CL image of the albite granite with remnant inclusions of microcline. c) Cross-polarized light image of the fayalite granite showing crosscutting relationship of flame lamellae. d) Higher magnification view of flame lamellae containing Fe oxides and unknown mineral phase.

alteration. Secondary mineral growth as a result of Na fluid alteration consists of albite, quartz, fluorite, apatite, and magnetite. Perthitic feldspar and clinopyroxene grains in the fayalite granite are distinct from that of the perthite granite. In feldspar grains, thin, straight, uniform lamellae are crosscut by hydrothermal alteration-related albite "flame lamellae" containing minute inclusions of Fe-oxides (Fig. 4-5c, d). Clinopyroxene grains contain exsolution lamellae of Fe-rich pyroxene that are not present in other LMG rock types (see mineral chemistry results below).

Ore deposits

Ore deposits in the LMG can be divided into two main types: clinopyroxene-magnetite (skarn-like deposits) and those associated with Na-rich fluid alteration and the growth of magnetite-apatite and quartz. Figure 4-3b shows the proposed sequence of mineral paragenesis for Fe-mineralization. The clinopyroxene-magnetite deposits are typified by the mineral assemblage clinopyroxene, magnetite ± apatite ± amphibole ± K-feldspar. Enclaves and pods of clinopyroxene-magnetite ore veins can be observed within the perthitic granite (e.g., Rutgers Mine, sample 06-4d) (Fig. 4-6a). The clinopyroxene-magnetite deposits are crosscut by granitic dikes and pegmatites, may contain miarolitic cavities (Fig. 4-6b), and in many localities have been overprinted and remobilized by subsequent Na-rich fluid alteration (Fig. 4-6c) to form a second generation of deposits (Fig. 4-6d). Deposits associated with Na alteration comprise magnetite, apatite, quartz, and zircon, and can contain albite ± fluorite ± clinopyroxene ± amphibole ± biotite ± titanite ± chlorite ± calcite. Inclusions from earlier assemblages (e.g., perthite granite, clinopyroxene-magnetite ore) are present at some localities. In

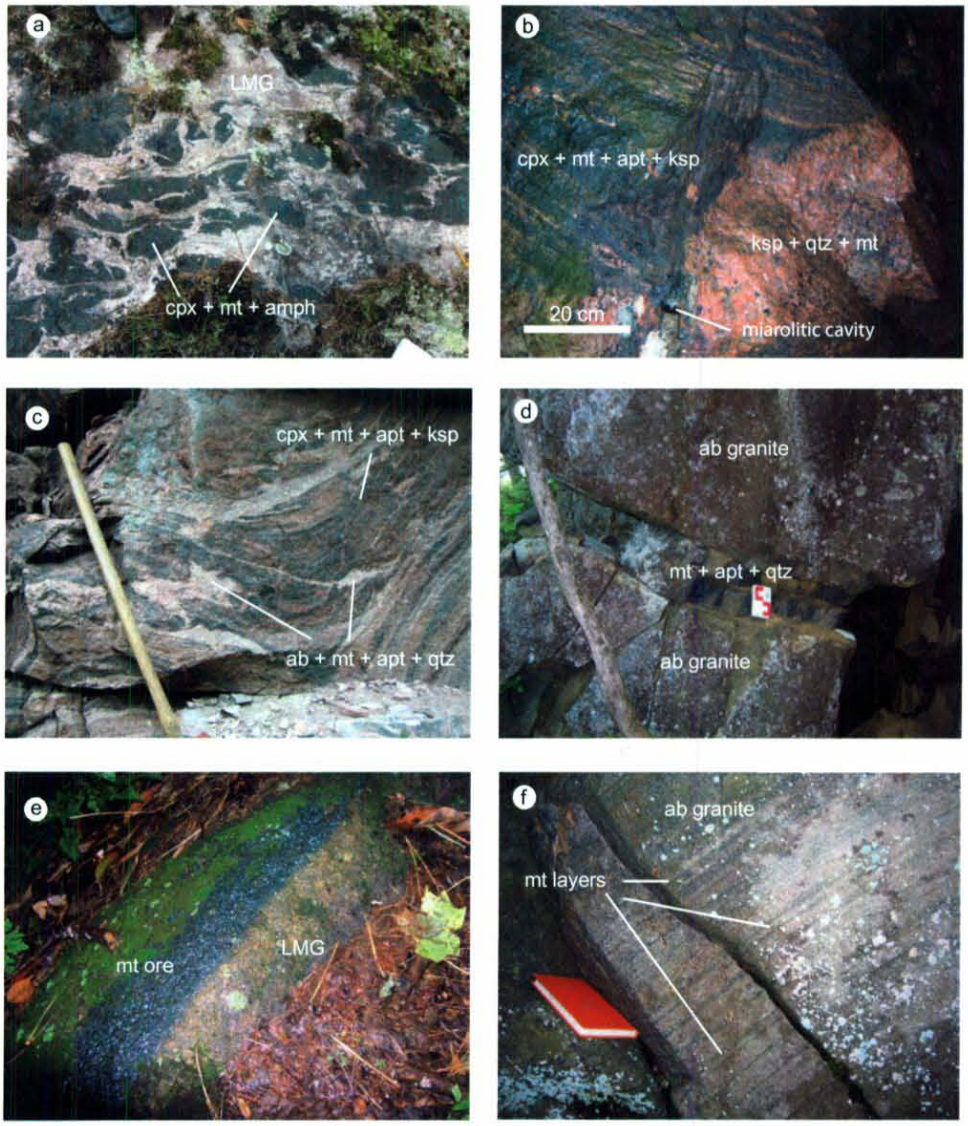

Figure 4-6. Various styles of Fe mineralization and fluid alteration in the Lyon Mountain granite. a) Enclaves of clinopyroxene-magnetite and amphibole, skarn ore in Lyon Mountain granite at the Rutgers mine. b) Main skarn ore body at the Chateaugay mine in Lyon Mountain. Ore consists primarily clinopyroxene (or amphibole)-magnetite-apatite and K-feldspar. The ore body is cut by a granitic pegmatite dike comprised of K-feldspar, quartz and magnetite. Note miarolitic cavity at the contact of the dike and ore body. The cavity contains large crystals of K-feldspar and amphibole. c) Sodic alteration and Fe remobilization overprinting earlier skarn ore assemblage and potassic altered rocks at the Chateaugay mine in Lyon Mountain. d) An ore seam at Skiff Mountain comprised of quartz-magnetite and apatite and enclosed by albite granite. e) Sharp contact between a magnetite ore body and Lyon Mountain granite near Mineville. f) Partial Fe mineralization in the form of thin, regular layers of magnetite in the albite granite near Mineville.

most samples zircon was not identified in thin section, and only identified later during heavy mineral separation.

Regardless of the ore type, certain physical features are shared between the different ores. The contacts between the ore and the host granite are either sharp (Figs. 4-6d and 6e) or in some localities gradational (Fig. 4-6f). Often, thin layers of magnetite (or magnetite and clinopyroxene) gradually increase in number and thickness until the main layer of the ore is reached (Fig. 4-6f). It is common above or below the mineralized zone to find the granite nearly devoid of disseminated magnetite, and for that matter any other ferromagnesian minerals that are present elsewhere in the rock further away from the ore-host contact. These barren zones range from a few meters (e.g., Lyon Mountain, Skiff Mountain) to approximately 100 meters (e.g., Palmer Hill).

Related rock types

Related minor units within the LMG include amphibolite layers, and crosscutting felsic dikes. These units, as well as, the nearby Hawkeye granite and AMCG suite-related charnockite were collected to better understand the evolution of the LMG, including the fluid alteration history, and Fe-mineralization

Amphibolite layers (e.g. Skiff Mountain, 00-11; Ausable Forks, F-06-1a) are relatively common within the LMG but constitute little of the total volume of the granite. Though not the focus of this study, they are considered here to help better characterize the LMG and its evolution and origin. The layers typically have a "salt and pepper" appearance and comprise varying amounts of biotite, amphibole, plagioclase, and apatite,

with minor orthoclase, magnetite or hematite-ilmenite intergrowths, titanite and zircon and in the sample collected at Skiff Mountain alteration related albite.

Granitic dikes and pegmatites are common throughout the LMG and the Adirondack Highlands. These dikes crosscut layering in the LMG and the regional fabric of the Highlands. Both potassium feldspar-rich dikes and plagioclase-rich dikes were observed. The potassium feldspar-rich dikes (e.g., Dannemora, sample 99-6b; Skiff Mountain, sample 00-03) typically contain coarse microcline, quartz, and minor magnetite, zircon, and apatite ± muscovite ± amphibole ± biotite ± calcite. A plagioclase-rich dike collected at Lyon Mountain (sample LM-06-1a) (and also reported in McLelland et al., 2001b), consists of coarse quartz, oligoclase, magnetite, microcline, apatite, titanite, calcite, zircon, and minor sulfides. This dike has been overprinted by minerals related to Na alteration (i.e., albite).

The Hawkeye granite (sample H-06-1c) mineral assemblage contains highly recrystallized quartz, perthitic feldspar, myrmekite plagioclase, and zircon ± amphibole ± orthopyroxene, ± garnet ± biotite ± ilmenite ± apatite. Perthite grains in the Hawkeye granite typically contain short, fat lamellae which are often absent in the rims of the grains. The mineral assemblage of the charnockite comprises plagioclase, perthitic feldspar (with short, or rounded lamellae), clinopyroxene (with exsolution lamellae), orthopyroxene, garnet, apatite, and zircon and minor quartz.

4-3-3 WHOLE ROCK MAJOR AND TRACE ELEMENTS

Whole rock geochemical analyses were done on the three main rock types of the LMG and the associated units mentioned above (including the Hawkeye granite and the

AMCG suite charnockite). These data are shown in Table 4-1 (locality stated here, and marked on the geologic map in Fig. 4-1). The whole rock geochemistry presented here is in general agreement with earlier findings from the different LMG rock types (e.g. Whitney and Olmsted, 1988; McLelland et al., 2002). The LMG shows a wide range of compositions in both major and trace elements as a result of the original composition of the rock types and the subsequent hydrothermal alteration and Fe-mineralization, and as such, it is not clear how much the major and trace element chemistry accurately reflects the original rock compositions. The SiO_2 content in LMG samples varies between 65.78 and 73.53 wt. % and total alkalis ($Na_2O + K_2O$) from 6.03 to 10.57 wt. %. It is unclear what portion of the alkali content is related to alteration and what is related to the original composition of the protolith. Some samples that have been subjected to complete alkali replacement contain up to 10 wt. % K_2O or Na_2O (Table 4-1). There is a one to one correlation between Na and K when normalized to aluminum (Figs. 4-7a). Lyon Mountain granite rock types range from peralkaline to peraluminous and both the microcline granite (K-alteration) and the albite granite (Na-alteration) and have a higher aluminum saturation index relative the perthite granite (least-altered) (Fig. 4-7b). Most samples from the LMG as well as the AMCG suite charnockite mentioned above have high Fe relative to Mg (Figs. 4-8) with the most Na altered samples (e.g., Arnold Hill, sample AH-06-1a, Mineville, sample BH-LMG-2) containing the highest levels of Fe (up to 10 wt. % Fe_2O_3 [tot]). The perthite granite typically averages 5 wt. % Fe_2O_3 (tot). Samples immediately adjacent to the ore body often show a depletion in Fe with Fe_2O_3 (tot) values as low as 1.69 wt. % (e.g., Lyon Mountain, sample LM-06-1c). Samples with

Table 4-1 Whole rock geochemistry of the Lyon Mountain granite and associated rocks

Location	Clintonville	Rutgers Mine	Lyon Mountain	Dannemora	Skiff Mountain	Skiff Mountain	Ausable Forks	Arnold Hill	Arnold Hill
Sample #	99-1a	06-4d	LM-06-2a	99-6c	00-04	00-02	95-1a	AH-06-1a	RC-06-2
Rock type	Perthite granite	Perthite granite	Perthite granite	Microcline granite	Microcline granite	Albite granite	Albite granite	Albite granite	Albite granite
Element									
wt %									
SiO2	71.52	67.18	68.13	68.98	68.20	73.53	69.14	68.84	65.78
TiO2	0.54	0.49	0.818	0.47	0.53	0.33	0.55	0.35	0.85
Al2O3	12.27	13.86	13.61	12.73	13.32	11.73	13.41	11.85	15.67
Fe2O3 (tot)	4.69	5.60	3.72	6.03	5.12	6.15	7.29	9.51	2.56
MnO	0.02	0.02	0.1	0.01	0.02	0.01	0.05	0.015	0.02
MgO	0.36	0.52	0.96	0.14	0.41	0.29	0.63	1.58	1.75
CaO	1.15	1.53	3.06	0.39	0.60	0.48	1.22	0.8	3.13
Na2O	3.35	4.55	3.83	1.27	2.11	6.57	6.69	5.79	7.16
K2O	5.75	5.97	6.01	9.30	8.03	0.33	0.77	0.24	1.67
P2O5	0.14	0.09	0.17	0.10	0.16	0.04	0.12	0.05	0.16
LOI	0.60	0.14	0.12	0.08	0.41	0.22	0.26	0.51	0.72
Total	100.39	99.94	100.5	99.50	98.91	99.66	100.10	99.53	99.46
ppm									
Ag	1.1	< 0.5	0.5	0.8	0.7	2.3	< 0.5	< 0.5	< 0.5
As	< 5	< 5	< 5	< 5	< 5	< 5	< 5	< 5	< 5
Ba	548	415	1331	3,510	889	12	61	8	223
Be	2	4	6	0.5	3	7	4	7	3
Bi	< 0.1	< 0.1	< 0.1	0.7	< 0.1	< 0.1	< 0.1	< 0.1	< 0.1
Co	1	144	166	5	3	2	299	195	301
Cr	< 20	< 20	< 20	< 20	< 20	< 20	< 20	< 20	50
Cs	0.1	0.2	0.4	0.6	1.6	0.05	0.05	0.1	0.6
Cu	75	< 10	< 10	74	42	< 10	< 10	< 10	10
Ga	23	26	28	23	23	42	28	31	21
Ge	1.7	1.9	2	3.0	2.0	2.6	1.4	2.3	1.8
Hf	14.7	16.6	17.4	14.0	9.7	38.7	15.6	34.1	6.9
In	< 0.1	< 0.1	0.2	< 0.1	< 0.1	< 0.1	< 0.1	< 0.1	< 0.1
Mo	< 2	< 2	< 2	< 2	< 2	< 2	< 2	2	< 2
Nb	20.6	21.7	23.2	23.5	13.9	55.0	15.9	25.3	11
Ni	< 20	< 20	< 20	< 20	< 20	< 20	< 20	< 20	< 20
Pb	< 5	< 5	< 5	< 5	< 5	< 5	< 5	< 5	< 5
Rb	116	143	196	315	236	5	9	5	48
Sb	< 0.2	< 0.2	< 0.2	< 0.2	< 0.2	< 0.2	< 0.2	0.2	< 0.2
Sc	5	5	11	5	7	1	12	4	15
Sn	7	10	6	16	20	11	7	10	4
Sr	73	79	119	81	50	24	101	33	151
Ta	1.37	4.01	3.46	1.82	2.82	4.08	3.94	4.18	3.45
Th	9.75	6.68	20.1	13.03	13.14	33.00	7.75	16.5	14.70
Tl	0.43	0.23	0.47	0.94	1.48	0.03	0.03	< 0.05	0.14
U	1.30	3.94	7.56	4.80	2.78	12.87	2.57	7.91	4.16
V	20	29	20	18	23	5	20	28	70
W	0.3	727	501	0.8	0.3	0.3	933	676	958
Y	71.5	81.2	88.8	71.5	56.4	362	73.2	52.9	43.6
Zn	< 30	< 30	40	< 30	< 30	< 30	50	< 30	< 30
Zr	525	708	692	500	360	1,220	590	1403	239
La	51.912	26.900	63.1	36.988	50.066	159.266	47.800	85.2	57.500
Ce	112.951	88.100	141	80.015	100.011	351.056	106.000	161	134.000
Pr	15.614	13.100	17.5	11.286	13.252	45.967	13.400	17.3	15.600
Nd	62.906	57.500	68.9	44.873	51.315	181.158	53.300	66.7	57.000
Sm	13.392	13.600	14.9	10.198	10.299	40.160	12.200	11.1	10.200
Eu	2.486	2.470	2.65	2.074	1.887	3.429	2.090	1.38	1.900
Gd	14.126	12.900	14.6	10.760	10.230	47.592	11.400	10	8.460
Tb	2.301	2.450	2.66	2.007	1.682	8.935	2.030	1.49	1.420
Dy	13.085	15.200	16.1	11.999	9.508	56.466	12.600	8.72	8.360
Ho	2.666	3.020	3.12	2.500	1.872	12.550	2.520	1.79	1.630
Er	7.599	9.540	9.58	7.612	5.287	37.163	7.830	5.97	4.870
Tm	1.187	1.570	1.46	1.273	0.810	5.901	1.200	1.01	0.734
Yb	7.098	10.200	9.62	7.877	4.869	32.452	7.780	7.69	4.720
Lu	1.003	1.520	1.5	1.152	0.714	4.452	1.150	1.36	0.685
Eu/Eu*	0.181	0.186	0.180	0.198	0.184	0.078	0.177	0.131	0.205

Table 4-1 Continued

Location	Dry Bridge	Mineville	Palmer Hill	Lyon Mountain	Lyon Mountain	Lyon Mountain	Arnold Hill	Arnold Hill	Fayalite granite
Sample #	99-2b	BH-LMG-2	99-4b	LM-06-1c	LM-06-1d	LM-06-2b	99-5a	RC-06-1	99-3a
Rock type	Albite granite	Albite granite	mixed alt. overall K	mixed alt. overall K	mixed alt. overall K	mixed alt. overall K	mixed alt. overall Na	mixed alt. overall K	partial Na-alt
Element									
wt %									
SiO2	71.38	71.78	71.96	72.76	70.61	69.28	68.06	71.38	70.62
TiO2	0.41	0.40	0.40	0.15	0.50	1.304	0.44	0.43	0.43
Al2O3	13.34	11.01	11.85	12.37	11.67	11.39	12.70	12.92	12.32
Fe2O3 (tot)	3.38	7.39	5.05	1.69	5.49	2.62	10.32	1.86	6.07
MnO	0.03	0.04	0.02	0.02	0.02	0.049	0.01	0.01	0.11
MgO	0.51	0.07	0.23	0.25	0.27	1.24	0.17	1.35	0.03
CaO	3.12	0.64	0.21	0.68	0.92	2.86	0.42	0.67	1.42
Na2O	7.61	5.29	2.43	2.70	2.62	1.51	5.34	3.26	4.14
K2O	0.10	1.97	6.81	7.51	6.64	8.21	2.84	6.69	5.12
P2O5	0.07	0.04	0.07	0.04	0.05	0.02	0.04	0.11	0.05
LOI	0.40	-0.03	0.25	0.43	0.05	0.49	0.10	0.42	0.08
Total	100.35	98.60	99.29	98.59	98.84	98.95	100.45	99.10	100.38
ppm									
Ag	1.9	2	1.8	< 0.5	< 0.5	0.5	1.8	< 0.5	3.5
As	< 5	< 5	< 5	< 5	< 5	< 5	< 5	< 5	< 5
Ba	8	115	406	573	778	787	194	449	200
Be	6	4	2	< 0.1	2	4	2	2	5
Bi	< 0.1	< 0.1	< 0.1	< 0.1	< 0.1	< 0.1	0.2	< 0.1	< 0.1
Co	0.5	331	2	185	270	198	6	208	0.5
Cr	< 20	< 20	< 20	< 20	< 20	50	< 20	< 20	< 20
Cs	0.05	0.05	0.4	0.3	0.4	0.4	0.1	0.7	0.1
Cu	< 10	20	40	30	< 10	< 10	68	10	< 10
Ga	33	36	24	21	21	18	32	21	38
Ge	4.2	2.2	2.5	1.3	1.7	1.8	1.8	1.8	2.7
Hf	25.2	38.6	21.0	9.6	13.2	13.7	26.6	7.8	36.1
In	0.3	< 0.1	< 0.1	< 0.1	< 0.1	< 0.1	< 0.1	< 0.1	< 0.1
Mo	< 2	2	< 2	< 2	3	2	< 2	< 2	< 2
Nb	39.5	61.9	22.7	12	17.8	19.6	33.8	10.4	32.5
Ni	< 20	< 20	< 20	< 20	< 20	20	23	< 20	< 20
Pb	8	< 5	< 5	19	< 5	< 5	< 5	< 5	< 5
Rb	2	29	200	168	181	232	46	191	199
Sb	0.3	< 0.2	< 0.2	< 0.2	< 0.2	< 0.2	< 0.2	< 0.2	< 0.2
Sc	6	1	5	2	5	8	2	13	2
Sn	20	12	18	3	5	8	11	4	3
Sr	33	45	30	44	48	42	44	42	29
Ta	2.86	8.45	1.30	4.74	3.89	2.91	2.45	2.84	1.72
Th	19.71	16.10	5.05	26.50	16.00	19.2	7.64	18.00	1.86
Tl	0.03	0.08	0.56	0.46	0.31	0.3	0.10	0.22	0.42
U	8.19	3.55	1.95	3.94	5.08	11.1	4.90	2.94	1.79
V	7	6	6	5	29	44	16	27	8
W	0.7	1090	0.3	932	910	624	0.3	722	0.3
Y	113	205	40.0	29.7	65.1	87.2	70.6	37.6	131
Zn	< 30	70	< 30	< 30	< 30	40	< 30	< 30	137
Zr	1,010	1362	902	272	458	516	1,060	260	1,370
La	111.116	91.100	26.705	40.700	38.300	71.3	14.363	9.300	48.511
Ce	204.757	248.000	60.772	71.500	92.200	163	50.487	27.100	132.627
Pr	25.645	33.000	8.466	7.300	11.500	21.3	5.975	3.860	20.916
Nd	97.261	138.000	34.388	25.600	45.400	82.1	26.098	17.800	92.263
Sm	18.778	33.000	7.259	5.080	10.600	16.2	8.525	4.860	22.686
Eu	3.075	2.670	0.940	0.714	1.530	2.74	1.911	0.775	2.920
Gd	19.604	32.800	7.226	4.780	10.300	15	9.772	5.310	25.506
Tb	3.304	6.150	1.246	0.920	1.950	2.65	2.120	1.090	4.370
Dy	19.205	38.300	7.265	5.680	11.900	15.6	13.054	7.010	25.737
Ho	3.919	7.440	1.479	1.120	2.340	2.98	2.733	1.420	5.225
Er	11.661	22.300	4.340	3.480	7.310	9.1	7.970	4.260	14.657
Tm	1.966	3.310	0.707	0.551	1.170	1.38	1.394	0.669	2.287
Yb	11.892	19.500	4.472	3.660	7.390	9	8.487	4.210	14.054
Lu	1.807	2.510	0.727	0.538	1.030	1.37	1.229	0.609	2.159
Eu/Eu*	0.160	0.081	0.130	0.145	0.146	0.176	0.209	0.153	0.121

Table 4-1 Continued

Location	Skiff Mountain	Ausable Forks	Lyon Mountain	Dannemora	Skiff Mountain	Near Skiff Mountain	Hawkeye	AGV-1	BCR-1
Sample #	00-11	F-06-1a	LM-06-1a	99-6b	00-03	00-09	H-06-1c	-	-
Rock type	amphibolite layer	amphibolite layer	tonalitic dike (alt)	granitic pegmatite dike	granitic pegmatite dike	AMCG suite charnockite	granite	-	-
Element									
wt %									
SiO2	49.79	45.36	64.29	64.55	72.41	56.64	71.52	60.17	54.32
TiO2	2.64	2.51	0.26	0.61	0.51	1.01	0.33	1.012	2.200
Al2O3	15.02	15.07	16.67	12.33	13.03	16.08	13.15	16.96	13.38
Fe2O3 (tot)	11.80	15.33	5.88	11.03	3.28	10.35	3.15	6.60	13.24
MnO	0.11	0.19	0.02	0.02	0.02	0.19	0.05	0.092	0.179
MgO	5.79	6.15	0.10	0.20	0.30	0.52	0.15	1.46	3.45
CaO	4.26	8.50	2.99	0.60	0.56	4.42	1.28	4.78	6.88
Na2O	5.92	3.84	6.43	1.12	1.99	4.69	2.85	4.26	3.35
K2O	1.68	1.67	1.75	8.71	7.68	4.38	5.79	3.12	1.86
P2O5	0.42	0.48	0.23	0.16	0.18	0.46	0.07	0.50	0.36
LOI	1.34	0.44	0.31	0.27	0.39	0.10	0.55	1.65	0.74
Total	98.79	99.53	98.94	99.60	100.34	98.86	98.88	100.59	99.95
ppm									
Ag	< 0.5	< 0.5	< 0.5	2.2	0.7	< 0.5	< 0.5	< 0.5	
As	7	< 5	< 5	< 5	< 5	< 5	< 5	< 5	< 5
Ba	248	263	397	2,510	1,210	2819	715	1,220	718
Be	7	3	6	0.5	1	1	1	2	1
Bi	< 0.1	< 0.1	< 0.1	< 0.1	0.2	< 0.1	< 0.1	0.1	< 0.1
Co	89	102	241	7	2	141	269	14	37
Cr	60	130	< 20	< 20	< 20	< 20	< 20	< 20	< 20
Cs	2.8	7.6	0.5	0.7	1.3	1.5	0.8	1.4	1.0
Cu	< 10	20	< 10	87	27	< 10	< 10	60	20
Ga	24	23	32	27	19	27	22	21	23
Ge	2	1.7	1.3	2.6	1.6	1.8	1.5	1.4	1.6
Hf	8.0	6.1	8.5	27.1	8.6	6.0	10.9	5.0	4.9
In	< 0.1	< 0.1	< 0.1	< 0.1	< 0.1	< 0.1	< 0.1	< 0.1	< 0.1
Mo	< 2	3	3	3	< 2	3	< 2	3	< 2
Nb	21.6	11.5	2.7	21.3	11.6	7.9	11.5	13.7	11.9
Ni	60	70	< 20	< 20	< 20	< 20	< 20	26	38
Pb	< 5	< 5	12	< 5	6	< 5	15	42	12
Rb	167	113	48	305	225	64	142	68	49
Sb	< 0.2	< 0.2	< 0.2	0.3	< 0.2	< 0.2	< 0.2	3.9	0.6
Sc	22	23	< 0.1	3	4	23	4	13	30
Sn	10	7	2	23	6	< 1	< 1	4	3
Sr	222	206	243	63	87	309	138	627	324
Ta	1.54	1.25	2.36	1.53	0.78	1.55	3.04	0.90	0.78
Th	8.39	4.33	9.50	13.36	6.54	2.55	1.97	6.27	5.86
Tl	0.32	0.98	0.25	0.85	1.40	0.33	1.07	0.54	0.28
U	3.89	2.35	2.87	3.79	1.78	0.79	1.34	2.32	1.72
V	158	166	5	26	15	< 5	6	119	405
W	206	184	757	3.4	0.3	420	896	0.6	0.5
Y	124	71.2	13.7	98.6	30.9	48.3	50.4	19.9	35.5
Zn	60	150	60	< 30	75	100	50	111	151
Zr	289	231	350	1,050	317	256	389	211	174
La	71.000	53.30	35.100	62.150	33.785	22.600	27.200	38.3	25.4
Ce	171.000	111.00	59.100	110.780	68.350	55.500	66.000	65.7	50.6
Pr	21.400	13.00	5.780	13.925	8.381	7.640	9.610	8.39	6.70
Nd	83.100	52.30	20.300	52.921	32.485	34.500	41.800	30.7	27.5
Sm	18.500	11.40	3.250	11.641	6.363	8.690	10.200	5.53	6.17
Eu	4.130	3.11	1.120	2.366	1.605	9.760	2.580	1.71	2.03
Gd	18.100	11.30	2.740	12.824	6.018	8.920	9.750	4.88	6.58
Tb	3.520	1.98	0.410	2.350	0.994	1.540	1.750	0.69	1.10
Dy	22.700	12.00	2.200	14.656	5.571	9.010	10.100	3.55	6.35
Ho	4.430	2.37	0.420	3.122	1.104	1.770	1.930	0.66	1.25
Er	13.700	7.11	1.250	9.492	3.120	5.040	5.540	1.80	3.58
Tm	2.120	1.09	0.188	1.583	0.456	0.747	0.781	0.244	0.530
Yb	13.300	6.90	1.270	9.785	2.931	4.870	4.780	1.67	3.31
Lu	1.820	0.97	0.196	1.485	0.425	0.741	0.675	0.253	0.488
Eu/Eu*	0.226	0.274	0.375	0.194	0.259	1.109	0.259	0.329	0.318

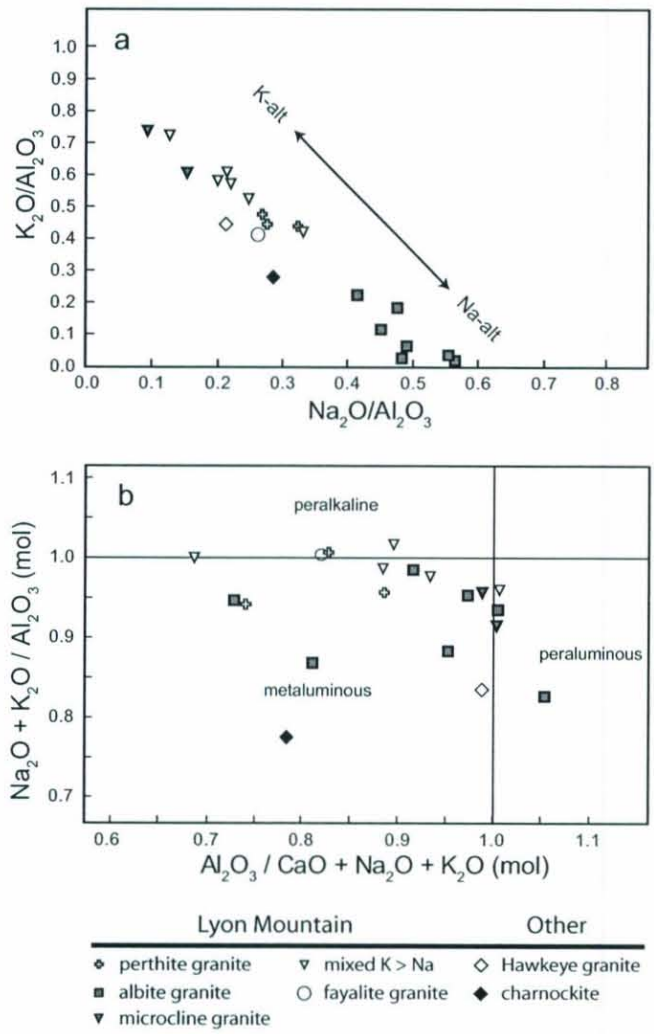

Figure 4-7. Whole rock geochemistry plots of major elements for the Lyon Mountain granite and associated rocks. a) Na_2O-K_2O normalized to Al_2O_3 plot showing one to one correlation between K and Na. b) Alumina saturation index. Values are in weight percent unless specified (after Shand, 1927).

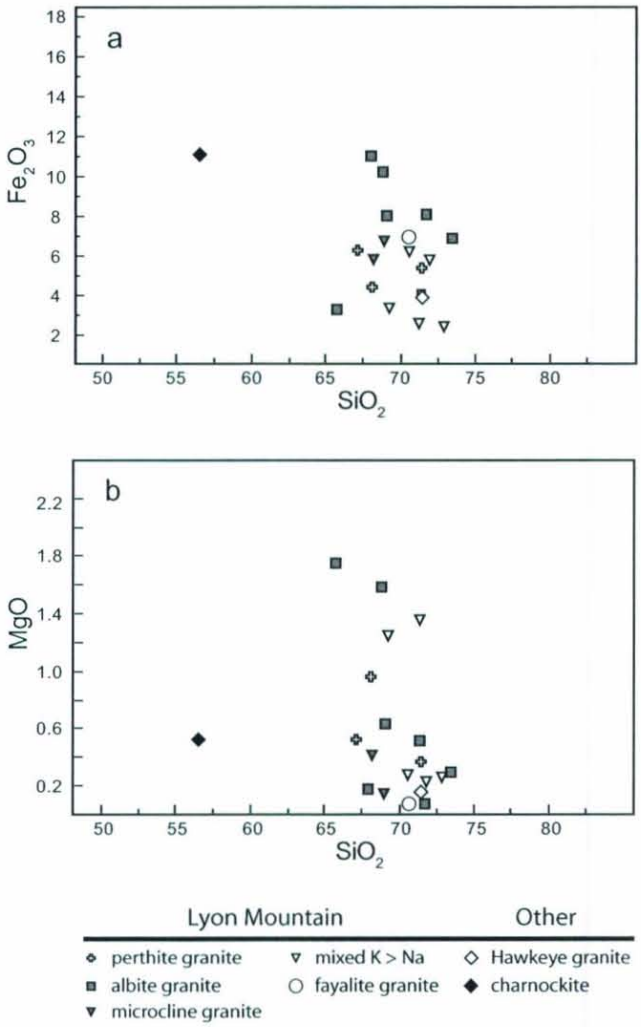

Figure 4-8. Whole rock geochemistry plots of major elements verses total silica plots for the Lyon Mountain granite and associated rocks. Values are in weight percent.

lower SiO_2 content typically have higher TiO_2 and Al_2O_3 values but with no clear correlation to a particular type of alteration (Figs. 4-9). Elevated Ca is observed in some samples regardless of rock type or alteration (e.g., Arnold Hill, RC-06-2; Dry Bridge, 99-2b) (Table 4-1; Fig 4-10a). Samples that have experienced K-alteration (Dannemora, 99-6c) are enriched in the large ion lithophile elements (LILE), Rb (170 % increase), Cs (333 % increase) and Ba (540 % increase), relative to the perthitic granite (Clintonville, 99-1a). Albite granite and Na altered samples are depleted in these same elements relative to the perthite granite (Figs. 4-10, -11 and -12).

Plots of elements generally considered to be immobile (e.g., Ti, Al, Zr, Y, and Nb) are presented in Figure 4-13. Titanium and Al contents are variable in the LMG with a slight decrease of TiO_2 with increasing Zr and a slight increase of Al with increasing Ti (Fig 4-13a, b). Most samples that have experienced Na-alteration are enriched in most high field strength elements (HFSE) (Figs. 4-13c, d, e, and f) (Table 4-1). Thorium does not increase with Na-alteration. A specific comparison between the least altered perthite granite from Clintonville (99-1a) and the Na-altered Albite granite at Skiff Mountain (00-02) shows that Zr increased by 522 %, Y 400 %, Nb 167 %, and Ta 197 % in the Albite granite.

Chondrite normalized whole rock REE concentrations for the LMG and associated rocks are plotted in Figure 4-14 and reported in Table 4-1. All LMG samples have similar negative slopes with minor variations in La in the least altered samples and a more pronounced negative Eu anomaly in the Na altered samples (Fig. 4-14a). Samples that have experienced extreme Na alteration have the highest whole rock REE

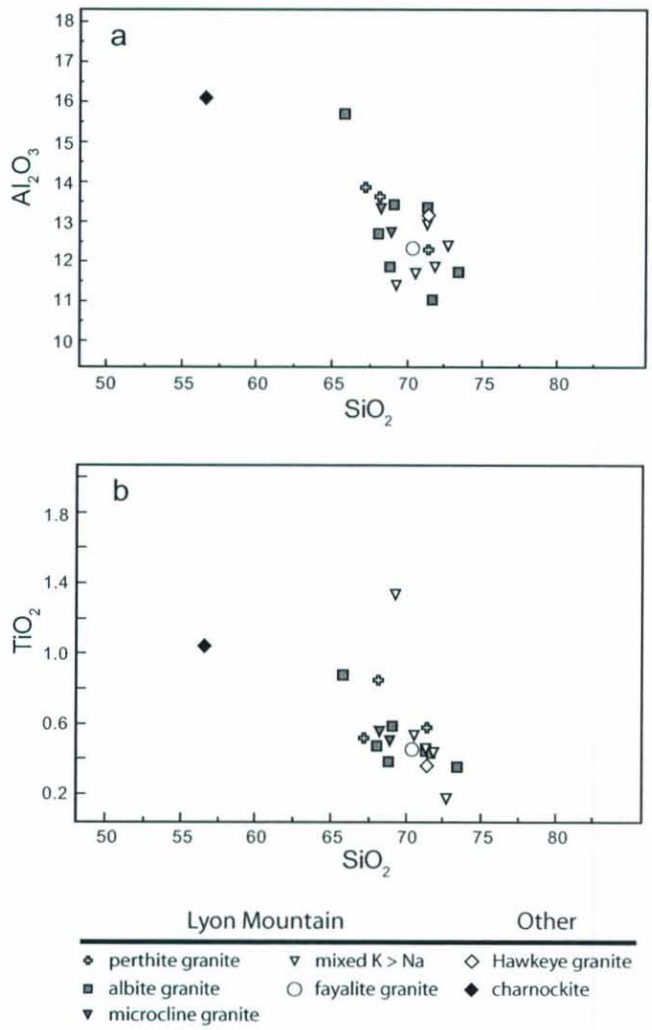

Figure 4-9. Whole rock geochemistry plots of major elements verses total silica plots for the Lyon Mountain granite and associated rocks. Values are in weight percent.

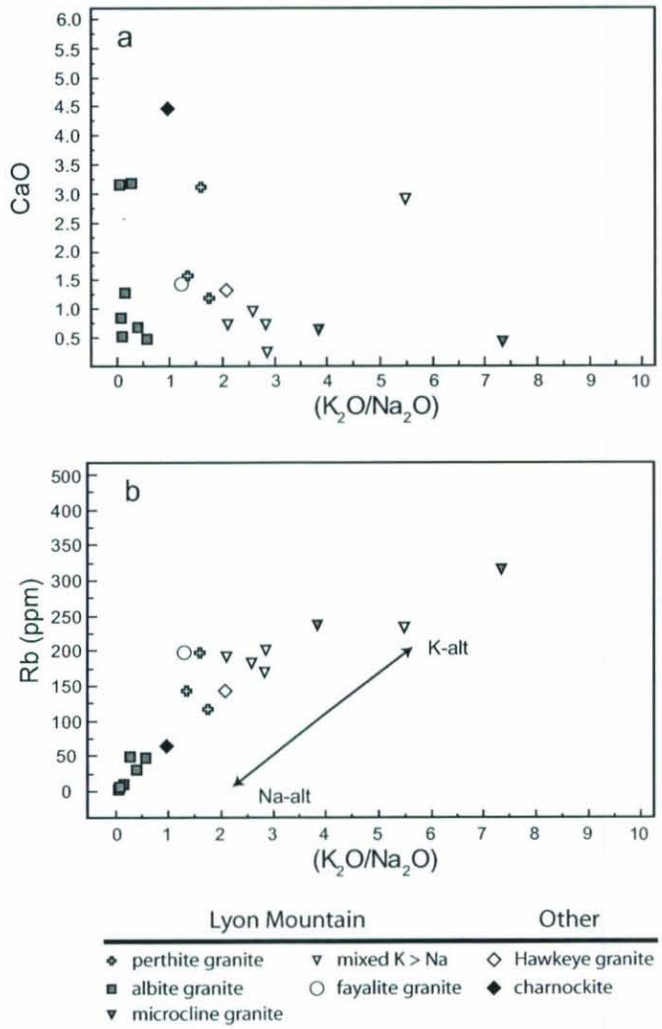

Figure 4-10. Whole rock geochemistry plots of Lyon Mountain granite and associated rocks. Large ion lithophiles verses alkalis. Values are in weight percent unless specified as parts per million (ppm).

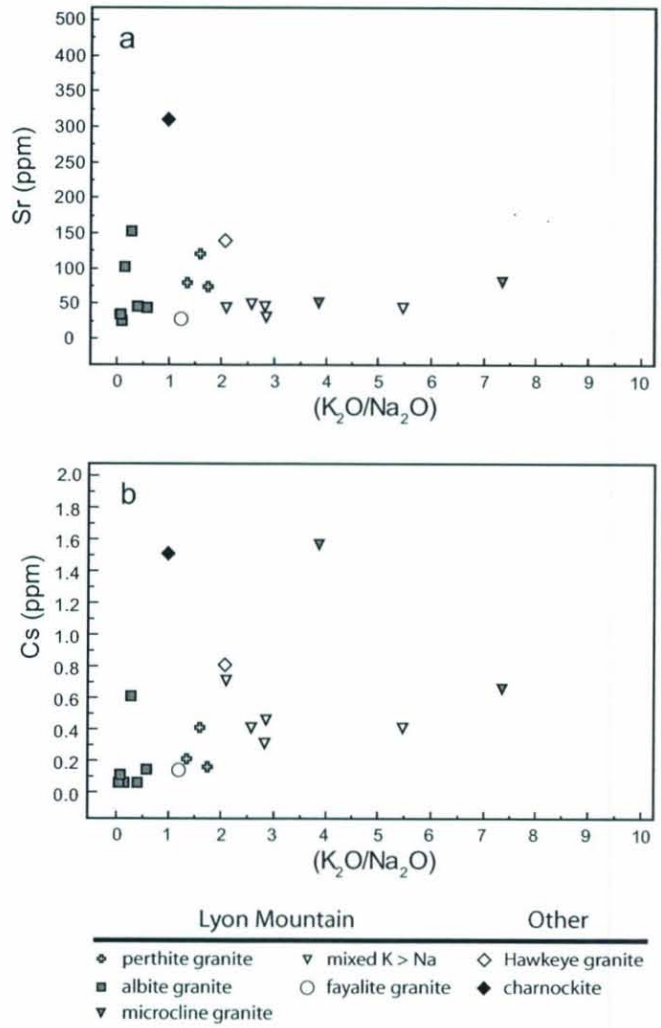

Figure 4-11. Whole rock geochemistry plots of Lyon Mountain granite and associated rocks. Large ion lithophiles verses alkalis. Values are in weight percent unless specified as parts per million (ppm).

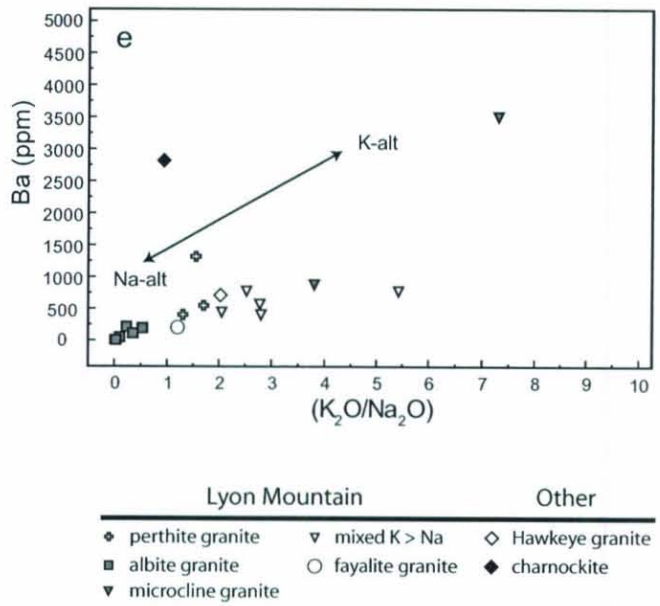

Figure 4-12. Whole rock geochemistry plots of Lyon Mountain granite and associated rocks. Large ion lithophiles verses alkalis. Values are in weight percent unless specified as parts per million (ppm).

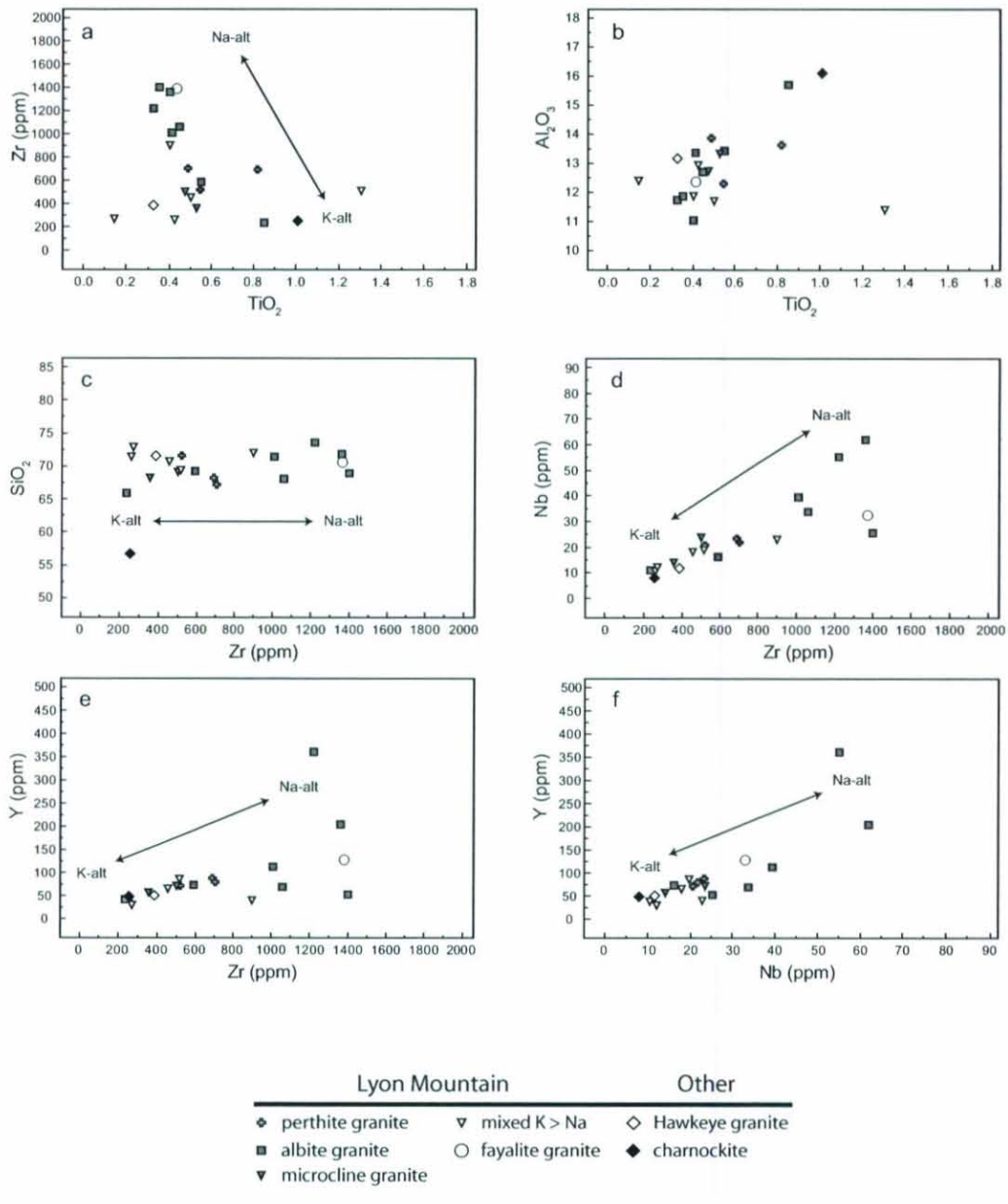

Figure 4-13. Immobile elements plots for Lyon Mountain granite and associated rocks. Values are in weight percent unless specified as parts per million (ppm).

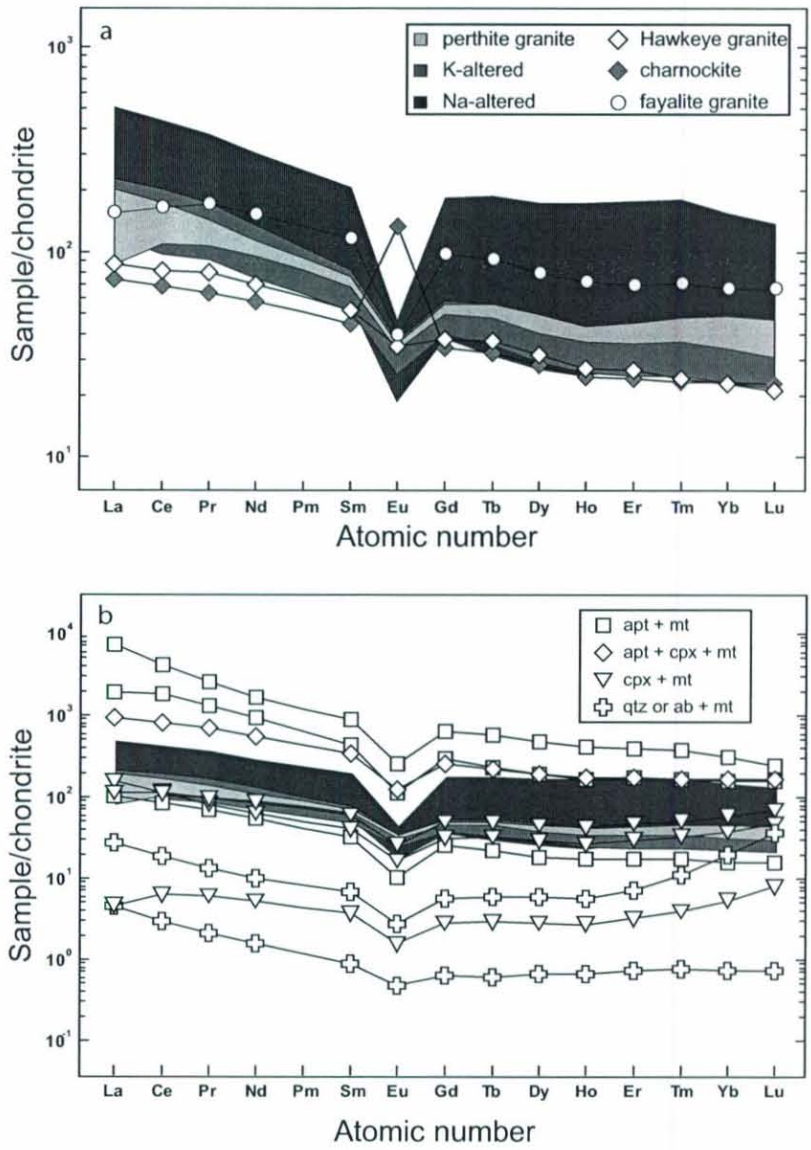

Figure 4-14. Chondrite normalized, whole rock rare earth element plots for the Lyon Mountain granite and associated rock types. Shaded areas in a) and b) are the range of rare earth element contents for the various Lyon Mountain granite rock types. a) Individual rare earth element patterns of representative samples of rocks associated with the Lyon Mountain granite. b) Rare earth element patterns for various ores within the Lyon Mountain granite categorized by the dominant mineral phases in the ore. Note the correlation of increased rare earth element content with the presence of apatite. Chondrite REE normalization of Boynton (1984).

Table 4-2 Rare earth element data of whole rock ore samples (ppm)

Location	Arnold Hill	Dannemora	Lyon Mountain	Mineville	Mineville	Palmer Hill*	Skiff Mountain*	Rutgers Mine	Rutgers Mine
Sample #	AH-06-6b	EM-06-1a	LM-06-1b	BH-06-2b	BH-06-1b	99-4a	00-02	06-4b	L-06-1a
Ore mineralogy	mt**-apt-qtz	cpx-mt	cpx-mt-ksp	qtz-mt	ab-qtz-mt-cpx	ab-apt-mt-qtz	mt-apt-qtz	apt-cpx-mt	cpx-mt
Element									
La	620	49.30	1.46	1.43	9.03	32.21	2300	298	36.00
Ce	1490	94.20	5.13	2.47	16.00	69.35	3390	667	91.70
Pr	159	10.20	0.76	0.26	1.68	8.81	311.40	85.50	12.00
Nd	575	39.20	3.20	0.96	6.23	33.65	993.36	339.00	52.40
Sm	87.90	8.12	0.73	0.18	1.37	6.32	175.67	67.50	12.10
Eu	8.40	1.25	0.12	0.04	0.21	0.77	19.49	9.17	1.95
Gd	77.50	8.31	0.74	0.17	1.52	6.70	168.23	68.50	13.30
Tb	11.40	1.57	0.14	0.03	0.30	1.06	28.28	10.70	2.40
Dy	64.50	9.60	0.92	0.22	1.97	6.05	153.30	61.60	15.00
Ho	12.20	1.95	0.20	0.05	0.43	1.25	30.67	12.50	3.15
Er	38.00	6.46	0.69	0.16	1.58	3.66	86.26	37.60	10.20
Tm	5.54	1.10	0.13	0.03	0.38	0.56	12.52	5.58	1.69
Yb	33.80	8.00	1.13	0.16	4.20	3.34	66.22	34.80	12.50
Lu	5.21	1.56	0.26	0.02	1.21	0.51	8.13	5.54	2.31

* from Valley et al., 2010 Chemical Geology v. 275 p. 208-220

** magnetite has been replaced by hematite

concentrations and the widest range of REE concentrations relative to the other samples. Lanthanum has increased by 205 %, Nd 191 % and Yb 357 % in the albite granite at Skiff Mountain compared to the perthite granite at Clintonville. The least altered samples and those dominated by potassic alteration are broadly similar in concentrations and variability (Fig. 4-14a; Table 4-1). Overall all rock types in the LMG have elevated REE relative to the Hawkeye granite and AMCG charnockite. The AMCG suite charnockite, however, has a pronounced positive Eu anomaly. The concentrations of REE in the ore deposits of the LMG are highly variable depending on the mineralogy of the ore (Fig. 4-14b and Table 4-2). Those ore samples containing abundant (i.e., 25 - 30 modal %) apatite are highly enriched in REE relative to those containing only pyroxene or those ore deposits associated with quartz and feldspar pegmatites (Fig. 4-14b).

4-3-4 MINERAL CHEMISTRY

Electron probe analyses of minerals from the different LMG rock types were analyzed to better understand the fluid geochemistry of alteration and the differences between primary and alteration-related minerals.

Feldspar

Representative samples of various feldspars from each of the three main LMG rock types were analyzed and are shown in Table 4-3 and plotted in Figure 4-15. Plagioclase chemistry from all lithologies is highly sodic containing 94 to 99 % Ab component. In the perthite granite, there is a distinction between alteration-related albite and the albite lamellae. Electron microprobe transects across single perthitic feldspar grains reveal that rims and patches of alteration related albite are consistently near end

member compositions (e.g., Ab_{99}), whereas albite lamellae contain up to 5% An (Fig. 4-15a;. 4-16a, b; Table 4-3). Alteration-related flame lamellae in the fayalite granite have similar end member compositions (e.g., Ab_{99}) (Figs. 4-15b and 4-16b; Table 4-3). The perthite grains in the fayalite granite also contain small, thin plagioclase lamellae related to granite crystallization and cooling, but these were too small for EPMA analysis (< 5 μm) (Figs. 4-5c, g). Plagioclase compositions in the albite granite have chemical composition of Ab 94-95 or contain near pure albite (e.g., Ab_{99}) (Fig. 4-15c; Table 4-3).

The microcline regions in the perthite granite range from Or_{92} to Or_{97} (Fig 4-14a; 4-16a and b; Table 4-3), while perthite grains in the fayalite granite are typically Or_{90} to Or_{94} (Fig. 4-15b and 4-16b; Table 4-3). Potassium feldspar in the microcline granite was the most variable in composition of all the samples analyzed. Orthoclase values typically range from Or_{86} to Or_{96}. This range of Or values may be due to remnant Na from the original perthitic feldspar or chemical variations in multiple generations of potassium feldspar growth (see microcline granite description). Barium was below the minimum detection limit (MDL) of the EPMA analyses for the conditions used in potassium feldspar of the perthitic granite and fayalite granite, but was as high as 1 wt. % BaO in the microcline granite.

Clinopyroxene

Clinopyroxene was not present in our samples of the microcline granite, but has been reported by other workers (Postel, 1952). The composition of all pyroxene grains (regardless of LMG rock type) is aegirine-augite with varying in the amount of Ca, Na, Fe, and Mg (Table 4-4). Clinopyroxene from the perthitic granite contains a greater

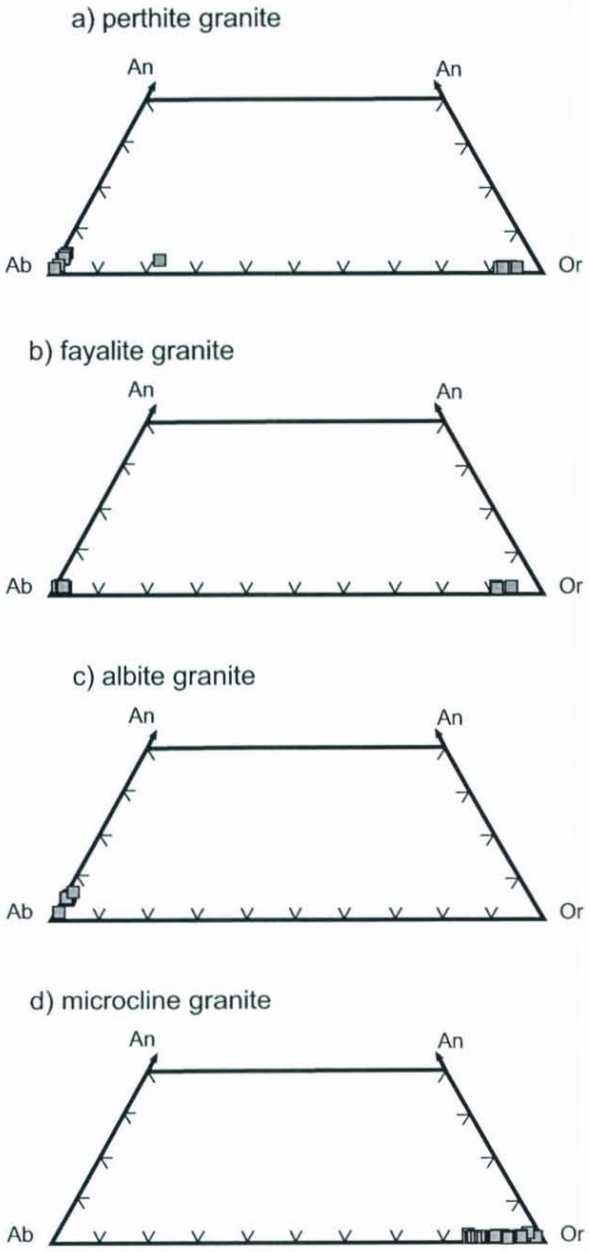

Figure 4-15. Ternary diagrams illustrating the feldspar compositions from crystals within the Lyon Mountain granite. a) Perthite granite (Rutgers Mine), b) fayalite granite (Ausable Forks), c) albite granite (Dry Bridge), and d) microcline granite (Dannemora).

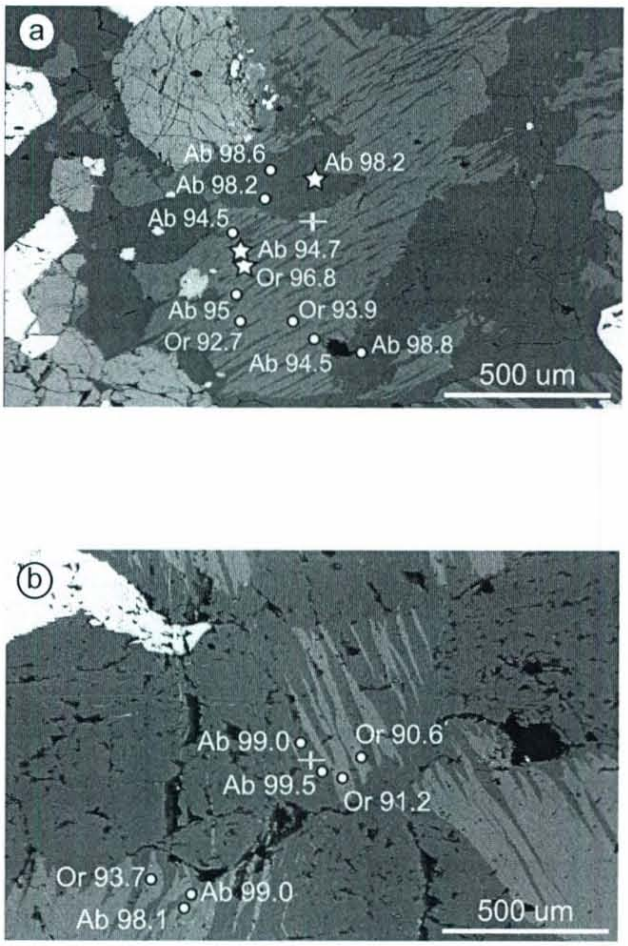

Figure 4-16. a) and b) Back-scattered electron images of perthitic feldspar grains analyzed by electron microprobe showing the locations and composition of individual analyses in the Ab-Or-An system.

Table 4-3 Feldspar EPMA analyses

Location	Rutgers Mine	Rutgers Mine	Ausable Forks	Dry Bridge	Rutgers Mine	Ausable Forks	Dannemora	Dannemora	Avg. MDL
Sample #	06-4d	06-4d	99-3a	99-2b	06-4d	99-3a	99-6c	99-6c	
Mineral	lamellae	albite grain	flame lamellae	albite grain	microcline	K-feldspar	microcline	microcline	
Element									
SiO_2	67.23	68.50	67.75	67.47	65.11	64.70	65.15	64.78	0.04
Al_2O_3	20.39	20.03	20.24	20.55	18.47	18.40	18.93	19.01	0.03
FeO[a]	< MDL	0.11	0.34	0.30	0.17	0.15	< MDL	< MDL	0.06
CaO	0.98	0.25	0.14	0.98	< MDL	< MDL	< MDL	< MDL	0.03
Na_2O	10.95	11.12	11.28	10.55	0.35	0.72	1.53	0.46	0.03
K_2O	0.12	0.10	0.06	0.07	16.24	16.24	14.20	15.07	0.05
BaO	< MDL	< MDL	< MDL	< MDL	< MDL	< MDL	0.55	1.01	0.02
Total	99.83	100.13	99.90	99.79	99.99	100.17	100.37	100.32	
Or	0.70	0.60	0.40	0.40	96.80	93.70	86.00	95.60	
Ab	94.70	98.20	99.00	94.70	3.20	6.40	14.10	4.50	
An	4.70	1.20	0.70	4.90	0.00	0.00	0.00	0.00	
number of cations on the basis of 8 oxygen									
Si	2.95	2.99	2.97	2.95	3.00	2.99	2.99	2.99	
Al	1.05	1.03	1.04	1.06	1.00	1.00	1.02	1.03	
Fe	< MDL	0.00	0.01	0.01	0.01	0.01	< MDL	< MDL	
Ca	0.05	0.01	0.01	0.05	< MDL	< MDL	< MDL	< MDL	
Na	0.93	0.94	0.96	0.90	0.03	0.07	0.14	0.04	
K	0.01	0.01	0.00	0.00	0.96	0.96	0.83	0.89	
Ba	< MDL	< MDL	< MDL	< MDL	< MDL	< MDL	0.01	0.02	

The mineral formulas calculated are based on 8 oxygen

[a] = total Fe

Table 4-4 Pyroxene and Olivine EPMA analyses

Location	Rutgers Mine	Rutgers Mine	Dry Bridge	Dry Bridge	Ausable Forks	Ausable Forks	Ausable Forks	Avg MDL
Sample #	06-4d	06-4d	99-2b	99-2b	99-3a	99-3a	99-3a	
Mineral	cpx	cpx	cpx	cpx	cpx	exsolution	olivine	
Element								
SiO_2	52.13	52.05	50.11	50.10	47.81	45.42	29.36	0.02
TiO_2	0.18	0.24	0.10	0.06	0.28	0.14	0.04	0.03
Al_2O_3	1.70	1.68	1.76	1.79	0.71	0.12	0.15	0.02
FeO[a]	13.37	13.67	22.23	22.34	30.41	51.38	67.93	0.05
MnO	0.18	0.18	0.23	0.34	0.93	1.98	2.05	0.05
MgO	9.70	9.86	4.34	4.30	0.28	0.29	0.22	0.02
CaO	20.06	20.15	16.82	16.59	18.00	0.46	0.05	0.03
Na_2O	2.50	2.40	4.03	4.23	1.66	0.06	0.07	0.03
K_2O	< MDL	< MDL	< MDL	< MDL	< MDL	< MDL	< MDL	0.02
Cr_2O_3	< MDL	< MDL	< MDL	< MDL	< MDL	< MDL	< MDL	0.05
Total	99.84	100.22	99.66	99.70	100.12	99.90	99.83	
Number of cations on the basis of 6O								
Si	1.99	1.98	2.00	2.00	1.98	2.00	1.00	
Ti	0.01	0.01	0.00	0.00	0.01	0.01	0.00	
Al	0.08	0.08	0.08	0.08	0.04	0.01	0.01	
Fe	0.43	0.44	0.74	0.74	1.05	1.88	1.93	
Mn	0.01	0.01	0.01	0.01	0.03	0.07	0.06	
Mg	0.55	0.56	0.26	0.26	0.02	0.02	0.01	
Ca	0.82	0.82	0.72	0.71	0.80	0.02	0.00	
Na	0.19	0.18	0.31	0.33	0.13	0.01	0.01	
K	< MDL	< MDL	< MDL	< MDL	< MDL	< MDL	< MDL	
Cr	< MDL	< MDL	< MDL	< MDL	< MDL	< MDL	< MDL	

The mineral formulas calculated are based on 6 oxygen for pyroxene and 4 oxygen for olivine

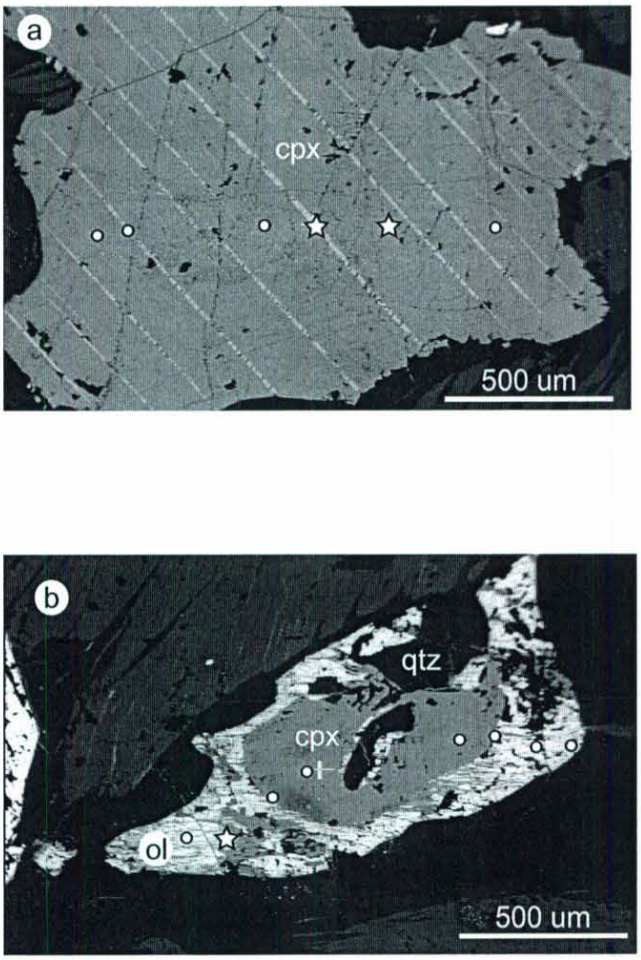

Figure 4-17. a and b) Back-scattered electron image of clinopyroxene and d) olivine and clinopyroxene grains from the fayalite granite analyzed by electron microprobe. Stars represent analyses presented in Table. 4-4.

Table 4-5 Magnetite EPMA analyses

Location	Rutgers (pg)*	Palmer Hill (grn.)**	Palmer Hill (ore)	Skiff Mtn (ore)	Avg. MDL
Sample #	06-4d	99-4b	99-4a	00-01	
Mineral	magnetite	hematite-magnetite	magnetite	magnetite	
Element					
SiO_2	< MDL	< MDL	< MDL	< MDL	0.02
TiO_2	< MDL	9.03	0.03	0.51	0.02
Al_2O_3	0.18	0.13	0.10	0.23	0.02
Fe_3O_4	99.62	87.75	99.76	98.89	0.04
MgO	< MDL	< MDL	0.05	0.06	0.04
MnO	0.19	0.12	< MDL	0.31	0.04
CaO	< MDL	0.01	< MDL	< MDL	0.02
Cr_2O_3	< MDL	< MDL	0.04	< MDL	0.03
V_2O_3	0.05	0.03	0.03	< MDL	0.03
ZnO	0.08	< MDL	< MDL	< MDL	0.04
Total	100.20	97.17	100.02	100.06	
Number of cations on the basis of 4O					
Si	< MDL	< MDL	< MDL	< MDL	
Ti	< MDL	0.26	0.00	0.02	
Al	0.01	0.01	0.01	0.01	
Fe	2.98	2.60	2.99	2.95	
Mg	< MDL	< MDL	0.00	0.00	
Mn	0.01	0.00	< MDL	0.01	
Ca	< MDL	0.00	< MDL	< MDL	
Cr	< MDL	< MDL	0.00	< MDL	
V	0.00	0.00	0.00	< MDL	
Zn	0.00	< MDL	< MDL	< MDL	

The mineral formulas calculated are based on 4 oxygen

* Samples collected near Rutgers mine

** Microcline granite overprinted by Na alteration

diopside component than either the albite or fayalite granites while clinopyroxene from the albite granite has increasing Na and Fe and decreasing Ca and Mg. Clinopyroxene from the fayalite granite have a higher ferrohedenbergite component (Fe-rich and Mg poor) than other LMG clinopyroxene grains and contain exsolution lamellae of near pure ferrosilite or inverted pigeonite (Figs. 17). Olivine grains in the fayalite granite are near end-member fayalite composition.

Magnetite

The chemistry of magnetite was compared between the perthite granite, a granite sample that has experienced both K and Na alteration (Palmer Hill) and various ore samples (Table 4-5). There are few differences in major elements between ore and granitic magnetite compositions. Magnetite is relatively low in Ti and other transition metals. One exception is the sample from the granite just a few meters above the ore body at the Palmer Hill mine which contained anomalously high Ti (up to 11 wt.%). This sample contains both microcline and albite, but no perthitic feldspar. The magnetite in this sample has undergone extensive oxidation and replacement by hematite (martite in some grains).

4-3-5 U-TH-PB GEOCHRONOLOGY

Three samples were chosen for zircon U-Th-Pb geochronology that represent the three main rock types within the LMG. Two additional samples from the LMG at Palmer Hill and Arnold Hill were previously published in Valley et al. (2009). In addition to the LMG samples, two amphibolite layers and three crosscutting dikes (discussed above) were dated to constrain the timing of fluid alteration and Fe-mineralization relative to the

regional tectonics of Adirondack Highlands. These dates along with previously published U-Th-Pb dates are summarized in Table 4-6. Individual U-Th-Pb analyses are presented in Tables 4-7, -8 and -9. All errors are given as 2 sigma and the stated mean square weighted deviation (MSWD) is of concordance and equivalence.

Lyon Mountain granite

A representative sample of the LMG perthite facies was collected along the Ausable River near Clintonville, New York (sample 99-1A) for geochronology (Fig. 4-1). Zircon grains from that sample are brown to pink or clear, well-faceted, and can contain irregular shaped cores that are highly fractured. Zircon grains are typically 200-400 μm in length with an aspect ratio that approximates 2:1. Some zircon grains exhibit growth zoning and relict cores (in BSE), whereas others (especially those lacking relict cores) are relatively homogeneous (e.g., Figs. 4-18a and b). Zircon grains without inherited cores and rims on zircon grains with cores from the perthitic granite at Clintonville, yield a concordant age of 1047.3 ± 9.2 Ma (2σ) (n = 7) (Fig. 4-19a).

A sample of microcline granite was collected one mile west of the town of Dannemora, New York (sample 99-6c) (Fig. 4-1). The zircon grains are typically 200-500 μm in length, with an aspect ratio that approximates 2:1, well-faceted, and brown to pink or clear in color, and in some cases have obvious cores (Fig. 4-18c, d) of AMCG suite age (e.g., ~1150 Ma) that are dark brown, and are often cracked relative to the outer regions in the zircon crystals. New zircon growth embays or cuts into these relict cores. Most zircon cores and outer regions show growth zoning in BSE images. Single age zircon grains, and rims on grains with cores, from the microcline granite give a

Table 4-6 Summary of zircon ages for the LMG and associated rocks.

Sample	Concordia Age	2 sigma%
Lyon Mountain granite		
Clintonville (99-1a)	1047.3	9.2
Dannemora (99-6c)	1050.5	5.2
Palmer Hill* (99-4b)	1062.6	5.5
Arnold Hill* (99-5a)	1060.7	4.5
Dry Bridge**	1055.0	7.0
Dry Bridge(alt.) (99-2b)	1033.0	8.6
Ausable Forks (fayalite granite)**	1047.3	2.2
Iron Oxide-Apatite ores		
Palmer Hill* (99-4a)	1038.9	4.4
Arnold Hill* (AH-06-6b)	1016.1	7.1
Mineville* (OBO)	1020.0	11.0
Skiff Mountain* (00-01)	1000.9	9.2
Mafic body		
Ausable Forks (F-06-1a)	1018.6	7.6
Skiff Mountain (00-11)	1046.0	11.0
Granitic dikes		
Lyon Mtn (LM-06-1a)	1040.9	6.8
Dannemora (99-6b)	1016.5	6.5
Skiff Mtn (00-03)	1030.4	11.0

* U-Th-Pb age from Valley et al. 2009
** U-Th-Pb age fromMcLelland et al. 2001

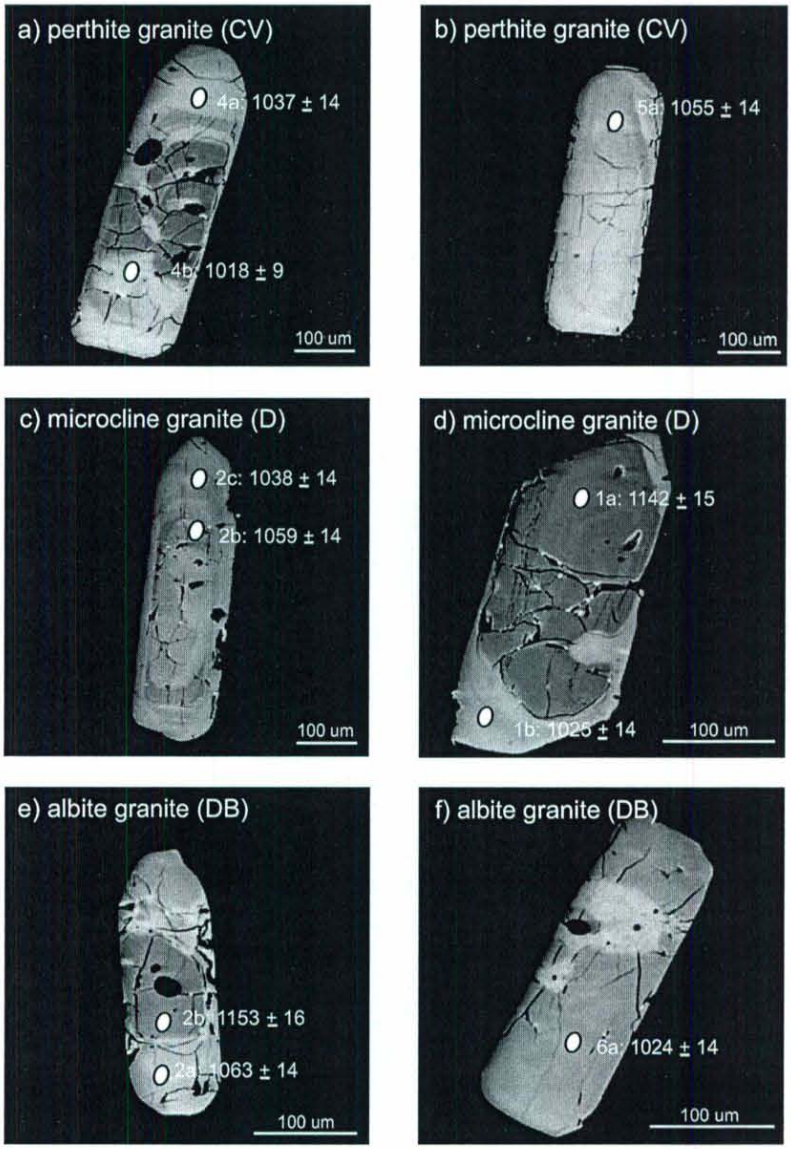

Figure 4-18. a) and b) Representative BSE images of zircon grains from the perthite granite collected at Clintonville (CV) (99-1a), b) and c) microcline granite collected at Dannemora (D) (99-6c) and d) and e) albite granite collected at Dry Bridge (DB) (99-2b). Single spot ages are given as $^{207}Pb/^{206}Pb$ ages corrected for common Pb. White ellipses are the approximate size ion probe craters.

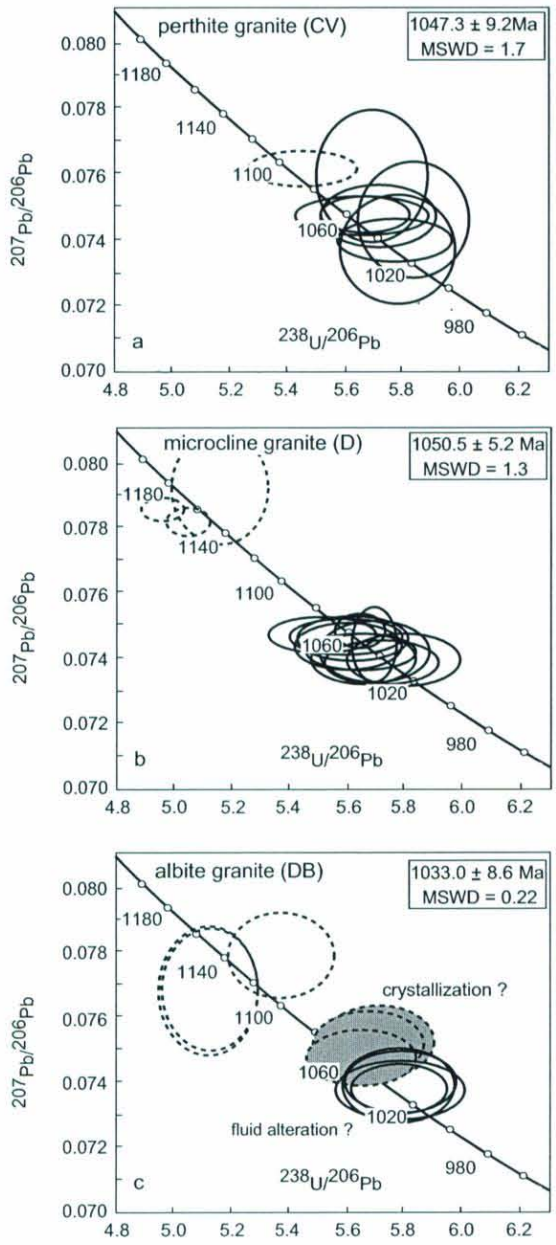

Figure 4-19. Tera-Wasserburg Concordia diagrams ($^{207}Pb/^{206}Pb$ versus $^{238}U/^{206}Pb$) showing zircon ages for a), perthite granite from Clintonville (CV) (99-1a) b), microcline granite at Dannemora (D) (99-6b) c), albite granite at Dry Bridge (DB) (99-2b). Uncertainties on quoted concordia ages (Ludwig 2003) are 2σ. Error ellipses are 2σ for all samples. Dashed error ellipses are not used in the age calculation. Filled error ellipses in figure c are used to show the similarity in ages to those from the perthitic and microcline granite.

Table 4-7 Zircon isotopic data Ion microprobe U-Th-Pb results for the Lyon Mountain granite

Sample	U(ppm)	Th (ppm)	Pb (ppm)	Th/U	f206 *	238U/206Pb	sigma%	207Pb/206Pb	sigma%	207Pb/206Pb	Ma error	206Pb/238U	Ma error
Perthite granite (Clintonville, 99-1a)													
4B	197	78	40	0.394	0.09	5.835	1.38	0.07459	0.96	1017.9	13.6	1019.7	13.0
2B	269	111	55	0.411	0.09	5.784	1.41	0.07364	0.90	1027.9	14.1	1028.1	13.5
3A	1268	318	252	0.251	0.03	5.775	1.39	0.07395	0.36	1028.9	13.9	1029.5	13.3
4A	861	165	170	0.192	0.04	5.723	1.38	0.07469	0.52	1037.0	13.8	1038.1	13.2
1B	124	52	26	0.424	0.04	5.694	1.38	0.07591	1.10	1040.5	14.0	1043.0	13.3
2A	1359	342	274	0.251	0.01	5.698	1.38	0.07468	0.33	1041.5	13.9	1042.4	13.3
5A	1553	404	317	0.260	0.01	5.621	1.41	0.07469	0.33	1055.3	14.4	1055.6	13.7
1A	1678	97	336	0.058	0.03	5.455	1.38	0.07639	0.28	1084.8	13.7	1084.1	14.4
Microcline granite (Dannemora, 99-6c)													
1b	911	164	177	0.180	0.03	5.796	1.38	0.07390	0.45	1025.4	13.7	1026.0	13.1
2C	1202	246	239	0.205	0.02	5.723	1.38	0.07380	0.39	1038.2	13.8	1038.1	13.2
3B	559	139	113	0.249	0.05	5.693	1.38	0.07412	0.52	1043.1	13.9	1043.2	13.3
1a	415	69	82	0.167	0.14	5.690	0.59	0.07436	0.63	1043.3	6.0	1043.7	5.7
5B3	941	141	186	0.150	0.05	5.659	1.29	0.07393	0.42	1049.5	13.2	1049.0	12.5
1d	1352	149	265	0.110	0.02	5.645	0.60	0.07481	0.28	1050.7	6.1	1051.3	5.8
4B	1567	328	316	0.210	{0.01}	5.644	1.38	0.07417	0.31	1051.8	14.0	1051.5	13.4
4C	1069	178	214	0.166	0.02	5.618	1.38	0.07459	0.39	1056.0	14.1	1056.1	13.4
2B	1207	212	243	0.176	0.03	5.603	1.38	0.07439	0.45	1058.9	14.1	1058.6	13.5
4A	1721	364	351	0.212	{0.01}	5.588	1.38	0.07459	0.29	1061.5	14.2	1061.3	13.5
5A	1619	290	331	0.179	0.01	5.514	1.38	0.07468	0.29	1075.1	14.3	1074.4	13.6
1a	188	81	44	0.433	{0.04}	5.152	1.38	0.07922	0.92	1141.5	15.3	1143.5	14.4
1b	1308	652	316	0.498	0.03	5.037	0.59	0.07813	0.24	1168.4	6.7	1167.4	6.3
3b	2229	1470	570	0.659	0.02	4.953	0.59	0.07850	0.18	1187.1	6.8	1185.5	6.4
Albite granite (Dry Bridge, 99-2b)													
6A	655	100	126	0.153	0.02	5.806	1.38	0.07380	0.46	1023.9	13.7	1024.5	13.1
1A	525	74	101	0.141	{0.02}	5.787	1.38	0.07401	0.51	1026.9	13.7	1027.5	13.1
8A	554	73	107	0.132	{0.03}	5.784	1.38	0.07387	0.64	1027.6	13.7	1028.1	13.1
4A	644	119	126	0.185	0.04	5.753	1.38	0.07368	0.49	1033.1	13.8	1033.1	13.1
3C	577	75	113	0.129	{0.02}	5.706	1.40	0.07520	0.62	1039.4	14.2	1041.0	13.5
5A	497	55	97	0.110	0.03	5.674	1.38	0.07519	0.52	1045.1	13.9	1046.4	13.3
7A	530	74	105	0.140	{0.01}	5.649	1.38	0.07467	0.50	1050.3	14.1	1050.8	13.4
3A	289	207	66	0.718	0.06	5.370	1.38	0.07787	0.69	1098.4	14.7	1100.8	14.0
1B	192	95	46	0.495	{0.09}	5.117	1.38	0.07671	1.04	1152.8	15.4	1150.7	14.5
2B	103	39	24	0.379	{0.10}	5.116	1.39	0.07677	1.05	1153.0	15.6	1151.0	14.6

Notes:
All errors are 1 sigma
*Percent of Pb206 that is common Pb, brackets indicate 204 was too small to measure

concordant age of 1050.5 ± 5.2 Ma (2σ) (n = 11) (Fig. 4-19b). This age agrees with the data of McLelland et al. (2001a) who obtained a U-Pb zircon age of 1055 ± 7Ma (2σ) by sensitive high-resolution ion microprobe (SHRIMP) from a sample collected at the same outcrop.

Samples of the albite granite were collected at Dry Bridge two miles northeast of the town of Ausable Forks, New York (sample 99-2b) (Fig. 4-1). Zircon grains are typically smaller, and much less abundant, than those of the microcline granite or the perthitic granite and have aspect ratios of 2:1 and range from 100 to 200 μm in length (Figs. 4-18e and f). Some of the zircon grains are similar to those of the perthite and microcline granites with dark irregular cores of ~1150 Ma and rims or single age zircon grains ~1060 Ma (filled error ellipses, Fig. 4-19c); however, these analyzes did not produce a statistically reliable concordia age. McLelland et al. (2001a) obtained a similar date of 1055 Ma ± 7. The albite granite at Dry Bridge, however, contains a significant population of zircon, which display patchy zoning, or no zoning whatsoever in BSE and CL, and are consistently younger than the typical 1060 to 1050 Ma zircon population found throughout the other LMG rock types. These zircon grains with patchy zoning yield a concordant age of 1033 ± 9 Ma (2σ) (n = 4) (Fig. 19c). We interpret this age to reflect hydrothermal zircon growth during Na alteration at the Dry Bridge locality. This interpretation is supported by U-Pb age data from nearby magnetite ore bodies associated with Na alteration that have been dated between 1040 and 1015 Ma (Valley et al., 2009). These ages have not been detected in the microcline granite despite several attempts to find younger zircon.

Crosscutting granitic dikes

Relatively undeformed granitic dikes that crosscut the fabric (when present) of the LMG are common. Representative samples were collected and dated to provide a minimum age for fabric development within the LMG and to better constrain the ages of various types of alteration.

A crosscutting, plagioclase-rich, granitoid dike was collected at the Chateaugay mine in the town of Lyon Mountain, New York (Fig. 4-1) (sample LM-06-1a). The dike crosscuts the granitic fabric as well as the main ore body. The dike itself has undergone secondary Na alteration, which in-turn was overprinted by a minor potassic alteration. Zircon grains from this sample are clear and elongate or equant. Equant grains are up to 300 μm on a side, and elongate grains are typically 400-600 μm with some grains as long as 900 μm. These zircon grains contain growth zoning or display patchy zonation in BSE and CL images (Figs. 20a and b). No obvious inherited cores were observed. These zircon yield a concordant age of 1040.9 ± 6.8 Ma (2σ) (n = 11) (Fig. 4-21). The age of this dike provides a maximum age for Na alteration at the Chateaugay mine in Lyon Mountain and minimum age for at least one stage of ore formation (e.g., clinopyroxene-magnetite ore).

A granite pegmatite dike was collected at the same locality as the dated microcline granite sample mentioned above, just west of the town of Dannemora, New York (sample 99-6b). Here the pegmatitic dike crosscuts the fabric in the microcline granite. Zircon grains are clear, elongate and 300-600 μm in length. Zircon grains typically exhibit patchy zonation and can contain obvious inherited cores in BSE images

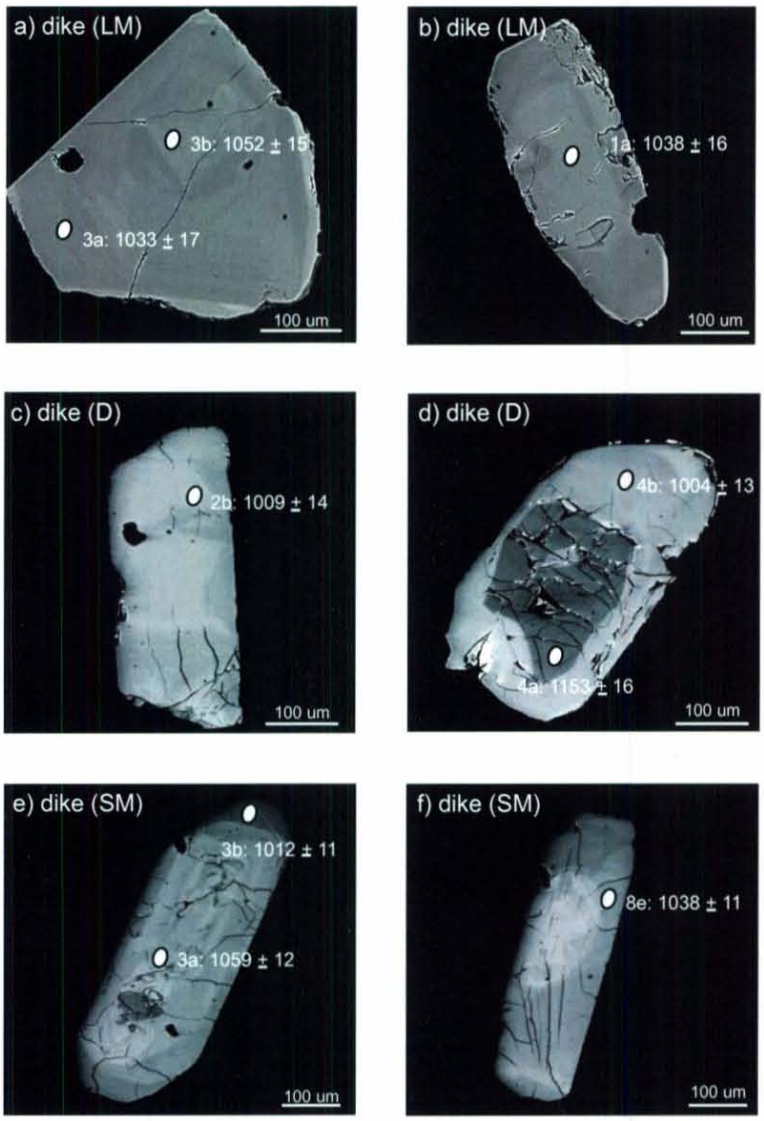

Figure 4-20. Representative BSE electron images of zircon grains from a) and b), crosscutting plagioclase-rich dike at Lyon Mountain (LM) (LM-06-1a) c) and d), granitic pegmatite dike at Dannemora (D) (99-6b) e) and f), granitic pegmatite dike at Skiff Mountain (SM) (00-03). Single spot ages are given as $^{207}Pb/^{206}Pb$ ages corrected for common Pb. White ellipses are the approximate size ion probe craters.

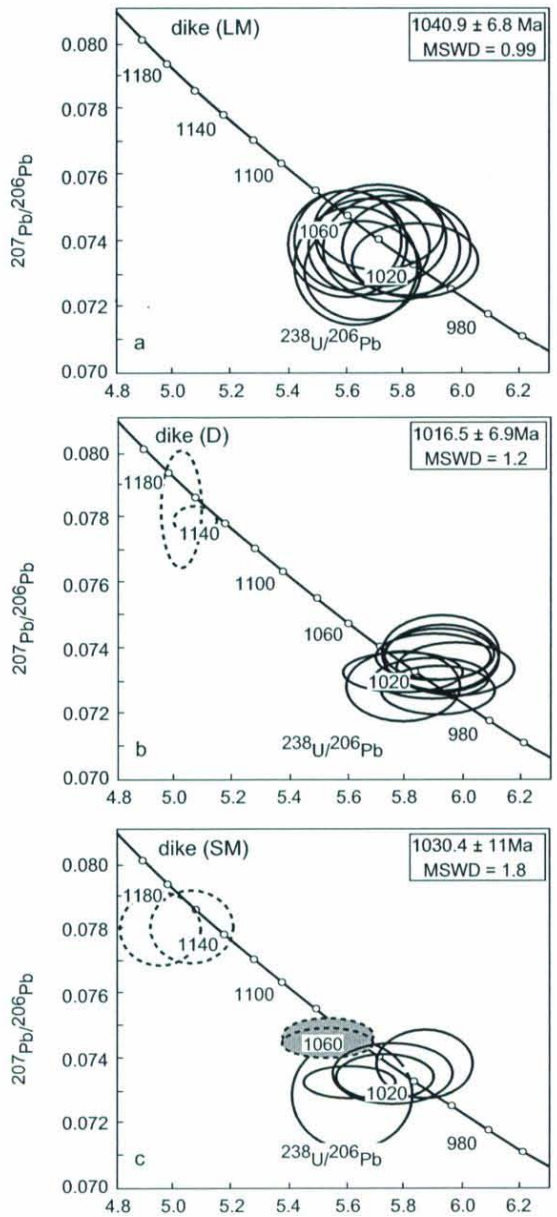

Figure 4-21. Tera-Wasserburg Concordia diagrams ($^{207}Pb/^{206}Pb$ versus $^{238}U/^{206}Pb$) showing zircon ages for a) crosscutting plagioclase-rich dike at Lyon Mountain (LM) (LM-06-1a) b), granitic pegmatite dike at Dannemora (D) (99-6b) c), granitic pegmatite dike at Skiff Mountain (SM) (00-03). Uncertainties on quoted concordia ages (Ludwig 2003) are 2σ. Error ellipses are 2σ for all samples. Dashed error elipses are not used in the age calculation. Filled error ellipses in figure c are used to show the similarity in ages to those from the perthitic and microcline granite and are not included in the calculation of the concordia age.

Table 4-8 Zircon isotopic data for dikes that crosscut the Lyon Mountain granite
Ion microprobe U-Th-Pb results for dikes in the LMG.

Sample	U(ppm)	Th (ppm)	Pb (ppm)	Th/U	f206 *	238U/206Pb	sigma%	207Pb/206Pb	sigma%	207Pb/206Pb	Ma error	206Pb/238U	Ma error
plagioclase-rich dike (Lyon Mtn., LM-06-1a)													
7a	841	274	168	0.326	0.03	5.836	1.52	0.07338	0.62	1019.3	15.1	1019.5	14.4
6b	419	173	86	0.412	0.03	5.805	1.58	0.07377	0.80	1024.0	15.7	1024.5	15.0
3a	354	204	77	0.576	0.04	5.751	1.68	0.07372	0.87	1033.5	16.8	1033.5	16.1
1a	362	216	79	0.597	0.02	5.721	1.58	0.07415	0.83	1038.2	15.9	1038.5	15.2
6a	477	195	100	0.409	0.04	5.709	1.59	0.07437	0.73	1040.0	16.1	1040.5	15.3
8a	333	196	73	0.588	0.01	5.670	1.48	0.07383	0.80	1047.6	15.0	1047.1	14.3
3d	272	114	58	0.419	0.03	5.651	1.44	0.07307	0.83	1051.9	14.7	1050.3	13.9
4b	494	324	112	0.656	0.02	5.629	1.54	0.07321	0.98	1055.7	15.8	1054.1	15.0
6c	292	156	64	0.535	0.05	5.612	1.44	0.07401	0.83	1057.8	14.8	1057.1	14.0
10b	313	133	67	0.426	0.06	5.610	1.43	0.07395	0.83	1058.2	14.7	1057.4	14.0
4a	268	115	58	0.431	0.09	5.592	1.45	0.07386	0.88	1061.7	14.9	1060.6	14.1
granitic dike (Dannemora, 99-6b)													
3A	1038	242	198	0.233	0.03	5.981	1.39	0.07336	0.46	995.3	13.4	996.6	12.8
1A	1186	338	232	0.285	0.03	5.930	1.38	0.07368	0.51	1003.3	13.5	1004.6	12.9
4B	1092	243	209	0.222	0.03	5.925	1.38	0.07383	0.64	1003.8	13.4	1005.3	12.8
7A	1197	250	229	0.209	0.02	5.914	1.40	0.07267	0.43	1007.1	13.6	1007.0	13.0
5A	1018	212	196	0.209	0.02	5.899	1.38	0.07370	0.42	1008.4	13.5	1009.5	12.9
2B	1725	463	337	0.268	0.02	5.898	1.41	0.07304	0.34	1009.4	13.8	1009.7	13.2
8B	1245	281	244	0.226	0.01	5.792	1.46	0.07324	0.36	1027.0	14.5	1026.8	13.8
5B	760	187	150	0.246	0.05	5.790	1.38	0.07279	0.59	1027.9	13.7	1027.0	13.1
4A	117	68	29	0.584	{0.06}	5.099	1.39	0.07951	1.12	1152.7	15.6	1154.5	14.7
3b	112	46	27	0.411	0.25	5.022	0.59	0.07820	0.93	1171.7	6.8	1170.6	6.4
3c	1135	614	276	0.541	0.03	5.069	0.60	0.07782	0.25	1161.9	6.8	1160.8	6.4
granitic dike (Skiff Mtn, 00-03)													
1B	349	130	70	0.371	{0.05}	5.874	1.17	0.07385	0.58	1012.2	11.4	1013.4	10.9
6CX	574	150	116	0.261	{0.01}	5.729	1.17	0.07338	0.39	1037.7	11.7	1037.1	11.2
8E2	1767	160	336	0.090	0.18	5.760	1.46	0.07355	0.51	1038.1	11.3	1032.0	14.0
1A	1533	54	296	0.035	0.02	5.609	1.17	0.07327	0.28	1059.4	12.0	1057.6	11.4
6F2	604	176	124	0.292	0.17	5.610	1.49	0.07284	0.92	1067.4	12.0	1057.5	14.5
5BX	981	122	197	0.124	{0.01}	5.535	1.19	0.07472	0.27	1071.1	12.3	1070.6	11.7
3A	1589	62	312	0.039	0.02	5.531	1.17	0.07448	0.25	1072.1	12.1	1071.3	11.5
3B	358	67	80	0.187	{0.03}	5.060	1.17	0.07805	0.58	1163.4	13.2	1162.5	12.4
6BX	174	55	41	0.317	{0.00}	4.951	1.17	0.07799	0.58	1188.3	13.5	1185.9	12.7
8D2	316	126	64	0.399	0.26	5.788	1.46	0.07186	1.26	1035.3	11.3	1027.4	13.9

All errors are 1 sigma

*Percent of Pb206 that is common Pb, brackets indicate 204 was too small to measure

(Fig. 4-20c, d). Zircon rims and single age zircon grains from this sample are concordant at 1016.5 ± 6.9 Ma (2σ) (n = 8) (Fig. 4-21b).

A granite pegmatite dike was collected from a road cut, at the base of Skiff Mountain, New York (sample 00-03), and crosscuts the microcline granite. Both the dike and the microcline granite have experienced minor sodic alteration. Zircon crystals from this sample are elongate (300-500 μm long), clear with patchy zonation in BSE images and typically contain large inherited cores of both AMCG (~1150 Ma) and LMG (~1060 Ma) age (Fig 20e, f). The zircon rims from zircon grains with relict cores and grains without cores have a concordant age of 1030.4 ± 1.8 Ma (2σ) (n = 5) (Fig. 21c).

Amphibolite Layers

At Skiff Mountain, two parallel amphibolite layers are present two meters below the upper ore seam on the west side of Skiff Mountain (sample 00-11) (Fig. 4-1, Fig. 4-30). These layers are continuous across the extent of the exposed outcrop. Zircon grains are small (100-200 μm), clear, and irregular-shaped (Fig. 22a), and yield a concordant age of 1046 ± 11 Ma (2σ) (n = 5) (Fig. 4-23a). Rare inherited cores (~1130 Ma) are sometimes present, as well as a subset of zircon that are younger and of an equivalent age to zircon from the ore body at Skiff Mountain (~ 1000 Ma) (Table 4-9).

Samples from an amphibolite layer were collected ~100 m east of the cemetery in the town of Ausable Forks, New York (sample F-06-1a). Its relation to the amphibolite layers within the LMG is unclear as this unit separates Na-altered LMG from outcrops of the fayalite granite mentioned above. This unit is probably related to the metagabbro and amphibolite bodies mapped locally by Postel (1952) and Whitney and Olmsted (1993).

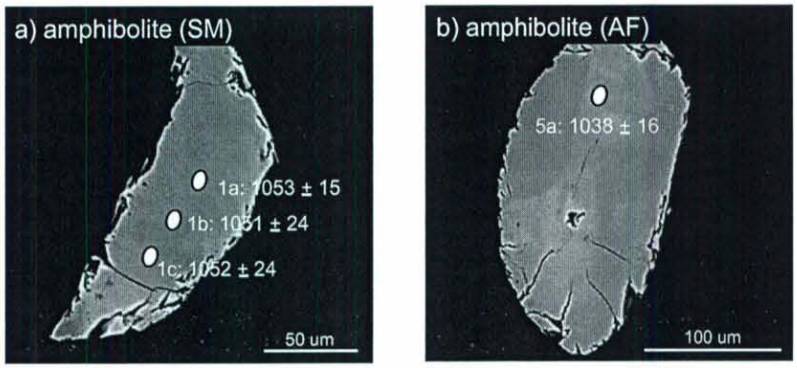

Figure 4-22. Representative BSE electron images of zircon grains from a) amphibolite layer at Skiff Mountain (SM) (00-11) and b), amphibolite layer which separates the fayalite granite from albite granite at Ausable Forks (AF) (f-06-1A. Single spot ages are given as $^{207}Pb/^{206}Pb$ ages corrected for common Pb. White ellipses are the approximate size ion probe craters.

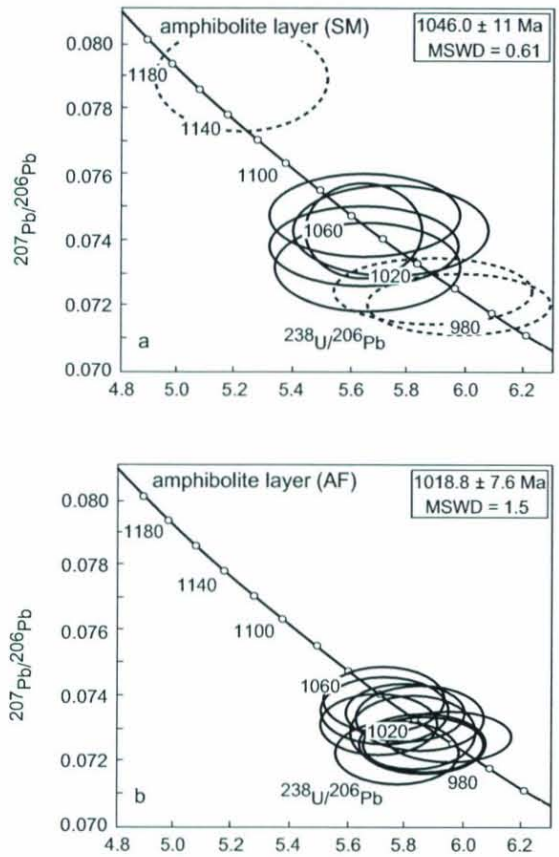

Figure 4-23. Tera-Wasserburg Concordia diagrams ($^{207}Pb/^{206}Pb$ versus $^{238}U/^{206}Pb$) showing zircon ages for a), amphibolite layer at Skiff Mountain (SM) (00-11) and b), amphibolite layer at Ausable Forks (AF) (F-06-1a). Uncertainties on quoted concordia ages (Ludwig 2003) are 2σ. Error ellipses are 2σ for all samples. Dasded error ellipses are not used in the age calculation.

Table 4-9 Ion microprobe U-Th-Pb results for zircon in amphibolite layers

Sample	U(ppm)	Th (ppm)	Pb (ppm)	Th/U	f206 *	238U/206Pb	sigma%	207Pb/206Pb	sigma%	207Pb/206Pb	Ma error	206Pb/238U	Ma error
Mafic layer (Skiff Mtn., 00-11)													
15a	1070	127	198	0.119	0.02	6.000	2.39	0.07206	0.52	993.9	23.1	993.7	22.1
7a	784	119	149	0.152	0.02	5.883	2.41	0.07248	0.57	1012.6	23.6	1012.0	22.6
11b	429	59	83	0.138	0.01	5.737	2.42	0.07431	0.76	1035.1	24.2	1035.8	23.2
1b	528	78	105	0.147	0.02	5.643	2.39	0.07478	0.69	1051.1	24.4	1051.6	23.3
11a	442	71	88	0.160	0.05	5.652	2.34	0.07321	0.76	1051.6	23.8	1050.1	22.7
1c	610	86	121	0.141	0.06	5.644	2.37	0.07385	0.68	1052.2	24.2	1051.5	23.0
1a	705	143	140	0.202	0.05	5.637	1.49	0.07434	0.78	1052.8	15.2	1052.7	14.5
14a	313	223	78	0.711	0.03	5.216	2.36	0.07891	0.82	1128.5	25.8	1130.8	24.5
Mafic layer (Ausable Forks, F-06-1a)													
11b	1697	366	325	0.216	0.03	5.948	1.50	0.07273	0.44	1001.6	14.6	1001.8	13.9
14a	796	107	151	0.135	0.03	5.862	1.45	0.07253	0.52	1016.1	14.3	1015.4	13.6
9a	906	117	172	0.129	0.03	5.848	1.52	0.07331	0.55	1017.3	15.0	1017.5	14.3
6a	940	112	178	0.119	0.02	5.853	1.49	0.07250	0.48	1017.5	14.7	1016.8	14.0
19a	974	130	186	0.134	0.01	5.821	1.50	0.07287	0.63	1022.5	14.9	1022.0	14.2
9c	832	104	159	0.125	0.04	5.797	1.44	0.07348	0.49	1025.8	14.3	1025.9	13.7
6b	824	104	159	0.126	0.03	5.768	1.50	0.07223	0.54	1032.5	15.0	1030.7	14.3
17b	772	99	150	0.129	0.02	5.723	1.49	0.07388	0.55	1038.1	15.0	1038.1	14.3
5b	1105	130	214	0.118	0.03	5.724	1.55	0.07355	0.57	1038.4	15.6	1038.0	14.9
17a	936	115	182	0.123	0.02	5.705	1.43	0.07312	0.52	1042.4	14.5	1041.2	13.8
14b	1005	143	197	0.143	0.04	5.687	1.53	0.07444	0.73	1043.7	15.5	1044.2	14.8
19b	1252	199	250	0.159	0.02	5.629	1.44	0.07486	0.50	1053.6	14.7	1054.2	14.0

All errors are 1 sigma

*Percent of Pb206 that is common Pb, brackets indicate 204 was too small to measure

Zircon grains are clear, small (100-200 μm), rounded or irregularly shaped with little internal zonation or obvious inherited cores in BSE images (Fig. 22b). This sample has a concordant age of 1018.8 ± 7.6 Ma (2σ) (n = 12) (Fig. 4-23b).

4-4 DISCUSSION

Understanding the origins, the subsequent timing and sequence of the Na and K hydrothermal fluid alteration, and Fe-mineralization, of the LMG, has important implications for the ore genesis of Kiruna-type deposits globally. The discussion below tries to relate petrographic and field observations, whole rock and mineral geochemistry, and U-Th-Pb zircon dates, to form a cohesive emplacement, fluid-alteration and mineralization history of the LMG and the associated magnetite-apatite deposits.

4-4-1 THE SEQUENCE OF ALTERATION

A model for the sequence of alteration of the LMG and related rocks is presented in Figure 4-24. Combining U-Th-Pb geochronology with field data, detailed petrography, and geochemistry, it is possible to put absolute ages or at least maximum and minimum ages on the various phases of alteration, mineralization, and tectonic conditions that have affected the LMG.

Age data presented here and in earlier work (e.g., McLelland et al., 2001a; Valley et al., 2009) suggests the LMG cannot be younger than ~1060-1050 Ma and likely intruded rocks of the AMCG suite at this time (see LMG evolution discussion below). The earliest mineral assemblage (e.g., perthite granite) consists of perthitic feldspar, quartz, magnetite, hematite-ilmenite intergrowths, titanite, apatite, and zircon (Fig. 4-3).

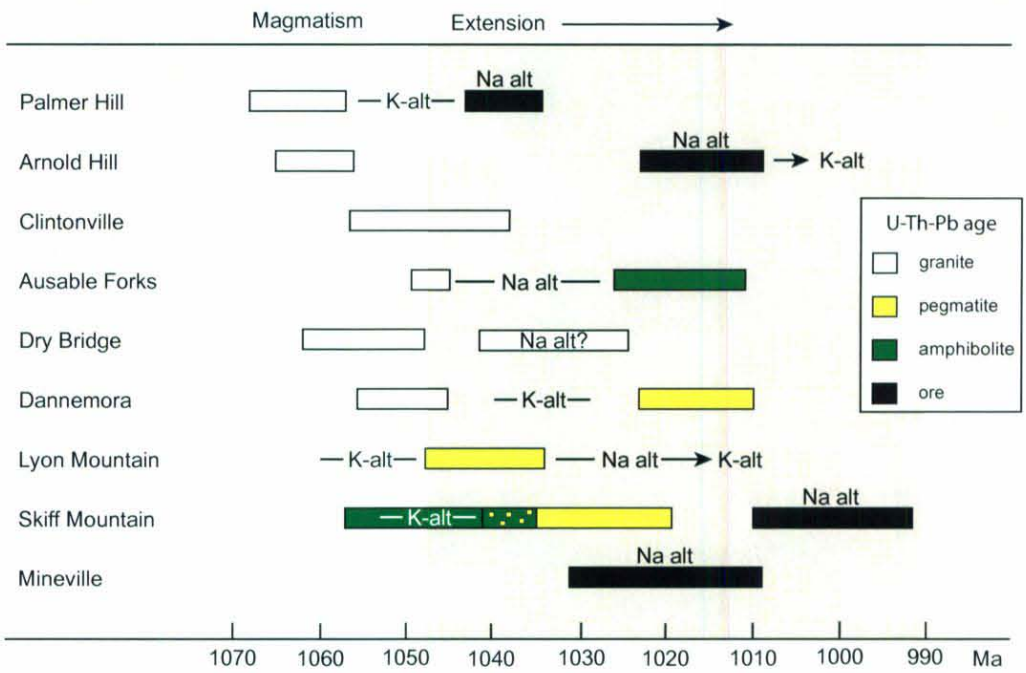

Figure 4-24. Diagram illustrating the relative and absolute (where possible) age relationships of magmatic, tectonic, mineralizing and alteration events within the Lyon Mountain granite and associated rocks. Uranium-Pb age ranges are 2σ.

Clinopyroxene and coarse magnetite are present in some samples of the perthite granite and forms subsequent to the primary mineral assemblage. The secondary growth of clinopyroxene and magnetite within the LMG and the textural similarities to the clinopyroxene-magnetite ± apatite ore bodies suggests they may be related. Secondary growth of titanite occurs after magnetite in both the granite and clinopyroxene-magnetite ore bodies.

In some localities, the perthite granite is unaltered or has experienced minor alteration. In other localities the perthite granite served as the protolith for the microcline and albite granites. The perthite granite is overprinted by widespread and pervasive potassic alteration associated mainly with the growth of microcline and quartz. Complete replacement of the primary perthitic feldspar results in the formation of the microcline granite. The similarity of zircon ages in the microcline granite and perthite granite suggests that K-alteration did little to modify preexisting zircon grains or promote new zircon growth, or that K-alteration took place within error of the zircon ages of the perthite granite. Whole rock geochemistry indicates that the LILE were mobile during K alteration (Table 4-1; Fig. 4-10, 11, 12). Potassic alteration must have occurred prior to ~1040 Ma, as the plagioclase-rich dike at Lyon Mountain crosscuts the microcline granite, and 1040 Ma hydrothermal zircon growth associated with sodic alteration Fe-mineralization at Palmer Hill also overprints the preexisting microcline granite (Valley et al., 2009).

Sodic alteration is associated with the growth of albite, quartz, apatite, titanite, hydrothermal zircon ± amphibole ± biotite ± fluorite ± garnet. Complete replacement of

perthitic feldspar or the microcline granite results in the formation of the albite granite. In rocks where partial replacement has occurred, varying proportions of earlier assemblages related to the perthite granite, microcline granite, and clinopyroxene-magnetite ore bodies are present. Additionally, some amphibolite layers and granitic dikes have been affected by Na-alteration. These overprinting relationships, when combined with zircon age data from the same samples, provide maximum ages for Na-rich fluid alteration at those localities (Fig. 4-24). The development of albite flame lamellae similar to what is observed in the fayalite granite, typically occurs during deformation at upper greenschist or lower amphibolite facies conditions (Pryer and Robin, 1995; 1996) suggesting that Na-alteration of the fayalite granite occurred under similar conditions and must be younger than ~1047 Ma age of the fayalite granite.

Whole rock geochemical data (and CL imaging of thin sections) suggests that the extreme variation in K and Na and an increase in Al in the hydrothermally altered rocks can be explained by alkali exchange in feldspar or the addition of feldspar during fluid alteration (Figs. 4-7). Many immobile elements (including Zr, Nb, Y, and Ta) and REE are enriched in Na-altered rocks relative the other LMG rock types, with apatite as the main repository for REE. The presence of fluorite and fluoroapatite (as well as fluoroamphibole and fluorotitanite; P. Whitney pers. comm.) and NaCl-rich fluid inclusions (McLelland et al., 2002) in the Na altered rocks, suggests Na-rich fluids were also rich in F and Cl, and most likely responsible for the transport of HFSE and REE (e.g., Bau and Dulski, 1995; Salvi et al., 2001).

Sodic alteration coincides with the probable remobilization of disseminated magnetite and the breakdown of clinopyroxene to form amphibole and biotite through hydration reactions. The remobilization of the clinopyroxene-magnetite ore deposits and further concentration of disseminated magnetite from the granite, results in the formation of second-generation ores comprised primarily of magnetite-apatite-quartz and zircon. Zirconium and REE are released from the clinopyroxene and apatite respectively and results in the growth of hydrothermal zircon rich in radiogenic Hf (Valley et al., 2010). These zircon ages from the ore directly date the Na-alteration and second-stage Fe-mineralization (Valley et al., 2009) (Fig. 4-24). Hydrothermal zircon growth occurs mainly in the magnetite-apatite ore bodies and possibly in the rocks of the LMG that have experienced extensive interaction with sodic fluids like at Dry Bridge. Zircon from Dry Bridge contain an age population that is significantly younger (~1033 Ma) than the zircon ages in the microcline and perthite granites (1060-1050 Ma). This 1033 Ma zircon population is similar to zircon ages from the ore bodies that range from ~1040 Ma at Palmer Hill to ~1000 Ma at Skiff Mountain (Valley et al., 2009). Based on these hydrothermal zircon ages, alteration by Na-rich fluids in the LMG must be episodic over a period of at least 40 m.y. Additionally, the age of hydrothermal zircon is similar to the zircon ages of crosscutting dikes and pegmatites (~ 1040 to 1016 Ma) found throughout the LMG (and elsewhere in the Adirondack Highlands; see Selleck et al., 2004), suggesting that fluid circulation and secondary ore formation coincide with dike emplacement and continued extension of the Adirondack Highlands during this time. The extent of Na-alteration is difficult to assess due to the lack of exposure. At Lyon

Mountain the Na-alteration in the hanging wall is approximately 10m wide. Other outcrops of albite granite are 100s of meters long.

A second, more limited period of K-rich fluid alteration (and locally including Ca alteration) postdates all previously mentioned mineral assemblages and fluid events. This late alteration was observed at Lyon Mountain, Arnold Hill, and Dannemora (see feldspar CL petrography discussion). This phase of K-alteration is limited to the growth of twinned and untwinned potassium feldspar on rims and grain boundaries or preexisting perthite, microcline and albite grains. This final stage of K-alteration overprints the plagioclase-rich granite dike at Lyon Mountain (~1040 Ma), the granite pegmatite at Dannemora (~1016 Ma) and Na-alteration and associated Fe-mineralization at Arnold Hill (~1016 Ma). Calcium alteration is present in the form of calcite and at Arnold Hill is associated with the growth of jasper, chlorite, and the nearly complete oxidation of magnetite to hematite.

4-4-2 IMPLICATIONS FOR EVOLUTION OF THE LMG

In addition to the timing and sequence of fluid alteration and Fe-mineralization in the LMG, the data presented here provide some information on the origins and evolution of the LMG and thus provides further constraints on the ore genesis of magnetite-apatite deposits. Debate over the origins of the LMG centers around the meaning of the 1060 to 1050 Ma zircon rims and single-age grains found in the LMG. First of all, whether the LMG was emplaced (or erupted) at ~1150 Ma and is coeval with the AMCG suite rocks in the Adirondacks (Whitney and Olmsted, 1988) and was subsequently metamorphosed and/or hydrothermally altered between 1060 and 1050 Ma. Second of all, if the LMG

was emplaced between 1060 and 1050 Ma during middle to late Ottawan orogeny (McLelland et al. 2001a; Selleck et al. 2005). If the former, the implication is that the LMG subsequently experienced granulite facies metamorphism during the Ottawan orogeny and that the 1060 to 1050 Ma zircon ages are metamorphic or a combination of metamorphic and hydrothermal recrystallization of the earlier formed zircon. If the LMG was emplaced between 1060 and 1050 Ma it is interpreted as a syn- to late-tectonic granite.

The Hawkeye granite (1100 Ma), which is geochemically similar to the LMG and clearly has experienced granulite facies metamorphism and Ottawan deformation, contains a pervasive quartz ribbon lineation that is lacking in the LMG. McLelland et al. (2001a) cited this as evidence that the LMG did not experience the main phase of Ottawan deformation and metamorphism and was emplaced post-Hawkeye (e.g., 1060 to 1050 Ma). The Hawkeye granite contains garnet and orthopyroxene which can be indicative of granulite facies metamorphism in certain rock types (e.g., Frost and Frost, 2008, and references therein) and the LMG lacks these minerals. Both the Hawkeye granite and the LMG contain perthitic feldspar with coarse plagioclase lamellae; however, the rims of perthite grains in the Hawkeye granite show evidence of recrystallization and elimination of the lamellae while perthite grains in the LMG do not (Figs. 4-4a and b; 4-31).

Zircon grains from the LMG are elongate and often contain facetted and well-developed terminations and growth zoning in BSE or CL imaging (McLelland et al., 2001, Fig. 12) (Fig. 4-18). The majority of zircon ages from the Hawkeye granite are

1090 Ma or older and with a small population of 1060-1050 Ma zircon ages (McLelland et al., 2001a, Valley unpublished data) despite being geochemically similar to the LMG. The differences in deformation, mineralogy and zircon ages suggest that the LMG and Hawkeye granite experienced different metamorphic and deformational histories.

This is not to say the LMG did not experience *any* metamorphism or deformation. Clearly the LMG experienced prolonged periods at elevated temperatures. The presence of coarse, wavy albite lamellae and triclinic microcline in perthite grains requires very slow cooling at temperatures below the transition from low sanidine to intermediate microcline (~ 500° C) (e.g., Yund and Davidson, 1978; Brown and Parsons, 1984). Additionally, the LMG has experienced regional scale upright folding or core complex development (Isachsen and Fisher, 1970, Whitney and Olmsted, 1988), locally exhibits a pronounced tectonic fabric (e.g., recumbent folding) and can contain boudinaged or stretched clinopyroxene and migmatite layers, or quartz veins (Fig. 4-2).

The third possibility for the origin of 1060-1050 Ma zircon ages in the LMG is that those zircon grains, or rims of grains, are hydrothermal in origin and this fluid event erased much of the tectonic fabric and metamorphic mineral assemblage. This idea is based on the unusual internal structures observed in BSE and CL imaging and the presence of embayments from the outer zircon regions intruding, with no obvious crystallographic control, into the inner regions of some zircon crystals (Fig. 4-18d). If this hypothesis is true it would suggest that the LMG protolith is ~1150 Ma, that Ottawan deformation has been obliterated by the hydrothermal alteration, or went unrecorded, and that the whole of the LMG experienced this hydrothermal event. This seems unlikely

given that: 1) This 1060-1050 Ma hydrothermal zircon event is not recorded in any of the ore bodies, as zircon ages in the ore deposits are 20 to 60 million years younger than those of the granite (Valley et al., 2009); 2) A pervasive 1060-1050 Ma fluid event would be concurrent with dry granulite facies metamorphism during the Ottawan orogeny (e.g. Valley et al., 1990; Rivers, 1997; McLelland et al., 2001); 3) If the whole of the LMG has experienced fluid alteration, then, why did this fluid event not affect the Hawkeye granite. The data obtained in this study suggest that the perthite granite (e.g., Clintonville, sample 99-1a; Rutgers Mine, sample 06-4d; Lyon Mountain, sample LM-06-2a) is *not* the product solely of hydrothermal fluid alteration given its ubiquitous presence away from the ore bodies and lack of zones of obvious fluid alteration. Thus, the perthite granite should retain any Ottawan deformational and metamorphic effects if it was emplaced at 1150 Ma; 4) If the LMG is 1150 Ma this forces one to explain previously mentioned differences between the Hawkeye granite and the LMG regarding metamorphism, deformation and mineralogy. A more likely reason for the observed zircon textures is that they are inherited zircon grains that were assimilated by 1060-1050 Ma LMG magmas.The simplest hypothesis suggested by the data presented here is that the LMG was originally a syn- to late-tectonic granite as proposed by McLelland et al. (2001a) and Selleck et al. (2005). Intrusion of the LMG occurred between ~1060 and ~1047 Ma and concurrent with the Ottawan Orogeny. Intrusion of the LMG probably marked the onset of extension (if melts are the result of decompression) or crustal anatexis from an over-thickened crust in the Adirondack Highlands (e.g., metamorphic dehydration melting, the input of mantle heat from delamination of the lower crust or

frictional heating during Ottawan thrusting). Syn-extensional intrusion of the LMG has been documented along the Carthage-Colton shear zone in the western Adirondack Mountains (Selleck et al., 2005). Similarly, extension in the Maurice region of Quebec was active from ~1090 to ~1040 Ma and is contemporaneous with emplacement of younger granitoids that have a similar chemistry to the LMG (Corrigan and van Breeman, 1997). The LMG must have experienced slow cooling for the development of coarse lamellae and triclinic microcline to develop in perthite grains and the formation of hematite-ilmenite intergrowths (e.g., Haggerty, 1991; Brownlee et al., 2010). By ~1047 Ma the orogen had cooled enough to allow for the preservation of feldspars and clinopyroxene (with Fe-rich exsolution lamellae) in the fayalite granite which are more typical of intrusive felsic igneous rocks that have not experienced long periods at elevated temperatures or experienced extensive deformation.

We suggest that the LMG intruded along extensional shear zones that developed near or along the anorthosite massif that acted as a ridged impermeable "barrier" (Figs. 4-1 and 4-25) prior to hydrothermal alteration and Fe-mineralization. Here initial clinopyroxene-magnetite ore deposits formed as a result of the late stages of LMG magmatism from immiscible Fe-rich liquids. From 1040 Ma to 1000 Ma a period of orogenic extension exists as evidenced by the emplacement of dikes which crosscut the regional fabric of the LMG and massive remobilization and modification of preexisting ore bodies took place by K, Na, Cl, Ca and F-rich fluids. In the northeastern Adirondacks, extension was dominantly to the northeast as evidenced by northeast plunging mineral lineations. Ore bodies are often coincident with these lineations.

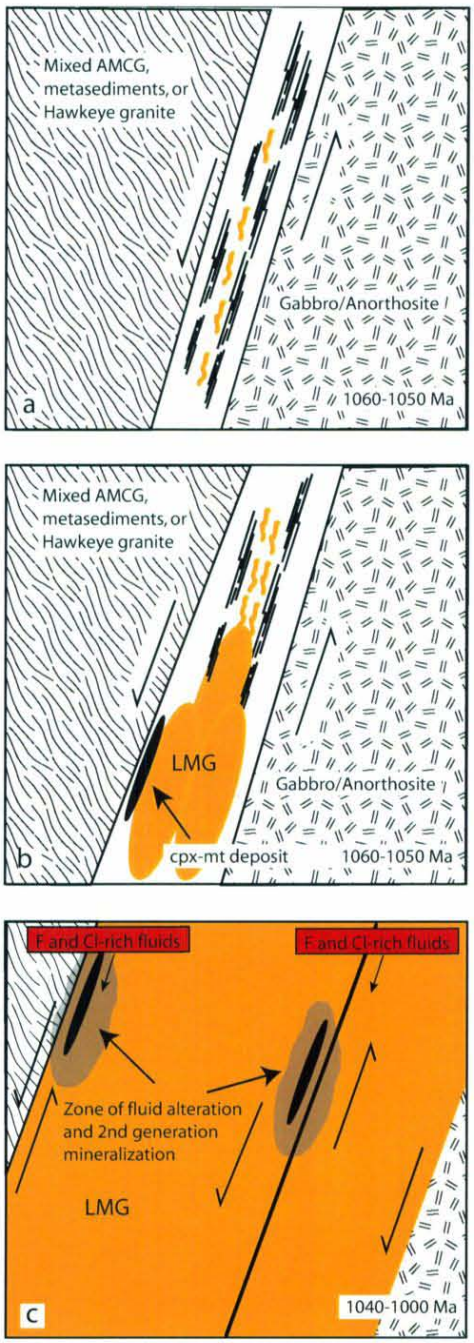

Figure 4-25. Cartoon illustrating the development and evolution of the Lyon Mountain granite and associated Fe mineralization and alteration.

Northeast-directed extension is supported by the development of the Tawachiche shear zone, a shear zone that records oblique northeast extension in the Maurice region of Quebec and occurs along strike to exposures of the LMG in the northeastern Adirondack Highlands (Corrigan and van Breeman, 1997).

Post-magmatic hydrothermal fluid circulation and mineralization was driven by rapid uplift of the hot interior of the orogen and juxtaposition against cooler upper level rocks. High heat flow is suggested by the presence of the aforementioned dikes. Given that the ages of hydrothermal zircon from the Lyon Mountain ores are 20 to 60 m.y. younger than zircon ages in the host granite, fluids responsible for hydrothermal zircon crystallization and secondary ore formation cannot be directly related to the LMG emplacement. Currently there are no major intrusive events younger than ~1040 Ma, (other than small granitic dikes and pegmatites), identified in the Adirondack Highlands. This suggests that the fluids responsible for ore remobilization and extensive Na-alteration were externally derived. Halogen-bearing fluids or brines could have penetrated the LMG along extensional shear zones and interacted with the clinopyroxene-magnetite ores and scavenged disseminated magnetite from the LMG to form new ore bodies associated with albitization (McLelland et al., 2002; Barton and Johnson, 2004; Valley et al., 2010). Many of the LMG ore bodies are located immediately above the contact of the LMG with other units (e.g., Hawkeye granite, calc silicate marbles, gabbros). This suggests that these contacts were fluid pathways. These contacts are typically covered with vegetation and direct observation of alteration in the adjacent rock types is not easily observed, but in many localities, ore deposits occur only 10s of meters

away. Near Skiff Mountain the LMG is in contact with a mixed calc silicate marble and gabbro unit. As the contact with the LMG is approached clinopyroxene in the marble is converted to biotite and amphibole, calcite grain size is reduced, and quartz and albite appear in the marble. Near Mineville, rare quartz-sillimanite veins and nodules occur with magnetite at the contact of the LMG and a metasedimentary unit suggesting chemical exchange between the metasedimentary rocks and the LMG. Field relations suggest these veins and nodules are contemporaneous with Na alteration.

Prograde metamorphism and penetrative deformation in the northeastern Adirondack Highlands must have ended by ~1045 Ma given the presence of dikes which crosscut the fabric in the LMG (e.g., Lyon Mountain dike, 1040.9 ± 6.8) the preservation of typical igneous minerals in the fayalite granite (dated at 1047.5 ± 2.2) and lack of a penetrative fabric in much of the LMG. Additionally, titanite from the eastern and central Adirondacks was dated between 1033 and 1021 Ma (Metzger et al, 1990). These ages are interpreted as cooling ages (~500° C), which further suggests that prograde metamorphism had ended by this time.

4-4-3 IMPLICATIONS FOR MAGNETITE-APATITE DEPOSITS AND RELATED ALTERATION

The formation of clinopyroxene-magnetite ore bodies occurred during the latest stages of pluton emplacement (see ore deposit description and Fig. 4-6). The formation of clinopyroxene-magnetite ore deposits during dry granulite facies metamorphism suggests that these initial deposits could be the result of Fe-rich immiscible liquids or the result of incorporation of mafic material from the AMCG suite. Alternatively these ores

could be hydrothermal in origin if the LMG magmas contained fluids derived from the dehydration melting of mica-rich metasedimentary rocks (e.g., Thompson, 1982; Patiño-Douce and Johnston, 1991) or produced residual magmatic fluids (McLelland et al., 2002; Selleck et al., 2004). The U-Th-Pb age data presented here and from Valley et al. (2009) shows that hydrothermal systems related to Kiruna-type magnetite-apatite deposits are episodic and may reuse the same "plumbing system" repeatedly over tens of millions of years. The Palmer Hill and Arnold Hill ore bodies are only 5 km apart, but their hydrothermal zircon ages are ~25 m.y. apart (~1040 Ma and ~1016 Ma respectively; Valley et al., 2009). Despite the age difference between the ore deposits at Palmer Hill and Arnold Hill, the host granite at both localities is nearly identical in age (~1060 Ma). Secondary Fe-mineralization and remobilization of preexisting clinopyroxene-magnetite ore bodies is associated with Na-alteration, and hydrothermal zircon growth. The similarities in ages between crosscutting dikes, pegmatites, and Na-alteration, suggest that Na-alteration and secondary Fe-mineralization was the result of fluid circulation during extension of the LMG and the Adirondack Highlands.

The source of Fe in the ore deposits is most likely the result of sequestration and concentration of disseminated magnetite from the adjacent granite. The previously mentioned depleted zones in the granite (see field relations section) can account for the Fe needed to form the *some* of the ore deposits. Mass-balance calculations done by Hagner and Collins (1967) indicate that the 100 m wide magnetite depleted zones on either side of the Palmer Hill ore could produce more than enough Fe to form the ore deposit. However, using these same calculations for the upper ore seam at Skiff

Table 4-10 Magnetite calculation (Skiff Mtn)

Ore Zone	
Length	100
Width	0.60
Depth	300
Total Vol. (m^3)	18000
avg % magnetite by vol in ore	50
Total vol. of magnetite (m^3) in ore body	9000
Host rock (granite) (hanging wall)	
Length	100
Width	4.00
Depth	300
Total vol. (m^3)	120000
avg % magnetite by vol in host	2.5
% magnetite removed from ore	2.50
Total vol magnetite available (m^3)	3000
Assume same for hanging wall	3000
Total vol magnetite available (m^3)	6000

All units are in meters
All values used in the calculation are visual estimations

Mountain (3m wide depleted zone, and 0.6m wide ore seam) we conclude that a maximum of 2/3s of the magnetite in the ore body can be accounted for by removal of disseminated magnetite from the host granite (see Table 4-10 for these calculations). We suggest that the rest of the magnetite came from remobilization of the early formed clinopyroxene-magnetite ores.

The various types and styles of Na- and K-rich fluid alteration in other magnetite-apatite Kiruna-type are typically associated with depth (i.e., changes in temperature and pressure) (Hitzman et al., 1992). The sequential nature of fluid alteration (Na overprints K) observed in the LMG further suggests that the crustal level of the LMG changed between 1050 and 1000 Ma. Fluid alteration in the LMG is episodic and lasted for at 40 m.y. as revealed by the ages of hydrothermal zircon ages in the ore bodies. The data presented here suggest that magnetite-apatite mineralization is both directly related (e.g., primary clinopyroxene-magnetite deposits) and indirectly related (e.g., secondary magnetite-apatite-quartz deposits) to magmatism and that the mineralization can continue long after magmatic crystallization.

4-5 CONCLUSIONS

A multidisciplinary approach using field relations, whole rock geochemistry, microscopy, mineral chemistry, and U-Th-Pb zircon geochronology has proven useful in unraveling the origins of the LMG, its tectonic history, and the sequence of fluid alteration, and subsequent Fe-mineralization. The data presented here show that the LMG most likely intruded the Adirondack Highlands between 1060 and 1050 Ma and

was hydrothermally altered tens of millions of years later. The data presented here suggests that these deposits in the LMG are related to both magmatism and to externally derived fluids (i.e. brines). Early clinopyroxene-magnetite mineralization is presumably related to granite emplacement and was subsequently altered and remobilized producing new deposits by Na-rich (and rarely K-rich) fluids during continued extension of the Adirondack Highlands. The presence of U-Th-Pb zircon ages 20 to 60 m.y. younger than the host granites of the ores, and the highly variable mineralogy of the ore deposits (e.g. clinopyroxene-magnetite and quartz-magnetite-apatite), suggests that multiple processes are responsible for ore formation and modification of preexisting ores. However, the presence of ore deposits almost exclusively within the LMG implies a "fertility" requirement of the host granite (or the presence of Fe-rich liquids or incorporation of mafic material by LMG magmas to form clinopyroxene-magnetite ores) and that magnetite-apatite mineralization may be directly or indirectly related to the magmatism that produced the LMG.

ACKNOWLEDGEMENTS

This research was supported by an NSERC Discovery Grant and startup funds to JMH provided by Memorial University of Newfoundland. The Nordsim ion microprobe facility is financed and operated under an agreement between the research councils of Denmark, Norway, Sweden, and the Geological Survey of Finland and the Swedish Museum of Natural History; this is Nordsim publication number xxx. We wish to thank

Marian Lupulescu, Phil Whitney, Pat Bickford, Bruce Selleck, William Peck, and James McLelland for their helpful discussions.

REFERENCES CITED

Armstrong, J.T., 1988, Quantitative analysis of silicates and oxide minerals: comparison of Monte-Carlo, ZAF and Phi-Rho-Z procedures. Microbeam Analysis 1988, Editor, D.E. Newbury, p. 239-246.

Barton, M.D., and Johnson, D.A., 1996, Evaporitic-source model for igneous-related Fe oxide- (REE-Cu-Au-U) mineralization: Geology, v. 24, p. 259-262.

Barton, M.D., and Johnson, D.A., 2004, Footprints of Fe-oxide (-Cu-Au) systems: SEG 2004 Predictive Mineral Discovery Under Cover - Extended Abstracts, Centre for Global Metallogeny, The University of Western Australia, v. 33, p. 112-116.

Bau, M., and Dulski, P., 1995, Comparative study of yttrium and rare-earth element behaviours in fluorine-rich hydrothermal fluids: Contributions to Mineralogy and Petrology, v. 119, p. 213-223

Boynton, W.V., 1984, Cosmochemistry of the rare earth elements: meteorite studies. In: Henderson PE (ed.) Rare Earth Element Geochemistry. Developments in Geochemistry. Elsevier, Amsterdam, pp 63-114.

Brown, W.L., and Parsons, I., 1984, Exsolution and coarsening mechanisms and kinetics in an ordered cryptoperthite series: Contributions to Mineralogy and Petrology, v. 86, p. 3-18.

Brownlee, S.J., Feinberg, J.M., Harrison, R.J., Kasama, T., Scott, G.R., and Renne, P.R., 2010, Thermal modification of hematite-ilmenite intergrowths in the Ecstall pluton, British Columbia, Canada: American Mineralogist, v. 95, p. 153-160.

Buddington, A.F., 1939, Adirondack igneous rocks and their metamorphism. Geological Society of America Memoir 7, 354 pp.

Corfu, F., Hanchar, J.M., Hoskin, P.W.O., and Kinny, P., 2003, Atlas of zircon textures. In J.M. Hanchar and P.W.O. Hoskin, Eds. Reviews in Mineralogy and Geochemistry, v. 53, p. 469-500.

Corriveau, L., Perreault, S., and Davidson, A., 2007, Prospecitive metallogenic settings of the Grenville Province, in Goodfellow,W.D., ed., Mineral Deposits of Canada: A Synthesis of Major Deposit-Types, District Metallogeny, the Evolution of Geological Provinces, and Exploration Methods: Geological Association of Canada, Mineral Deposits Division, Special Publication No. 5, p. 819-847.

Corrigan, D., and van Breeman, O., 1997, U-Pb age constraints for the lithotectonic evolution of the Grenville Province along the Mauricie transect, Quebec: Canadian Journal of Earth Sciences, v 34, p. 299-316.

Davidson, A., 1998, Geological map of the Grenville Province, Canada and adjacent parts of the United States of America. Geol. Surv. Can., Map 1947A (scale 1:2,000,000).

Day, H.W., and Brown, V.M., 1980, Evolution of perthite composition and microstructure during progressive metamorphism of hypersolvus granite, Rhode Island, USA: Contributions to Mineralogy and Petrology, v. 72, p. 353-365.

Finch, A.A., Klein, J., 1999, The causes and petrological significance of cathodoluminescence emissions from alkali feldspars: Contrib. Mineral. Petrol., v. 135, p. 234 - 245.

Foose, M.P., and McLelland, J.M., 1995, Proterozoic low-Ti iron-oxide deposits in New York and New Jersey; relation to Fe-oxide (Cu-U-Au-rare earth element) deposits and tectonic implications: Geology (Boulder), v. 23, p. 665-668.

Frietsch, R., 1978, On the magmatic origin of iron ores of the Kiruna type: Economic Geology and the Bulletin of the Society of Economic Geologists, v. 73, p. 478-485.

Frost, B.R., and Frost, C.D., 2008, On charnockites: Gondwana Research, v. 13, p. 30.

Gallagher, D., 1937, Origin of the magnetite deposits at Lyon Mountain, N. Y: New York State Museum Bulletin, p. 85.

Govindaraju, K., 1994, Compilation of Working Values and Descriptions for 383 Geostandards, Geostandards Newsletter, 18:1-158.

Haggerty, S.E., 1991, Oxide textures—A mini-atlas. In D.H. Lindsley, Ed., Oxide Minerals: Petrologic and Magnetic Significance, Reviews in Mineralogy, v 25, p. 129-137.

Harlov, D.E., Andersson, U.B., Foerster, H.-J., Nystrom, J.O., Dulski, P., and Broman, C., 2002, Apatite-monazite relations in the Kiirunavaara magnetite-apatite ore, northern Sweden: Chemical Geology, v. 191, p. 47-72.

Hitzman, M.W., Oreskes, N., and Einaudi, M.T., 1992, Geological characteristics and tectonic setting of proterozoic iron oxide (Cu-U-Au-REE) deposits: Precambrian Research, v. 58, p. 241-287.

Hoskin, P.W.O., and Schaltegger, U., 2003, The composition of zircon and igneous and metamorphic petrogenesis: In J.M. Hanchar and P.W.O. Hoskin, Eds. Reviews in Mineralogy and Geochemistry, v. 53, p. 27-62.

Isachsen, Y. W., and Fisher, D. W., 1970, Geologic map of New York State Adirondack Sheet. New York State Museum Science Service Map Chart Series 16.

Lindberg, M L., and Ingram, B., 1964, Rare-earth silicatian apatite from the Adirondack Mountains, New York. U.S. Geological Survey Professional Paper 501-B, p. 864-865.

Ludwig, K.R., 2003, User's Manual for Isoplot 3.00, A geochronological toolkit for Microsoft Excel: Berkley Geochronology Center Special Publication No. 4

McLelland, J., and Isachsen, Y. W., 1985, Geologic evolution of the Adirondack Mountains: a review, *in* Tobi, A., and Touret, J., eds., The deep Proterozoic crust in the North Atlantic provinces: NATO Advanced Study Institute Series C, v. 158, 175-215

McLelland, J., and Isachsen, Y., 1986, Synthesis of geology of the Adirondack Mountains, New York, and their tectonic setting within the southwestern Grenville Province, In: Moore, J.M., Davidson, A., Baer, A., (Eds.), The Grenville Province. Geological Association of Canada Special Paper 31, p. 75–94.

McLelland, J. and Chiarenzelli, J., 1988, Geochronology and geochemistry of 1.3 Ga tonalitic gneisses of the Adirondack Highlands and their implications for the tectonic evolution of the Grenville Province: *In* Middle Proterozoic Crustal evolution of the North American and Baltic Shields, Geological Association of Canada Special paper 38, p. 175-196.

McLelland, J., Hamilton, M., Selleck, B., McLelland, J., Walker, D., and Orrell, S., 2001a, Zircon U-Pb geochronology of the Ottawan Orogeny, Adirondack Highlands, New York; regional and tectonic implications: Precambrian Research, v. 109, p. 39-72.

McLelland, J.M., Foose, M.P., and Morrison, J., 2001b, Kiruna-type low Ti, Fe oxide ores and related rocks, Adirondack Mountains, New York; high-temperature hydrothermal processes: Guidebook Series (Society of Economic Geologists (U S), v. 35, p. 7-17.

McLelland, J., Morrison, J., Selleck, B., Cunningham, B., Olson, C., and Schmidt, K., 2002, Hydrothermal alteration of late- to post-tectonic Lyon Mountain granitic gneiss, Adirondack Mountains, New York; origin of quartz-sillimanite segregations, quartz-albite lithologies, and associated Kiruna-type low-Ti Fe-oxide deposits: Journal of Metamorphic Geology, v. 20, p. 175-190.

Mezger, K., Rawnsley, C.M., Bohlen, S.R., and Hanson, G.N., 1991, U-Pb garnet, sphene, monazite, and rutile ages - Implications for the duration of high-grade metamorphism and cooling histories, Adirondack Mountains, New York: Journal of Geology, v. 99, p. 415-428.

Parak, T., 1975, Kiruna iron ores are not "intrusive-magmatic ores of the Kiruna type": Economic Geology and the Bulletin of the Society of Economic Geologists, v. 70, p. 1242-1258.

Parsons, I., Thompson, P., Lee, M.R., and Cayzer, N., 2005, Alkali feldspar microtextures as provenance indicators in siliciclastic rocks and their role in feldspar dissolution during transport and diagenesis: Journal of Sedimentary Research, v. 75, p. 921-942.

Patiño-Douce, A.E., and Johnston, A.D., 1991, Phase equilibria and melt productivity in the pelitic system: implications for the origin of peraluminous granitoids and aluminous granulites: Contributions to Mineralogy and Petrology, 107: 202-218.

Postel, A.W., 1952, Geology of the Clinton County magnetite district: United States Geological Survey Professional Paper, v. 237, p. 88.

Pryer, L.L., and Robin, P.Y.F., 1995, Retrograde metamorphic reactions in deforming granites and the origin of flame perthite: Journal of Metamorphic Geology, v. 13, p. 645-658.

Pryer, L.L., and Robin, P.Y.F., 1996, Differential stress control on the growth and orientation of flame perthite; a palaeostress-direction indicator: Journal of Structural Geology, v. 18, p. 1151-1166.

Reynolds L.J., 2000, Geology of the Olympic Dam Cu-U-Au-Ag-REE Deposit, In Porter T.M. (Ed.) Hydrothermal Iron Oxide Copper-Gold & Related Deposits: A Global Perspective. Volume 1. PGC Publishing, Adelaide, pp.93-104.

Roeder, P.L., MacArthur, D., Ma, X.-P., Palmer, G.R., and Mariano, A.N., 1987, Cathodoluminescence and microprobe study of rare-earth elements in apatite: American Mineralogist, v. 72, p. 801-811.

Salvi, S., Tagirov, B., Moine, B., 2001, Hydrothermal mineralization of Zr and other "immobile elements": field evidence and experimental constraints. In: Cidu, R. (Ed.), Water-Rock Interaction: Proceedings of the Tenth International Symposium of Water-Rock Interaction, 1, pp. 745–748.

Selleck, B.W., McLelland, J.M., and Hamilton, M. A., 2004, Magmatic-hydrothermal leaching and origin of late- to post-tectonic quartz-rich rocks, Adirondack Highlands, New York; in Tollo, R.P., Corriveau, L., McLelland, J., and Bartholomew, M. J., eds., Proterozoic Tectonic Evolution of the Grenville Orogen in North America: Geological Society of America Memoir no. 197, p. 379-390.

Selleck, B.W., McLelland, J.M., and Bickford, M.E., 2005, Granite emplacement during tectonic exhumation: The Adirondack example: Geology, v. 33, p. 781-784.

Shand, S.J., 1927, Eruptive Rocks: Their genesis, composition, and classification with a chapter on meteorites. Wiley, New York. 360 pp.

Stacey, J.S., and Kramers, J.D., 1975, Approximation of terrestrial lead isotope evolution by a two-stage model: Earth and Planetary Science Letters, v. 26, p. 207.

Thompson, A.B., 1982, Dehydratation melting of pelitic rocks and the generation of H_2O-undersaturated granitic liquids: American Journal of Science., v. 282: 1567-l 595.

Valley, J.W., Bohlen, S.R., Essene, E.J., and Lamb, W., 1990, Metamorphism in the Adirondacks; II, The role of fluids: Journal of Petrology, v. 31, p. 555-596.

Valley, P.M., Hanchar, J.M., and Whitehouse, M.J., 2009, Direct dating of Fe oxide-(Cu-Au) mineralization by U/Pb zircon geochronology: Geology, v. 37, p. 223-226, doi: 10.1130/G25439A.1.

Valley, P.M., Fisher, C.M., Hanchar, J.M., Lam, R., and Tubrett, M., 2010, Hafnium isotopes in zircon: A tracer of fluid-rock interaction during magnetite-apatite ("Kiruna-type") mineralization: Chemical Geology, v. 275, p. 208-220.

Whitehouse, M.J., Kamber, B.S., and Moorbath, S., 1999, Age significance of U-Th-Pb zircon data from early Archaean rocks of west Greenland--a reassessment based on combined ion-microprobe and imaging studies: Chemical Geology, v. 160, p. 201.

Whitehouse, M.J., and Kamber, B.S., 2005, Assigning dates to thin gneissic veins in high-grade metamorphic terranes: A cautionary tale from Akilia, Southwest Greenland: J. Petrology, v. 46, p. 291-318.

Whitney, P.R., and Olmsted, J.F., 1988, Geochemistry and origin of albite gneisses, northeastern Adirondack Mountains, New York: Contributions to Mineralogy and Petrology, v. 99, p. 476–484, doi: 10.1007/BF00371938.

Whitney, P.R., Olmsted, J.F., and New York State Geological, S., 1993, Bedrock geology of the Au Sable Forks quadrangle, northeastern Adirondack Mountains, New York: Albany, N.Y., University of the State of New York, State Education Dept., New York State Museum/Geological Survey.

Wiedenbeck, M., Alle, P., Corfu, F., Griffin, W.L., Meier, M., Oberli, F., Quadt, A.V., Roddick, J.C., and Spiegel, W., 1995, Three natural zircon standards for U-Th-Pb, Lu-Hf, trace element and REE analyses: Geostandards and Geoanalytical Research, v. 19, p. 1-23.

Yund, R.A., and Davidson, P., 1978, Kinetics of lamellar coarsening in cryptoperthites: American Mineralogist, v. 63, p. 470-477.

4-6 DATA REPOSITORY 1

ROCK DESCRIPTIONS AND PETROGRAPHY

The Lyon Mountain granite

The LMG consists of three primary end-member rock types based on the dominant feldspar present: perthite granite; microcline granite; and albite granite. The three rock types are fine to medium grained, in some cases with a "sugary" granoblastic texture, and are often difficult to differentiate in the field. The LMG has a foliation or layering that can be locally pronounced but lacks continuity especially along strike (Whitney and Olmsted, 1988).

Perthite granite

The perthite granite is the most prevalent rock type of the LMG. In outcrop, the unit appears pinkish-white to "salmon" colored and contain thin coarse-grained quartz-potassium feldspar-rich pegmatite layers. Unit ranges from gneissic to unfoliated or massif with "blocky" layering.

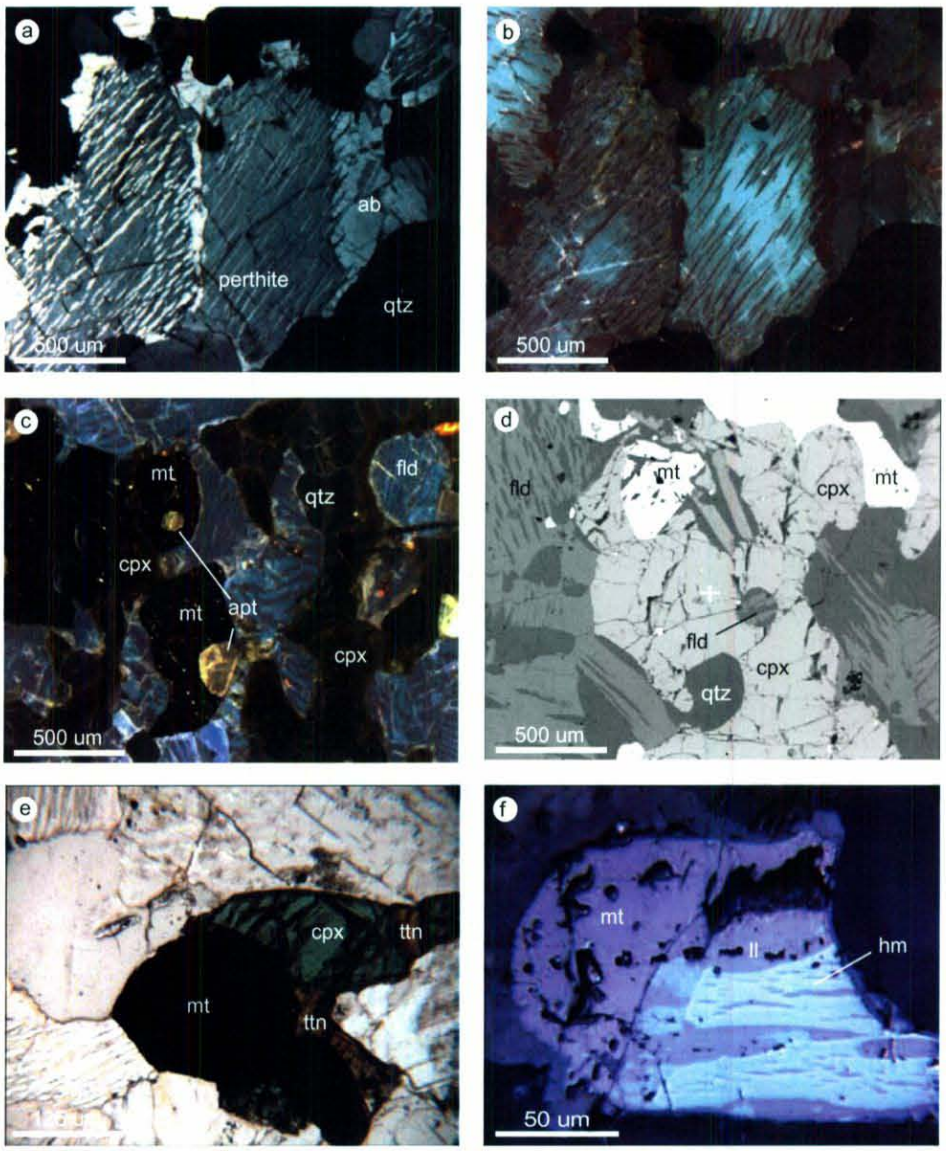

Figure 4-26. Photomicrographs of the perthitic granite near Skiff Mountain. a) Cross-polarized light image and b) color CL image of perthite grains with minor Na-alteration in the form of albite rims and veins. c) Color CL image showing the relationship of clinopyroxene and grains of perthitic feldspar and the location of apatite grains within the photomicrograph. d) Grain of perthitic feldspar enclosed by clinopyroxene (center of photo). e) Plane light photomicrograph showing the intimate relationship of clinopyroxene and magnetite and subsequent growth of titanite. f) Reflected light image of hematite-ilmenite exsolution with magnetite from the perthite granite.

The primary mineral assemblage in the perthite granite is perthitic feldspar, quartz, euhedral magnetite, hematite-ilmenite intergrowths and minor zircon and apatite. Perthitic feldspar grains in this unit contain coarse, sinuous, anastomosing or discontinuous lozenge shaped albite lamellae in microcline with well-developed twinning (Fig. 4-26a, b). Quartz grains are equant and in some cases contain zircon. Zircon also occurs along feldspar grain boundaries.

Clinopyroxene is present in most samples, is intimately associated with coarse-grained magnetite, and contains inclusions of perthite or partially enclose perthite grains (Fig. 4-26c and d). It is unclear if this is the result of recrystallization during deformation, hydrothermal alteration, or the growth of clinopyroxene during skarn development in the latest stages of crystallization of the LMG (Valley et al., 2010).

In some samples the perthite granite has experienced varying amounts of alteration by sodic fluids. Sodic alteration is associated with the crystallization of albite, quartz, magnetite, zircon, and apatite along grain boundaries, and replacement of perthitic feldspars by albite. Additionally, sodic-alteration is accompanied by the growth of titanite, amphibole (optically determined as arfedsonite and hornblende), garnet and biotite. Titanite rims or encloses grains of coarse magnetite (Fig. 4-26e) and amphibole and biotite replace pyroxene but are later than titanite. Rarely ilmenite or rutile appears as rims on magnetite in the absence of titanite.

In CL, microcline regions in perthite grains typically luminesce blue (typical of microcline) (e.g., Finch and Klein, 1999) and albite lamellae are brownish-gray-green to red. Red CL in feldspars is generally attributed to the presence of Fe^{3+} or trivalent REE

(e.g., Sm, or Eu) (Finch and Klein, 1999). Preliminary CL spectroscopic measurements (J. Götze, J.M. Hanchar, and P. Valley, unpublished results) of the CL suggests that the red CL emission is due to Fe^{3+} and not trivalent REE based on the relatively broad full width at half maximum (FWHM) CL emission peak typical of d-electron elements and the position of the red CL peak centered at ~755 nm (Wenzel and Ramseyer, 1992). The red CL tends to be patchy and discontinuous. Apatite in the perthite granite typically occurs along grain boundaries in the least altered samples and in some cases as inclusions in magnetite (Fig. A1c). Both occurrences luminesce purple-orange, which in apatite is indicative of trivalent REE and not Mn^{2+} CL activation which is the more common color of the CL emission in plutonic rocks (Roeder et al., 1987).

Reflected light microscopy reveals that some oxides are a mixture of magnetite grains and minor hematite-ilmenite intergrowths (Fig. 4-26f) or magnetite rimmed by ilmenite. The visible characteristics of these oxide intergrowths are nearly identical to the perthitic feldspar.

Microcline granite - Potassic alteration

The microcline granite is most likely the result of hydrothermal Na and K-rich fluid alteration of pre-existing granitoid rocks and in many cases there are no remnants of the perthite granite. The unit appears pink to orange and rarely reddish-orange in outcrop. Foliations in the microcline granite are much less distinct and difficult to observe than in the perthite granite owing to the lack of mafic and planar minerals or subsequent K alteration and recrystallization.

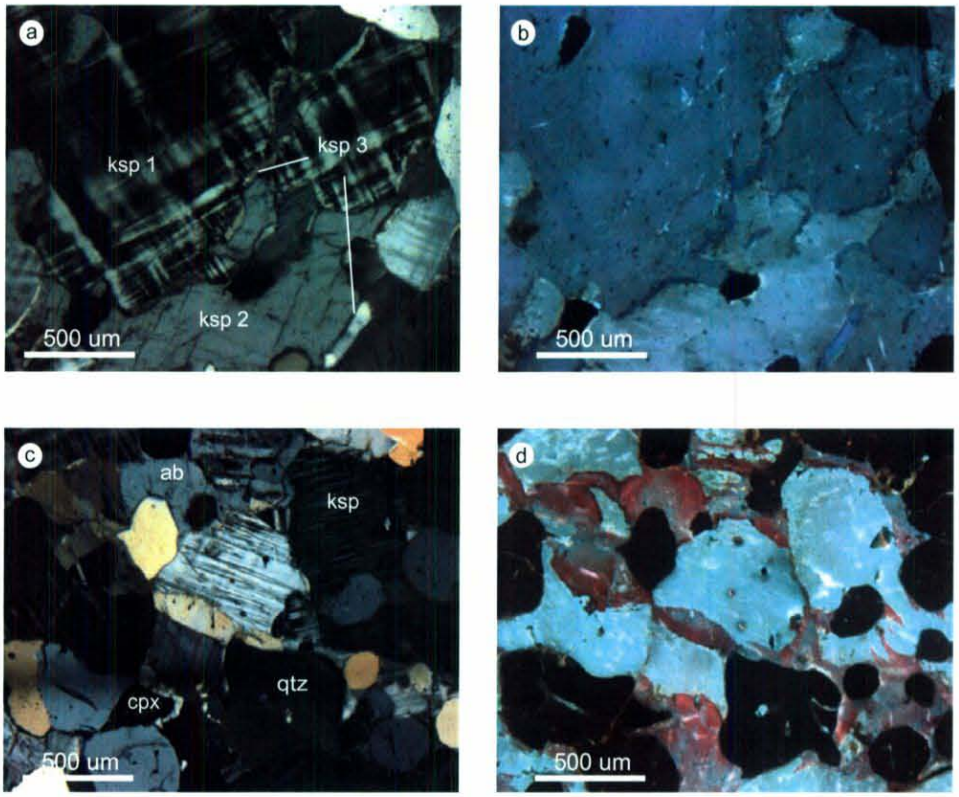

Figure 4-27. Photomicrograph the microcline granite. a) Cross-polarized light image and b) color cathodoluminescence image of three generations of potassium feldspar. c) Cross-polarized light image and d) color cathodoluminescence image of partial sodium alteration of the microcline granite. Albite growth related to Na fluid alteration luminesces red.

The microcline granite is the simplest mineralogically and typically more homogeneous than either the perthite or albite granite. The mineral assemblage consists predominately of microcline, quartz, magnetite, and minor titanite, apatite, and zircon. The microcline texture is granoblastic and mafic silicates are rare. Quartz occurs interstitially or as rounded grains within microcline grains and locally shows evidence of recrystallization and shape preferred orientation. Euhedral magnetite grains, quartz, zircon, and trace perthitic feldspar are found as inclusions in microcline or secondary quartz. Apatite typically occurs at grain boundaries in contact with quartz. Rare pyroxene is altered to biotite or chlorite. Coarse euhedral magnetite are present without pyroxene and titanite rims are ubiquitous on both magnetite and pyroxene grains.

The microcline granite can appear "pristine" (i.e., unaltered) when distal to the ore deposits (Fig. 4-27a, b) but is typically overprinted near the ore zones by minerals related to Na alteration (Fig. 4-27c, d) and Fe mineralization. Minerals associated with Na alteration observed in the microcline granite include albite, quartz, apatite, zircon, and magnetite. Additionally, some samples show multiple generations of potassium feldspar growth (Fig. 4-27a, b). A second period of K-alteration overprints all earlier assemblages as revealed by thin rims or veins of potassium feldspar crosscutting the earlier formed microcline grains and, in samples where Na-alteration has occurred, on albite grains.

In CL microscopy, the microcline luminesces blue, a characteristic CL emission color of potassium feldspar (e.g., Finch and Klein, 1999). In some samples, three distinct shades of blues are visible (Fig. 4-27b). These differences in luminescence could represent different generations of potassium feldspar growth. Blue-gray luminescent

grains can form larger grains than those that are darker blue, have less developed twinning, and crosscut darker blue grains (Fig. 4-27a, b). A third, brighter blue, potassium feldspar appears along grains boundaries of both dark blue and blue-gray grains. In the microcline granite, apatite luminesces orange-purple.

Albite granite - Sodic alteration

The albite granite, like its potassium counterpart the microcline granite, is the product of pervasive fluid alteration. The albite granite is typically white, gray, or pink, but can appear red due to hematite staining.

The mineral assemblage of the albite granite is the most variable of LMG lithologies that were studied. The dominant mineral assemblage in the albite granite consists of granoblastic albite, quartz, zircon, apatite, magnetite ± clinopyroxene ± amphibole ± titanite ± garnet ± fluorite (Fig. 4-28). Grains of rounded quartz, euhedral magnetite, titanite, zircon, apatite and remnant perthite and microcline grains are found as inclusion within albite. Clinopyroxene and magnetite are intimately associated with each other. Rims or grains of titanite typically form around or in close proximity to pyroxene and magnetite. In some samples garnet is associated with pyroxene instead of magnetite. Pleochroic blue-green amphibole (i.e., arfvedsonite) and hornblende grew at the expense of preexisting clinopyroxene and both amphibole and pyroxene are subsequently altered to biotite or biotite-quartz intergrowths. Apatite is typically associated with albite, quartz, and coarse magnetite. Zircon occurs predominately within grains of quartz and albite and along grain boundaries.

The albite granite in some localities has recorded subsequent alteration events by K-, Ca-, or Si-rich fluids. Thin rims of potassium feldspar on albite were observed in some samples. Calcium alteration is recorded typically by the growth of calcite and is associated with brittle deformation and a lower temperature mineral assemblage (e.g., chlorite, hydrothermal quartz) and hematization.

Replacement of preexisting feldspar by albite ranges from near completion in some samples to only grain margins in other. In samples where Na replacement is complete, well-twinned granoblastic albite is predominant (Figs. 4-28a, b) and only small remnants of earlier formed feldspar are present (Figs. 4-28c, d). In samples that have experienced partial or limited Na-alteration flame or patch perthite is often present (Fig. 4-28e, f). Alteration of feldspar in the perthite granite shows replacement of the microcline portions of grains leaving earlier exsolution related albite lamellae protruding into the replacement albite (Fig. 4-26a, and b) and as rims of albite around the perthite.

Cathodoluminescence imaging of the albite granite samples shows that alteration related albite is most often associated with red luminescence (Figs. 4-26-4-29), though dark gray, gray-green, and purple-gray luminescence is also present. Red areas can grade into gray within the same grain or area of alteration. In samples with near-complete albitization red luminescence tends to be more subdued. Preliminary CL spectroscopy measurements (J. Götze, J.M. Hanchar, and P. Valley, unpublished results) of the red CL suggests that the red CL is due to Fe^{3+} and not trivalent REE as noted above for the microcline. However, EPMA data shows there is not a significant difference in the iron content between any of the feldspars analyzed (see EPMA discussion below). Apatite

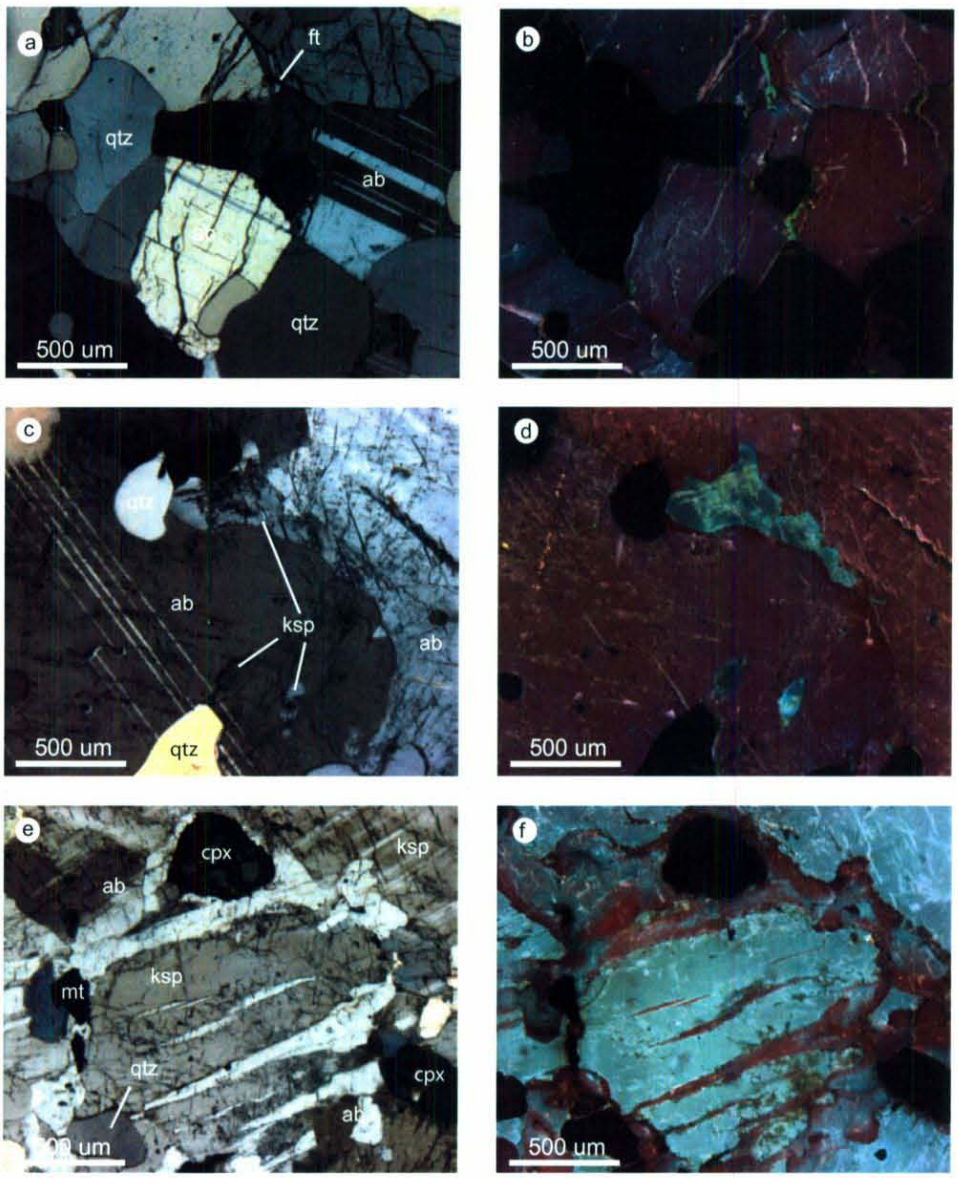

Figure 4-28. Photomicrograph images of the albite granite and various stage of sodium alteration. a) Cross-polarized light image and b) cathodoluminescence image of typical albite granite. Note green luminescent interstitial fluorite in figure b. c) and d) Nearly complete replacement of microcline in microcline granite by albite during sodium alteration. e) and f) Partial replacement of microcline by albite. Note "pseudo lamellae" of albite in microcline. Alteration related albite typically luminesces red.

grains luminesce purple to orange indicative of high REE content and trivalent REE CL activation (Roeder et al., 1987).

Related rock types

Fayalite granite

A body of fayalite granite in Ausable Forks, NY is separated from outcrops of albite granite on its western edge by a layer of coarse-grained amphibolite and its eastern, northern, and southern, margins are covered. This unit appears dark green-brown to rust-colored, is massive, and is medium grained.

The fayalite granite is mineralogically distinct from other lithologies in the LMG. The primary igneous assemblage consists of perthitic feldspar, quartz, clinopyroxene, and zircon (Fig. 4-29). It is not clear if the fayalite is primary or the result of hydrothermal alteration. Secondary mineral growth as a result of Na-rich fluid alteration consists of albite, quartz, fluorite, apatite, and magnetite. Perthitic feldspar and clinopyroxene grains in the fayalite granite are clearly distinct from those of the perthite granite Fig 4-29 In the feldspar grains, thin, straight, uniform lamellae are crosscut by hydrothermal alteration-related "flame lamellae" containing minute inclusions of Fe-oxides and other unidentified phases (Figs. 4-29c, d). Twinning in the potassium regions of perthitic feldspar is not well developed. Clinopyroxene grains contain exsolution lamellae of Fe-rich pyroxene. Fayalite grains often altered extensively to iddingsite and associated with

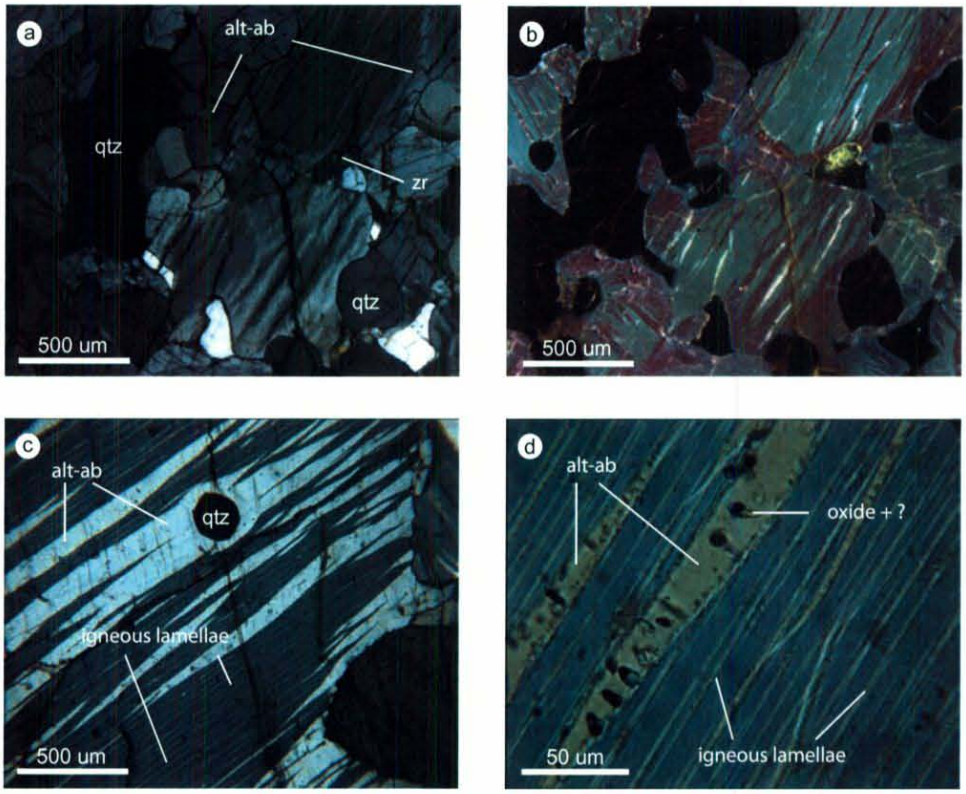

Figure 4-29. Photomicrograph of the fayalite granite. a) Cross-polarized light image and b) color CL image of typical fayalite granite that has experienced partial alteration by sodium bearing fluids. Alteration related albite typically luminesces red. c) Cross-polarized light image of alteration related albite penetrating igneous feldspar grain forming "flame lamellae" and cross-cutting earlier exsolution lamellae. d) Close up image of alteration related albite containing micro inclusions of an Fe oxide and unknown mineral which crosscuts exsolution related lamellae of albite.

clinopyroxene. The clinopyroxene is not altered to amphibole or biotite in this sample. Zircon is present along grain boundaries and inclusions in quartz and feldspar. Apatite, fluorite and quartz typically occur together.

In CL microscopy, Na-alteration related "flame lamellae" are bright red and potassium feldspar grains luminesce gray-green. Apatite grains luminesce purple-orange which is similar to the other samples investigated, indicative of high REE content and trivalent REE CL activation (Roeder et al., 1987).

Ore deposits / F-mineralization

Iron mineralization in the LMG is characterized by magnetite as the main Fe-bearing oxide phase; however, a few deposits contain appreciable quantities of martite (incomplete pseudomorphic replacement of magnetite by hematite) and hematite. The ore deposits can be divided into two main types: clinopyroxene-magnetite and those associated with Na-rich fluid alteration and the growth of albite and quartz. A smaller subset of magnetite deposits consist of either quartz and/or potassium feldspar pegmatites and magnetite with minor apatite and zircon, or more rarely some magnetite deposits are associated with K-alteration and the microcline granite (Postel, 1952). Alteration and mineralization can be highly variable within a single deposit and multiple overprinting fluid events recorded in these rocks are common.

Clinopyroxene-magnetite deposits typically occur in layers ranging from less than a meter up to 4 meters wide. Clinopyroxene-magnetite migmatite or granite "contaminated" by the clinopyroxene-magnetite assemblage is also present. Enclaves of clinopyroxene-magnetite ore observed within the perthitic granite suggest that the

clinopyroxene-magnetite ore is contemporaneous with the emplacement of the LMG. Clinopyroxene-magnetite deposits are typified by the mineral assemblage clinopyroxene, magnetite ± apatite ± amphibole. Coarse magnetite is typically secondary to pyroxene but small euhedral crystals of magnetite appear as inclusions within clinopyroxene. Secondary amphibole commonly rims clinopyroxene and encloses magnetite. Apatite luminesces intense orange-purple which is indicative of the high REE content (Lindberg and Ingram, 1964; Roeder et al., 1987). In clinopyroxene-magnetite migmatites, coarse microcline or orthoclase rim pods of clinopyroxene-magnetite or form alternating layers with clinopyroxene and magnetite (Fig. 4-6b main paper). Inclusions of perthite or other early feldspars are present within magnetite or pyroxene grains in clinopyroxene-magnetite" contaminated" granites. Apatite occurs interstitially along grain boundaries of magnetite and pyroxene and often makes up a significant portion of the rock. Apatite luminesces purple-orange in cathodoluminescence. Zircon was not observed in thin sections from clinopyroxene-magnetite ore samples or in heavy mineral separates (e.g., Rutgers mine).

The most prevalent type of ore deposit is associated with Na-alteration and albitization. Field and petrographic observations clearly show that Na-alteration overprints and is subsequent to clinopyroxene-magnetite ore formation and that Na-alteration can occur at the same locality as clinopyroxene-magnetite deposits (e.g., Lyon Mountain, Palmer Hill, and Arnold Hill). Deposits associated with Na-alteration are typified by coarse or massive magnetite, apatite, quartz, and zircon but also contain albite ± fluorite ± clinopyroxene ± amphibole ± titanite ± garnet ± chlorite ± calcite.

Apatite occurs interstitially between magnetite grains and exhibits intense orange-purple luminescence. In most samples zircon was not identified in thin section, and only identified during heavy mineral separation. However, some samples (e.g., Mineville) contain extremely large zircon (and apatite) (e.g., mm scale). These large zircon are highly metamict from the high U content and subsequent radiation damage.

The position of the ore bodies is structurally controlled. Ore bodies occur in the hinges, or limbs, of folds and immediately above the contact of the LMG with various other units and are tabular, or rod-like (Postel, 1952). One or more of the following characteristics are locally present at a given ore deposit: migmatization, mylonitization, boudinage of the ore and host rocks, breccias, crosscutting dikes and pegmatites, and miarolitic cavities.

Amphibolite layers

Amphibolite layers of uncertain origin are common within the LMG but constitute little of the total volume. Though not the focus of this study, they are considered here to better characterize the LMG and its evolution and origin. Layers range from a few centimeters to 3 or 4 meters in width and can appear as a single layer or occur in groups spaced a few centimeters apart to many meters (Fig 4-30). The layers can be followed the length of the outcrop with little variation. The layers typically have a "salt and pepper" or banded appearance and are conformable with the local granitic fabric when present. Early workers describe the amphibolite layers as anastomosing and pinching out and that some samples contain pyroxene or relict pyroxene (though none was observed in this study) (Gallagher, 1937; Postel, 1952). The samples collected in

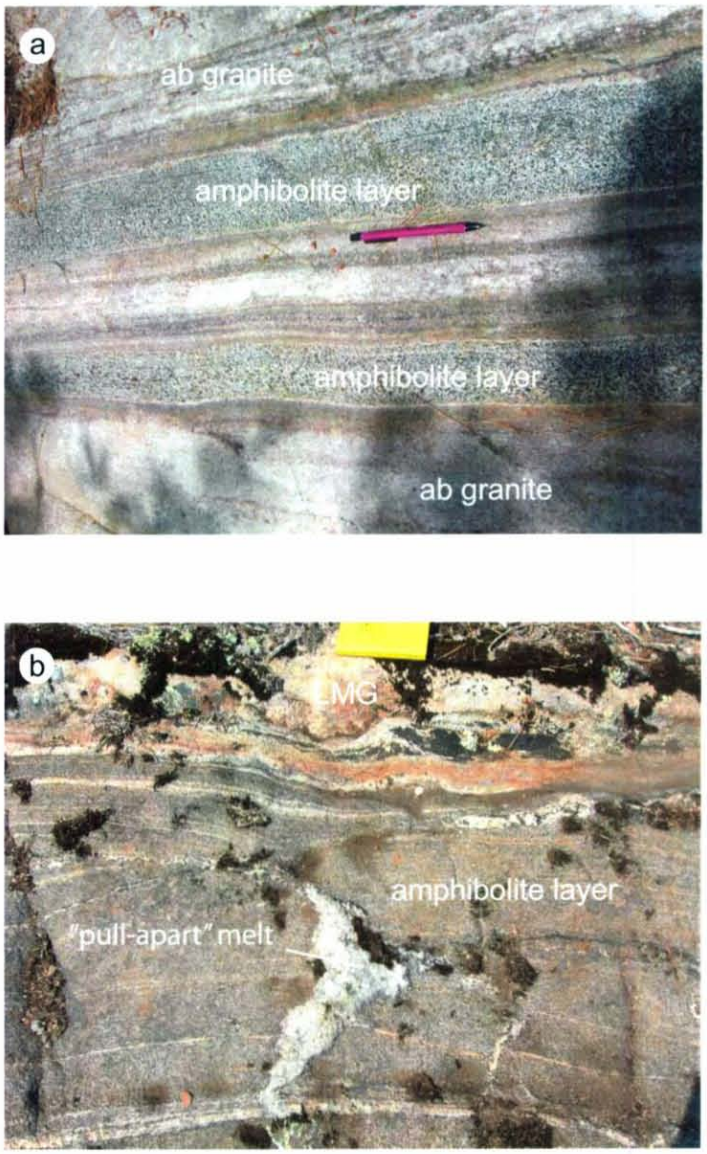

Figure 4-30. a) Parallel amphibolite layers surrounded by sodium altered Lyon Mountain granite, 2 meters below an ore seam at Skiff Mountain. b) Pull-apart melting related to brittle extension of an amphibolite layer at Skiff Mountain. Note sharp upper contact with the Lyon Mountain granite.

this study comprise varying amounts of biotite, amphibole, plagioclase apatite, minor orthoclase, magnetite or hematite-ilmenite intergrowths, titanite and zircon. Plagioclase is generally granoblastic. Biotite in thin section is "fresh" in appearance and ranges from brown to green pleochroic in plane light microscopy. Plagioclase luminescence ranges from blue-gray to red. Apatite typically luminesces purple-orange.

Two amphibolite layers (~ 10 and 20 cm thick) just below the ore horizon at Skiff Mountain have relatively sharp contacts with thin layers (1-2 cm) of albite separating the amphibolite from the albite granite (Fig. 4-30a). An amphibolite layer at the top of Skiff Mountain has a lower contact with the LMG that appears to be gradational with thin layers of amphibolite gradually increasing in thickness and abundance until becoming one massive layer 3 or 4 meters across (Fig. 4-30b). The upper contact with the LMG is sharp, but wavy with evidence for partial melting and shearing at the interface of the granite and the amphibolite and partial melting within the amphibolite as a result of the layer being pulled apart.

In addition to the amphibolite layers within the LMG, an amphibolite layer approximately 10m across separates the LMG from the fayalite granite at Ausbale Forks. The relationship between this sample and the amphibolite layers that are clearly internal to the LMG is uncertain, but they are considered here together based on the similarity of mineralogy and texture. The amount of amphibole and biotite varies between 20 % to nearly 100 % across the outcrop with some areas of the outcrop consisting entirely of biotite or amphibole. Apatite is ubiquitous, typically occurs along grain boundaries and contain inclusions of plagioclase (e.g., Ausable Forks). The oxide and Ti-bearing phases

are different in the amphibolite layer at Ausable Forks and the one collected at Skiff Mountain. The amphibolite body at Ausable Forks contains magnetite with rims of ilmenite whereas the amphibolite layer at Skiff Mountain contains hematite-ilmenite intergrowths and minor magnetite with ubiquitous titanite throughout the thin section.

Crosscutting dikes

Granitic dikes are common throughout the LMG and the Adirondack Highlands. These dikes crosscut layering in the LMG. Two main types of dikes are present in the LMG: potassium feldspar-rich dikes which appear orange to pink in the field; and plagioclase-rich dikes that appear white or light gray. Some dikes contain coarse masses of magnetite and minor pyrite.

The potassium feldspar-rich dikes typically contain coarse microcline, quartz, and minor magnetite, zircon, and apatite ± muscovite ± amphibole ± biotite ± calcite. The dike samples collected at Dannemora and Skiff Mountain are pegmatitic. Limited fluid-enhanced Na-alteration has added albite and calcite to the mineral assemblage of these samples. Blue or blue-gray luminescent microcline is typical. Two populations of apatite are present; yellow luminescent grains (typical of igneous apatite, Roeder et al., 1987) which occur with quartz and magnetite and those with purple-orange luminescence typical of REE-enriched apatite, Roeder et al., 1987) which occur with quartz and microcline. Zircon grains are present at grain boundaries and rarely along fractures in magnetite.

The plagioclase-rich dike collected at Lyon Mountain consists of coarse quartz, oligoclase (McLelland et al., 2001b), magnetite, microcline, apatite, titanite, calcite,

zircon, and minor sulfides. Secondary Na- and K-alteration has masked the original igneous composition and mineral assemblage (Table 4-1). Primary oligoclase (blue-gray CL) is replaced first by albite (with red CL) and then by potassium feldspar (blue CL) along grain boundaries. Apatite occurs near quartz, in areas of fine-grained alteration, and is associated with clusters of titanite grains which grew later than apatite. Apatite typically luminesces yellow with a subset of purple orange luminescent grains. Zircon grains are present along grain boundaries and in association with quartz.

Hawkeye granite

The Hawkeye granite is dated at 1100 Ma, is highly deformed and metamorphosed as a result of the Ottawan orogeny, and intrudes rocks of the 1150 Ma AMCG suite (e.g., Buddington, 1939; McLelland et al. 2001a). The Hawkeye granite is white to light-gray or pink and contains a distinctive quartz ribbon lineation with lineations reaching up to 10 cm.

The Hawkeye granite mineral assemblage contains highly recrystallized quartz, perthitic feldspar, myrmekite plagioclase, and zircon ± amphibole ± orthopyroxene, ± garnet ± biotite ± ilmenite ± apatite. Perthite grains in the Hawkeye granite typically contain short, fat lamellae which are often absent in the rims of the grains (Fig 4-31). Zircon occurs at grain boundaries and as inclusion in perthite grains. The mafic mineral content is variable in the Hawkeye granite with some samples containing only minor magnetite while others would be better classified as charnockite. Potassium feldspar luminesces blue with brown to gray-brown plagioclase lamellae, and apatite, when present, luminesce orange-purple.

AMCG suite charnockite

Charnockite is common throughout the Adirondack Highlands as part of the circa 1150 Ma AMCG suite. A charnockite sample, near Skiff Mountain was collected for this study as a comparison between the LMG and granitoid rocks of the AMCG suite that have not experienced alteration and mineralization. The unit is typically orange to orange-gray and with a "tiger-striped" appearance as a result of the presence of elongated mafic minerals and gneissic layering.

The mineral assemblage consists of plagioclase, perthitic feldspar, clinopyroxene (with exsolution lamellae), orthopyroxene, garnet, apatite, and zircon and minor quartz. Perthite grains contain short, fat, or rounded lamellae. Feldspar grains and quartz are typically granoblastic and can form composite "strings" between clinopyroxene and garnet-rich layers. Clinopyroxene and garnet are rimmed by amphibole and magnetite and all exhibit a shape-preferred orientation. Additionally magnetite occurs as small euhedral grains within orthopyroxene and garnet. Elongated apatite grains are present throughout the thin section. Plagioclase luminesces brown-green and perthitic feldspar luminesces blue with brown-green lamellae. Apatite exhibit a purple-orange luminescence.

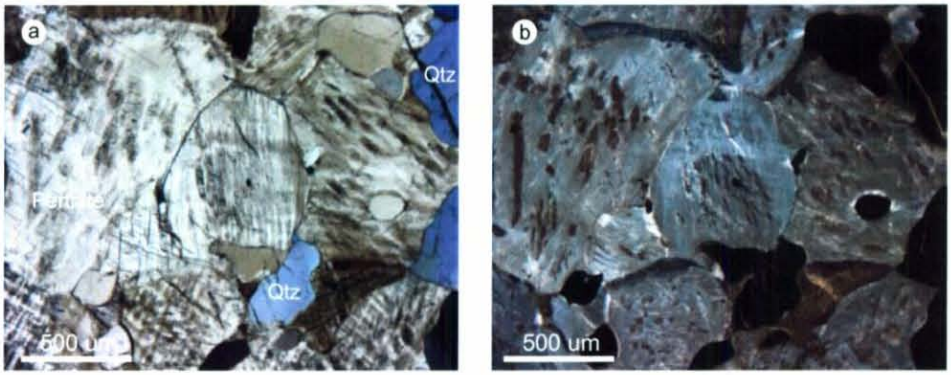

Figure 4-31. Cross-polarized light image a) and b) color CL image of perthitic feldspars in the Hawkeye granite. Note the lack of lamellae in rims of feldspar grains.

SUMMARY

The data presented in this thesis suggest that the LMG intruded the northeastern Adirondack Highlands between 1060 and 1050 Ma. The earliest preserved mineral assemblage of the granite comprises perthitic feldspar, quartz, magnetite, hematite-ilmenite intergrowths and minor clinopyroxene, zircon, titanite and apatite. First generation ore deposits consisting of clinopyroxene, magnetite and apatite formed as a result of granite crystallization. The perthite granite and clinopyroxene-magnetite ores were subsequently altered by external K- and Na-rich fluids that penetrated the LMG during or following the Ottawan orogeny or by fluids associated with late dike and pegmatite emplacement or unrecognized contemporaneous intrusions. Clinopyroxene and apatite from the initial ore bodies broke down during this subsequent fluid alteration and released Zr and radiogenic Hf, and magnetite was remobilized to form new deposits. These second generation ore deposits comprise magnetite, apatite, quartz, albite, minor zircon, and converted clinopyroxene to secondary amphibole and biotite. Perthitic feldspar in the granite was converted to microcline during K alteration and then to albite during Na alteration.

Fluid alteration and Fe mineralization associated with the development of magnetite-apatite (Kiruna-type) deposits may occur episodically, long after crystallization or formation of the ore host rock and ores associated with granite magmatism. The presence U-Th-Pb zircon ages 20 to 60 m.y. younger than the host granites of the ores, and the highly variable mineralogy of the ore deposits (e.g. clinopyroxene-magnetite and quartz-magnetite) suggests that multiple processes are

responsible for ore formation and periodic modification of preexisting ores. However, the presence of ore deposits almost exclusively within the LMG implies a "fertility" requirement of the host granite and that magnetite-apatite mineralization is directly or indirectly related to magmatism.

APPENDIX 1

MINERAL ASSEMBLAGE AND CATHODOLUMINESCENCE

A comprehensive table for the observed mineral assemblages in samples studied is presented in appendix Table A1-1. Additionally the observed luminescence for certain minerals important to this study are listed here. The implication of the mineral assemblage and luminescence has been discussed in detail in Chapter 4.

Table A1-1 Petrology and CL of the Lyon Mountain granite and associated rock types

Sample	Rock Type	Alteration	perthitic feldspar	K-feldspar	K-feldspar CL	plg
Arnold Hill						
99-5A	mixed LMG	Na	x	x (some may xcut)	blue-gray	2 gen
AH-06-1A	albite granite	Na	-	-	-	x
AH-06-6B	ore	-	-	-	-	-
RC-06-1	mixed LMG	K + Na		x	blue	late
RC-06-2	albite granite	Na		a few patches	gray-brown	dominant
Ausable Forks						
95-1A	albite granite	Na	-	trace	blue	x
Barton Hill						
BH-06-1B	ore-pegmatite	Na	-	x	blue	x-cut
BH-06-1F	mafic layer	Na?	-	-	-	w/alt cores
BH-LMG-2	mixed LMG	Na	trace	trace	blue-gray	x-cut
BH-06-2A	def. pegmatite	Na	-	trace	blue	x
BH-06-2B	ore-pegmatite	-	-	-	-	-
Clintonville						
99-1A	perthite granite	Na	x	as perthite	blue	x (some x-cut)
Dannemora						
99-6B	pegamtite	K (?)	-	dominant		
99-6C	microcline granite	K	-	dominant		
D-06-1B	metasediment	K (?)	-	X blue-gray in CL	blue-gray	x
D-06-1G	mafic layer	K (?)	-	-		turbid
EM-06-1A	ore	Ca	dominant	as perthite	blue	as lamellae
Dry Bridge						
99-2B	albite granite	Na	-	-	-	x
Ellenberg						
EB-07-01	microcline granite	K	-	dominant	blue	?
EB-07-02	albite granite	Na	patch, anti, typical	x	blue	x
Fayalite granite						
99-3A	fayalite granite	Na	flame	as perthite	gray-green	x
F-06-1A	amphibolite	?				x
F-06-4B	fayalite granite	Na	braid, flame	as perthite	gray-green	x

Table A1-1 Continued

Sample	Rock Type	Alteration	perthitic feldspar	K-feldspar	K-feldspar CL	plg
Hawkeye locality						
H-06-1A	aplite dike	-	x	as perthite	blue-gray	x
H-06-1C	Hawkeye granite	-	"blobs"	as perthite	blue-gray	x
H-06-2A	pegmatite	-	x	as perthite	gray	x
H-06-2B	mafic layer	-	-	in veins or patches	blue	x
HSL-1-06	Hawkeye granite	-	"blobs"	as perthite	blue-gray	as lamellae
Lyon Mtn						
LM-06-1A	dike	Na		x	blue-gray	2 gen
LM-06-1B	ore	-	remnant	-	-	-
LM-06-1C	mixed LMG	K + Na		x	blue-gray	xcut
LM-06-1D	microcline granite	K + Na	trace	x	blue-gray	x
LM-06-1E	mylonite	Na	porph (lam not red)	porph	blue-gray	recrystallized
LM-06-2A	perthite granite	Na	dominant	as perthite	blue-gray	some late
LM-06-2B	microcline granite	K + Na	Flame pos.	w/ dusty patches	blue	limted late
NW mixed rock						
MR-06-1	mafic gneiss	-	x	x	blue	x
MR-06-2A	granite gneiss	-	graphic ?	x	blue	x
Palmer Hill						
99-4A	ore	-	-	trace	blue	some turbid
99-4B	mixed LMG	K + Na		x	gray	xcut
99-4C	lean ore	K + Na	flame	x	blue-gray	xcut
Piercefield						
99-7A	pegamtite	K		x	gray	x
99-7E	microcline granite	K	some	x	blue	-
Rutgers						
L-06-1A	lean ore	-	x	x	blue	x
06-4B	ore	-	-	-	-	-
06-4D	perthite granite	Na (?)	x	as perthite	blue-gray	some xcut
HOG-1A	mixed	K + Na	limited flame	dominant	blue-gray	x
Skiff Mtn						
00-01	ore	-	-	-	-	-
00-02	albite granite	Na	-	-	-	x
00-03	pegmatite	K	x	x	blue-gray	some xcut
00-04	microcline granite	K	x	x	blue-gray	x
00-09	charnockite	-	x	as perthite	blue	x
00-11	amphibolite	Na ?	-	-	-	x

Table A1-1 Continued

Sample	plg CL	quartz	cpx	opx	amphibole	olivine
Arnold Hill						
99-5A	red + gray	x	-			
AH-06-1A	red + gray	x	altered		alt	
AH-06-6B	-	x	-			
RC-06-1	brown + red	x	DNO			
RC-06-2	blue-gray + red	x	inc in plg, along plg grb		tr.	
Ausable Forks						
95-1A	dull red	some round	-		blue-green	
Barton Hill						
BH-06-1B	red	x	x			
BH-06-1F	red + gray	-			blue-green	
BH-LMG-2	red	some x-cut	trace			
BH-06-2A	red	some x-cut	x			
BH-06-2B	-	x	-			
Clintonville						
99-1A	red + gray	x	-		tr. in mag layer	
Dannemora						
99-6B		some SPO, xcut	-			
99-6C		some SPO, xcut	-			
D-06-1B	gray	some SPO and round	-			
D-06-1G		trace	-		x	
EM-06-1A	dark gray	?	alt, w/ mt, cc, chl			
Dry Bridge						
99-2B	red	some round	emerald green			
Ellenberg						
EB-07-01	-	some xcut				
EB-07-02	red	x	SPO			
Fayalite granite						
99-3A	red	w/ olivine, inc of perth in SPO qtz	with opx lamllae		?	rare
F-06-1A	blue-gray	-	-		x	
F-06-4B	red	some round	with opx lamllae		?	rare

Table A1-1 Continued

Sample	plg CL	quartz	cpx	opx	amphibole	olivine
Hawkeye locality						
H-06-1A	brown	some SPO				
H-06-1C	brown	ribbon			x	
H-06-2A	dark gray	large				
H-06-2B	green	-	?	elongate		
HSL-1-06	dark gray	large				
Lyon Mtn						
LM-06-1A	red + gray	some "crushed"	remants			
LM-06-1B	-	recrystallized	x		late, as. w/ cpx, mt	
LM-06-1C	red	some round	trace		x	
LM-06-1D	red	some vein	trace		w/ mt, ttn	
LM-06-1E	red	assume fine grain				
LM-06-2A	red	x-cut, rd, SPO, feld inc	SPO w/amph, ttn, mt		blue-green w/cpx	
LM-06-2B	red	round in ksp	SPO, w/ ttn, mt			
NW mixed rock						
MR-06-1	brown	some round	w/ mt, late plg rim	elongate	w/ mt	
MR-06-2A	dark gray	large, small round	remnant w/ mt, layer		trace	
Palmer Hill						
99-4A	red	coarse	-			
99-4B	red	round in fld, some late	-			
99-4C	red	layers				
Piercefield						
99-7A	red	x				
99-7E		x	x			
Rutgers						
L-06-1A	red	x	much (rims of ttn, mag)		blue-green	
06-4B	-	tr.	going to mag and amph		inc of mt, apt, cpx	
06-4D	red	w/ late plg	small (ttn, mag)			
HOG-1A	red	w/ late plg	rims of ttn, inc in mt, plg			
Skiff Mtn						
00-01	-	x				
00-02	dull red	x (rd or as inc)				
00-03	dark gray	x (some xcut and rd)	tr.			
00-04	brown	x (some late) inc of fld				
00-09	brown-gray	tr.	x	x (w/cpx, mag, grt	after cpx + grt	
00-11	blue-gray, red	tr.			blue-green	

Table A1-1 Continued

Sample	garnet	oxide	titanite	biotite
Arnold Hill				
99-5A		mt		
AH-06-1A		mt, late hem		
AH-06-6B		hem		
RC-06-1			x	w/ late alt.
RC-06-2		w/ cpx	inc of mt , near cpx	
Ausable Forks				
95-1A		mt	w/ mafics, inc in qtz + ab	w/ amph and mt
Barton Hill				
BH-06-1B		mt	w/cpx-mt	
BH-06-1F		mt	w/ mt-amph	x
BH-LMG-2		trace. mt	w/ mt	
BH-06-2A		trace. mt	trace	
BH-06-2B		mt	in qtz	
Clintonville				
99-1A		mt		
Dannemora				
99-6B		mt, hem exs.		
99-6C		mt	rims mt	
D-06-1B		mt w/hem rim		brown w/ mt
D-06-1G		mt, hem exs.		brown
EM-06-1A		mt		
Dry Bridge				
99-2B	w/ cpx + ttn	trace mt	x	
Ellenberg				
EB-07-01		hem		
EB-07-02		rare mt	ubiquitous	
Fayalite granite				
99-3A		mt		
F-06-1A		mt		defines foliation
F-06-4B		mt		

Table A1-1 Continued

Sample	garnet	oxide	titanite	biotite
Hawkeye locality				
H-06-1A				remnants w/ rt, il
H-06-1C				
H-06-2A				
H-06-2B		?		defines foliation
HSL-1-06		mt, il		
Lyon Mtn				
LM-06-1A		mt w/ ttn, apt)	rim mt, near apt	
LM-06-1B		mt (inc of cpx, qtz, plg)		
LM-06-1C		trace	x	
LM-06-1D		mt w/ ttn	ubiquitous	trace
LM-06-1E		mt and il, late hem	def. with tails of mt	
LM-06-2A		mt (hem cleav)	w/ mt, cpx, amph	
LM-06-2B		trace	w/ cpx	trace
NW mixed rock				
MR-06-1		mt, w/ sul.	none	x
MR-06-2A		mt w/ qtz, cpx		
Palmer Hill				
99-4A		mt		
99-4B		mt		
99-4C		mt		
Piercefield				
99-7A			surounded by il	
99-7E			x (as. with scap)	
Rutgers				
L-06-1A		mt, hem exs., rims of ttn	w/ mt, cpx	trace
06-4B		mt		trace
06-4D		mt w/ cpx, ttn, inc of perth	w/ mt, cpx	w/ ttn, cpx, mt
HOG-1A		mt, patch hem	w/ mt, cpx	late
Skiff Mtn				
00-01		mt		x
00-02		mt		
00-03		mt		x
00-04		mt		x
00-09	x (rims of cpx)	x after cpx, in opx		
00-11		mt (amph, bt (inc))	rims amph	x

Table A1-1 Continued

Sample	apatite (CL)	zircon (CL, D = dark, Y = yellow)	fluorite	myrmekite	accessory
Arnold Hill					
99-5A	grb (purple-orange), mt (yellow)	qtz, small (D), plg (Y),gbd (zoned)			bt, much chl, tremolite ?
AH-06-1A	w/ alt. mafics, grb (orange)	qtz (Y) small (D), grb, ab (zoned)			bt/rt/il
AH-06-6B	alt zone w/ Cc + qtz, (purple)	?			il/ Cc/Chl ?)
RC-06-1	alt zones, large, small at grb (orange)	ksp (D)			epi/zoi
RC-06-2	grb (purple-orange)	ab (zoned), small (all D)			
Ausable Forks					
95-1A	in plg, w/ mafics (purple-orange)	grb (Y), ab (Y), qtz (D)		sympl bt-qtz	
Barton Hill					
BH-06-1B	-	?			
BH-06-1F	plg, bt, mt, grb (orange-purple)	plg/grb/bt-mt (Y)			
BH-LMG-2	ksp-plg (orange-purple), big (yellow)	qtz, ksp, grb, (D)(Y fract)			cpx
BH-06-2A	grb, alt. cpx (orange-purple)(yellow rims)	plg, large			
BH-06-2B	-	?			chl or bt
Clintonville					
99-1A	w/ mt, qtz, ab, inc in mt (orange)	grb,perth,qtz (Y), alt plg (zoned)			rt/il/ttn/bt
Dannemora					
99-6B	grb, alt. zone (yellow)	grb, (Y, zoned), fract of mt (Y + D)			mus w/ mt, Cc
99-6C	grb w/ qtz, mt, fld (purple)	grb (Y), ksp, qtz (zoned)			
D-06-1B	w/ bt, mt, fld (yellow)	small, in qtz + feld (D)			sec. feld, ms, cc alt
D-06-1G	ubiquitous (yellow, purple core)	amph, btwn mt-fld (D)			chl
EM-06-1A	w/ mt, cpx (purple, yellow rim + fract)	perth, cpx, alt zone (Y)		w/ plg	scapolite, chl, cal, sil (?)
Dry Bridge					
99-2B	alt zones (purple-orange)	qtz, grb, plg (D), grb (Y)			Cc alt cuts apt
Ellenberg					
EB-07-01	alt zones (orange-purple)	gb, qtz, ksp (Y)			Lots of Chl
EB-07-02	grb, in cpx (large) (purple-orange)	?			
Fayalite granite					
99-3A	alt zones, near fl, in qtz (orange)	grb (Y), qtz (zoned), cpx (Y)	x		bt, iddingsite
F-06-1A	ubiquitous (purple-orange)	?			rutile,bt,il
F-06-4B	rare (purple)	grb, fld, qtz (Y)			

Table A1-1 Continued

Sample	apatite (CL)	zircon (CL, D = dark, Y = yellow)	fluorite	myrmekite	accessory
Hawkeye locality		few grb (Y)			
H-06-1A	many small, at grb (orange)	few grb (Y) perth, qtz		w/ plg	rutile/il
H-06-1C	many as.w/ vein (orange)	perth, vein, (D + Y)		w/ plg	rutile/il
H-06-2A	-	?			
H-06-2B	w/ ksp, grb small, in bt (yellow)	plg (Y) ksp (D), Bt (?)			
HSL-1-06	-	grb (D)			rt
Lyon Mtn					
LM-06-1A	alt zones, (yellow) some (P)	some large @ grb near grunge (Y), qtz			much Cc, some sulp,
LM-06-1B	w/ mt, qtz (purple)	?			rt/il/chl/cal
LM-06-1C	grb, qtz (orange-purple)	qtz (D), grb (D), Ksp (Y)			chl/msc/cal/bt/rt/il
LM-06-1D	-	qtz, grb, ksp (D, little Y)			chl/epi/bt/apt?
LM-06-1E	many small (orange-purple)	?			deformed porhryoclasts
LM-06-2A	w/ late plg (orange)	grb near qtz and in qtz (Y)	?		
LM-06-2B	-	small, qtz, alt fld, grb, (D)			
NW mixed rock					
MR-06-1	grb, as.w/ mt (all purple-orange)	grb (zoned)		as. w/ plg	
MR-06-2A	w/ mt, cpx, grb (orange)	(Y or zoned)			
Palmer Hill					
99-4A	alt zones, w/ fl (orange-purple)	many small (D) in qtz, Large (Y) in mt	x		bt
99-4B	alt zones, grb(orange-purple)	many small in qtz, plg and grb (zoned)	x		chl/bt
99-4C	alt zones, grb(orange-purple)	ksp, grb (Y)	x		
Piercefield					
99-7A	alt zones, grb (purple-orange)	grb (Y), alt fld, in ksp w/ qtz inc (zoned)			Cc
99-7E	ubiquitous (purple)	grb (zoned) many small all (zoned)	x		scapolite (much)(ttn as.)
Rutgers					
L-06-1A	alt zones,grb, inc in hbl (orange)	small, perth, grb, qtz, (D)			
06-4B	large, w/cpx, mt, in amph (purple-orange)	?			qtz/bt
06-4D	alt zones (orange)	in qtz, few perth, (small + D)			bt
HOG-1A	alt zones fractured cpx, (orange-purple)	small in qtz (D) larger @ grb, mc			
Skiff Mtn					
00-01	multi-gen. (intense orange-purple)	?	?		rt/bt
00-02	1grain (purple)	grb (Y) in ab (D)			chl-epi
00-03	as. plg + qtz (orange, yellow rim)	in fld, grb (D)		x	msc
00-04	as. plg + qtz (orange, yellow rim)	ksp, qtz, bt, grb (D), in fract (Y)		x	
00-09	grb, w/ cpx, amph, grt (purple-orange)	?			qtz
00-11	grb (purple-orange)	grb, ab (Y + D)			

APPENDIX 2

WHOLE ROCK GEOCHEMISTRY

Whole rock geochemistry for the all of the samples studied is presented in appendix Tables A2-1 – A2-6. A detailed discussion on the implication of whole rock geochemistry for the LMG and associated rock types has been presented in Chapter 4.

Table A2-1 Major element geochemistry (weight percent) of the Lyon Mountain granite and associated rock types

Element				SiO2	Al2O3	Fe2O3	MnO	MgO	CaO	Na2O	K2O	TiO2	P2O5	LOI	TOTAL
Sample	Rock type	Location	specifics												
Lyon Mountain granite															
99-1A	perthite granite	Clintonville	outcrop	71.52	12.27	4.69	0.02	0.36	1.15	3.35	5.75	0.54	0.14	0.60	100.39
06-4D	perthite granite	Rutgers Mine	30m west of ore	67.18	13.86	5.60	0.02	0.52	1.53	4.55	5.97	0.49	0.09	0.14	99.94
LM-06-2A	perthite granite	Lyon Mountain	40m below ore	68.13	13.61	3.72	0.1	0.96	3.06	3.83	6.01	0.818	0.17	0.12	100.5
99-6C	microcline granite	Dannemora	outcrop	68.98	12.73	6.03	0.01	0.14	0.39	1.27	9.30	0.47	0.10	0.08	99.50
99-7E	microcline granite	Piercefield	outcrop	68.81	11.99	5.10	0.13	0.31	2.07	1.40	7.62	0.65	0.16	0.34	98.59
00-04	microcline granite	Skiff Mountain	outcrop	68.20	13.32	5.12	0.02	0.41	0.60	2.11	8.03	0.53	0.16	0.41	98.91
LM-06-2B	microcline granite	Lyon Mountain	30m above ore	69.28	11.39	2.62	0.049	1.24	2.86	1.51	8.21	1.304	0.02	0.49	98.95
AH-06-1A	albite granite	Arnold Hil	waste pile	68.84	11.85	9.51	0.015	1.58	0.8	5.79	0.24	0.35	0.05	0.51	99.53
99-2B	albite granite	Dry Bridge	outcrop	71.38	13.34	3.38	0.03	0.51	3.12	7.61	0.10	0.41	0.07	0.40	100.35
00-02	albite granite	Skiff Mountain	0.5m below ore	73.53	11.73	6.15	0.01	0.29	0.48	6.57	0.33	0.33	0.04	0.22	99.66
RC-06-2	albite granite	Arnold Hil	1km E. of ore	65.78	15.67	2.56	0.02	1.75	3.13	7.16	1.67	0.85	0.16	0.72	99.46
95-1A	albite granite	Ausable Forks	outcrop	69.14	13.41	7.29	0.05	0.63	1.22	6.69	0.77	0.55	0.12	0.26	100.10
99-5A	mixed	Arnold Hil	waste pile	68.06	12.70	10.32	0.01	0.17	0.42	5.34	2.84	0.44	0.04	0.10	100.45
99-4B	mixed	Palmer Hill	0.5m above ore	71.96	11.85	5.05	0.02	0.23	0.21	2.43	6.81	0.40	0.07	0.25	99.29
BH-LMG-2	mixed	Barton Hill	3m above ore	71.78	11.01	7.39	0.04	0.07	0.64	5.29	1.97	0.40	0.04	-0.03	98.60
LM-06-1C	mixed	Lyon Mountain	0.5m above ore	72.76	12.37	1.69	0.02	0.25	0.68	2.70	7.51	0.15	0.04	0.43	98.59
LM-06-1D	mixed	Lyon Mountain	15m below ore	70.61	11.67	5.49	0.02	0.27	0.92	2.62	6.64	0.50	0.05	0.05	98.84
RC-06-1	mixed	Ausable Forks	1km E. of ore	71.38	12.92	1.86	0.01	1.35	0.67	3.26	6.69	0.43	0.11	0.42	99.10
99-3A	fayalite granite	Ausable Forks		70.62	12.32	6.07	0.11	0.03	1.42	4.14	5.12	0.43	0.05	0.08	100.38
Dikes and pegmatites															
99-6B	pegmatite	Dannemora	crosscuts granite	64.55	12.33	11.03	0.02	0.20	0.60	1.12	8.71	0.61	0.16	0.27	99.60
99_7A	pegmatite	Piercefield	migmatite	64.74	14.85	4.65	0.08	0.03	1.94	1.74	10.30	0.52	0.12	0.58	99.56
00-03	dike	Skiff Mountain	crosscuts granite	72.41	13.03	3.28	0.02	0.30	0.56	1.99	7.68	0.51	0.18	0.39	100.34
LM-06-1A	dike	Lyon Mountain	crosscuts granite	64.29	16.67	5.88	0.02	0.10	2.99	6.43	1.75	0.26	0.23	0.31	98.94
BH-06-2A	dike	Barton Hill	deformed	74.38	12.11	2.58	0.05	0.86	1.49	7.32	0.30	0.10	0.03	0.32	99.54
H-06-1A	LMG (?) dike	Hawkeye	cuts Hawkeye	69.84	14.23	3.39	0.04	0.28	1.48	3.38	5.78	0.40	0.15	0.68	99.65
Ore															
AH-06-6B	hem	Arnold Hil	waste pile	11.91	0.97	73.92	0.049	1.67	1.93	0.05	< 0.01	0.19	0.66	1.77	93.12
99-4A	mt + apt	Palmer Hill		18.14	1.42	75.48	0.17	0.16	0.47	0.13	0.60	4.44	0.33	-1.33	100.00
99-4C	mt	Palmer Hill	lean ore	45.60	8.37	38.10	0.04	0.12	0.07	1.64	4.72	0.74	0.04	-0.72	98.73
00-01	mt + apt	Skiff Mountain		10.06	0.72	87.79	0.04	0.11	1.44	0.00	0.01	0.45	0.92	-1.91	99.66
BH-06-1B	feld + mt	Barton Hill		63.19	10.91	12.89	0.04	1.02	2.49	5.90	1.88	0.25	0.02	0.25	98.84
BH-06-2B	qtz + mt	Barton Hill		74.20	1.67	21.94	0.02	0.05	0.18	0.78	0.29	0.11	0.01	-0.66	98.60
LM-06-1B	cpx + mt	Lyon Mountain		6.69	1.00	90.18	0.11	0.90	1.68	0.29	0.07	0.35	0.01	-2.65	98.61
EM-06-1A	cpx + mt	Dannemora	lean ore	37.55	6.03	37.1	0.154	5.09	7	1.46	2.6	0.577	0.07	1.16	98.78
L-06-1A	cpx + mt	Lavake	lean ore	57.03	11.11	11.83	0.073	4.63	6.4	3.85	4.16	0.289	0.32	0.23	99.92
06-4B	cpx + mt	Rutgers		20.52	1.21	52.89	0.11	4.41	14.22	1.00	0.11	0.41	5.48	-1.39	98.97
Mafic layers															
BH-06-1F	biotite-rich	Barton Hill	1m below ore	46.11	14.18	15.92	0.04	5.73	4.37	5.08	2.71	3.05	0.55	1.16	98.89
D-06-1G	amphibolite	Dannemora	within metasediments	44.67	15.21	16.17	0.21	6.09	7.66	2.36	2.68	3.36	0.61	0.89	99.91
F-06-1A	amphibolite	Ausable Forks		45.36	15.07	15.33	0.19	6.15	8.50	3.84	1.67	2.51	0.48	0.44	99.53
00-11	amphibolite	Skiff Mountain	1m below ore	49.79	15.02	11.80	0.11	5.79	4.26	5.92	1.68	2.64	0.42	1.34	98.79
H-06-2B	biotite-rich	Hawkeye		49.23	22.71	10.13	0.10	3.72	2.82	4.75	4.20	0.81	0.14	1.09	99.70
MR-06-1	amphibolite	Rt 458		55.94	13.49	13.99	0.24	1.76	5.17	4.05	3.11	1.68	0.65	-0.29	99.77
Other															
00-09	charnockite	Skiff Mountain	AMCG suite	56.64	16.08	10.35	0.19	0.52	4.42	4.69	4.38	1.01	0.46	0.10	98.86
HSL-1-06	Hawkeye granite	Hawkeye		78.47	11.61	0.4	0.001	0.1	0.32	2.47	5.91	0.087	0.02	0.28	99.67
H-06-1C	Hawkeye granite	Hawkeye		71.52	13.15	3.15	0.05	0.15	1.28	2.85	5.79	0.33	0.07	0.55	98.88
H-06-2A	pegmatite	Hawkeye		69.53	15.53	0.88	0.01	0.02	0.52	3.13	8.63	0.03	0.03	0.21	98.51
D-06-1B	metasediment	Dannemora		63.63	12.64	9.59	0.059	1.33	0.65	0.69	8.64	0.734	0.14	0.69	98.8
MR-06-2A	granite	Lake Titus		70.20	13.63	4.59	0.02	0.87	1.76	4.76	3.21	0.56	0.16	0.55	100.30
99-6A	diabase dike	Dannemora		48.71	15.21	12.39	0.16	4.56	6.64	4.63	1.95	3.11	0.94	1.49	99.80
99-6D	trachyte dike	Dannemora		62.29	17.15	5.47	0.04	0.40	1.10	6.74	5.44	0.20	0.05	1.14	100.00

Table A2-2 Trace element geochemistry (ppm) of the Lyon Mountain granite and associated rock types

Element				Sc	Be	V	Cr	Co	Ni	Cu	Zn	Ga	Ge	As
Sample	Rock type	Location	specifics											
Lyon Mountain granite														
99-1A	perthite granite	Clintonville	outcrop	5	2	20	10	1	10	75	15	23	1.7	2
06-4D	perthite granite	Rutgers Mine	30m west of ore	5	4	29	10	144	10	5	15	26	1.9	2
LM-06-2A	perthite granite	Lyon Mountain	40m below ore	11	6	20	< 20	166	< 20	< 10	40	28	2	< 5
99-6C	microcline granite	Dannemora	outcrop	5	0.5	18	10	5	10	74	15	23	3.0	2
99-7E	microcline granite	Piercefield	outcrop	8	2	19	10	4	10	82	83	22	2.2	2
00-04	microcline granite	Skiff Mountain	outcrop	7	3	23	10	3	10	42	15	23	2.0	2
LM-06-2B	microcline granite	Lyon Mountain	30m above ore	8	4	44	50	198	20	< 10	40	18	1.8	< 5
AH-06-1A	albite granite	Arnold Hil	waste pile	4	7	28	< 20	195	< 20	< 10	< 30	31	2.3	< 5
99-2B	albite granite	Dry Bridge	outcrop	6	6	7	10	0.5	10	5	15	33	4.2	2
00-02	albite granite	Skiff Mountain	0.5m below ore	1	7	5	10	2	10	5	15	42	2.6	2
RC-06-2	albite granite	Arnold Hil	1km E. of ore	15	3	70	50	301	10	10	15	21	1.8	2
95-1A	albite granite	Ausable Forks	outcrop	12	4	20	10	299	10	5	50	28	1.4	2
99-5A	mixed	Arnold Hil	waste pile	2	2	16	10	6	23	68	15	32	1.8	2
99-4B	mixed	Palmer Hill	0.5m above ore	5	2	6	10	2	10	40	15	24	2.5	2
BH-LMG-2	mixed	Barton Hill	3m above ore	1	4	6	10	331	10	20	70	36	2.2	2
LM-06-1C	mixed	Lyon Mountain	0.5m above ore	2	0.5	5	10	185	10	30	15	21	1.3	2
LM-06-1D	mixed	Lyon Mountain	15m below ore	5	2	29	10	270	10	5	15	21	1.7	2
RC-06-1	mixed	Ausable Forks	1km E. of ore	13	2	27	10	208	10	10	15	21	1.8	2
99-3A	fayalite granite	Ausable Forks		2	5	8	10	0.5	10	5	137	38	2.7	2
Dikes and pegmatites														
99-6B	pegmatite	Dannemora	crosscuts granite	3	0.5	26	10	7	10	87	15	27	2.6	2
99_7A	pegmatite	Piercefield	migmatite	3	0.5	14	10	2	10	107	69	26	1.9	10
00-03	dike	Skiff Mountain	crosscuts granite	4	1	15	10	2	10	27	75	19	1.6	2
LM-06-1A	dike	Lyon Mountain	crosscuts granite	0.5	6	5	10	241	10	5	60	32	1.3	2
BH-06-2A	dike	Barton Hill	deformed	3	3	17	10	287	10	5	15	31	1.3	2
H-06-1A	LMG (?) dike	Hawkeye	cuts Hawkeye	5	1	13	10	238	10	5	60	22	1	2
Ore														
AH-06-6B	hem	Arnold Hil	waste pile	4	7	175	< 20	117	50	< 10	40	22	2.7	41
99-4A	mt + apt	Palmer Hill		9	0.5	42	10	21	71	36	103	16	2.7	7
99-4C	mt	Palmer Hill	lean ore	1	0.5	39	24	17	10	25	57	15	11.1	2
00-01	mt + apt	Skiff Mountain		2	0.5	54	10	10	132	13	70	40	9.2	34
BH-06-1B	feld + mt	Barton Hill		12	6	9	10	251	10	5	15	32	2.9	2
BH-06-2B	qtz + mt	Barton Hill		1	0.5	11	10	368	10	5	15	10	1.1	2
LM-06-1B	cpx + mt	Lyon Mountain		2	4	326	10	92	100	5	15	22	1.4	2
EM-06-1A	cpx + mt	Dannemora	lean ore	13	16	288	< 20	101	60	< 10	70	21	4.6	< 5
L-06-1A	cpx + mt	Lavake	lean ore	19	19	61	< 20	119	30	< 10	50	30	4	< 5
06-4B	cpx + mt	Rutgers		25	23	234	10	56	70	5	40	30	4.6	361

Table A2-2 Continued

Element				Sc	Be	V	Cr	Co	Ni	Cu	Zn	Ga	Ge	As
Sample	Rock type	Location	specifics											
Mafic layers														
BH-06-1F	biotite-rich	Barton Hill	1m below ore	23	4	121	70	80	50	5	15	20	2.3	16
D-06-1G	amphibolite	Dannemora	within metasediments	27	3	206	110	154	70	80	80	23	1.6	2
F-06-1A	amphibolite	Ausable Forks		23	3	166	130	102	70	20	150	23	1.7	2
00-11	amphibolite	Skiff Mountain	1m below ore	22	7	158	60	89	60	5	60	24	2	7
H-06-2B	biotite-rich	Hawkeye		6	162	< 5	10	122	10	5	700	55	1.6	2
MR-06-1	amphibolite	Rt 458		24	3	20	10	102	10	20	220	28	2	2
Other														
00-09	charnockite	Skiff Mountain	AMCG suite	23	1	< 5	10	141	10	5	100	27	1.8	2
HSL-1-06	Hawkeye granite	Hawkeye		< 1	< 1	< 5	< 20	221	< 20	< 10	< 30	22	1.4	< 5
H-06-1C	Hawkeye granite	Hawkeye		4	1	6	10	269	10	5	50	22	1.5	2
H-06-2A	pegmatite	Hawkeye		0.5	0.5	< 5	10	241	10	5	15	17	0.9	2
D-06-1B	metasediment	Dannemora		13	3	58	20	165	20	< 10	50	26	2.2	< 5
MR-06-2A	granite	Lake Titus		7	2	64	10	238	10	5	15	22	1.5	2
99-6A	diabase dike	Dannemora		17	3	197	24	33	56	33	154	26	2.0	6
99-6D	trachyte dike	Dannemora		3	11	5	10	0.5	36	67	41	56	2.3	2

Table A2-3 Trace element geochemistry (ppm) of the Lyon Mountain granite and associated rock types

Element				Mo	Ag	In	Sn	Sb	Ta	W	Tl	Bi	Pb	U
Sample	Rock type	Location	specifics											
Lyon Mountain granite														
99-1A	perthite granite	Clintonville	outcrop	1	1.1	-0.1	7	0.1	1.37	0.3	0.43	0.1	3	1.30
06-4D	perthite granite	Rutgers Mine	30m west of ore	1	0.2	< 0.1	10	0.1	4.01	727	0.23	0.1	3	3.94
LM-06-2A	perthite granite	Lyon Mountain	40m below ore	< 2	< 0.5	0.2	6	< 0.2	3.46	501	0.47	0.1	< 5	7.56
99-6C	microcline granite	Dannemora	outcrop	1	0.8	-0.1	16	0.1	1.82	0.8	0.94	0.7	3	4.80
99-7E	microcline granite	Piercefield	outcrop	1	1.0	0.1	6	0.3	1.51	0.3	2.00	0.1	9	5.54
00-04	microcline granite	Skiff Mountain	outcrop	1	0.7	-0.1	20	0.1	2.82	0.3	1.48	0.1	3	2.78
LM-06-2B	microcline granite	Lyon Mountain	30m above ore	< 2	< 0.5	0.1	8	< 0.2	2.91	624	0.3	< 0.1	< 5	11.1
AH-06-1A	albite granite	Arnold Hil	waste pile	< 2	< 0.5	0.1	10	< 0.2	4.18	676	< 0.05	< 0.1	< 5	7.91
99-2B	albite granite	Dry Bridge	outcrop	1	1.9	0.3	20	0.3	2.86	0.7	0.03	0.1	8	8.19
00-02	albite granite	Skiff Mountain	0.5m below ore	1	2.3	-0.1	11	0.1	4.08	0.3	0.03	0.1	3	12.87
RC-06-2	albite granite	Arnold Hil	1km E. of ore	1	0.2	< 0.1	4	0.1	3.45	958	0.14	0.1	3	4.16
95-1A	albite granite	Ausable Forks	outcrop	1	0.2	0.1	7	0.1	3.94	933	0.03	0.1	3	2.57
99-5A	mixed	Arnold Hil	waste pile	1	1.8	-0.1	11	0.1	2.45	0.3	0.10	0.2	3	4.90
99-4B	mixed	Palmer Hill	0.5m above ore	1	1.8	-0.1	18	1.1	1.30	0.3	0.56	0.1	3	1.95
BH-LMG-2	mixed	Barton Hill	3m above ore	2	2	< 0.1	12	0.1	8.45	1090	0.08	0.1	3	3.55
LM-06-1C	mixed	Lyon Mountain	0.5m above ore	1	0.2	< 0.1	3	0.1	4.74	932	0.46	0.1	19	3.94
LM-06-1D	mixed	Lyon Mountain	15m below ore	3	0.2	< 0.1	5	0.1	3.89	910	0.31	0.1	3	5.08
RC-06-1	mixed	Ausable Forks	1km E. of ore	1	0.2	< 0.1	4	0.1	2.84	722	0.22	0.1	3	2.94
99-3A	fayalite granite	Ausable Forks		1	3.5	0.1	3	0.1	1.72	0.3	0.42	0.1	3	1.79
Dikes and pegmatites														
99-6B	pegmatite	Dannemora	crosscuts granite	3	2.2	-0.1	23	0.3	1.53	3.4	0.85	0.1	3	3.79
99_7A	pegmatite	Piercefield	migmatite	1	1.1	-0.1	20	0.8	1.21	2.6	1.92	0.2	7	3.56
00-03	dike	Skiff Mountain	crosscuts granite	1	0.7	-0.1	6	0.1	0.78	0.3	1.40	0.2	6	1.78
LM-06-1A	dike	Lyon Mountain	crosscuts granite	3	0.2	< 0.1	2	0.1	2.36	757	0.25	0.1	12	2.87
BH-06-2A	dike	Barton Hill	deformed	1	0.2	< 0.1	3	0.1	2.64	896	0.03	0.1	3	0.49
H-06-1A	LMG (?) dike	Hawkeye	cuts Hawkeye	1	0.2	< 0.1	0.5	0.1	2.55	837	1.19	0.1	16	1.39
Ore														
AH-06-6B	hem	Arnold Hil	waste pile	< 2	< 0.5	0.2	7	3.8	0.52	333	< 0.05	0.1	11	13.6
99-4A	mt + apt	Palmer Hill		4	0.2	1.0	327	10.9	9.09	0.3	0.08	0.1	3	1.55
99-4C	mt	Palmer Hill	lean ore	2	0.2	-0.1	12	2.1	1.24	0.3	0.37	0.2	3	0.40
00-01	mt + apt	Skiff Mountain		1	0.2	0.3	91	0.1	20.0	1.2	0.03	0.1	9	7.88
BH-06-1B	feld + mt	Barton Hill		1	0.2	0.3	56	0.1	1.98	810	0.07	0.1	7	0.55
BH-06-2B	qtz + mt	Barton Hill		1	0.2	< 0.1	11	0.1	3.33	1300	0.03	0.1	3	0.12
LM-06-1B	cpx + mt	Lyon Mountain		1	0.2	0.2	3	0.1	0.31	99.4	0.03	0.1	3	0.15
EM-06-1A	cpx + mt	Dannemora	lean ore	< 2	< 0.5	0.5	6	< 0.2	0.52	176	0.16	< 0.1	< 5	1.07
L-06-1A	cpx + mt	Lavake	lean ore	< 2	< 0.5	0.3	11	< 0.2	1.22	339	0.24	< 0.1	< 5	1.98
06-4B	cpx + mt	Rutgers		1	0.2	0.4	11	0.1	0.28	109	0.07	0.1	11	8.72

Table A2-3 Trace element geochemistry (ppm) of the Lyon Mountain granite and associated rock types

Element				Mo	Ag	In	Sn	Sb	Ta	W	Tl	Bi	Pb	U
Sample	Rock type	Location	specifics											
Mafic layers														
BH-06-1F	biotite-rich	Barton Hill	1m below ore	1	0.2	0.1	23	7.7	1.38	232	0.35	0.1	3	1.79
D-06-1G	amphibolite	Dannemora	within metasediments	3	0.2	0.1	2	0.1	1.4	274	0.68	0.3	3	0.88
F-06-1A	amphibolite	Ausable Forks		3	0.2	< 0.1	7	0.1	1.25	184	0.98	0.1	3	2.35
00-11	amphibolite	Skiff Mountain	1m below ore	1	0.2	0.1	10	0.1	1.54	206	0.32	0.1	3	3.89
H-06-2B	biotite-rich	Hawkeye		1	0.2	< 0.1	2	0.1	1.44	363	1.99	0.1	38	20.80
MR-06-1	amphibolite	Rt 458		3	0.2	0.1	4	0.1	2.12	301	0.29	0.1	10	0.95
Other														
00-09	charnockite	Skiff Mountain	AMCG suite	3	0.2	< 0.1	1	0.1	1.55	420	0.33	0.1	3	0.79
HSL-1-06	Hawkeye granite	Hawkeye		< 2	< 0.5	< 0.1	< 1	< 0.2	2.14	750	0.65	< 0.1	11	0.92
H-06-1C	Hawkeye granite	Hawkeye		1	0.2	< 0.1	0.5	0.1	3.04	896	1.07	0.1	15	1.34
H-06-2A	pegmatite	Hawkeye		1	0.2	< 0.1	0.5	0.1	2.12	765	1.27	0.1	14	0.25
D-06-1B	metasediment	Dannemora		< 2	< 0.5	0.1	7	< 0.2	2.39	486	1.57	0.2	6	2.35
MR-06-2A	granite	Lake Titus		1	0.2	< 0.1	4	0.1	2.65	823	0.28	0.1	7	1.11
99-6A	diabase dike	Dannemora		4	0.2	-0.1	3	0.1	3.72	0.8	0.27	0.1	7	1.36
99-6D	trachyte dike	Dannemora		4	0.2	0.1	14	0.1	18.9	0.8	0.31	0.1	11	7.51

Table A2-4 Large ion lithophile element geochemistry (ppm) of the Lyon Mountain granite and associated rock types

Element				Rb	Sr	Cs	Ba
Sample	Rock type	Location	specifics				
Lyon Mountain granite							
99-1A	perthite granite	Clintonville	outcrop	116	73	0.1	548
06-4D	perthite granite	Rutgers Mine	30m west of ore	143	79	0.2	415
LM-06-2A	perthite granite	Lyon Mountain	40m below ore	196	119	0.4	1331
99-6C	microcline granite	Dannemora	outcrop	315	81	0.6	3,510
99-7E	microcline granite	Piercefield	outcrop	338	70	1.6	789
00-04	microcline granite	Skiff Mountain	outcrop	236	50	1.6	889
LM-06-2B	microcline granite	Lyon Mountain	30m above ore	232	42	0.4	787
AH-06-1A	albite granite	Arnold Hil	waste pile	5	33	< 0.1	8
99-2B	albite granite	Dry Bridge	outcrop	2	33	0.05	8
00-02	albite granite	Skiff Mountain	0.5m below ore	5	24	0.05	12
RC-06-2	albite granite	Arnold Hil	1km E. of ore	48	151	0.6	223
95-1A	albite granite	Ausable Forks	outcrop	9	101	0.05	61
99-5A	mixed	Arnold Hil	waste pile	46	44	0.1	194
99-4B	mixed	Palmer Hill	0.5m above ore	200	30	0.4	406
BH-LMG-2	mixed	Barton Hill	3m above ore	29	45	0.05	115
LM-06-1C	mixed	Lyon Mountain	0.5m above ore	168	44	0.3	573
LM-06-1D	mixed	Lyon Mountain	15m below ore	181	48	0.4	778
RC-06-1	mixed	Ausable Forks	1km E. of ore	191	42	0.7	449
99-3A	fayalite granite	Ausable Forks		199	29	0.1	200
Dikes and pegmatites							
99-6B	pegmatite	Dannemora	crosscuts granite	305	63	0.7	2,510
99_7A	pegmatite	Piercefield	migmatite	442	68	1.0	1,100
00-03	dike	Skiff Mountain	crosscuts granite	225	87	1.3	1,210
LM-06-1A	dike	Lyon Mountain	crosscuts granite	48	243	0.5	397
BH-06-2A	dike	Barton Hill	deformed	2	46	0.05	34
H-06-1A	LMG (?) dike	Hawkeye	cuts Hawkeye	159	174	1.2	1243
Ore							
AH-06-6B	hem	Arnold Hil	waste pile	2	25	0.1	10
99-4A	mt + apt	Palmer Hill		18	7	0.05	51
99-4C	mt	Palmer Hill	lean ore	145	38	0.3	745
00-01	mt + apt	Skiff Mountain		2	20	0.05	7
BH-06-1B	feld + mt	Barton Hill		24	44	0.05	92
BH-06-2B	qtz + mt	Barton Hill		5	12	0.05	23
LM-06-1B	cpx + mt	Lyon Mountain		2	7	0.05	9
EM-06-1A	cpx + mt	Dannemora	lean ore	58	58	0.1	589
L-06-1A	cpx + mt	Lavake	lean ore	110	64	0.4	426
06-4B	cpx + mt	Rutgers		2	31	0.05	18

Table A2-4 Large ion lithophile element geochemistry (ppm) of the Lyon Mountain granite and associated rock types

Element				Rb	Sr	Cs	Ba
Sample	Rock type	Location	specifics				
Mafic layers							
BH-06-1F	biotite-rich	Barton Hill	1m below ore	173	202	1.2	403
D-06-1G	amphibolite	Dannemora	within metasediments	108	222	1.3	284
F-06-1A	amphibolite	Ausable Forks		113	206	7.6	263
00-11	amphibolite	Skiff Mountain	1m below ore	167	222	2.8	248
H-06-2B	biotite-rich	Hawkeye		306	172	10.3	462
MR-06-1	amphibolite	Rt 458		67	208	0.1	574
Other							
00-09	charnockite	Skiff Mountain	AMCG suite	64	309	1.5	2819
HSL-1-06	Hawkeye granite	Hawkeye		141	30	0.2	102
H-06-1C	Hawkeye granite	Hawkeye		142	138	0.8	715
H-06-2A	pegmatite	Hawkeye		236	351	0.8	3127
D-06-1B	metasediment	Dannemora		279	48	0.8	947
MR-06-2A	granite	Lake Titus		62	204	0.05	561
99-6A	diabase dike	Dannemora		45	635	0.8	693
99-6D	trachyte dike	Dannemora		160	11	0.3	27

Table A2-5 High field strength element geochemistry (ppm) of the Lyon Mountain granite and associated rock types

Element				Y	Zr	Nb	Hf	Th
Sample	Rock type	Location	specifics					
Lyon Mountain granite								
99-1A	perthite granite	Clintonville	outcrop	72	525	20.6	14.7	9.75
06-4D	perthite granite	Rutgers Mine	30m west of ore	81	708	21.7	16.6	6.68
LM-06-2A	perthite granite	Lyon Mountain	40m below ore	89	692	23.2	17.4	20.1
99-6C	microcline granite	Dannemora	outcrop	71	500	23.5	14.0	13.03
99-7E	microcline granite	Piercefield	outcrop	82	483	19.9	13.4	15.94
00-04	microcline granite	Skiff Mountain	outcrop	56	360	13.9	9.7	13.14
LM-06-2B	microcline granite	Lyon Mountain	30m above ore	87	516	19.6	13.7	19.2
AH-06-1A	albite granite	Arnold Hil	waste pile	53	1403	25.3	34.1	16.5
99-2B	albite granite	Dry Bridge	outcrop	113	1010	39.5	25.2	19.71
00-02	albite granite	Skiff Mountain	0.5m below ore	362	1220	55.0	38.7	33.00
RC-06-2	albite granite	Arnold Hil	1km E. of ore	44	239	11.0	6.9	14.70
95-1A	albite granite	Ausable Forks	outcrop	73	590	15.9	15.6	7.75
99-5A	mixed	Arnold Hil	waste pile	71	1060	33.8	26.6	7.64
99-4B	mixed	Palmer Hill	0.5m above ore	40	902	22.7	21.0	5.05
BH-LMG-2	mixed	Barton Hill	3m above ore	205	1362	61.9	38.6	16.10
LM-06-1C	mixed	Lyon Mountain	0.5m above ore	30	272	12.0	9.6	26.50
LM-06-1D	mixed	Lyon Mountain	15m below ore	65	458	17.8	13.2	16.00
RC-06-1	mixed	Ausable Forks	1km E. of ore	38	260	10.4	7.8	18.00
99-3A	fayalite granite	Ausable Forks		131	1370	32.5	36.1	1.86
Dikes and pegmatites								
99-6B	pegmatite	Dannemora	crosscuts granite	99	1050	21.3	27.1	13.36
99_7A	pegmatite	Piercefield	migmatite	70	545	17.5	13.4	10.46
00-03	dike	Skiff Mountain	crosscuts granite	31	317	11.6	8.6	6.54
LM-06-1A	dike	Lyon Mountain	crosscuts granite	14	350	2.7	8.5	9.50
BH-06-2A	dike	Barton Hill	deformed	15	482	3.6	12.3	0.91
H-06-1A	LMG (?) dike	Hawkeye	cuts Hawkeye	20	303	10.5	7.8	10.70
Ore								
AH-06-6B	hem	Arnold Hil	waste pile	344	30	6.8	2.5	101
99-4A	mt + apt	Palmer Hill		34	140	267.6	4.4	5.13
99-4C	mt	Palmer Hill	lean ore	7	181	39.5	4.9	0.61
00-01	mt + apt	Skiff Mountain		804	59	12.2	4.5	58.70
BH-06-1B	feld + mt	Barton Hill		13	36	3.2	2.3	0.65
BH-06-2B	qtz + mt	Barton Hill		2	31	1.5	0.7	0.08
LM-06-1B	cpx + mt	Lyon Mountain		6	41	2.1	1.2	0.18
EM-06-1A	cpx + mt	Dannemora	lean ore	58	179	2.9	4.3	0.58
L-06-1A	cpx + mt	Lavake	lean ore	96	682	8.1	16.5	23.4
06-4B	cpx + mt	Rutgers		427	58	9.0	2.4	109.00

Table A2-5 High field strength element geochemistry (ppm) of the Lyon Mountain granite and associated rock types

Element				Y	Zr	Nb	Hf	Th
Sample	Rock type	Location	specifics					
Mafic layers								
BH-06-1F	biotite-rich	Barton Hill	1m below ore	130	211	27.0	5.5	8.02
D-06-1G	amphibolite	Dannemora	within metasediments	47	248	11.0	6.4	2.36
F-06-1A	amphibolite	Ausable Forks		71	231	11.5	6.1	4.33
00-11	amphibolite	Skiff Mountain	1m below ore	124	289	21.6	8.0	8.39
H-06-2B	biotite-rich	Hawkeye		52	1186	10.6	33.9	112.00
MR-06-1	amphibolite	Rt 458		103	455	19.1	12.1	1.57
Other								
00-09	charnockite	Skiff Mountain	AMCG suite	48	256	7.9	6.0	2.55
HSL-1-06	Hawkeye granite	Hawkeye		3	187	1.5	6.3	0.57
H-06-1C	Hawkeye granite	Hawkeye		50	389	11.5	10.9	1.97
H-06-2A	pegmatite	Hawkeye		4	31	1.4	0.8	0.63
D-06-1B	metasediment	Dannemora		88	579	17.9	15.4	15.3
MR-06-2A	granite	Lake Titus		26	440	7.9	11.5	36.60
99-6A	diabase dike	Dannemora		48	390	54.0	9.4	3.86
99-6D	trachyte dike	Dannemora		84	1830	228.4	42.4	33.71

Table A2-6 Rare earth element geochemistry (ppm) of the Lyon Mountain granite and associated rock types

Element			La	Ce	Pr	Nd	Sm	Eu	Gd	Tb	Dy	Ho	Er	Tm	Yb	Lu
Sample	Rock type	Location														
Lyon Mountain granite																
99-1A	perthite granite	Clintonville	51.91	112.95	15.61	62.91	13.39	2.49	14.13	2.30	13.09	2.67	7.60	1.19	7.10	1.00
06-4D	perthite granite	Rutgers Mine	26.90	88.10	13.10	57.50	13.60	2.47	12.90	2.45	15.20	3.02	9.54	1.57	10.20	1.52
LM-06-2A	perthite granite	Lyon Mountain	63.10	141.00	17.50	68.90	14.90	2.65	14.60	2.66	16.10	3.12	9.58	1.46	9.62	1.50
99-6C	microcline granite	Dannemora	36.99	80.02	11.29	44.87	10.20	2.07	10.76	2.01	12.00	2.50	7.61	1.27	7.88	1.15
99-7E	microcline granite	Piercefield	54.94	116.42	15.67	59.77	12.71	2.56	13.33	2.34	14.00	2.83	8.29	1.35	8.35	1.24
00-04	microcline granite	Skiff Mountain	50.07	100.01	13.25	51.32	10.30	1.89	10.23	1.68	9.51	1.87	5.29	0.81	4.87	0.71
LM-06-2B	microcline granite	Lyon Mountain	71.30	163	21.30	82.10	16.20	2.74	15.00	2.65	15.60	2.98	9.10	1.38	9.00	1.37
AH-06-1A	albite granite	Arnold Hil	85.20	161.00	17.30	66.70	11.10	1.38	10.00	1.49	8.72	1.79	5.97	1.01	7.69	1.36
99-2B	albite granite	Dry Bridge	111.12	204.76	25.64	97.26	18.78	3.08	19.60	3.30	19.20	3.92	11.66	1.97	11.89	1.81
00-02	albite granite	Skiff Mountain	159	351	46	181	40.16	3.43	47.59	8.94	56.47	12.55	37.16	5.90	32.45	4.45
RC-06-2	albite granite	Arnold Hil	57.50	134	15.60	57.00	10.20	1.90	8.46	1.42	8.36	1.63	4.87	0.73	4.72	0.69
95-1A	albite granite	Ausable Forks	47.80	106	13.40	53.30	12.20	2.09	11.40	2.03	12.60	2.52	7.83	1.20	7.78	1.15
99-5A	mixed	Arnold Hil	14.36	50.49	5.97	26.10	8.53	1.91	9.77	2.12	13.05	2.73	7.97	1.39	8.49	1.23
99-4B	mixed	Palmer Hill	26.71	60.77	8.47	34.39	7.26	0.94	7.23	1.25	7.27	1.48	4.34	0.71	4.47	0.73
BH-LMG-2	mixed	Barton Hill	91.10	248	33.00	138.00	33.00	2.67	32.80	6.15	38.30	7.44	22.30	3.31	19.50	2.51
LM-06-1C	mixed	Lyon Mountain	40.70	71.50	7.30	25.60	5.08	0.71	4.78	0.92	5.68	1.12	3.48	0.55	3.66	0.54
LM-06-1D	mixed	Lyon Mountain	38.30	92.20	11.50	45.40	10.60	1.53	10.30	1.95	11.90	2.34	7.31	1.17	7.39	1.03
RC-06-1	mixed	Ausable Forks	9.30	27.10	3.86	17.80	4.86	0.78	5.31	1.09	7.01	1.42	4.26	0.67	4.21	0.61
99-3A	fayalite granite	Ausable Forks	48.51	132.63	20.92	92.26	22.69	2.92	25.51	4.37	25.74	5.22	14.66	2.29	14.05	2.16
Dikes and pegmatites																
99-6B	pegmatite	Dannemora	62.15	110.78	13.93	52.92	11.64	2.37	12.82	2.35	14.66	3.12	9.49	1.58	9.79	1.48
99_7A	pegmatite	Piercefield	44.44	84.45	11.06	43.33	9.75	2.10	10.31	1.79	11.01	2.31	6.90	1.17	7.38	1.14
00-03	dike	Skiff Mountain	33.78	68.35	8.38	32.49	6.36	1.61	6.02	0.99	5.57	1.10	3.12	0.46	2.93	0.42
LM-06-1A	dike	Lyon Mountain	35.10	59.10	5.78	20.30	3.25	1.12	2.74	0.41	2.20	0.42	1.25	0.19	1.27	0.20
BH-06-2A	dike	Barton Hill	5.13	13.20	1.62	6.62	1.54	0.23	1.70	0.33	2.20	0.48	1.61	0.28	2.02	0.36
H-06-1A	LMG (?) dike	Hawkeye	65.00	143	16.00	57.70	10.00	2.33	6.76	0.87	4.34	0.76	2.05	0.29	1.83	0.30
Ore																
AH-06-6B	hem	Arnold Hil	620	1490	159	575	87.90	8.40	77.50	11.40	64.50	12.20	38.00	5.54	33.80	5.21
99-4A	mt + apt	Palmer Hill	32.21	69.35	8.81	33.65	6.32	0.77	6.70	1.06	6.05	1.25	3.66	0.56	3.34	0.51
99-4C	mt	Palmer Hill	10.74	18.50	1.97	6.87	1.23	0.17	1.18	0.20	1.14	0.24	0.72	0.12	0.77	0.12
00-01	mt + apt	Skiff Mountain	2300	3390	311	993	176	19.49	168.23	28.28	153.30	30.67	86.26	12.52	66.22	8.13
BH-06-1B	feld + mt	Barton Hill	9.03	16.00	1.68	6.23	1.37	0.21	1.52	0.30	1.97	0.43	1.58	0.38	4.20	1.21
BH-06-2B	qtz + mt	Barton Hill	1.43	2.47	0.26	0.96	0.18	0.04	0.17	0.03	0.22	0.05	0.16	0.03	0.16	0.02
LM-06-1B	cpx + mt	Lyon Mountain	1.46	5.13	0.76	3.20	0.73	0.12	0.74	0.14	0.92	0.20	0.69	0.13	1.13	0.26
EM-06-1A	cpx + mt	Dannemora	49.30	94.20	10.20	39.20	8.12	1.25	8.31	1.57	9.60	1.95	6.46	1.10	8.00	1.56
L-06-1A	cpx + mt	Lavake	36.00	91.70	12.00	52.40	12.10	1.95	13.30	2.40	15.00	3.15	10.20	1.69	12.50	2.31
06-4B	cpx + mt	Rutgers	298	667	85.50	339	67.50	9.17	68.50	10.70	61.60	12.50	37.60	5.58	34.80	5.54

Table A2-6 Rare earth element geochemistry (ppm) of the Lyon Mountain granite and associated rock types

Element			La	Ce	Pr	Nd	Sm	Eu	Gd	Tb	Dy	Ho	Er	Tm	Yb	Lu
Sample	Rock type	Location														
Mafic layers																
BH-06-1F	biotite-rich	Barton Hill	187	309	31.90	112	21.90	4.39	20.20	3.56	21.90	4.43	13.60	2.15	13.30	1.81
D-06-1G	amphibolite	Dannemora	23.10	57.20	7.73	34.30	8.54	2.66	8.82	1.51	8.88	1.75	5.06	0.76	4.79	0.69
F-06-1A	amphibolite	Ausable Forks	53.30	111	13.00	52.30	11.40	3.11	11.30	1.98	12.00	2.37	7.11	1.09	6.90	0.97
00-11	amphibolite	Skiff Mountain	71.00	171	21.40	83.10	18.50	4.13	18.10	3.52	22.70	4.43	13.70	2.12	13.30	1.82
H-06-2B	biotite-rich	Hawkeye	257	571	75.20	288	63.00	2.84	37.40	3.43	12.10	1.73	4.70	0.68	4.43	0.68
MR-06-1	amphibolite	Rt 458	55.90	134	17.80	77.40	18.30	4.68	18.00	3.24	19.50	3.73	11.00	1.65	10.50	1.52
Other																
00-09	charnockite	Skiff Mountain	22.60	55.50	7.64	34.50	8.69	9.76	8.92	1.54	9.01	1.77	5.04	0.75	4.87	0.74
HSL-1-06	Hawkeye granite	Hawkeye	13.60	17.20	1.48	4.93	0.76	0.67	0.58	0.09	0.53	0.12	0.41	0.07	0.53	0.09
H-06-1C	Hawkeye granite	Hawkeye	27.20	66.00	9.61	41.80	10.20	2.58	9.75	1.75	10.10	1.93	5.54	0.78	4.78	0.68
H-06-2A	pegmatite	Hawkeye	9.66	11.80	1.09	3.73	0.78	2.81	0.70	0.13	0.80	0.15	0.41	0.06	0.33	0.05
D-06-1B	metasediment	Dannemora	57.40	132	15.90	67.20	15.00	3.11	15.80	2.73	15.70	3.02	8.69	1.21	7.41	1.06
MR-06-2A	granite	Lake Titus	75.00	129	12.50	40.40	6.50	1.95	5.28	0.87	5.02	0.98	2.89	0.43	2.82	0.45
99-6A	diabase dike	Dannemora	50.09	104.27	14.14	57.41	11.82	3.60	11.21	1.70	8.97	1.62	4.52	0.61	3.97	0.56
99-6D	trachyte dike	Dannemora	160.07	296.14	33.28	112.77	20.13	0.94	17.33	2.88	15.59	2.86	8.01	1.30	7.55	1.07

APPENDIX 3

Electron Probe Microanalysis

Feldspars

Electron probe micro analysis was performed on representative feldspars grains from the perthite, microcline, albite, granite and fayalite granites. Physical descriptions and discussion on EPMA data have been presented in Chapter 4 as well as data collection methods. The complete feldspar EPMA data set is presented in appendix Table A3-1 - A3-5. Plagioclase feldspars are typically Ab 92-97 in all samples, but may approach Ab 100 in plagioclase related to partial sodic alteration.

Pyroxene/amphibole/olivine

Pyroxene (and olivine) was analyzed by EPMA in 3 different rocks types from the LMG; the perthite granite (Rutgers Mine, sample 06-4d), the albite granite (Dry Bridge, sample 99-2b), and the fayalite granite (Ausable Forks, sample 99-3a) and is presented in appendix Table A3-6- A3-8. Data from an additional sample of the perthite granite containing amphibole without pyroxene is presented in appendix Table A3-9. Pyroxene compositions and textures are discussed in detail in Chapter 3. Pyroxene compositions in the LMG are aegerine-augite with slightly variable Na and Ca contents between rock types. However, the fayalite granite contains pyroxenes of different composition. These pyroxene grains are hedenbergite with exsolution lamellae of Fe-rich orthopyroxene. In addition to pyroxene the fayalite granite contains fayalite olivine. Amphibole compositions mimic that of the clinopyroxene in that they comprise Ca, Na, Fe, and Mg in various proportions.

Magnetite

Magnetite was analyzed by EPMA in all the different rock types of the LMG as well as two different ore samples. Magnetite compositions are discussed in detail in chapter 3 and the complete data set is presented in appendix Table A3-10- and A3-11. Magnetite compositions are indistinguishable between the ore and LMG except at Palmer Hill. The magnetite at Palmer Hill is enriched in Ti relative to the other LMG and ore samples. Additionally, the fayalite granite contains magnetite with slightly elevated Ti relative to the LMG

Titanite

Titanite from the 3 main rock types of the LMG were analyzed by EPMA. The complete data set is presented in table A3-12. These data are not reported elsewhere as measured weight present totals are not acceptable for publication. However this preliminary data set does provide important information on the geochemistry of titanite in the LMG. Cerium was measured as a proxy for the REE content of titanite. The perthite granite and the albite granite both contain titanite with 1 to 1.5 weight percent Ce (the microcline granite typically has ~0.5 weight percent Ce). This high concentration of Ce may explain the low weight percent totals for titanite analyses in that other REE, especially LREE, may be present but were not measured by EPMA. All titanite grains analyzed contain F, regardless of the rock type.

Garnet

The albite granite at Dry Bridge contains garnet. This was the only LMG rock type observed that contains garnet. Garnet associated with Na alteration in the alteration

halo of some deposits have been reported elsewhere (Hagner and Collins, 1967) These garnet grains at Dry Bridge were analyzed by EPMA but weight percent totals are too low for publication. The measured data is presented appendix Table A3-12. These data suggest that the garnet are andradite in composition as the garnet contain significant Fe and little Al. The distribution of garnet in the alteration of halo of some ore deposits and the association of garnet with Na alteration suggests that the growth of andradite is related to hydrothermal alteration

Table A3-1 Feldspar EPMA analyses from the perthite granite

Element	SiO_2	Al_2O_3	FeO	CaO	Na_2O	K_2O	BaO	Total	Ab	An	Or
Sample											
Clintonville (99-1a)											
Un 21 991a perth grn1											
95	64.75	17.96	0.19	0.03	0.33	15.97	0.00	99.23	3.1	0.1	96.8
Un 22 991a perth grn1a											
96	63.14	20.17	0.01	-0.03	0.85	14.63	0.05	98.83	8.1	0	92
Un 23 991a perth grn1b											
97	67.20	20.86	0.10	1.21	10.69	0.33	-0.09	100.31	92.3	5.8	1.9
Un 24 991a perth grn1c											
98	63.95	19.28	0.02	0.04	0.29	17.26	0.17	101.02	2.5	0.2	97.3
Un 25 991a perth grn1d											
99	67.88	19.91	0.04	0.75	10.72	0.20	0.00	99.40	95.2	3.7	1.1
Un 26 991a perth grn1e											
100	66.10	21.52	0.23	0.86	10.33	0.17	0.00	99.04	94.6	4.3	1
Un 27 991a perth grn2											
101	36.55	12.44	0.25	0.96	9.56	0.06	0.00	59.70	94.3	5.2	0.4
Un 28 991a perth grn2a											
102	34.77	11.52	-0.04	0.00	0.61	14.80	0.15	61.82	5.9	0	94.1
Un 29 991a perth grn2b											
103	66.98	20.03	0.17	0.79	11.25	0.11	0.00	99.24	95.7	3.7	0.6
104	67.47	20.78	0.16	0.76	10.95	0.14	0.23	100.49	95.5	3.7	0.8
Un 30 991a perth grn2c											
105	64.77	18.97	0.01	0.01	0.82	15.73	0.11	100.41	7.3	0	92.6
Un 31 991a perth grn2d											
106	63.72	22.55	0.20	0.96	10.30	0.20	0.00	97.72	93.9	4.9	1.2
107	63.64	22.04	0.05	0.48	5.80	6.89	0.00	98.83	54.8	2.5	42.8
Un 32 991a perth grn2e											
108	65.57	19.24	0.05	0.55	7.49	5.29	0.25	98.44	66.4	2.7	30.9
Un 33 991a perth grn2f											
109	65.68	18.76	0.13	0.05	1.11	15.13	0.00	100.82	10	0.2	89.8
Un 34 991a perth grn2g											
110	66.46	21.20	0.13	0.98	10.81	0.11	0.00	99.42	94.6	4.7	0.7
Un 35 991a perth grn2h											
111	63.80	18.42	0.02	-0.01	0.61	15.94	0.00	98.65	5.5	0	94.6
Un 36 991a perth grn2i											
112	64.78	18.52	0.01	0.01	0.63	16.13	0.00	100.03	5.6	0.1	94.3
Un 37 991a perth grn2j											
113	67.00	20.18	0.33	0.65	9.59	2.56	0.00	100.31	82.4	3.1	14.5
114	65.11	18.59	0.13	-0.01	2.68	13.12	0.04	99.66	23.7	0	76.3
Un 38 991a perth grn2k											
115	67.27	21.39	0.16	1.12	10.73	0.08	0.12	100.87	94.1	5.4	0.5

Table A3-1 Continued

Element	SiO_2	Al_2O_3	FeO	CaO	Na_2O	K_2O	BaO	Total	Ab	An	Or
Sample											
Rutgers (06-4d)											
116	40.50	12.58	0.15	0.19	10.16	0.05	0.11	63.74	98.6	1	0.3
117	40.26	13.48	0.17	0.23	10.22	0.08	0.22	64.66	98.3	1.2	0.5
Un 40 064d perth grn1a											
118	68.76	20.35	0.13	0.18	11.06	0.09	0.00	100.53	98.6	0.9	0.5
119	68.50	20.03	0.11	0.25	11.12	0.10	0.02	100.13	98.2	1.2	0.6
120	68.75	19.81	0.11	0.25	10.68	0.09	0.00	99.60	98.2	1.3	0.6
Un 41 064d perth grn1b											
121	67.41	21.00	0.31	0.98	10.47	0.10	0.00	100.18	94.5	4.9	0.6
Un 42 064d perth grn1c											
122	67.23	20.39	0.06	0.98	10.95	0.12	0.11	99.83	94.7	4.7	0.7
Un 43 064d perth grn1d											
123	65.11	18.47	0.17	0.00	0.35	16.24	0.00	99.99	3.2	0	96.8
Un 44 064d perth grn1e											
124	67.37	20.51	0.19	0.90	10.62	0.09	0.08	99.76	95	4.4	0.6
Un 45 064d perth grn1f											
125	65.76	19.05	0.11	0.00	0.73	15.87	0.30	101.82	6.5	0	93.4
126	65.75	18.67	0.10	0.00	0.81	15.66	0.21	101.19	7.3	0	92.7
Un 46 064d perth grn1g											
127	67.17	19.60	0.29	0.62	8.66	3.68	0.12	100.13	75.8	3	21.2
Un 47 064d perth grn1h											
128	65.67	19.39	0.17	0.00	0.70	16.34	1.06	103.34	6.1	0	93.9
129	65.03	19.15	0.04	-0.02	0.94	15.80	0.00	100.90	8.3	0	91.8
Un 48 064d perth grn1j											
130	67.72	19.86	0.08	0.82	10.80	0.09	0.04	99.41	95.5	4	0.5
Un 49 064d perth grn1k											
131	68.40	19.48	0.23	0.18	11.14	0.05	0.10	99.58	98.8	0.9	0.3
Un 50 064d perth grn2											
132	64.53	20.12	0.18	0.48	11.19	0.07	0.12	96.68	97.3	2.3	0.4
133	68.16	20.28	0.16	0.57	11.12	0.05	0.00	100.30	97	2.8	0.3
134	67.27	20.56	0.14	0.78	11.22	0.13	0.00	100.08	95.6	3.7	0.7
135	68.70	19.96	0.27	0.17	11.04	0.11	0.06	100.31	98.5	0.9	0.6
Un 51 064d perth grn2a											
136	68.45	19.32	0.01	0.25	10.77	0.10	0.04	98.93	98.1	1.3	0.6
Un 52 064d perth grn2b											
137	67.43	20.19	0.16	0.56	10.88	0.07	0.00	99.22	96.9	2.7	0.4
Un 53 064d perth grn2c											
138	64.93	18.77	0.22	0.01	0.50	16.02	0.06	100.52	4.6	0	95.4
Un 54 064d perth grn2d											
139	67.37	19.70	0.18	0.51	11.21	0.10	0.04	99.11	97	2.4	0.6
Un 55 064d perth grn2e											

Table A3-1 Continued

Element			SiO_2	Al_2O_3	FeO	CaO	Na_2O	K_2O	BaO	Total	Ab	An	Or
Sample													
		140	68.53	20.68	0.14	0.51	11.13	0.12	0.05	101.17	96.9	2.5	0.7
		141	68.10	19.19	0.17	0.39	11.09	0.05	0.00	98.90	97.8	1.9	0.3
Un	56	064d perth grn2f											
		142	66.81	20.72	0.50	0.58	10.56	0.12	0.05	99.35	96.3	2.9	0.7
Un	57	064d perth grn2g											
		143	64.87	18.38	0.08	0.00	0.53	16.16	0.15	100.17	4.8	0	95.2
Un	86	064d perth trans grn1											
		217	68.17	20.01	0.27	0.50	11.00	0.13	0.06	100.14	96.9	2.4	0.7
		219	68.21	20.28	0.20	0.56	10.92	0.09	0.00	100.25	96.7	2.8	0.5
		220	64.86	18.54	-0.02	-0.01	0.64	16.03	0.18	100.23	5.7	0	94.3
		221	67.08	20.01	0.24	0.44	11.05	0.11	0.00	98.92	97.2	2.1	0.6
		222	66.83	20.09	0.17	0.20	11.11	0.09	0.00	98.35	98.5	1	0.5
		223	64.05	19.18	0.06	0.01	0.62	15.62	0.27	99.82	5.7	0	94.2
		224	67.60	19.55	0.16	0.49	11.16	0.09	0.00	99.05	97.1	2.4	0.5
		226	64.59	18.90	0.14	0.00	0.69	16.36	0.00	100.67	6	0	94
		227	66.81	20.02	0.09	0.76	10.79	0.10	0.00	98.54	95.7	3.7	0.6
		228	66.10	19.96	0.21	0.70	10.73	0.10	0.06	97.86	95.9	3.4	0.6
Un	87	064d perth trans grn2											
		229	65.20	18.63	0.26	0.00	0.69	16.49	0.09	101.37	6	0	94
		230	67.89	20.16	0.11	0.76	10.87	0.09	-0.24	99.66	95.7	3.7	0.6
		231	65.33	18.67	0.13	-0.05	0.64	16.27	0.30	101.28	5.6	0	94.6
		232	64.91	18.83	0.17	-0.01	0.65	15.87	0.06	100.48	5.9	0	94.2
		233	67.68	20.11	0.02	0.62	10.93	0.16	0.03	99.55	96.1	3	0.9
		234	65.22	18.94	0.11	0.01	0.75	15.98	0.15	101.17	6.7	0.1	93.3
Un	88	064d perth single pt											
		235	68.06	19.93	0.19	0.45	11.13	0.06	0.09	99.90	97.5	2.2	0.3
Un	89	064d ab around mt 1-1											
		236	67.31	20.58	0.21	1.03	10.64	0.11	0.00	99.85	94.3	5.1	0.6
Un	90	064d ab around mt 1-2											
		237	67.15	20.00	0.09	0.89	11.05	0.14	-0.12	99.21	95	4.2	0.8
Un	91	064d ab around mt 1-3											
		238	67.76	19.67	0.17	0.27	10.86	0.08	0.00	98.51	98.2	1.4	0.5
Un	92	064d ab around mt 1-4											
		239	67.16	19.96	0.53	0.37	10.66	0.23	0.06	98.98	96.8	1.8	1.4
		240	67.93	20.12	0.03	0.47	11.00	0.16	0.09	99.79	96.8	2.3	0.9

Table A3-2 Feldspar EPMA analyses from the microcline granite

Element		SiO_2	Al_2O_3	FeO	CaO	Na_2O	K_2O	BaO	Total	Ab	An	Or
Sample												
Dannemora (99-6c)												
Un	7 996c grn 1 kfs											
	54	65.34	19.14	0.02	0.00	1.04	14.92	0.26	100.70	9.60	0.00	90.60
	55	65.16	19.71	0.14	0.02	1.72	14.63	0.38	101.75	15.10	0.10	84.80
	56	64.49	19.10	0.02	0.00	1.03	14.86	0.84	100.33	9.50	0.00	90.50
Un	8 996c grn 2 kfs											
	57	65.47	18.39	0.12	0.00	1.12	15.46	0.25	100.80	9.90	0.00	90.10
	58	66.09	19.62	0.05	0.01	0.97	15.73	1.43	103.90	8.60	0.00	91.40
	59	64.95	19.41	0.07	0.00	1.17	15.56	0.21	101.34	10.30	0.00	89.90
Un	9 996c grn 3 kfs											
	60	65.68	19.16	0.03	0.00	0.74	15.37	0.40	101.32	6.80	0.00	93.40
	61	64.63	19.32	-0.04	0.00	1.06	15.07	0.88	100.93	9.70	0.00	90.30
	62	65.20	18.86	-0.03	0.00	0.80	15.74	0.16	100.72	7.20	0.00	92.80
Un	10 996c grn 4 kfs											
	63	65.62	18.73	0.03	0.00	1.00	15.03	0.33	100.70	9.20	0.00	91.00
	64	64.86	18.72	0.04	0.01	1.67	14.77	0.53	100.60	14.60	0.00	85.30
	65	65.41	19.20	0.09	0.01	1.27	15.05	0.91	101.94	11.40	0.00	88.60
Un	11 996c grn 5 kfs											
	66	65.08	19.03	0.04	0.00	1.06	15.67	0.57	101.45	9.30	0.00	90.70
	67	65.40	19.12	0.09	0.00	0.99	15.10	0.60	101.31	9.00	0.00	91.00
	68	65.19	19.87	0.02	0.01	1.11	15.03	0.77	102.01	10.10	0.10	89.80
Un	12 996c grn 6 kfs											
	69	65.15	18.93	0.00	0.00	1.53	14.20	0.55	100.37	14.10	0.00	86.00
	70	65.71	18.85	0.05	0.02	1.33	14.59	0.59	101.13	12.10	0.10	87.80
	71	64.85	19.28	0.05	0.01	0.91	15.50	0.80	101.40	8.20	0.00	91.70
Un	13 996c grn 7 kfs											
	72	65.41	18.95	-0.01	0.00	1.14	15.53	0.38	101.41	10.10	0.00	89.90
	73	65.32	18.83	0.10	0.04	0.98	15.38	0.67	101.32	8.80	0.20	91.00
	74	65.50	19.34	0.01	0.00	0.79	16.26	1.42	103.32	6.90	0.00	93.20
Un	14 996c grn 8 kfs											
	75	62.56	20.12	0.02	0.00	1.12	14.33	0.81	98.96	10.70	0.00	89.40
	76	65.16	19.41	0.04	0.02	1.14	15.88	0.59	102.24	9.80	0.10	90.10
	77	64.67	18.98	0.07	0.04	1.04	15.02	0.47	100.29	9.50	0.20	90.30
Un	15 996c grn 9 kfs											
	78	65.38	19.01	0.06	0.01	1.62	14.86	1.07	102.01	14.20	0.00	85.80
	79	64.46	19.31	0.07	0.01	1.13	15.15	0.62	100.75	10.20	0.00	89.70
	80	64.78	19.01	0.00	0.00	0.46	15.07	1.01	100.32	4.50	0.00	95.60

Table A3-2 Continued

Element	SiO_2	Al_2O_3	FeO	CaO	Na_2O	K_2O	BaO	Total	Ab	An	Or
Sample											
Un 83 996c mc trans grn1 st											
183	64.21	19.15	0.00	0.02	0.70	15.80	0.96	100.83	6.30	0.10	93.60
184	64.93	18.86	0.00	0.04	0.89	15.66	0.60	100.97	7.90	0.20	91.90
185	64.61	19.12	0.00	0.00	1.38	15.09	0.51	100.67	12.20	0.00	87.90
186	64.69	18.98	0.10	0.02	1.13	15.46	0.51	100.88	10.00	0.10	90.00
187	64.69	19.01	0.03	0.01	1.06	15.20	0.69	100.69	9.60	0.10	90.40
188	64.48	18.65	0.04	0.03	0.46	15.60	0.60	99.85	4.30	0.20	95.50
189	64.48	18.84	0.05	0.00	0.96	15.85	0.66	100.84	8.40	0.00	91.60
190	65.11	19.02	0.12	0.06	1.03	15.53	0.60	101.47	9.10	0.30	90.60
191	65.15	19.23	0.09	0.01	1.34	15.07	0.78	101.66	11.90	0.00	88.10
192	64.30	19.03	0.03	0.00	1.00	15.48	0.63	100.45	8.90	0.00	91.10
193	64.43	18.82	0.02	0.00	1.34	14.85	0.33	99.77	12.00	0.00	88.10
194	0.00	19.26	0.04	0.00	0.89	14.64	0.57	35.23	8.50	0.00	91.70
195	64.60	18.66	0.04	0.00	0.86	16.07	0.42	100.60	7.50	0.00	92.10
196	65.33	19.04	0.07	0.00	1.57	14.54	0.75	101.31	14.10	0.00	85.90
197	65.08	19.01	0.08	0.00	1.23	15.38	0.75	101.50	10.80	0.00	89.30
Un 84 996c mc trans grn2											
198	64.84	18.84	0.10	0.01	0.87	15.58	0.75	100.99	7.80	0.00	92.10
199	65.24	19.34	0.02	0.00	1.47	15.24	0.45	101.74	12.80	0.00	87.30
200	64.68	19.09	0.14	0.01	0.86	15.83	0.66	101.28	7.60	0.10	92.30
201	64.36	19.14	0.08	0.07	1.05	15.91	0.51	101.11	9.10	0.30	90.60
202	64.87	19.08	0.07	0.00	0.84	15.74	0.33	100.89	7.50	0.00	92.70
203	64.45	19.21	0.08	0.00	1.19	15.60	0.60	101.11	10.40	0.00	89.70
205	64.45	19.15	0.08	0.00	1.04	15.79	0.36	100.84	9.10	0.00	91.00
206	63.57	19.46	0.32	0.00	1.22	14.93	0.60	100.08	1.10	0.00	89.00
207	64.96	19.27	0.05	0.04	1.29	15.10	0.63	101.34	11.50	0.20	88.30
208	64.99	19.17	0.00	0.03	1.52	14.80	0.84	101.31	13.50	0.10	86.40
209	77.18	22.95	0.10	0.15	0.33	19.28	0.68	120.65	2.50	0.60	96.90
210	64.11	18.90	0.04	0.02	1.19	15.27	0.24	99.77	10.60	0.10	89.30
211	64.75	18.86	0.03	0.00	1.12	15.64	0.87	101.28	9.80	0.00	90.20
212	64.98	19.40	0.00	0.08	1.69	14.58	0.66	101.33	14.90	0.40	84.70

Table A3-3 Feldspar EPMA analyses from the albite granite

Element	SiO_2	Al_2O_3	FeO	CaO	Na_2O	K_2O	BaO	Total	Ab	An	Or
Sample											
Dry Bridge (99-2b)											
Un 16 992b ab test											
81	60.08	18.14	2.11	1.01	8.24	0.11	0.12	89.82	92.90	6.30	0.80
82	67.47	20.55	0.30	0.98	10.55	0.07	0.00	99.79	94.70	4.90	0.40
Un 17 992b ab grn1											
83	66.49	20.37	0.17	1.10	10.68	0.07	0.16	99.04	94.20	5.30	0.40
84	67.59	20.39	0.12	0.99	11.25	0.04	0.44	100.83	95.10	4.60	0.20
85	66.71	20.83	0.21	1.05	10.45	0.11	0.00	99.27	94.10	5.20	0.70
Un 18 992b ab grn2											
86	67.31	20.23	0.33	0.98	11.17	0.10	0.00	99.98	94.80	4.60	0.60
87	66.82	20.56	0.33	1.03	10.36	0.14	0.07	99.31	94.00	5.20	0.80
88	66.83	20.10	0.22	0.92	10.31	0.14	0.00	98.42	94.50	4.70	0.80
Un 19 992b ab grn3											
89	102.00	0.03	-0.02	0.03	0.02	0.06	0.08	102.20	94.30	5.10	0.60
90	100.96	0.11	0.03	0.01	0.01	0.00	0.00	100.77	95.00	4.20	0.80
91	99.72	0.90	0.03	0.03	0.04	0.03	0.00	100.70	98.20	1.40	0.50
Un 20 992b ab grn4											
92	67.60	20.88	0.11	0.86	10.46	0.16	0.00	99.98	94.70	4.30	1.00
93	67.08	20.56	0.12	0.90	10.92	0.15	0.00	99.62	94.80	4.30	0.90
94	67.43	20.76	0.18	0.90	10.94	0.12	0.03	100.36	95.00	4.30	0.70
Un 93 99-2b ab day2 grn1											
241	66.76	19.95	0.20	1.04	10.59	0.15	0.00	98.39	94.00	5.10	0.90
242	67.28	20.42	0.29	0.94	10.68	0.14	0.00	99.75	94.60	4.60	0.80
Un 95 99-2b ab day2 grn3											
244	67.51	20.08	0.08	0.91	10.82	0.13	0.06	99.58	94.80	4.40	0.70

Table A3-4 Feldspar EPMA analyses from the fayalite granite

Element	SiO_2	Al_2O_3	FeO	CaO	Na_2O	K_2O	BaO	Total	Ab	An	Or
Sample											
Ausable Forks (99-3a)											
Un 3 993a fld grn 1											
41	67.90	19.99	0.13	0.11	10.96	0.07	0.13	99.29	99.00	0.60	0.40
42	67.65	19.96	0.16	0.09	11.45	0.03	0.00	99.00	99.40	0.40	0.20
43	68.88	20.21	0.17	0.08	11.25	0.02	0.00	100.52	99.50	0.40	0.10
Un 4 993a fld grn 1-kfs											
44	65.48	18.85	0.10	0.00	0.97	15.37	0.00	100.67	8.70	0.00	91.30
45	65.57	18.78	0.11	0.00	0.90	15.51	0.20	101.07	8.10	0.00	91.90
46	65.67	18.70	0.11	0.03	1.00	16.06	0.17	101.73	8.60	0.10	91.20
47	65.62	18.98	0.02	0.00	1.06	15.45	0.37	101.49	9.50	0.00	90.60
Un 5 993a fld grn 2-kfs											
48	65.20	19.14	0.10	0.02	0.96	15.42	0.00	100.72	8.60	0.10	91.30
49	64.70	18.40	0.15	0.00	0.72	16.24	0.00	100.17	6.40	0.00	93.70
50	64.57	18.75	0.65	0.07	1.06	15.28	0.25	100.62	9.50	0.40	90.20
Un 6 993a fld grn 2-ab											
51	67.75	20.24	0.34	0.14	11.28	0.06	0.08	99.90	99.00	0.70	0.40
52	68.71	19.85	0.31	0.13	11.05	0.07	0.00	99.93	98.90	0.60	0.40
53	69.04	19.63	0.27	0.08	11.63	0.27	0.08	100.99	98.10	0.40	1.50

Table A3-5 Feldspar EPMA analyses from mixed alteration granite

Element / Sample	SiO_2	Al_2O_3	FeO	CaO	Na_2O	K_2O	BaO	Total	Ab	An	Or
Palmer Hill (99-4b)											
Un 58 994b fld grn1											
144	65.60	18.99	0.20	0.00	0.36	17.37	0.00	102.39	3.10	0.00	96.90
Un 59 994b fld grn1a											
145	65.65	19.13	0.18	0.00	0.46	16.39	0.34	102.15	4.10	0.00	96.00
146	65.57	19.31	0.21	0.00	0.47	16.50	0.09	102.13	4.20	0.00	95.90
Un 60 994b fld grn test											
147	65.09	18.83	0.30	0.00	0.40	16.46	0.12	101.18	3.50	0.00	96.60
Un 61 994b fld ab test											
148	68.14	19.95	0.31	0.10	11.77	0.06	0.00	100.28	99.20	0.50	0.40
Un 62 994b fld perth grn1											
149	68.02	20.06	0.30	0.11	11.36	0.11	0.10	100.06	98.80	0.50	0.60
Un 63 994b fld perth grn1a											
150	65.34	18.55	0.13	0.00	0.56	16.40	0.00	100.93	4.90	0.00	95.10
Un 64 994b fld perth grn1b											
151	68.49	20.13	0.25	0.03	11.58	0.11	0.00	100.53	99.20	0.20	0.60
Un 65 994b fld perth grn1c											
152	65.09	18.67	0.32	0.00	0.53	16.40	0.48	101.48	4.70	0.00	95.30
153	64.80	18.59	0.19	0.02	0.46	16.19	0.30	100.55	4.10	0.10	95.80
Un 66 994b fld perth grn1d											
154	67.69	19.86	0.23	0.88	10.47	0.19	0.41	99.72	94.50	4.40	1.10
Un 67 994b fld perth grn1e											
155	67.34	20.76	0.22	0.67	10.59	0.13	0.00	99.61	95.90	3.40	0.80
Un 68 994b fld perth grn2											
156	61.71	20.36	0.32	0.12	10.89	0.08	0.03	93.52	98.90	0.60	0.50
157	66.25	20.86	0.54	0.09	10.85	0.09	0.00	98.46	99.00	0.50	0.50
Un 69 994b fld perth grn2a											
158	68.40	20.36	0.32	0.05	11.64	0.07	0.37	101.21	99.40	0.20	0.40
159	69.12	19.74	0.23	0.06	11.56	0.07	0.05	100.83	99.30	0.30	0.40
Un 70 994b fld perth grn2b											
160	65.17	19.02	0.22	0.00	0.38	16.16	0.25	101.20	3.50		96.50
161	65.45	18.82	0.20	0.00	0.47	17.00	0.06	101.99	4.00	0.00	96.10
Un 71 994b fld perth grn2c											
162	68.21	19.89	0.32	0.02	11.67	0.06	0.00	100.14	99.60	0.10	0.30
Un 72 994b fld perth grn2d											
163	65.56	18.87	0.28	0.00	0.54	16.08	0.14	101.45	4.90		95.20
164	65.50	18.53	0.25	0.00	0.55	16.47	0.32	101.60	4.80	0.00	95.30
Un 73 994b fld perth grn2e											
165	69.30	19.96	0.14	0.05	11.55	0.09	0.00	101.05	99.30	0.20	0.50

Table A3-6 Clinopyroxene EPMA analyses from the perthite granite

Element	SiO_2	TiO_2	Al_2O_3	FeO[a]	MnO	MgO	CaO	Na_2O	K_2O	CrO	Total
Sample											
Rutgers (06-4d)											
Un 60 06-4d cpx grn1											
118	51.34	0.19	1.58	13.12	0.20	9.86	20.20	2.40	0.02	0.02	98.95
Un 61 06-4d cpx grn1-2											
119	51.70	0.18	1.62	13.29	0.22	9.81	20.13	2.54	0.00	0.00	99.42
Un 62 06-4d cpx grn1-3											
120	52.13	0.18	1.70	13.37	0.18	9.70	20.06	2.50	0.01	0.00	99.84
Un 63 06-4d cpx grn1-4											
121	51.85	0.26	1.67	13.42	0.14	9.79	20.53	2.30	0.01	0.00	99.93
Un 64 06-4d cpx grn2-1											
122	52.05	0.24	1.68	13.67	0.18	9.86	20.15	2.40	0.02	0.00	100.22
Un 65 06-4d cpx grn2-2											
123	51.70	0.16	1.63	13.49	0.19	9.92	20.50	2.34	0.00	0.01	99.93
Un 66 06-4d cpx grn2-3											
124	51.37	0.23	1.65	13.22	0.18	9.85	20.31	2.44	0.02	0.00	99.27
Un 67 06-4d cpx grn2-4											
125	51.99	0.20	1.66	13.19	0.15	9.66	20.45	2.37	0.01	0.03	99.71

Table A3-7 Clinopyroxene EPMA analyses from the albite granite

Element	SiO_2	TiO_2	Al_2O_3	FeO[a]	MnO	MgO	CaO	Na_2O	K_2O	CrO	Total
Sample											
Dry Bridge (99-2b)											
Un 47 992b cpx grn1-1											
102	50.09	0.13	1.73	22.23	0.28	4.20	16.56	4.00	0.02	0.00	99.22
103	50.33	0.07	1.66	22.02	0.33	4.30	16.59	4.12	0.03	0.04	99.50
104	49.53	0.07	1.72	22.00	0.20	4.20	16.76	4.14	0.01	0.01	98.63
Un 48 992b cpx grn1-2											
105	49.47	0.00	1.74	22.00	0.26	4.31	16.89	4.14	0.00	0.00	98.77
Un 49 992b cpx grn1-3											
106	50.11	0.10	1.76	22.23	0.23	4.34	16.82	4.03	0.02	0.02	99.66
Un 50 992b cpx grn1-4											
107	49.95	0.14	1.71	22.16	0.18	4.20	16.90	3.95	0.00	0.01	99.20
Un 51 992b cpx grn1-5											
108	49.84	0.11	1.74	21.96	0.28	4.23	16.87	4.02	0.04	0.00	99.09
Un 52 992b cpx grn2-1											
109	49.69	0.12	1.81	21.98	0.25	4.23	16.68	4.18	0.01	0.00	98.94
Un 53 992b cpx grn2-2											
110	49.44	0.09	1.66	22.21	0.30	4.14	16.52	3.91	-0.01	0.00	98.25
Un 54 992b cpx grn3-1											
111	50.10	0.06	1.79	22.34	0.34	4.30	16.59	4.23	0.00	0.00	99.70
Un 55 992b cpx grn3-2											
112	50.06	0.07	1.70	21.53	0.21	4.44	16.70	4.04	0.00	0.04	98.80

Table A3-8 Clinopyroxene and olivine EPMA analyses from the fayalite granite

Element / Sample	SiO_2	TiO_2	Al_2O_3	FeO^a	MnO	MgO	CaO	Na_2O	K_2O	CrO	Total
Ausable Forks (99-3a)											
Un 5 993a cpx test											
44	47.54	0.24	0.64	28.57	0.87	0.28	18.48	1.89	0.09	0.02	98.61
45	47.70	0.22	0.70	30.68	0.97	0.24	17.64	1.50	0.01	0.05	99.70
46	48.30	0.24	0.64	28.74	0.94	0.25	18.64	1.72	0.01	0.00	99.48
Un 6 993a cpx test2											
47	47.94	0.24	0.78	29.82	0.85	0.28	18.32	1.65	0.00	0.02	99.88
Un 7 993a cpx test2a											
48	47.83	0.20	0.62	29.44	0.94	0.26	18.37	1.49	0.02	0.03	99.22
Un 8 993a cpx test2b											
49	48.00	0.16	0.64	29.07	0.73	0.27	18.53	1.51	0.02	0.00	98.94
Un 9 993a cpx grain2											
50	45.75	0.23	0.65	28.36	0.81	0.26	18.28	1.60	0.04	0.02	96.02
Un 12 cpx grn2 a											
70	41.19	0.24	0.69	26.61	0.82	0.27	17.25	1.58	0.00	0.00	88.65
Un 17 cpx grn2 a											
71	41.00	0.24	0.55	27.93	0.87	0.11	16.70	1.32	0.02	0.02	88.77
Un 18 cpx grn2 b											
72	39.60	0.06	0.30	44.56	1.62	0.30	3.87	0.28	0.02	0.04	90.65
Un 19 cpx grn2 c											
73	39.86	0.16	0.64	28.86	0.83	0.25	15.28	1.33	0.05	0.03	87.28
Un 20 cpx grn2 d											
74	40.15	0.22	0.66	26.95	0.83	0.10	17.44	1.59	0.01	0.01	87.96
Un 22 cpx grn2 a											
76	48.45	0.19	0.61	30.61	0.82	0.31	18.03	1.47	0.01	-0.06	100.43
Un 23 cpx grn2 b											
77	46.40	0.17	0.62	40.62	1.29	0.26	9.75	0.84	0.10	-0.01	100.03
Un 24 cpx grn2 c											
78	46.99	0.21	0.72	32.27	0.98	0.28	15.92	1.34	0.01	0.02	98.73
Un 25 cpx grn2 d											
79	47.76	0.28	0.68	29.23	0.84	0.29	18.50	1.46	0.00	0.05	99.09
Un 26 cpx grn2 e											
80	48.37	0.27	0.73	31.33	0.90	0.25	17.27	1.47	0.00	0.00	100.59
Un 27 cpx grn2 f											
81	46.23	0.24	0.41	43.65	1.40	0.29	8.07	0.14	0.00	0.00	100.40
Un 28 cpx grn2 g											
82	47.80	0.18	0.70	29.34	0.87	0.28	18.65	1.63	0.01	0.00	99.46
Un 29 cpx grn2 h											
83	48.07	0.21	0.62	29.80	1.00	0.09	18.43	1.52	0.01	0.02	99.78
Un 30 cpx grn2 i											
84	48.06	0.16	0.64	29.38	0.82	0.28	18.58	1.68	0.02	0.01	99.64
Un 31 cpx grn2 j											

85	47.57	0.22	0.71	29.87	0.87	0.24	17.96	1.56	0.01	0.00	98.98

Table A3-8 Continued

Element	SiO_2	TiO_2	Al_2O_3	FeO^a	MnO	MgO	CaO	Na_2O	K_2O	CrO	Total
Sample											
Un 32 cpx grn2 k											
86	47.69	0.14	0.59	30.30	0.87	0.27	18.21	1.43	0.02	0.00	99.52
Un 33 cpx grn3-1											
87	47.95	0.23	0.69	30.05	0.88	0.26	18.20	1.64	0.01	0.00	99.88
Un 34 cpx grn3-2											
88	45.75	0.14	0.11	52.14	1.92	0.30	0.46	0.06	0.02	0.00	100.87
Un 35 cpx grn3-3											
89	48.36	0.23	0.72	29.35	0.87	0.26	18.40	1.55	0.01	0.03	99.78
Un 36 cpx grn3-4											
90	45.42	0.14	0.12	51.38	1.98	0.29	0.46	0.06	0.02	0.01	99.90
Un 37 cpx grn3-5											
91	47.81	0.28	0.71	30.41	0.93	0.28	18.00	1.66	0.04	0.00	100.12
Un 38 cpx grn3-6											
92	47.64	0.22	0.68	29.90	0.84	0.23	18.25	1.68	0.03	0.00	99.47
Un 39 ol grn1-1											
93	29.03	-0.01	0.02	68.02	2.07	0.20	0.06	0.02	0.04	0.02	99.48
Un 40 ol grn1-2											
94	29.36	0.04	0.15	67.93	2.05	0.22	0.05	0.07	0.00	-0.05	99.83
Un 41 ol grn1-3											
95	35.46	0.00	0.06	83.13	2.63	0.27	0.09	0.06	0.04	0.00	121.73
Un 42 cpx grn1-4											
96	47.53	0.14	0.62	32.13	0.94	0.33	16.36	1.46	0.02	0.00	99.48
Un 43 cpx grn1-5											
97	47.65	0.15	0.68	29.30	0.86	0.39	18.26	1.60	0.04	0.00	98.87
98	47.70	0.14	0.63	29.34	0.87	0.43	18.01	1.64	0.04	0.00	98.80
Un 44 cpx grn1-6											
99	48.23	0.14	0.65	29.87	0.81	0.38	18.38	1.54	0.00	0.00	99.99
Un 45 ol grn1-7											
100	36.12	-0.02	0.03	83.98	2.62	0.20	0.05	0.09	0.00	0.00	123.04
Un 46 ol grn1-8											
101	29.29	0.03	0.02	69.09	2.02	0.20	0.04	0.11	0.02	0.01	100.81

Table A3-9 Amphibole EPMA analyses from the perthite granite

Element	SiO_2	TiO_2	Al_2O_3	FeO^a	MnO	MgO	CaO	Na_2O	K_2O	Cr_2O_3	Total
Sample											
Clintonville (99-1a)											
Un 68 991a amph grn1-1											
126	44.31	1.07	7.56	16.60	0.05	11.64	10.67	2.48	1.54	0.00	95.92
Un 69 991a amph grn1-2											
127	44.65	1.15	7.49	16.80	0.11	11.47	10.66	2.46	1.48	0.01	96.29
Un 70 991a amph grn2-1											
128	45.40	1.10	7.20	16.59	0.07	11.97	11.01	2.14	1.49	0.05	97.01
Un 71 991a amph grn2-2											
129	45.18	0.86	7.18	16.21	0.18	12.32	11.53	1.65	1.44	0.00	96.54

Table A3-10 Magnetite EPMA analyses from the Lyon Mountain granite

Element	SiO_2	TiO_2	Al_2O_3	Fe_3O_4	MgO	MnO	CaO	Cr_2O_3	V_2O_3	ZnO	Total
Sample											
Rutgers (06-4d)(perthite granite)											
Un 16 064d mt test											
75	0.05	0.00	0.13	100.06	0.03	0.06	0.02	0.01	0.09	0.00	100.42
Un 17 064d mt grn1											
76	0.05	0.03	0.17	99.62	0.04	0.00	0.02	0.00	0.04	0.00	99.90
77	0.01	0.01	0.30	99.69	0.05	0.29	0.00	0.00	0.05	0.00	100.39
Un 18 064d mt grn2											
78	0.05	0.00	0.18	99.62	0.02	0.19	0.00	0.01	0.05	0.08	100.20
Un 19 064d mt grn3											
79	0.03	0.00	0.18	98.53	-0.01	0.21	0.00	0.00	0.08	0.00	99.01
Un 20 064d mt grn4											
80	0.06	0.03	0.17	97.94	0.04	0.00	0.00	0.02	0.09	0.01	98.04
81	0.03	0.04	0.21	99.13	-0.01	0.15	0.02	0.03	0.06	0.00	99.64
Clintonville (99-1a)(perthite granite)											
Un 21 991a mt test											
82	0.34	0.06	0.42	96.61	0.06	0.00	0.00	0.03	0.09	0.00	97.51
83	0.09	0.01	0.19	97.24	0.03	0.00	0.00	0.02	0.07	0.00	97.48
Un 22 991a mt grn1											
84	0.12	0.57	0.16	99.56	0.01	0.00	0.01	0.02	0.04	0.02	100.50
85	0.99	0.05	0.37	95.12	0.03	0.00	0.02	0.02	0.04	0.02	96.62
Un 23 991a mt grn2											
86	0.10	0.00	0.19	98.50	0.00	-0.14	0.02	0.00	0.03	0.02	98.67
87	0.09	0.05	0.21	99.99	0.08	0.22	0.00	0.00	0.03	0.00	100.66
Un 24 991a mt grn3											
88	2.67	0.00	0.00	0.04	0.00	0.02	46.06	0.00	0.00	0.00	48.69
89	3.77	0.01	0.02	0.06	0.00	0.00	46.66	0.01	0.01	0.00	50.14
Un 25 991a mt grn4											
90	0.10	0.02	0.14	99.34	0.01	0.00	0.01	0.00	0.00	0.01	99.55
Un 26 991a mt grn5											
91	0.12	0.01	0.18	98.55	0.00	0.04	0.00	0.00	0.05	0.00	98.87
Un 27 991a mt grn6											
92	0.10	0.12	0.34	98.01	0.06	0.10	0.00	0.00	0.12	0.01	98.85
93	0.10	0.13	0.22	100.12	0.02	0.11	0.01	0.00	0.02	0.02	100.73
Dannemora (99-6c)(microcline granite)											
Un 13 996c mt grn1											
71	0.05	0.06	0.15	99.39	0.00	0.00	0.00	0.02	0.03	0.02	99.64
Un 14 996c mt grn2											
72	0.02	0.07	0.44	101.19	0.00	0.00	0.00	0.01	0.00	0.00	101.39
Un 15 996c mt grn3											
73	0.02	0.05	0.20	99.09	0.00	0.00	0.01	0.02	0.01	0.04	99.27
mt grn 4 (2nd Un 15 pt)											
74	0.07	0.04	0.34	100.36	0.08	0.17	0.02	0.01	0.03	0.02	101.15

Table A3-10 Magnetite EPMA analyses from the Lyon Mountain granite

Element	SiO_2	TiO_2	Al_2O_3	Fe_3O_4	MgO	MnO	CaO	Cr_2O_3	V_2O_3	ZnO	Total
Sample											
Palmer Hill (99-4b)(mixed granite)											
Un 11 994b mt grn1											
65	0.03	10.99	0.07	82.09	0.00	0.25	0.01	0.01	0.01	0.04	93.48
66	0.07	11.18	0.07	84.82	0.00	0.32	0.00	0.00	0.00	0.00	96.41
Un 12 994b mt grn test											
67	0.10	8.49	0.06	88.78	0.04	0.00	0.01	0.02	0.02	0.00	97.18
68	0.08	9.03	0.13	87.75	0.04	0.12	0.01	0.00	0.03	0.00	97.17
69	0.01	0.00	0.12	99.19	0.01	0.12	0.02	0.01	0.01	0.01	99.46
70	0.03	8.50	0.08	88.21	0.13	0.00	0.00	0.02	0.00	0.00	96.90
Ausable forks (99-3a)(fayalite granite)											
Un 28 993a mt grn1											
94	0.16	1.86	0.27	98.57	0.00	0.11	0.01	0.00	0.01	0.15	101.07
Un 29 993a mt grn1a											
95	0.18	2.59	0.44	96.08	0.00	0.24	0.01	0.02	0.00	0.28	99.77
Un 30 993a mt grn2											
96	0.12	2.01	0.20	98.08	0.03	0.45	0.00	0.03	0.00	0.09	101.02
97	0.14	1.95	0.29	97.82	0.06	0.01	0.00	0.01	0.02	0.18	100.45
Un 31 993a mt grn2a											
98	0.15	1.11	0.36	98.97	0.00	0.30	0.00	0.00	0.05	0.19	101.11
99	0.13	1.27	0.31	98.67	0.00	-0.03	0.01	0.00	0.01	0.13	100.47
100	0.22	1.09	0.78	97.95	0.03	0.14	0.00	0.01	0.01	0.25	100.48
Un 32 993a mt grn3											
101	0.15	1.93	0.36	98.09	0.05	0.00	0.01	0.00	0.00	0.25	100.73
Un 33 993a mt grn4											
102	0.19	1.54	0.34	98.53	0.00	0.25	0.00	0.01	0.01	0.03	100.85
Un 34 993a mt grn4a											
103	0.18	2.66	0.41	95.94	0.02	0.18	0.00	0.00	0.00	0.12	99.51

Table A3-11 Magnetite EPMA analyses from Lyon Mountain ore bodies

Element	SiO_2	TiO_2	Al_2O_3	Fe_3O_4	MgO	MnO	CaO	Cr_2O_3	V_2O_3	ZnO	Total
Sample											
Palmer Hill (99-4a)											
Un 4 994a mt test											
45	0.03	0.04	0.14	98.94	0.00	0.04	0.00	0.02	0.01	0.00	99.16
46	0.06	0.03	0.10	99.76	0.05	0.00	0.00	0.04	0.03	0.01	100.02
47	0.05	0.03	0.16	101.00	0.03	0.00	0.00	0.00	0.04	0.00	101.18
Un 5 994a hem grn1											
48	0.05	0.02	0.12	96.76	0.06	0.00	0.00	0.01	0.02	0.00	96.64
49	0.04	0.51	0.13	95.92	0.09	0.34	0.00	0.00	0.00	0.00	97.00
Un 6 mt grn 2											
50	0.06	0.01	0.09	100.90	0.00	0.28	0.00	0.01	0.00	0.03	101.31
51	0.05	0.03	0.23	100.54	0.03	0.28	0.00	0.00	0.01	0.00	101.15
52	0.08	0.01	0.14	99.87	0.00	0.07	0.00	0.00	0.01	0.03	100.18
Un 7 mt grn 3											
53	0.09	0.00	0.19	99.92	0.10	0.07	0.00	0.00	0.03	0.00	100.33
54	0.07	0.03	0.09	101.08	0.00	0.02	0.01	0.00	0.01	0.02	101.32
55	0.08	0.03	0.13	100.02	0.00	0.00	0.00	0.01	0.00	0.01	100.11
Un 8 mt grn 4											
56	0.06	0.06	0.10	100.91	0.03	0.00	0.00	0.00	0.00	0.00	101.01
57	0.04	0.02	0.12	100.48	0.00	0.26	0.00	0.00	0.01	0.03	100.90
58	0.02	0.00	0.12	100.21	0.05	0.60	0.00	0.01	0.00	0.02	101.02
Un 9 mt grn 5											
59	0.05	0.01	0.30	100.53	0.04	0.00	0.00	0.00	0.00	0.00	100.79
60	0.05	0.02	0.08	99.58	0.04	0.00	0.01	0.00	0.00	0.03	99.69
61	0.02	0.03	0.08	100.45	0.07	0.00	0.02	0.00	0.03	0.01	100.60
Un 10 mt grn 6											
62	0.03	0.01	0.13	100.23	0.05	0.19	0.01	0.01	0.00	0.01	100.66
63	0.10	0.01	0.28	99.22	0.08	0.00	0.00	0.02	0.01	0.00	99.52
64	0.03	0.01	0.12	100.74	0.03	0.00	0.00	0.00	0.01	0.02	100.48
Skiff Mountain (00-01)											
Un 35 0001 mt grn1											
104	0.06	0.52	0.18	99.54	0.07	0.00	0.00	0.00	0.00	0.05	100.28
105	0.06	0.53	0.21	100.53	0.03	0.02	0.00	0.00	0.04	0.00	101.38
106	0.06	0.49	0.18	99.83	0.00	0.12	0.00	0.00	0.02	0.00	100.66
Un 36 0001 mt grn2											
107	0.04	0.49	0.21	100.16	0.09	0.00	0.01	0.02	-0.03	0.00	100.84
Un 37 0001 mt grn2a											
108	0.09	0.50	0.17	99.61	0.07	0.07	0.00	0.01	0.00	0.03	100.56
Un 38 0001 mt grn3											
109	0.08	0.44	0.22	99.85	0.10	0.15	0.00	0.01	0.02	0.01	100.90
Un 39 0001 mt grn4											
110	0.04	0.37	0.20	99.76	0.03	0.13	0.00	0.03	0.02	0.01	100.56

Table A3-11 Continued

Element	SiO_2	TiO_2	Al_2O_3	Fe_3O_4	MgO	MnO	CaO	Cr_2O_3	V_2O_3	ZnO	Total
Sample											
Un 40 0001 mt grn5											
111	0.07	0.46	0.19	97.87	0.06	0.00	0.00	0.01	0.01	0.03	98.65
112	0.06	0.51	0.20	98.81	0.09	0.05	0.00	0.00	0.00	0.01	99.71
113	0.05	0.51	0.23	98.89	0.06	0.31	0.00	0.02	0.01	0.00	100.06
Un 41 0001 mt grn6											
114	0.05	0.44	0.21	99.99	0.10	0.00	0.00	0.00	0.00	0.02	100.64

Table A3-12 Titanite EPMA analyses for the Lyon Mountain granite

Element / Sample	SiO_2	TiO_2	Al_2O_3	Fe_2O_3	CaO	Ce_2O_3	F	Total
Rutgers (06-4d) (perthite granite)								
Un 96 064d ttn grn1-1								
625	29.32	29.74	2.29	4.48	25.07	1.37	1.68	95.16
Un 97 064d ttn grn1-2								
626	29.25	30.00	2.38	4.82	25.06	1.36	1.75	95.80
Un 98 064d ttn grn1-3								
627	29.24	30.25	2.26	4.70	25.21	1.40	1.57	95.84
Un 99 064d ttn grn2-1								
628	30.24	32.83	2.06	3.28	26.83	0.65	1.54	98.63
Un 100 064d ttn grn2-2								
629	30.08	32.85	2.18	3.36	26.49	0.74	1.65	98.56
Un 103 064db ttn grn2-3								
677	30.00	32.59	2.20	3.27	27.07	1.01	1.57	98.91
Un 104 064d ttn grn3-1								
678	28.80	32.18	2.07	3.62	26.32	1.07	1.58	96.83
Un 105 064d ttn grn3-2								
679	28.38	31.29	2.21	4.05	25.26	1.20	1.56	95.16
Un 106 06-4d ttn grn3-3								
680	29.73	31.49	2.22	4.02	25.75	1.26	1.57	97.24
Dannemora (99-6c) (microcline granite)								
Un 107 99-6c ttn grn1-1								
681	30.23	30.69	3.73	3.38	26.46	0.53	1.84	98.07
Un 108 99-6c ttn grn1-2								
682	30.24	30.23	3.79	2.96	26.33	0.62	1.78	97.15
Un 109 99-6c ttn grn2-1								
683	30.31	31.32	3.54	2.76	27.43	0.76	1.75	99.07
Un 110 99-6c ttn grn2-2								
684	29.45	30.54	3.74	3.01	23.86	0.65	1.69	94.14
Un 111 99-6c ttn grn2-3								
685	29.95	30.95	3.48	2.73	27.46	0.92	1.75	98.45
Un 112 99-6c ttn grn3-1								
686	30.07	30.55	3.57	2.96	26.41	0.56	1.87	97.18
Un 113 99-6c ttn grn3-2								
687	30.53	30.99	3.71	2.97	26.41	0.54	1.88	98.23
Un 114 99-6c ttn grn4								
688	30.09	30.57	3.79	3.02	25.45	0.86	1.84	96.83
Un 115 99-6c ttn grn4-2								
689	30.41	30.96	3.87	2.88	27.22	0.71	1.93	99.18
Un 116 99-6c ttn grn4-3								
690	30.10	30.52	3.94	3.01	27.07	0.58	2.00	98.43

Table A3-12 Continued

Element / Sample	SiO_2	TiO_2	Al_2O_3	Fe_2O_3	CaO	Ce_2O_3	F	Total
Dry Bridge (99-2b) (albite grnaite)								
Un 86 992b ttn grn1 add Al								
614	29.93	29.95	2.34	5.59	26.91	0.98	2.06	98.96
615	30.01	29.46	2.40	5.51	26.93	1.11	2.15	98.78
Un 87 992b ttn grn1-1								
616	30.16	29.99	2.40	5.56	27.41	0.92	2.10	99.75
Un 88 992b ttn grn1-2								
617	30.38	30.01	2.37	5.24	27.16	0.84	2.13	99.33
Un 89 992b ttn grn1-3								
618	30.18	29.54	2.31	5.36	26.71	1.10	2.11	98.50
Un 90 992b ttn grn2-1								
619	30.25	29.84	2.48	5.56	26.99	1.16	2.20	99.68
Un 91 992b ttn grn2-2								
620	30.51	29.95	2.47	5.56	26.88	0.78	2.10	99.45
Un 92 992b ttn grn3-1								
621	30.13	30.30	2.36	5.24	26.74	1.36	2.09	99.41
Un 93 992b ttn grn3-2								
622	30.29	30.27	2.57	5.02	27.46	0.56	2.10	99.48
Un 94 992b ttn grn3-3								
623	30.12	29.53	2.26	5.50	26.94	1.01	2.03	98.60
Un 95 992b ttn grn3-4								
624	30.45	29.90	2.21	5.51	27.03	0.92	2.03	99.25

Table A3-13 Garnet EPMA analyses for the albite granite

Element	SiO_2	TiO_2	Al_2O_3	Fe_2O_3	MnO	MgO	CaO	Na_2O	K_2O	Cr_2O_3	Total
Sample											
Dry Bridge (99-2b)											
Un 56 992b grt grn1-1											
113	34.78	0.98	1.84	28.78	0.21	0.11	30.74	0.05	0.01	0.00	97.47
114	34.76	0.95	1.87	28.25	0.27	0.15	30.80	0.08	0.00	0.02	97.15
Un 57 992b grt grn1-2											
115	34.97	0.78	1.85	28.57	0.35	0.13	30.65	0.09	0.01	0.04	97.44
Un 58 992b grt grn2-1											
116	34.50	0.97	1.94	28.44	0.32	0.13	30.66	0.06	0.00	0.00	97.01
Un 59 992b grt grn2-2											
117	34.69	1.00	1.82	28.08	0.25	0.14	30.51	0.10	0.00	0.00	96.55

APPENDIX 4

FLUID INCLUSION STUDY

Fluid inclusions from representative samples were studied to try and directly characterize the fluids responsible for alteration and Fe mineralization within the Lyon Mountain granite (LMG). These samples include the 3 main rock types that make up the LMG (perthite granite, microcline granite [K alteration] and albite granite [Na alteration]), one sample that has experienced both K and Na alteration, fayalite granite and two magnetite ore samples. With few exceptions, the fluid inclusion assemblages (FIA) studied were from grains of quartz which contained little petrographic evidence as to the time of mineral growth. Additionally many of the FIA have been stretched or deformed since their entrapment and thus calculated temperatures of formation will not be accurate. FIA occur as liner arrays (probably along healed fractures) and as isolated patches, typically in the cores of quartz grains. In addition, the FIA assemblages, two sets of solid inclusions were analyzed by ICPMS. One set occurred as inclusions in flame lamellae in the fayalite granite, the other as inclusions within altered biotite in the albite granite sample.

Fluid inclusion microthermometric studies were performed on doubly polished thin section chips using a USGS-type gas-flow heating and cooling stage. Individual fluid inclusions were then analyzed by laser ablation ICPMS using a Agilent 7500ce ICPMS coupled with a Geolas laser ablation system at the Virginia Polytechnic Institute. A wide range of major and minor elements were collected (Si, K, Na, Ca, Mn, Fe, Rb, Sr, Ba, La, Ce, Yb, Ti, Sc, Y, Zn, Pb, U, and Zr) as a way to characterize fluid chemistry associated with Fe mineralization and fluid alteration. The presence of fluorine could not be

measured because the ionization potential of fluorine is higher than that of the argon plasma (27 for F and 15 for Ar). The roll of fluorine is important in samples from the LMG because of its ability to form and transport metal ions, and rare earth and high field strength elements (e.g., Bau and Dulski, 1995; Salvi and Williams-Jones, 1996). Fluorine is present in apatite, amphibole and in veins of fluorite suggesting that fluorine was present as a fluid phase during alteration.

RESULTS

Perthite granite (99-1A, Clintonville)

A representative sample of the perthite granite was collected along the Ausable River in Clintonville, NY. The geochemistry, petrology, and U-Th-Pb age data was collected and previously reported in Chapter 4. The FIA in this sample (and other perthite samples) are plentiful but typically too small for microthermometric analysis and ICPMS data collection. The FIA consisted of single and multiphase inclusions. One multiphase inclusion was large enough for microthermometry. In this sample first melting occurred at -56.2° C and final melting at -2.2° C for a calculated salinity of 3.71 % NaCl (Table A4-1).

Microcline granite (99-6C, Dannemora)

A sample of microcline granite was collected one mile west of the town of Dannemora, New York. The FIA is variable within this sample. The FIA are typically 2 phase vapor-dominated, CO_2 rich as indicated by first melting temperatures at -56.6° C, but a smaller subset of FI comprise multiple solid phases as well as liquid and vapor that have inconsistent first melting temperatures ~ -40° C (appendix Table A4-1). This behavior may be the result of chloride complexing with Fe, Ca, or K (Robert Bodner,

personal communication). Major and trace element data from multiphase FI is presented in appendix Table A4-1 and plotted in appendix Figure A4-1a. Fluid inclusions in the microcline granite are rich in Ca, Mn, and Fe.

Albite granite (95-1A, Ausable Forks)

A sample of the albite granite was collected just east of the town of Ausable Forks along highway 9N. The FIA in this albite granite sample was a mixture of two phase (V+L) and multiphase (V+L+S). Multiphase FI typically have final melting temperatures between -3.5 ° C and 4.5 ° C 9 (Table A4-1). This corresponds to a salinity between 5.5 and 7 %. First melting could not be accurately measured. Major and trace element chemistry for FI in the albite granite is presented in appendix Table A4-3 and appendix Figure A4-1b. In addition the FI analyzed by ICPMS, solid inclusions in biotite were also analyzed. These form part of a "wormy" texture in by biotite similar to a symplectite texture. The inclusions analyzed are surrounded by a "ring" or "moat" of quartz. Their composition is presented in appendix Table A4-3. These inclusions are Fe and K-rich and may represent remnant amphibole.

Mixed granite (99-4B, Palmer Hill)

A sample of the Lyon Mountain granite was taken a few meters above the ore body at Palmer Hill, just outside the town of Ausable Forks. This sample has been altered by K-rich fluids and subsequently overprinted by Na-rich fluids. The FIA assemblage in this sample is dominated by multiphase (V+L+S) inclusions. One or more solids may be present in the FI. This FIA has inconsistent and complicated melting behavior probably as a result of the previously mentioned chloride complexing with Ca or Fe. First melting occurred below -70° C with and intermediate melting steps at -50 ° C

and -32 ° C (Table A4-1). Final melting could not be accurately observed. Major and trace element data are presented in appendix Table A4-4 and Figure A4-1b. This FIA is rich in Na and Ca and rarely contains anomalous La.

Fayalite granite (99-3A, Ausable Forks)

A sample of the fayalite granite was taken in the town of Ausable Forks. The sample has experienced partial Na alteration. The dominant FIA in the fayalite granite are CO_2 rich with first melting occurring at -56.6° C. Solid inclusions were observed in flame lamellae produced by Na alteration of preexisting perthitic feldspars. These inclusion contain an oxide mineral and at least one other unidentified phase. These inclusion were analyzed by ICPMS and the data are presented in appendix Table A4-5 and appendix Figure A4-2b. The inclusions are rich in Na, Al, K and Fe suggesting that in addition to the observed oxide phase, the unidentified mineral is probably feldspar. Host feldspar analyses are presented for comparison.

Ore (99-4a, Palmer Hill)

Samples from the Palmer Hill ore body were collected for FI analysis. This sample (as well as the ore sample from Skiff Mountain) contain large (up to 100 μm), ubiquitous, 2 phase fluid inclusions. These FI are typically stretched or "necked". These fluid inclusions exhibit the complex and irregular melting phenomenon of multiphase FIA in other samples. First melting occurs below -60 ° C with an intermediate melting or phase change at -22 ° C and final melting typically between -7° C and -10° C (Table A4-1). Between first melting and final melting numerous phase changed can be observed during heating. Geochemical data indicate that this FIA is Na-rich with minor K and Ca (appendix Table A4-6, appendix Figure A4-3a).

Ore (00-01, Skiff Mountain)

The FIA assemblage from the Skiff Mountain ore body are similar to those of the Palmer Hill ore except that they typically contain at least one solid phase whereas those at Palmer Hill typically do not. The FIA is pervasive and may large (up to 100 μm). First melting occurs below -70° C and final melting between -29° C and -35° C (Table A4-1). Numerous phase changes can be observed between first melting and final melting. Geochemical data show that these FI are rich in Na and Ca with minor K and Sr (appendix Table A4-7, appendix Figure A4-3b). Rarely FI contain anomalously high La, Sc, Al, and Ti. The widespread occurrence and extremely large size of the FI in both ore samples suggests that these are primary inclusions, trapped at the time of ore formation.

REFERENCES

Bau, M., and Dulski, P., 1995, Comparative study of yttrium and rare-earth element behaviours in fluorine-rich hydrothermal fluids. Contributions to Mineralogy and Petrology, v. 119, p. 213.

Hagner, A.F., and Collins, L.G., 1967, Magnetite ore formed during regional metamorphism, Ausable magnetite district, New York: Economic Geology, v. 62, p. 1034-1071.

Salvi, S., and Williams-Jones, A.E., 1996, The role of hydrothermal processes in concentrating high-field strength elements in the Strange Lake peralkaline complex, northeastern Canada. Geochimica et Cosmochimica Acta, v. 60, p. 1917.

Table A4-1 Fuid Inclusion microthermometry results

Sample ID	Type	First Melting (C)	Intermediate	Final Melting (C)	Homogenization (C)	% CO_2	% Salinity
99-1A	V + L	-56.6		-2.2			3.71
99-6C	V + L	-56.6			2		
99-6C	V + L	-56.6			3.1		
99-6C	V + L	-56.6			3.4		
99-6C	V + L + S	~ -40					
95-1A	V + L + S			-3.8			6.16
95-1A	V + L + S			-3.5			5.56
95-1A	V + L + S			-4.5			7.17
99-4B	V + L + S	~ -75.6	-50, -31.9				
99-4B	V + L + S	-82	-50.9, -32				
99-4B	V + L + S	-82.	-51				
99-4B	V + L + S	-90.					
99-4B	V + L + S	-74.5					
99-3A	V + L	-56.6		+ 8 (clathrate)	17.1	~60	
99-3A	V + L	-56.6		+ 9 (clathrate)	22.1		
99-3A	V + L	-56.6		-2.4			~ 4
99-4A	V + L	-65	-22	-2			
99-4A	V + L	-70	-21.7	-9.8			
99-4A	V + L	-66.8	-22.4	-7.2			
99-4A	V + L	~ -65	-22	-7.2			
00-01	V + L + S	-70.00		-29.80			
00-01	V + L + S	-74.0		-29.0			
00-01	V + L + S	-70.6		-35.3			
00-01	V + L + S	-73.20		-35.00			

Table A4-2 Fuid Inclusion major and trace element results for Microcline granite sample (99-6C)

Type	multi-phase	multi-phase	multi-phase
Element			
Na (23)	1,067	-	-
Al (27)	64	143	-
K (39)	-	-	-
Ca (40)	678,616	682,046	678,800
Sc (45)	68	54	177
Ti (49)	68	83	260
Mn (55)	7,303	10,219	9,955
Fe (56)	29,274	24,302	26,247
Zn (66)	-	-	-
Rb (85)	-	-	-
Sr (88)	230	229	179
Y (89)	439	164	464
Zr (90)	-	-	-
Ba (138)	-	8	41
La (139)	-	9	316
Ce (140)	4	34	865
Yb (172)	238	64	85
Pb (208)	-	-	-
U (238)	-	-	-

Table A4-3 Fuid Inclusion major and trace element results for Albite granite sample (95-1A)

Type	V + L + S	V + L + S	solid inclusion
Element			
Na (23)	11,272	7,253	1,298
Al (27)	356	1,423	168,937
K (39)	7,902	11,565	239,381
Ca (40)	3,339	-	16,325
Sc (45)	143	-	-
Ti (49)	-	-	12,380
Mn (55)	-	776	10,338
Fe (56)	-	622	256,668
Zn (66)	399	793	1,753
Rb (85)	-	-	380
Sr (88)	9	-	11
Y (89)	-	6	16
Zr (90)	-	0	20
Ba (138)	8	6	837
La (139)	300	0	-
Ce (140)	4	0	-
Yb (172)	3	0	8
Pb (208)	14	-	47
U (238)	-	0	-

Table A4-4 Fuid Inclusion major and trace element results for mixed alteration sample (99-4B)

Type	multi-phase	multi-phase	multi-phase (?)	multi-phase	multi-phase
Element					
Na (23)	62,172	49,031	39,530	41,104	44,324
Al (27)	634	222	-	3,858	-
K (39)	-	1,349	-	9,808	-
Ca (40)	26,264	52,646	-	48,576	51,402
Sc (45)	-	177	-	700	2,355
Ti (49)	450	76	-	469	1,299
Mn (55)	-	440	-	869	-
Fe (56)	-	-	-	-	-
Zn (66)	498	1,515	-	486	-
Rb (85)	-	-	-	-	-
Sr (88)	436	4,285	5,460	2,375	2,707
Y (89)	-	-	-	-	-
Zr (90)	18	3	-	0	0
Ba (138)	97	1,060	1,369	93	204
La (139)	26,929	-	0	65	-
Ce (140)	-	-	27	10	0
Yb (172)	-	-	0	0	0
Pb (208)	122	762	247	507	-
U (238)	-	1	0	0	0

Table A4-5 Solid inclusions in flame perthite, major and trace element results for fayalite granite (99-3a)

Type	host feldspar	host feldspar	solid inclusion	solid inclusion	host feldspar	solid inclusion
Element						
Na (23)	53,320	151,651	161,710	119,599	51,094	49,498
Al (27)	287,433	302,736	247,997	233,474	292,776	260,436
K (39)	313,249	172,293	38,474	122,421	303,481	237,328
Ca (40)	-	1,212	58,191	81,950	-	7,168
Sc (45)	51	52	58	-	-	51
Ti (49)	134	76	595	672	108	88
Mn (55)	29	121	1,204	2,900	85	1,718
Fe (56)	3,844	9,808	141,735	100,050	7,389	109,367
Zn (66)	-	10	163	129	-	-
Rb (85)	1,466	799	169	664	1,438	1,153
Sr (88)	76	42	68	437	98	115
Y (89)	0	0	2	2	1	5
Zr (90)	-	-	-	-	-	-
Ba (138)	638	368	135	351	747	627
La (139)	1	1	23	21	2	6
Ce (140)	0	1	41	44	-	19
Yb (172)	-	-	-	-	-	2
Pb (208)	3	1	-	9	-	-
U (238)	-	-	-	-	0	-

Table A4-6 Fluid inclusion major and trace element results for Palmer Hill ore (99-4a)

Type	multi-phase	multi-phase	multi-phase	multi-phase	multi-phase	multi-phase	multi-phase	multi-phase
Element								
Na (23)	42,612	41,282	38,585	39,769	43,873	35,964	34,210	35,142
Al (27)	160	-	124	363	63	586	2,049	2,626
K (39)	6,212	4,117	4,871	4,295	3,624	5,565	3,842	3,845
Ca (40)	5,483	8,006	9,050	8,422	6,104	7,120	6,152	6,776
Sc (45)	-	-	-	155	-	193	487	796
Ti (49)	128	177	835	244	32	382	924	1,459
Mn (55)	-	157	152	72	122	449	1,349	63
Fe (56)	-	-	-	-	125	3,278	500	-
Zn (66)	30	35	74	37	111	381	366	-
Rb (85)	-	-	37	42	40	46	-	41
Sr (88)	916	873	976	947	983	1,041	993	901
Y (89)	0	0	-	-	-	-	1	0
Zr (90)	0	-	0	0	0	0	0	0
Ba (138)	415	394	397	367	525	830	465	352
La (139)	0	0	0	459	73	2	2,816	0
Ce (140)	0	0	0	0	0	2	0	0
Yb (172)	1	0	0	0	0	0	2	0
Pb (208)	7	16	5	28	9	45	41	13
U (238)	0	-	0	0	-	-	0	0

Table A4-7Fluid inclusion major and trace element results for Skiff Mountain ore (00-01)

Type	multi-phase	multi-phase	multi-phase	multi-phase	multi-phase	multi-phase	multi-phase	multi-phase
Element								
Na (23)	78,321	83,646	35,233	30,204	38,847	46,778	77,482	-
Al (27)	1,451	49	1,847	451	308	533	535	40,143
K (39)	5,583	2,641	4,061	4,306	5,090	3,202	5,379	-
Ca (40)	25,506	24,780	61,648	70,080	61,975	55,847	26,126	-
Sc (45)	182	-	778	170	114	64	275	11,495
Ti (49)	415	-	1,147	265	263	337	454	23,364
Mn (55)	-	72	39	-	107	166	-	-
Fe (56)	143	32	-	-	152	-	-	-
Zn (66)	59	190	710	686	642	616	167	-
Rb (85)	-	31	112	117	95	72	52	-
Sr (88)	780	1,366	2,953	3,812	3,428	3,105	3,192	-
Y (89)	1	-	-	0	-	-	0	0
Zr (90)	0	0	-	0	-	-	0	0
Ba (138)	60	110	245	324	321	291	512	536
La (139)	19	1,053	-	0	-	-	0	598,685
Ce (140)	0	0	4	0	4	1	0	142
Yb (172)	0	0	-	0	-	-	1	0
Pb (208)	34	55	109	21	100	169	-	-
U (238)	0	0	-	0	-	-	0	-

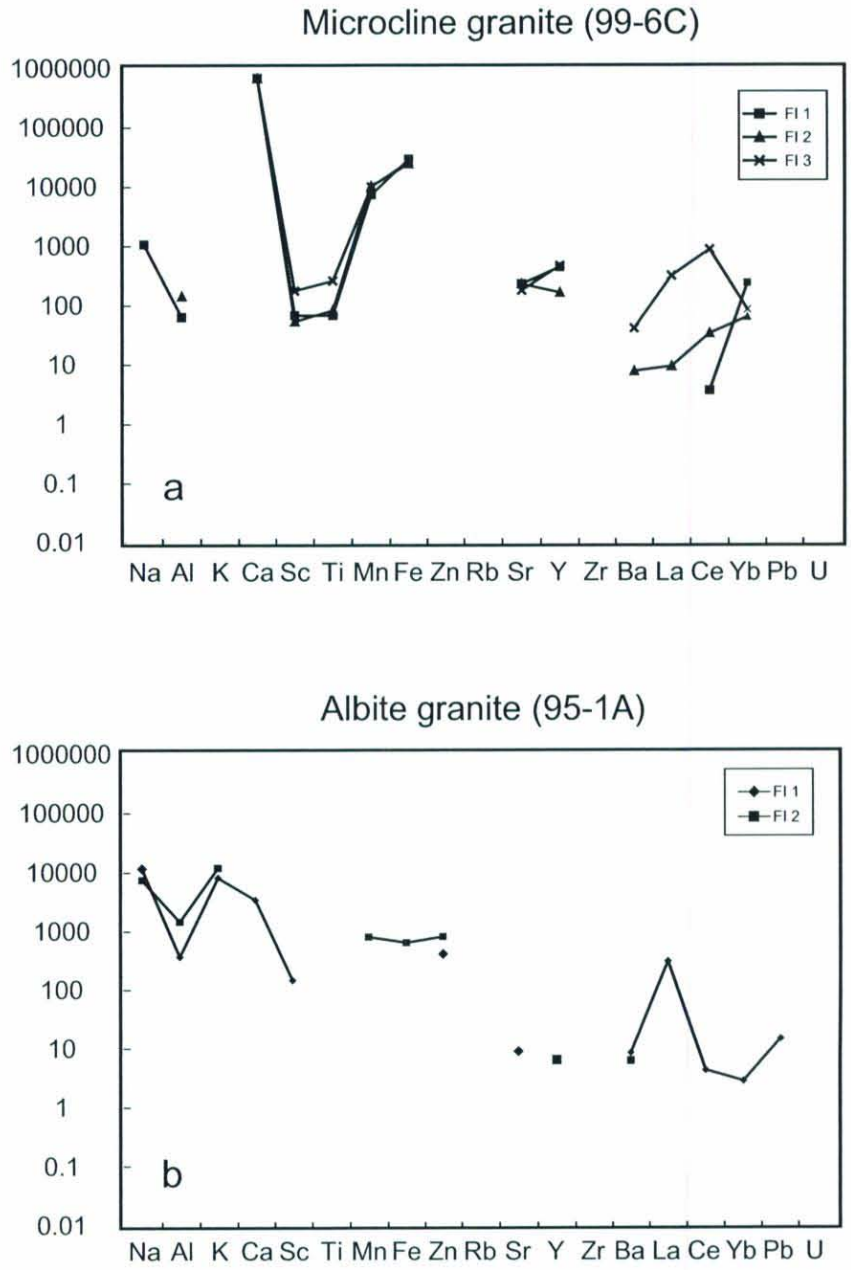

Figure A4-1. Major and trace element chemistry of fluid inclusions in the a), microcline granite (Dannemora) and b), albite granite (Ausable Forks).

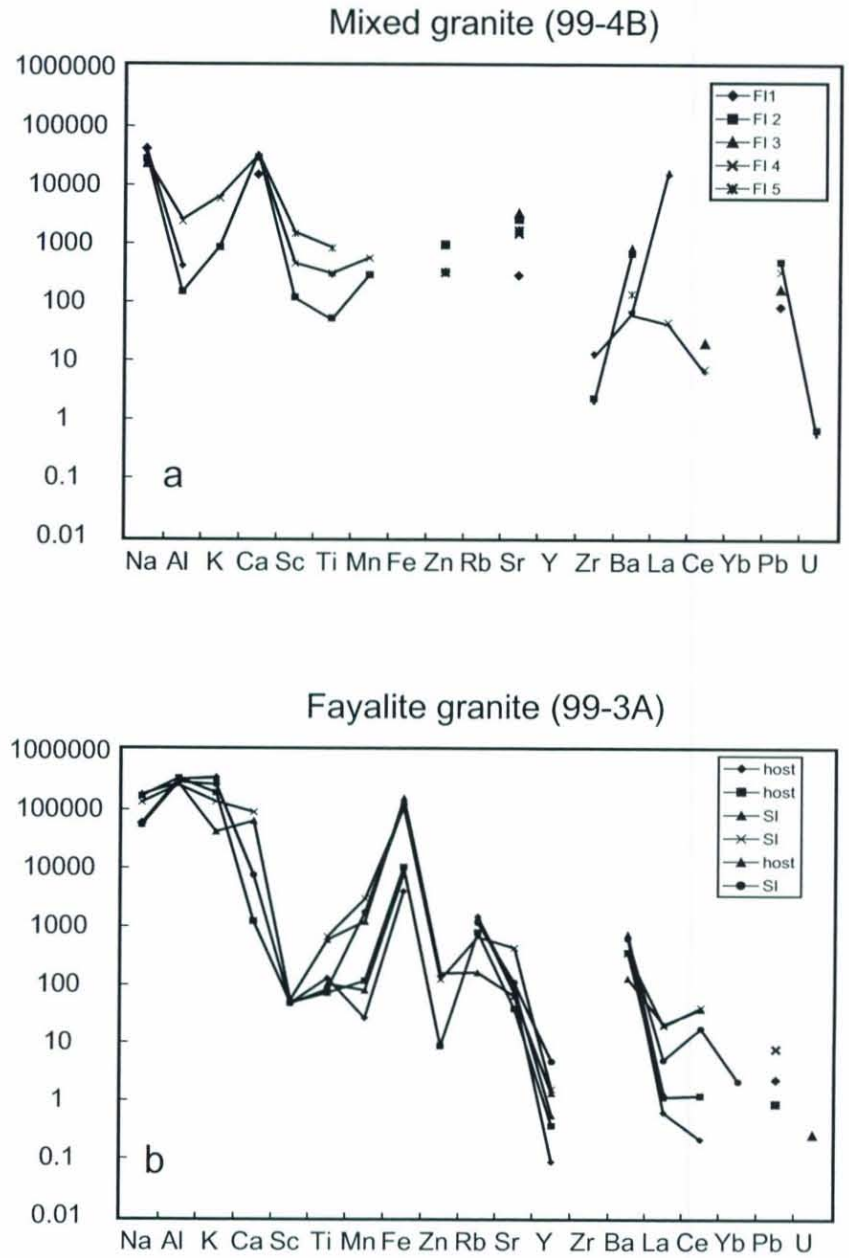

Figure A4-2. Major and trace element chemistry of fluid inclusions in the a), mixed granite (Palmer Hill) and b), fayalite granite (Ausable Forks). SI = solid inclusion.

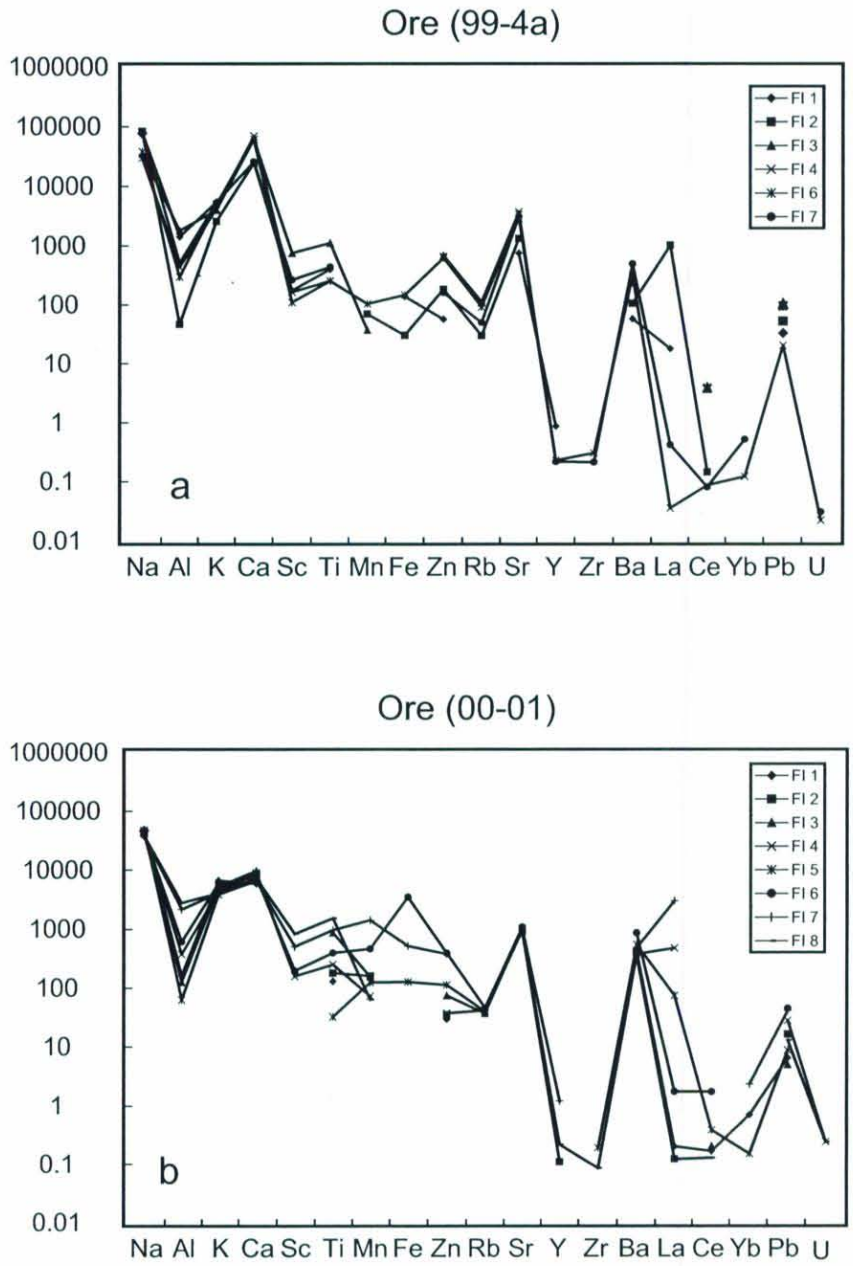

Figure A4-3. Major and trace element chemistry of fluid inclusions in the LMG ore a), 99-4a (Palmer Hill) and b), 00-01 (Skiff Mountain).